Compressive Behaviour of C-Shaped Confined Masonry Boundary Elements

ALA' TALEB MUFLEH OBAIDAT

A Thesis

In the Department

of

Building, Civil and Environmental Engineering

Presented in Partial Fulfillment of the Requirements

For the Degree of

Doctor of Philosophy (Building Engineering) at

Concordia University

Montréal, Québec, Canada

August 2017

CONCORDIA UNIVERSITY

School of Graduate Studies

This is to certify that the thesis prepared

By: **Ala' Taleb Mufleh Obaidat**

Entitled: **Compressive behaviour of C-shaped confined masonry boundary elements**

and submitted in partial fulfillment of the requirements for the degree of

DOCTOR OF PHILOSOPHY (Building Engineering)

complies with the regulations of the university and meets the accepted standards with respect to originality and quality.

Signed by the final examining committee:

_____ Chair
Dr. Sabine Bergler

_____ External Examiner
Dr. Edward G. Sherwood

_____ External to Program
Dr. Rajamohan Ganesan

_____ Examiner
Dr. Anjan Bhowmick

_____ Examiner
Dr. Ashutosh Bagchi

_____ Thesis supervisor
Dr. Khaled Galal

Approved by _____

Dr. Fariborz Haghighat, , Graduate Program Director
Department of Building, Civil and Environmental Engineering

_____
Dr. Amir Asif, Dean
Faculty of Engineering and Computer Science
Date August 21, 2017

Abstract

Compressive Behaviour of C-Shaped Confined Masonry Boundary Elements

Ala' Taleb Mufleh Obaidat, Ph.D.
Concordia University, 2017

Reinforced masonry (RM) shear walls are commonly used in mid- and high-rise masonry buildings as the main lateral load resisting system. The seismic performance of RM shear walls can be enhanced by integrating reinforced boundary elements at the wall most stressed zone (i.e. wall ends). Evaluating the compression behaviour of the boundary elements is key for predicting the seismic response of the RM shear walls. Unlike reinforced concrete (RC), the experimental studies that focused on compressive stress-strain behaviour of reinforced masonry are scarce.

This study quantifies the stress-strain relationship of sixteen C-shape full-scale and fifty four C-shape half-scale fully grouted unreinforced and reinforced masonry boundary element (RMBE) specimens tested under concentric compression loading up to failure. The effect of changing hoop spacing, vertical reinforcement ratio, the strength of grout, and aspect ratio (height to thickness) on the axial compressive stress-strain behaviour of RMBE is investigated. Enhancement in both peak and post peak stress-strain behaviour were observed by decreasing the hoop spacing, increasing the grout strength, decreasing the aspect ratio, and increasing the vertical reinforcement ratio. Out of the studied parameters, the hoop spacing had the most noticeable effect on the stress-strain relationship.

Finite element modelling (FEM) numerical simulations are employed to simulate the compression behaviour of the full-scale RMBE. The proposed FEM procedure provides good

prediction of the compression stress-strain behaviour of RMBEs and captures the influence of the confinement reinforcement ratio on the RMBE response. In addition, this study investigates the capability of three existing stress-strain models in predicting the RMBE stress-strain relationship. The considered models overestimated the enhancement in the RMBE stress and significantly overestimated the enhancement in the RMBE strain.

Finally, an analytical compressive stress-strain model capable of predicting the RMBE compressive response considering various confinement effects is proposed. The proposed empirical stress-strain model is capable of capturing the overall compressive stress-strain behaviour where a good agreement with the test results was achieved. This model can be implemented in different design and assessment frameworks aiming at better prediction of the seismic response of RM walls with boundary elements.

DEDICATION

To my beloved parents

To my lovely wife Eng. Ala'a Al-ayyoub

To my sons; Abdullah, Abd Alruhman, and Mohammad and daughter Bana

To my brothers and sisters

Acknowledgements

First and foremost, I would like to thank Allah for giving me the health and patient throughout this research work. I would like to thank my supervisor, Professor Khaled Galal for his support, help, and guidance throughout this research study. Although he had thirteen graduate student, Professor Khaled Galal has been able to keep me motivated, challenged, productive and on the right track at all time. His encouragement has given me the confidence to focus and proceed. I would like also to thank postdoctoral fellow Drs. Ahmed Ashour and Ahmad Abo El Ezz for their support, vital comments, valuable suggestions, and guidance. Also, Special thanks for my examination committee members, Dr. Edward Sherwood, Dr. Rajamohan Ganesan, Dr. Ashutosh Bagchi, and Dr. Anjan Bhowmick.

Also, I would like to acknowledge and appreciate the structure laboratory staff at Concordia University (Riccardo Gioia, Andy Shin-Pong, Roberto Avila, and Jaime Yeargans) and at Ecole Polytechnique Montreal QC (Xavier Willem, Patrice Belanger, and David Ek) for their assistance and technical support during my experimental work.

I will be failing in my duty if I do not mention special thanks to my friends Khalid Alotaibi, Omar Yagob, Hamid Arabzadeh, Mohammed Albotainy, Nader Ali, Mohamed Yosry, Hany Seif, Siamak Pejmanfer, Zakaria Maamar, Gaith Sabouni, Jimi Adoumie and Rebecca Mossa for their help, endless support and valuable hints throughout the experimental and analytical work of this research study.

I would like to acknowledge the financial support from the Natural Science and Engineering Research Council of Canada (NSERC), l'Association des Entrepreneurs en Maçonnerie du Québec (AEMQ), the Canadian Concrete Masonry Producers Association (CCMPA) and Canada Masonry Design Centre (CMDC).

Finally, I would like to thank my main pillars in my life (parents) without them, I would not be definitely achieve this success. It is also a rare blessing to have a wife as supportive as Eng. Ala'a Al-Ayyoub whose love, encouragement, continuous motivation, advises, support, and patience have inspired me to complete this academic journey. I would like to thank my kids as well for their kisses and hugs which they gave me a positive energy. Also, I would like to acknowledge my brothers and my sisters for their invaluable supporting over the past four years throughout my study.

Co-Authorship

This thesis has been prepared in accordance with the regulations for a sandwich thesis format. This research presents experimental, numerical, and empirical work carried out solely by Ala' Taleb Mufleh Obaidat. Advice and guidance provided for the whole thesis by the academic supervisor Professor Khaled Galal. Dr. Ahmad Abo El Ezz reviewed the third chapter in the thesis. Dr. Ahmed Ashour has reviewed the fourth and fifth chapters in this thesis. This thesis consists of the following chapters:

Chapter 3

Obaidat, A., Abo El Ezz, A., and Galal, K. (2017). "Compression behaviour of confined concrete masonry boundary elements". *Journal of Engineering Structures*, Elsevier, 132, 562-575.

Obaidat, A., Abo El Ezz, A., and Galal, K. (2015). "Evaluation of the compression behaviour of confined boundary elements in ductile reinforced concrete block masonry structural walls". 11th Canadian Conference on Earthquake Engineering, Victoria, BC, Canada.

Chapter 4

Obaidat, A., Ashour, A., and Galal, K. (2017) "Compression behaviour of confined concrete masonry boundary elements." *Journal of Structural Engineering*, ASCE, submitted for publication in June 2017.

Chapter 5

Obaidat, A., Ashour, A., and Galal, K. (2017) "Empirical stress-strain model for c-shape confined concrete masonry boundary elements of RM shear wall." *Journal of Engineering Structures*, Elsevier, submitted for publication in July 2017.

Table of Contents

List of Figures

List of Tables

Chapter1

Introduction

1.1 Background and Motivation

Masonry is one of the oldest building material that is still used to date in North America and all over the globe. Reinforced masonry systems are vital alternative for low- and mid-rise residential and commercial buildings. In general, the perception that masonry structures have a limited ductility and poor seismic performance may be due to the poor performance of unreinforced masonry (URM) structures under seismic loading. However, several studies have shown that reinforced masonry (RM) seismic force resisting systems (SFRS) can survive extreme seismic events with minimal damage (e.g. Abrams 1986, Seible et al. 1994).

Shear walls are commonly used as the SFRS in RM structures to provide lateral strength, stiffness, and energy dissipation that is required to resist the lateral loads arising from wind or from earthquakes. As shown in Figure 1.1, when an earthquake strikes, the inertia forces will be distributed through the diaphragm in-plane stiffness to the RM shear walls. Designing the RM shear wall to behave elastically during severe ground motion is not economical and unpractical. As such, RM shear walls are expected to undergo inelastic deformation during severe ground motion. Hence, enhancing the wall ductility is a key factor for enhancing the building seismic performance. This could be attained by achieving a better reinforcement detailing.

Reinforced concrete (RC) shear walls usually accommodate more than one layer of vertical steel reinforcement that are commonly enclosed by horizontal reinforcement (i.e. hoops) at the wall toes; wall's most stressed zone. However, a rectangular RM wall typically accommodates only one layer of vertical reinforcement bars. Consequently, this single bar per cell will not allow the placement of confinement hoops at the end zones of the wall, which are subjected to high inelastic strains during an earthquake. Adding boundary elements, BEs, to RM shear walls' toes was recently introduced (CSA) to allow the placement of at least four vertical reinforcing bars enclosed by transversal hoops. This offers a reinforcement cage that provides core confinement to the wall's toes and thus enhances the seismic performance of the RM wall which was not attained in rectangular RMSW (Shedid et al. 2010, and Banting and El-Dakhakhni 2012).

The failure mechanism of RM shear wall systems can be categorized into two main mechanisms, shear failure and flexural failure. Shear failure is sub categorized into sliding shear failure along mortar bed joints and formation of diagonal shear cracks. Shear failure mode is relatively brittle and is usually accompanied with rapid strength and stiffness degradation. Flexure failure is characterized by the formation of cracks along the bed joints and tensile yielding of the vertical reinforcement at the ends of the wall (Toes). This is followed by the formation of a plastic hinge zone at the bottom of the wall. Finally, flexural failure is characterized by compression crushing of the masonry and the grout in the plastic hinge region, buckling, and fracture of vertical reinforcement under compression and tension, respectively. Flexural failure is the favoured failure mode compared to shear failure. It dissipates energy effectively, due to the tensile yielding of the vertical reinforcement and its ductile nature, in addition to its inelastic deformation of the masonry.

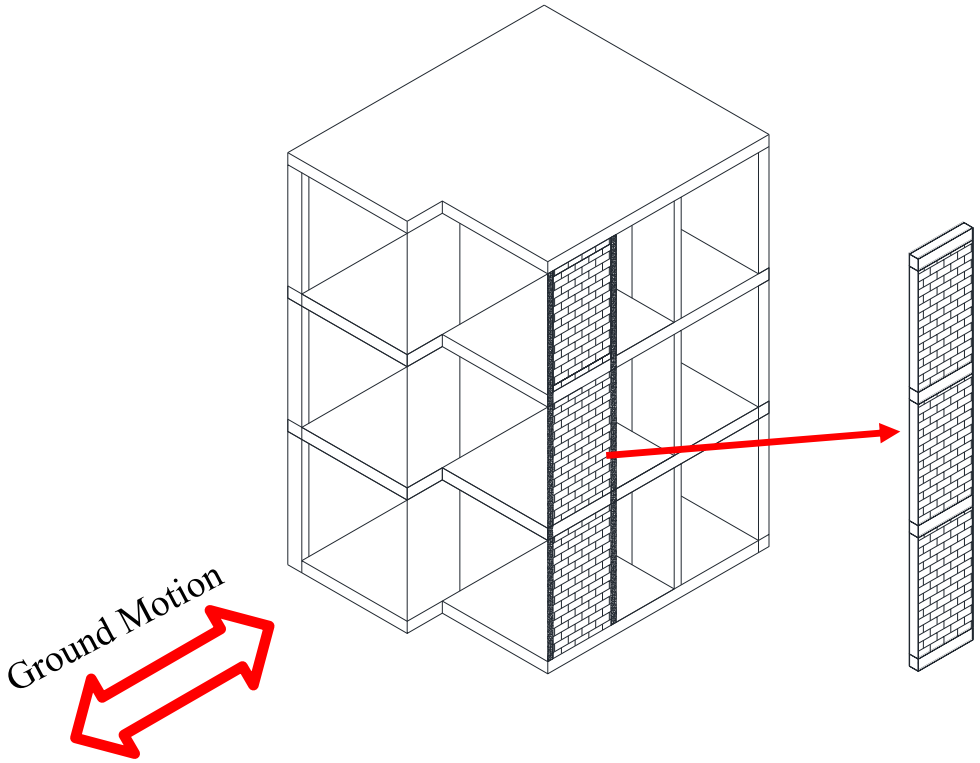

Figure 1.1 Schematic of a masonry building with RM walls

Improving the ductility of masonry prisms by adding confinement was investigated in a number of studies in the literature (Priestley and Elder 1983, Hart et al. 1988, Shing et al. 1993, Dhanasekar and Shrive 2002, Malmquist 2004, and Abo Elzz et al. 2015). Moreover, experimental Studies on the seismic performance of RM shear walls with boundary elements (Shedid et al. 2010, and Banting and El-Dakhakhni 2012) concluded that the wall ductility and lateral response can be improved by integrating boundary elements at the wall's end zones. Adding BEs at RM shear walls' toes increases the area at the wall ends and thus decreasing the compression stress block depth (Park et al., 2007). Subsequently, this will result in enhancing the ultimate compression strain, the RM wall's curvature and displacement ductility (Paulay and Priestley, 1992). Moreover, the transversal hoops delays both the buckling of vertical reinforcement and compression crushing of the masonry at the plastic hinge region which improves the seismic performance of RM shear wall (Shedid, 2010).

In order to improve the displacement ductility capacity of the RM walls, recent North American codes and masonry standards (MSJC, 2013 and CSA S304-14, 2014) have introduced the use of ductile RM walls with boundary elements. The U.S. Building Code Requirements and Specifications for Masonry Structures (MSJC, 2013) allow integrating BE with RM walls, however, MSJC (2013) only imposes some geometric rules with no emphasis on the effect of confinement on the wall performance. Also, in the most recent Canadian Standard for the Design of Masonry Structures (CSA S304, 2014), the correlation between specific parameters (e.g., detailing of confinement reinforcement) and the corresponding enhancement of the strength and strain capacity is yet to be presented. The 2014 CSA S304 code recently added a new clause discussing RM shear walls with boundary elements. The new clause allowed, with experimental evidence, the use of higher ultimate strain values for RM shear walls with confined end zones. As such, understanding the stress-strain response of the RM boundary element is key in the analysis and design of RM shear walls with boundary elements. Therefore, there is a need for experimental research to investigate the stress-strain response of RM boundary elements considering the effect of different parameters.

Recently, the compression stress-strain behaviour of RM boundary elements made of standard block was investigated by Abo Elzz et al. (2015) based on the experimental study of 17 full scale, fully grouted concrete masonry boundary elements that represented the end zones of a RM shear wall. It was concluded that the confinement reinforcement increased the axial

compression capacity and the strain ductility of the boundary elements. It should be noted that Abo Elzz et al. (2015) utilized standard concrete block to build the RMBE which introduce some limitations on the hoop spacing and placement. However, C-shaped blocks (Fig. 1.2) offer a larger single core where the mass of the block is lower compared to the standard hollow block, which makes the placement of reinforcement and grout easier. According to the literature, the stress-strain behaviour of RMBE constructed with C-shaped blocks is yet to be investigated.

Figure 1.2 Half-Scale C-Shaped Concrete Masonry Block Unit

1.2 Objectives

This dissertation presents a part of an ongoing research project focusing on the seismic response of RM boundary elements at Concordia University. As illustrated in the previous section, investigating the compression behaviour of RMBE is essential to understand the nonlinear response of RM boundary element walls under lateral loading.

The main objective of this study is to investigate, experimentally, numerically, and analytically, the compression stress-strain behaviour of unreinforced and reinforced RMBE built using C-shaped concrete block (see Figure 1.3). Throughout this study, the effect of the following parameters on the stress-strain behaviour of RMBE were investigated;

1. Vertical reinforcement ratio, ρ_v
2. Volumetric ratio of lateral reinforcement, ρ_h
3. Strength of the grout, f_{gr}

4. Aspect ratio of boundary element (height to thickness), h/t
5. The effect of changing the gauge length on the measured axial strain.

In addition to the aforementioned objectives, other objectives were adopted based on the analyzed research results:

- Introducing equations of strains at the peak load, 75% of the peak load, and 50% of the peak load, CSA S304 permits the use of the maximum compressive strain of masonry more than 0.0025 by either adding boundary elements or another technique which can be shown through testing.
- Proposing an empirical stress-strain model that can be adopted in different analysis and assessments frameworks.

Figure 1.3 Reinforced masonry boundary element, RMBE

1.3 Scope of Work

The scope of this work is divided into three phases.

1.3.1 Phase I

The main objectives of this phase are:

- Investigating the compression behaviour of full-scale RMBE, having different confinement ratios, under compression concentric loading.
- Complementary to experimental investigations, a Finite element modeling (FEM) procedure, using ABAQUS software, need to be employed to simulate the compression behaviour of the RMBE.
- The FEM procedure shall be validated with experimental results on the full-scale confined RMBE by comparing stress-strain curves and damage progression.

To achieve these objectives, a total of 16 full-scale fully grouted RMBE were constructed and tested. These specimens were divided into six groups. Some of the groups had three identical specimens and some of them had two. All of the reinforced specimens contained four vertical rebars, except the first group. The first group was unreinforced, the second group was unconfined but vertically reinforced, and the rest of groups were confined with horizontal reinforcement (hoops) with different confinement ratios. The total length of the test unit was 1250 mm with an effective (gauge) length of 1000 mm. Each RMBE consisted of five block layers placed on a concrete footing with dimensions of 400 mm x 400 mm x 250 mm (length x width x depth). Each course of the RMBE was made of two block units placed together in alternating directions along its height. Complementary to the experimental investigation, a nonlinear finite element ABAQUS software package was employed for the numerical simulation of the compression stress-strain behaviour of the tested RMBE.

1.3.2 Phase II

The main objectives of this phase are:

- Investigating the effect of changing the volumetric ratio of transverse reinforcement, the longitudinal reinforcement ratio, and grout strength on the compression stress-strain behaviour of half scale RMBE.

- Introducing Equations of strains at the peak load, 75% of the peak load, and 50% of the peak load function with confinement ratio, vertical reinforcement ratio, and grout strength.
- Investigating the capability of three existing stress-strain models in predicting the RMBE stress-strain relationship.

In order to achieve these objectives, thirty half scale RMBE with an aspect ratio of 5 (i.e. height to thickness ratio h/t) were tested, until failure, under concentric compression loading. The specimens were divided into ten groups, each group had three identical specimens. All the confined specimens contained four vertical bars. The first and second groups were unreinforced and grouted with 15 and 45 MPa grout, respectively. The rest of the groups were vertically reinforced with different vertical reinforcement ratios, confined with hoops with different confinement ratios, and constructed with 15 and 45 MPa grout strength.

1.3.3 Phase III

The main objectives of this phase are:

- Investigating the compression stress-strain behaviour of half scale RMBE with different aspect ratios under compression concentric loading.
- Investigating the effect of changing gauge length on the compression stress-strain behaviour of the half scale RMBE.
- Proposing an empirical model to predict the compressive stress-strain curve of the unconfined and confined RMBE.

Thirty RMBE were constructed and tested, up to failure, to achieve these objectives. Phase III specimens were detailed similar to those of Phase II but they had different aspect ratios (i.e. 2 and 3). The specimens were divided into ten groups with different aspect ratios, each group had three identical specimens. All the specimens were constructed using 15 MPa grout strength and they all had a different h/t. They contained two layers of vertical reinforcement with two bars of #3 per each layer and confined with hoops with different confinement ratios, except the first and second groups, which were un-grouted.

Finally, a stress-strain empirical model is proposed. This model is capable of predicting the complete stress-strain relationship of both the unconfined and confined zone for RMBE. The

model formulation take into account the effect of changing, the grout strength, aspect ratio, volumetric ratio of lateral reinforcement and vertical reinforcement ratio on the axial stress-strain behaviour of RMBE. Hence, the proposed compression stress-strain analytical model can be adopted in forced- or displacement-based design frameworks to predict the seismic response of RM shear walls with boundary elements.

1.4 Organization of the Dissertation

The dissertation is comprised of six chapters (including the present one), a list of figures and tables, notations, appendix, and references. These chapters provide all the experimental, numerical, and analytical details of this research project. These details are used to investigate the compression stress-strain behaviour of the RMBE. The content of the chapters are as follows:

- Chapter 1 presents the problem statement, the research significance and motivation of the dissertation, the main objectives followed by the scope of work to achieve the research objectives, and the organization of the dissertation.
- Chapter 2 reviews the previous research on confined RC columns, RM boundary elements, the applications and techniques of confinement in improving the seismic performance of RC and RM boundary elements, and the effect of adding boundary elements to the end of RM shear walls.
- Chapter 3 contains a description of an experimental and numerical compression behaviour of full scale RMBE considering the effect of changing the confinement ratio. The properties of materials that were used in the construction of RMBE specimens were obtained by tests conducted at the structures laboratory of Concordia University. These tests are presented in this chapter. Furthermore, the setup utilized for testing the specimens of RMBE is described. This chapter also presents the numerical model including: the details of finite element, the definition of constitutive materials, details of boundary conditions and meshes, and the employed software for simulation of the RMBE behaviour. Finally, the results of the experimental and the numerical study are presented in this chapter. These results include: validation of the numerical model, comparison of results, the effect of changing confinement ratio on the strength of RMBE, and ductility capacity at 75% and 50% of the peak stress.

It should be noted that this chapter presents a separate accepted paper.

- Chapter 4 focuses on the compression stress-strain behaviour of half scale confined concrete masonry boundary elements considering the effect of changing the volumetric ratio of transverse reinforcement, vertical reinforcement ratio, and grout strength. The chapter starts by reporting the significance of investigating the compression stress-strain behaviour that can be employed for any masonry analysis process. This chapter documents the effect of aforementioned parameters on the RMBE ultimate strength, strain corresponding to peak, and post-peak behaviour. Also, this chapter presents a linear relationship that can be used by engineers to predict the RMBE stress and strain corresponding to the ultimate stage, 25%, and 50% stress degradation. Finally, this study investigated the capability of three existing stress-strain models in predicting the RMBE stress-strain relationship.

It should be noted that this chapter presents a separate submitted paper.

- Chapter 5 presents the compression stress-strain behaviour of half scale confined concrete masonry boundary elements considering the effect of changing the aspect ratio (height to thickness), confinement ratio of transverse reinforcement, and gauge length. In addition, this chapter presents the proposed empirical compressive stress-strain model which can be adopted in forced- or displacement-based design frame work to predict the seismic response of RM shear walls with boundary elements. The proposed model is important in a numerical analysis especially that this model capture nicely the descending part of the copressive stress-strain curve especially the sudden stress drop after the peak stress due to the face shell spalling

It should be noted that this chapter presents a separate submitted paper.

- Chapter 6 presents a summary, the main conclusions of the dissertation, and recommendations for future research.

Chapters 3, 4, and 5 complement each other.

Chapter 2

Literature Review

2.1 Background

This chapter presents a concise review of the response of reinforced concrete (RC) columns, reinforced masonry (RM) boundary elements, RM prisms, and RM shear walls with boundary elements under compression and lateral cyclic loading. Due to the wealth of knowledge that exists on the stress-strain axial response of RC columns, this chapter starts by presenting a summary of some relevant studies.

On the other hand, experimental studies that investigate and quantify the compression strain ductility of reinforced masonry boundary elements (RMBEs) are scarce. Abo El Ezz et al. (2015) experimentally investigated the compression behaviour of boundary elements with standard concrete blocks. More research was conducted on the evaluation of compression behaviour of confined RC columns, and several analytical stress-strain models were proposed (e.g. Vallenas et al., 1977; Mander et al., 1988; Kent and Park, 1971 and Hoshikuma et al., 1997). That being said, the compression behaviour of a confined RM column is not necessarily similar to that of RC columns since there are complex interactions between the mortar, grout, the block, and the longitudinal and transverse steel reinforcement. On the other hand, most of the experimental, analytical, and numerical work on the RM columns were focused on evaluation of the ultimate compression strength (Köksal et al. 2004, Sturgeon et al. 1980, and Khalaf et al. 1993).

Three different expressions are used in this chapter in order to describe masonry boundary elements. “Unreinforced masonry” is used to describe unreinforced and unconfined masonry boundary elements. On the other hand, “unconfined reinforced” is implemented to describe vertically reinforced masonry boundary elements. Finally, “confined reinforced” is used to describe vertically and transversely reinforced masonry boundary elements.

2.2 Behaviour of Unconfined and Confined Concrete Columns

Early experimental research (e.g. Park and Paulay 1975), reported that the stress-strain relationship of a RC member is almost identical to the plain concrete column subjected to uniaxial load after excluding the contribution of the vertical reinforcement in increasing strength. However, in the post-peak strains, the relationship is completely different. In the plain concrete, the lateral expansion is too large when the vertical strain in the concrete exceeds the strain corresponding to the peak stress, due the absence of confinement, which leads to a brittle failure. In the absence of the lateral support (no confinement), the failure of RC prism is characterized by splitting and crushing of the concrete followed by the buckling of longitudinal reinforcement rebars (MacGregor and Wight, 2004).

2.2.1 Vallenas et al. (1977)

Vallenas et al. (1977) proposed a more reliable compression stress-strain relationship for the confined RC columns considering the effect of the following parameters: concrete cover, horizontal reinforcement (hoops), and longitudinal reinforcement. Fourteen one-third scale specimens of plain and reinforced concrete were tested under concentric loading. These specimens had square cross sections of 254 mm x 254 mm with their cover, 229 mm x 229 mm without a cover, and 762 mm in height. These specimens represented the boundary elements of wall specimens used for the ongoing project on structural walls. The specimens were longitudinally reinforced with ratios of 0.0353 and 0.0434 for the specimens with a cover and without a cover, respectively. The axial strain was measured using three different gauge lengths in order to record the deformation in the most heavily damaged branch. The first one was at the middle and used four LVDT's that were mounted on the embedded crossing bars in the concrete core. The second one, at the region on the ends of the specimens, used two linear potentiometers that were attached on one end of the specimen and on one of the embedded bars. The last one was placed at the whole height of the specimens and measured the relative displacement of the heads of the testing machine, using wire potentiometers (see Figure 2.1). It was concluded that adding longitudinal reinforcement improved the confinement of the concrete, increased the strength stress, and prevented slippage of the end hook of the hoops. The buckling of longitudinal reinforcement rebars was observed at an axial strain in the range of 0.023 to 0.03, therefore it was not considered to affect the stress-strain relationship of the confined reinforced

concrete. It was found that the load capacity of the specimens without a cover was similar to that of the specimens with a cover, before cover spalling. Moreover, no sudden drop in load capacity was observed after the start of spalling. Finally, adding lateral confinement in the form of hoops showed an increase in strength, concrete stress, and ductility compared to the unreinforced concrete specimens. A lower modulus of elasticity was seen for the confined reinforced concrete, as compared to the unreinforced concrete specimens, due to the disruption of the continuity of the concrete from the hoops. Moreover, not all of the hoops had yielded when the maximum stress in concrete was reached.

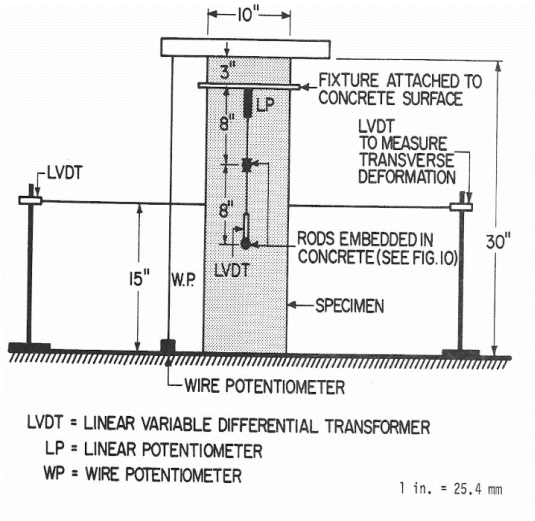

Figure 2.1 External instrumentation
(Vallenas et al., 1977)

Vallenas et al. (1977) proposed the following stress-strain relationship based on the analysis of experimental results shown in Figure 2.2. The stress-strain relationship consists of three branches as follows:

For branch AB $\left(\varepsilon_L \leq \varepsilon_0\right)$ is given by Eq. 2.1 and Eq. 2.2.

$$\frac{f_c}{f_c^{'}} = \frac{\frac{E_c \varepsilon_0}{f_c^{'}}\left(\frac{\varepsilon_L}{\varepsilon_0}\right) - k\left(\frac{\varepsilon_L}{\varepsilon_0}\right)^2}{1 + \left[\frac{E_c \varepsilon_0}{k f_c^{'}} - 2\right]\left(\frac{\varepsilon_L}{\varepsilon_0}\right)} \qquad \text{Eq. 2.1}$$

$E_c = 46{,}000\sqrt{f_c^{'}}$, $f_c^{'}$ in psi (for the specimen tested) and ε_0 is the strain corresponding to the maximum stress.

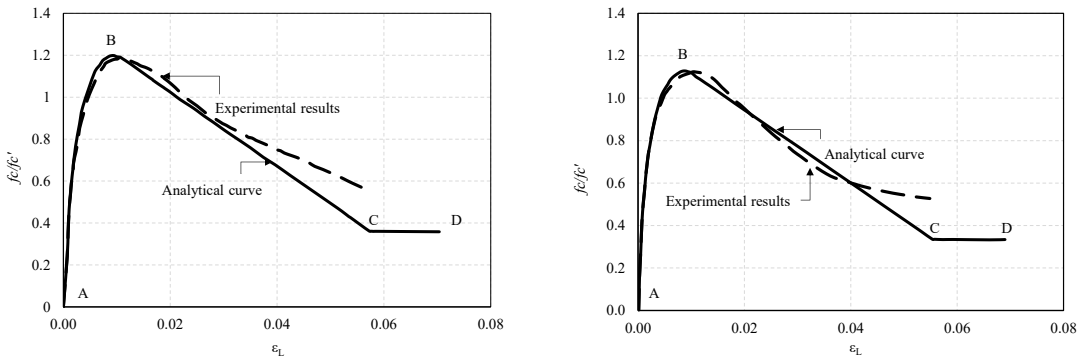

Figure 2.2 Analytical curve and experimental results for: (a) confined reinforced concrete with longitudinal reinforcement; and (b) confined concrete without longitudinal reinforcement (redrawn from Vallenas et al., 1977)

k is the maximum stress ratio and it's a function of lateral, longitudinal confinement, and the concrete strength as seen in the following equation.

$$k = 1 + 0.0091\left(1 - 0.245\frac{s}{h''}\right)\frac{\left(\rho'' + \frac{d''}{d}\rho\right)f_y''}{\sqrt{f_c'}} \qquad \text{Eq. 2.2}$$

s is the lateral reinforcement spacing, h'' is the width of the confined reinforced concrete, d and d'' are the nominal diameter of the longitudinal and lateral reinforcement, respectively. f_y'' is the yield strength of the lateral reinforcement, f_c' is the compressive strength of concrete, ρ and ρ'' are the longitudinal reinforcement ratio and volumetric ratio of lateral reinforcement, respectively.

For branch BC $\left(\varepsilon_0 \le \varepsilon_L \le \varepsilon_{0.k}\right)$ is given by Eq. 2.3 and Eq. 2.4.

$$\frac{f_c}{f_c'} = k\left[1 - z\,\varepsilon_0\left(\frac{\varepsilon_L}{\varepsilon_0} - 1\right)\right] \qquad \text{Eq. 2.3}$$

where

$$z = \frac{0.5}{\frac{3}{4}\rho''\sqrt{\frac{h''}{s}} + \left(\frac{3 + 0.002 f_c'}{f_c' - 1000}\right) - 0.002} \qquad \text{Eq. 2.4}$$

For branch CD $\left(\varepsilon_{0.k} \le \varepsilon_L\right)$ is given by Eq. 2.5.

$$\frac{f_c}{f_c'} = 0.3k \qquad \text{Eq. 2.5}$$

2.2.2 Kent and Park (1971)

Kent and Park (1971) proposed a compression stress-strain model for both unreinforced and confined reinforced square concrete columns. This model generalized Hognestad's (1951) equation to completely describe the post-peak stress-strain behaviour. Based on the experimental results, the compression stress-strain curve for confined reinforced concrete consists of three branches: the ascending branch, the falling branch, and the horizontal linear branch. This model considers the increase in ductility due to the confinement steel (hoops), however, neglects the increase in concrete strength, as depicted in Figure 2.3. The ascending branch is formulated by modifying the Hognestad's (1951) second degree parabola and is considered to be unaffected by confinement, the $0.85f_c^{'}$ and ε_0 are replaced by $f_c^{'}$ and 0.002, respectively. The ascending branch is given by Eq. 2.6 as follows:

$$f_c = f_c^{'}\left[\frac{2\varepsilon_c}{\varepsilon_{co}} - \left(\frac{\varepsilon_c}{\varepsilon_{co}}\right)^2\right] \qquad \text{Eq. 2.6}$$

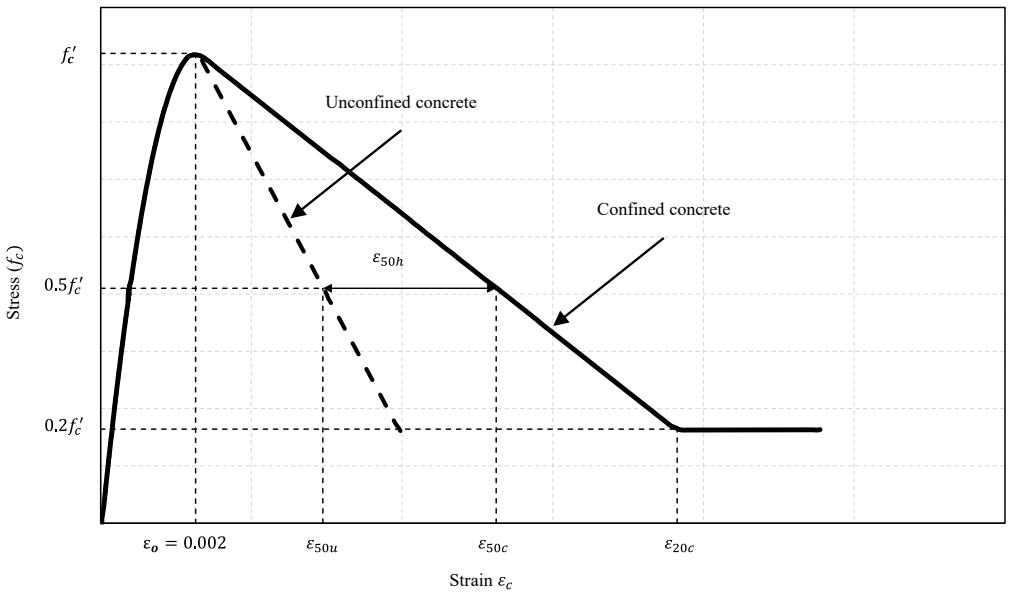

Figure 2.3 Proposed stress-strain model for confined reinforced and unreinforced concrete (redrawn from Kent and Park, 1971**)**

The falling branch (post-peak) is idealized by a sloping line, which is a function of concrete strength, and given by Eq. 2.7 to Eq. 2.8.

$$f_c = f_c^{'}\left[1 - Z\ (\varepsilon_c - \varepsilon_{co}\right] \qquad \text{Eq. 2.7}$$

in which

$$Z = \frac{0.5}{\varepsilon_{50u} - \varepsilon_{co}} \quad \text{Eq. 2.8}$$

where ε_{50u} is the strains corresponding to the stress of 50% of the maximum concrete strength for unreinforced concrete as follows:

$$\varepsilon_{50u} = \left[\frac{3 + 0.29 f_c^{'}}{145 f_c^{'} - 1000} \right] \quad \text{Eq. 2.9}$$

The third portion is formulated by horizontal linear with stress equal to the 20% of the maximum concrete stress at the end of the descending curve at a strain beyond the ε_{20c}.

2.2.3 Scott et al. (1982)

Scott et al. (1982) tested twenty five square RC columns vertically reinforced with either 8 or 12 rebars and confined by overlapping hoop sets. This test was conducted with rapid strain rates, which is typical for seismic loading, to investigate the stress-strain behaviour of confined RC concrete. It was observed that the strength enhanced due to the presence of the confinement of hoops, unlike the Kent and Park (1971) model. In order to incorporate the effect of confinement to increase the strength of confined reinforced concrete (see Figure 2.4), simple modifications were made to the Kent and Park (1971) model. The maximum concrete stress is reached to the $Kf_c^{'}$ at a strain of $0.002K$. The modified Kent and Park stress-strain relationship consists of two branches:

For $\varepsilon_c \le 0.002K$ is given by Eq. 2.10.

$$f_c = Kf_c^{'} \left[\frac{2\varepsilon_c}{0.002\mathrm{K}} - \left(\frac{\varepsilon_c}{0.002\mathrm{K}} \right)^2 \right] \quad \text{Eq. 2.10}$$

For $\varepsilon_c > 0.002K$ is given by Eq. 2.11 to Eq. 2.13.

$$f_c = Kf_c^{'} \left[1 - Z_m \left(\varepsilon_c - 0.002K \right) \right] \quad \text{Eq. 2.11}$$

but not less than $0.2Kf_c^{'}$, in which

$$z_m = \frac{0.5}{\frac{3 + 0.29 f_c^{'}}{145 f_c^{'} - 1000} + \frac{3}{4} \rho_s \sqrt{\frac{h''}{s_h}} - 0.002K} \quad \text{Eq. 12}$$

The value of K is obtained from the following expression:

$$K = 1 + \frac{\rho_s f_{yh}}{f_c^{'}} \qquad \text{Eq. 13}$$

where $f_c^{'}$ is the maximum strength of concrete in MPa, ρ_s is the ratio of the volume of hoops to the volume of concrete core measured to the outside of the peripheral of the hoop, $h^{''}$ is the width of concrete core measured to the outside of the peripheral of the hoop, s_h is the center to center spacing of the hoop sets, and f_{yh} is the yield strength of the hoop reinforcement.

The modified Kent and Park relationship can be used for high strain rates by applying a multiplying factor of 1.25 to the peak stress, the strain corresponding to the peak stress, and the slope of the post peak descending curve. Hence, the stress-strain relationship for the high strain is given by Eq. 2.10 and Eq. 2.11, however the values of K and z_m are changed to:

$$K = 1.25\left(1 + \frac{\rho_s f_{yh}}{f_c^{'}}\right) \qquad \text{Eq. 2.14}$$

and

$$z_m = \frac{0.625}{\frac{3 + 0.29 f_c^{'}}{145 f_c^{'} - 1000} + \frac{3}{4}\rho_s \sqrt{\frac{h''}{s_h}} - 0.002K} \qquad \text{Eq. 2.15}$$

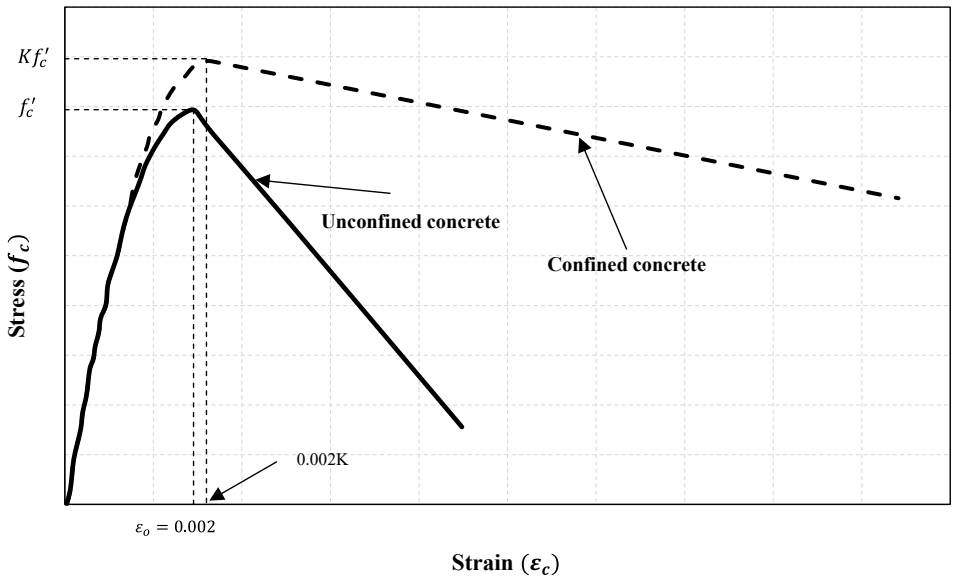

Figure 2.4 Proposed stress-strain model for confined reinforced and unreinforced concrete-Modified Kent and Park (Scott et al., 1982) model
(redrawn from Scott et al., 1982)

2.2.4 Mander et al. (1988a)

Mander et al. (1988a) developed a stress-strain model for confined reinforced concrete subjected to uniaxial compressive loading with cross sections that were either spiral or rectangular hooped steel confinement. The proposed stress-strain model for confined reinforced and unreinforced concrete under monotonic loading with slow strain rate is illustrated in Figure 2.5. The longitudinal compressive concrete stress f_c is given by Eq. 2.16 to Eq. 2.32.

$$f_c = \frac{f'_{cc}\, x\, r}{r - 1 + x^r} \qquad \text{Eq. 2.16}$$

where f'_{cc} = compressive strength of confined reinforced concrete.

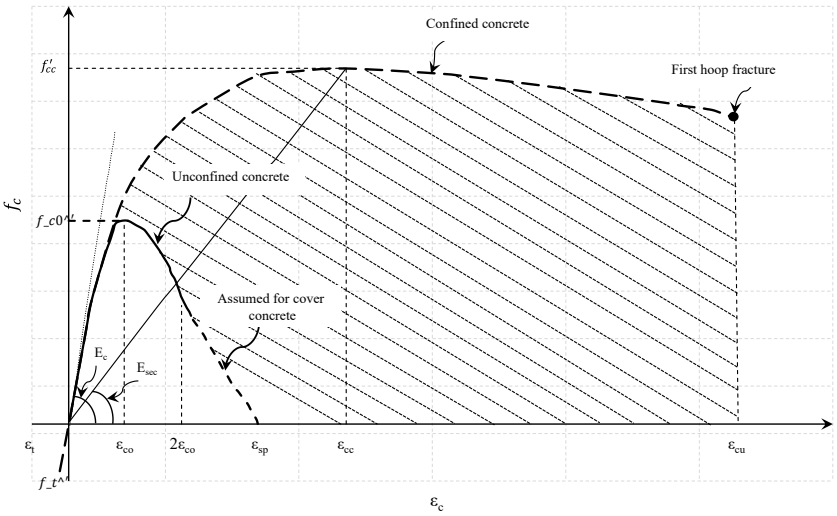

Figure 2.5 Stress-strain model proposed for monotonic loading of confined reinforced and unreinforced concrete
(redrawn from Mander et al., 1988a)

$$x = \frac{\varepsilon_c}{\varepsilon_{cc}} \qquad \text{Eq. 2.17}$$

where ε_c = longitudinal compressive concrete strain.

$$\varepsilon_{cc} = \varepsilon_{co}\left[1 + 5\left(\frac{f'_{cc}}{f'_{co}} - 1\right)\right] \qquad \text{Eq. 2.18}$$

where f'_{co} and ε_{co} are the unreinforced concrete strength and corresponding strain, respectively, and r is given by Eq. 2.19.

$$r = \frac{E_c}{E_c - E_{sec}} \qquad \text{Eq. 2.19}$$

$E_c = 5{,}000\sqrt{f_c^{'}}$, $f_c^{'}$ in MPa, is the tangent modulus of elasticity of concrete, and $E_{sec} = f_{cc}^{'} / \varepsilon_{cc}$.

The behaviour of the concrete cover is assumed to be a straight line at the end of the descending curve, at a strain beyond the $2\varepsilon_{co}$.

The core section is susceptible to the maximum pressure of transverse reinforcement when the confining stress has fully developed due to the arching action. The arching occurs horizontally and vertically between vertical and horizontal reinforcement rebars, respectively, with second degree parabolas that have an initial slope of 45°. The effective lateral confining pressure is given by Eq. 2.20.

$$f_l^{'} = f_l k_e \qquad \text{Eq. 2.20}$$

f_l is the lateral reinforcement confining pressure which is assumed to be uniformly distributed over the surface of the concrete core. The confinement effectiveness coefficient is given by Eq. 2.21.

$$k_e = \frac{A_e}{A_{cc}} \qquad \text{Eq. 2.21}$$

where A_e is the area of confined concrete core, and A_{cc} is given by Eq. 2.22.

$$A_{cc} = A_c\left(1 - \rho_{cc}\right) \qquad \text{Eq. 2.22}$$

ρ_{cc} is the ratio of the area of the longitudinal reinforcement to the area of the core of section. A_c is the area of the core section enclosed by the centerlines of the perimeter hoop.

The effective confined area of concrete is calculated by subtracting the area of the parabolas containing the ineffectively confined concrete (Eq. 2.23) from the confined core section as shown in Figure 2.6;

$$A_i = \sum_{i=1}^{n} \frac{\left(w_i^{'}\right)^2}{6} \qquad \text{Eq. 2.23}$$

Then the area of effectively confined concrete between the hoops (at the mid-way) is given by Eq. 2.24.

$$A_e = \left(b_c d_c - \sum_{i=1}^{n} \frac{\left(w_i'\right)^2}{6} \right) \left(1 - \frac{s'}{2b_c}\right) \left(1 - \frac{s'}{2d_C}\right) \quad \text{Eq. 2.24}$$

Hence, from Eq. 2.21, the confinement effectiveness coefficient for rectangular hoops is;

$$k_e = \frac{\left(1 - \sum_{i=1}^{n} \frac{\left(w_i'\right)^2}{6 b_c d_c}\right) \left(1 - \frac{s'}{2b_c}\right) \left(1 - \frac{s'}{2d_C}\right)}{1 - \rho_{cc}} \quad \text{Eq. 2.25}$$

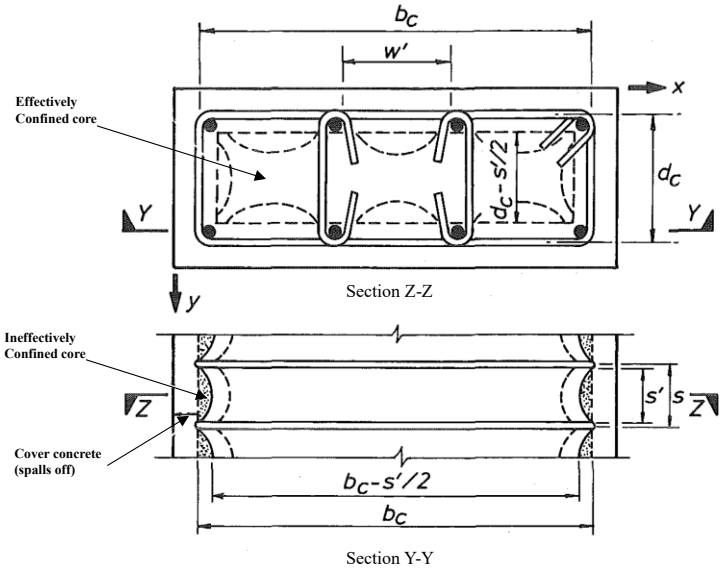

Figure 2.6 Effectively confined core for rectangular hoop reinforcement (redrawn from Mander et al., 1988a)

Basically, the rectangular section has different quantities of transverse confining steel in the x and y directions and they may be expressed by Eq. 2.26 and Eq. 2.27, respectively.

$$\rho_x = \frac{A_{sx}}{s d_c} \quad \text{Eq. 2.26}$$

$$\rho_y = \frac{A_{sy}}{s b_c} \quad \text{Eq. 2.27}$$

The total area of longitudinal reinforcement is equal to the summation of the A_{sx} and A_{sy}. The lateral confining pressure stress coming from the hoop on the concrete is the total area of transverse steel rebars divided by vertical area of confined concrete and is given by Eq. 2.28.

$$f = \frac{p}{A} \quad \text{Eq. 2.28}$$

By substituting in Eq. 2.20, the effective confining stresses in x and y directions are given in Eq. 2.29 and Eq. 2.30, respectively.

$$f_{lx}^{'} = k_e \rho_x f_{yh} \quad \text{Eq. 2.29}$$

and,

$$f_{ly}^{'} = k_e \rho_y f_{yh} \quad \text{Eq. 2.30}$$

Finally, the confined reinforced compressive strength $\left(f_{cc}^{'}\right)$ and the corresponding strain $\left(\varepsilon_{cc}\right)$ are given by Eq. 2.31 and Eq. 2.32.

$$f_{cc}^{'} = f_{co}^{'}\left(-1.254 + 2.254\sqrt{1 + \frac{7.94 f_i^{'}}{f_{co}^{'}}} - 2\frac{f_i^{'}}{f_{co}^{'}}\right) \quad \text{Eq. 2.31}$$

$$\varepsilon_{cc} = \varepsilon_{co}\left[1 + 5\left(\frac{f_{cc}^{'}}{f_{co}^{'}} - 1\right)\right] \quad \text{Eq. 2.30}$$

It was concluded that the proposed stress-strain curve for confined reinforced concrete required three control parameters: $f_c^{'}$, ε_{cc} and E_c. The ultimate concrete compressive strain of the section is defined as the strain corresponding to the first hoop fracture.

2.2.5 Mander et al. (1988b)

Mander et al. (1988b) tested thirty one concrete columns with circular, rectangular, and rectangular wall cross sections under compression. These columns were tested in order to investigate compression stress-strain behaviour of the columns and compare it with the predicted theoretical model considering the effects of strain rate, configuration of the confinement reinforcement, and cyclic loading. Longitudinal strain was measured using four potentiometers which were mounted on embedded cross bars in the core concrete with gauge lengths of 450 mm. It was concluded that the most significant parameter that has influence on the longitudinal stress-strain behaviour was the quantity of the confining reinforcement, for all the different sections of columns. The circular column that was confined and reinforced with spiral reinforcement exhibited an increase in strength and ultimate strain more than the square column. It was found that as the confinement ratio of lateral reinforcement increased, the strength increased, the slope of the post peak descending curve decreased, and the strain corresponding to the first hoop fracture increased. Finally, it was shown that the proposed analytical stress-strain model is in agreement with experimental results for all shapes of the columns.

2.2.6 Hoshikuma et al. (1997)

Hoshikuma et al. (1997) proposed a stress-strain curve for the behaviour of RC columns under compression considering the effect of confinement. Thirty one RC column specimens with square, circle, and wall type sections were tested. This test was conducted to study the compression behaviour of RC columns considering the effects of confinement reinforcement in terms of the volumetric ratio, hoop's spacing, configurations of the hoops, cross sectional shape, and cross ties. Two linear potentiometers were used to measure the axial strain with gauge lengths equal to the height of the specimen. It was found that the buckling of the longitudinal reinforcement and the crushing of the core concrete occurred after 50% degradation. Based on these observations, the ultimate strain was assumed to be the strain corresponding the 50% of the peak stress. It was found that as the confinement ratio increases the peak stress, the strain corresponding to the peak stress, and the strain ductility. The results show that the confinement decreased the deterioration of the specimens after the peak. In addition, as the spacing of hoops increases the deterioration of the specimen increases. The stress-strain model proposed by Hoshikuma et al. (1997) was based on the results of compression loading tests. This model consists of three branchs; an ascending branch, a falling branch, and a sustaining branch. The ascending branch of proposed stress-strain models is formulated by a second order parabola with the following four boundary conditions:

Initial condition $f_c = 0$ at $\varepsilon_c = 0$, Initial stiffness condition $df_c / d\varepsilon_c = E_c$ at $\varepsilon_c = 0$, Peak condition $f_c = f_{cc}$ at $\varepsilon_c = \varepsilon_{cc}$, Peak stiffness condition $df_c / d\varepsilon_c = 0$ at $\varepsilon_c = \varepsilon_{cc}$

where f_{cc} is the peak stress; ε_{cc} is the strain at peak stress; E_c is the initial stiffness.

The second-order parabola of the ascending branch is expressed in Eq. 2.33:

$$f_c = f_{cc}\left[\frac{2\varepsilon_c}{\varepsilon_{cc}} - \left(\frac{\varepsilon_c}{\varepsilon_{cc}}\right)^2\right] \qquad \text{Eq. 2.33}$$

By satisfying the boundary conditions and substituting in Eq. 2.33, the Eq. 2.34 is obtained.

$$f_c = E_c\varepsilon_c\left[1 - \frac{1}{n}\left(\frac{\varepsilon_c}{\varepsilon_{cc}}\right)^{n-1}\right] \qquad \text{Eq. 2.34}$$

where n is a coefficient and is given by Eq. 2.35.

$$n = \frac{E_c \varepsilon_{cc}}{E_c \varepsilon_{cc} - f_{cc}} \qquad \text{Eq. 2.35}$$

The falling branch of proposed stress-strain curve is idealized by a straight line as indicated by the test results shown in Figure 2.7, and is formulated as in Eq. 2.36.

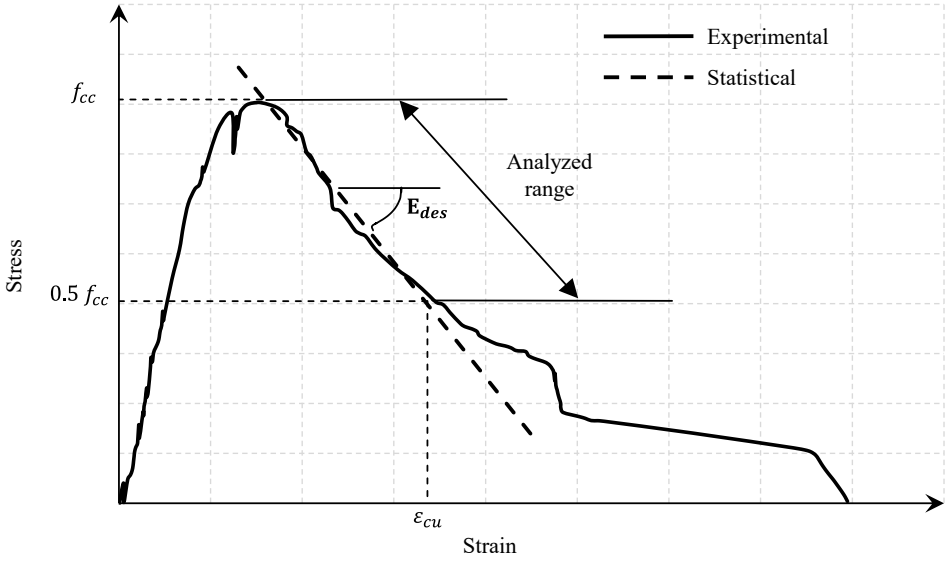

Figure 2.7 Definition of ultimate strain and deterioration rate (redrawn from Hoshikuma et al., 1997)

$$f_c = f_{cc} - E_{des}\left(\varepsilon_c - \varepsilon_{cc}\right) \qquad \text{Eq. 2.36}$$

where, E_{des} is the deterioration rate which is developed from regression analysis of test data in the range of ε_{cc} to ε_{cu}. The ultimate strain can be obtained by substituting $f_c = 0.5 f_{cc}$ into Eq. 2.36, as in Eq. 2.37.

$$\varepsilon_{cu} = \varepsilon_{cc} + \frac{f_{cc}}{2E_{des}} \qquad \text{Eq. 2.37}$$

In this proposed model, the sustained branch is not formulated, since that branch is not critical in the seismic design of bridges.

2.3 Behaviour of Unconfined and Confined Masonry Prisms

The failure mechanism of unreinforced fully-grouted masonry prisms tested under concentric compression axial loading is defined as a combined compression-tension failure. As the compression load increases, the lateral expansion of mortar and grout increases, leading to tensile splitting of the block face shell and compression-tension failure of the unreinforced grout cores (Drysdale and Hamid 2005). However, when unconfined RM prisms fail, their vertical reinforcement buckles. Therefore, the failure mode of the unreinforced and the unconfined RM prisms is characterized by a brittle failure mechanism. Adding confinement reinforcement in masonry prisms prevents the brittle failure mechanism and provides a more ductile response to the tested prism. Different techniques have been implemented in the literature to confine the masonry prisms. However, the conventional technique of confining reinforced masonry wall ends using transversal hoops is typically restricted due to the geometry of the available concrete blocks.

2.3.1 PRIESTLEY AND ELDER (1983)

In 1974, Priestley and Bridgeman (1974) introduced the steel plate technique to confine the bed joint which became known as the Priestley plate. Priestley and elder (1983) tested twenty one masonry prisms, with heights of 980 mm, to investigate the compressive stress-strain relationship of the grouted concrete masonry prisms. The test program aimed to investigate the influence of the block width, strain rate, vertical reinforcement, and confining steel plate (Priestley plate) on the failure modes and compressive stress-strain relationship of masonry prisms. The Priestley plate was fabricated from 3.1 mm of stainless steel with an area slightly smaller than the block's net area (see Figure 2.8). The results showed that the failure mechanism of unreinforced masonry prism was similar to the failure mechanism suggested by Drysdale and Hamid (1979). The failure of a masonry unit/mortar occurs earlier by vertically splitting and it is initiated by lateral expansion of the crushing mortar which leads to lower strain corresponding to the peak stress. The width of the block and the presence of the vertical reinforcement exhibited no significant effect on the masonry prism's behaviour. Increasing the strain rate from 0.005 to 0.5 percent/sec produced an increase in strength and exhibited a steeper descending curve of the compressive stress-strain relationship for confined reinforced prisms. Adding a stainless steel confining plate eliminated the vertical splitting of the block and changed the failure mechanism

to a shear/crushing failure within one or two courses of the block. In addition, the stainless steel confining plate produced a more gradual descending curve on the compressive stress-strain relationship.

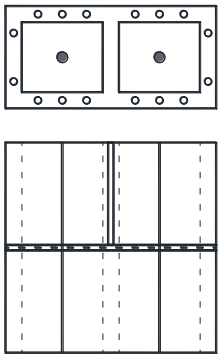

Figure 2.8 Priestley plate for concrete masonry prism

Priestley and Elder (1983) applied a modified Kent-Park curve with a modification to consider the low strain at peak stress (i.e. $\varepsilon_c = 0.0015$ instead of 0.002 0.002). Priestley and elder's (1983) model for confined reinforced and unreinforced masonry consists of three branches:

Unreinforced masonry

- Rising branch is given by Eq. 2.38.

$$f_m = 1.067 f_m^{'} \left[\frac{2\varepsilon_m}{0.002} - \left(\frac{\varepsilon_m}{0.002} \right)^2 \right] \qquad \text{for } \varepsilon_c \le 0.0015 \qquad \text{Eq. 2.38}$$

where, f_m and ε_m are stress and axial strain in masonry, respectively, and $f_m^{'}$ is the maximum compressive strength of concrete masonry prism.

- Falling branch is given by Eq. 2.39.

$$f_m = f_m^{'} \left[1 - Z_m \left(\varepsilon_c - 0.0015 \right) \right] \qquad \text{for } \varepsilon_c > 0.0015 \qquad \text{Eq. 2.39}$$

- Horizontal plateau, f_m is assumed equivalent to $0.2 f_m^{'}$

Confined reinforced masonry

- Rising branch is given by Eq. 2.40.

$$f_m = 1.067\mathrm{K}f_m^{'}\left[\frac{2\varepsilon_c}{0.002\mathrm{K}} - \left(\frac{\varepsilon_c}{0.002\mathrm{K}}\right)^2\right] \quad \text{for } \varepsilon_c \le 0.002K \qquad \text{Eq. 2.40}$$

- Falling branch is given by Eq. 2.41.

$$f_m = Kf_m^{'}\left[1 - Z_m\left(\varepsilon_c - 0.002\mathrm{K_d}\right)\right] \quad \text{for } \varepsilon_c < 0.002K \qquad \text{Eq. 2.41}$$

The value of K_d and Z_m are obtained from the Eq. 2.42 and Eq. 2.43, respectively:

$$K_d = 1.17\left[1 + \frac{\rho_s f_{yh}}{f_m^{'}}\right] \qquad \text{Eq. 2.42}$$

$$z_m = \frac{0.5}{\frac{3 + 0.29 f_m^{'}}{145 f_m^{'} - 1000} + \frac{3}{4}\rho_s\sqrt{\frac{h''}{s_h}} - 0.002K_d} \qquad \text{Eq. 2.43}$$

- Horizontal plateau

f_m is assumed equivalent to $0.2f_m^{'}$

2.3.2 HART ET AL. (1988)

Hart et al. (1988) used different types and techniques of confinement to confine masonry prisms, including: closed wire mesh and open wire mesh. A total of 71 prisms with a height of 4 courses each were tested. This test was conducted to investigate the compression stress-strain behaviour of masonry prisms considering the following five confinement techniques: modified Priestly plate, square steel ties equivalent to the minimum confinement reinforcement required by the 1988 UBC for masonry (#3 bars (9.5 mm diameter) at 8" (203 mm) spacing), cage (hoop) reinforcement, spiral reinforcement, and cage (spiral) reinforcement.

Figure 2.9 shows the different confinement techniques that were used by Hart et al. (1988) to confine the masonry prisms. Based on the experimental results of each confinement configuration, a compression stress-strain curve for typical confined reinforced concrete masonry shown in Figure 2.10 was defined. It was observed that the curve can be divided into four strain branches.

It was concluded that the unreinforced and unconfined reinforced specimens failed in a brittle manner. The result showed that the different confinement configurations had a minimal effect on the ascending portion of stress-strain curve, however, it had a significant effect on post-peak curves. Henceforth, enhancing the prism's ductility and its energy dissipation. The study

concluded that the most effective confinement technique was the Priestley plate, which produced a more gradual descending curve.

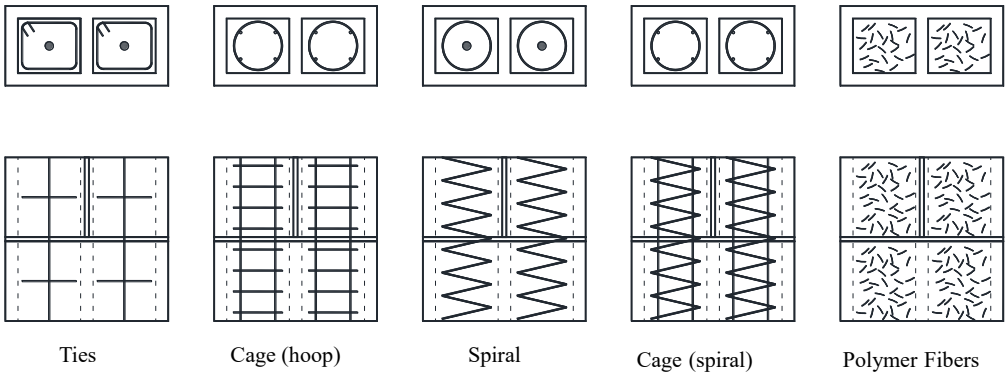

Figure 2.9 Confinement techniques
(redrawn from Hart et al. (1988))

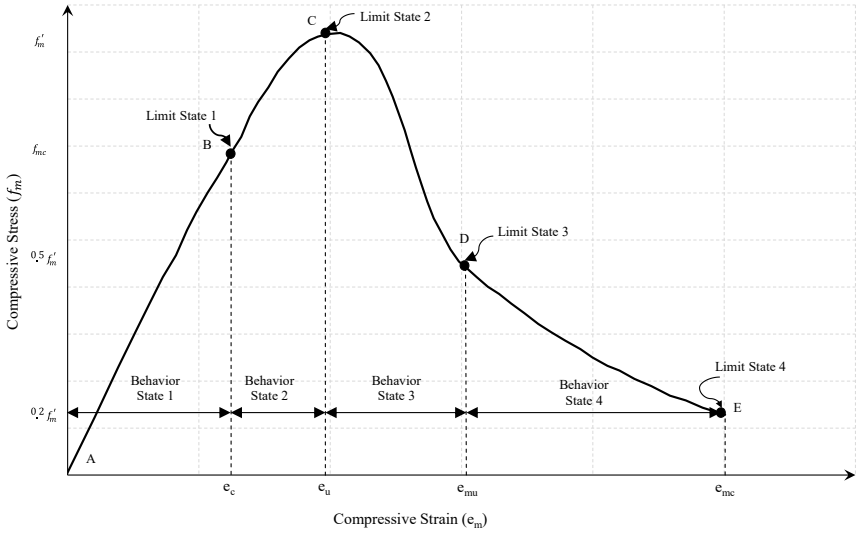

Figure 2.10 Confined reinforced concrete masonry stress-strain curve
(redrawn from Hart et al., 1988)

2.3.3 HART ET AL. (1989)

Hart et al. (1989) presented two analytical models for the stress-strain behaviour of masonry in compression for both confined reinforced and unreinforced concrete. One hundred and six concrete masonry prisms were tested including unreinforced, unconfined reinforced, and confined reinforced masonry prisms. The confined reinforced prisms utilized seven confinement techniques. Based on the experimental results, two analytical models were developed: acceptable fit model and the best fit model. Acceptable fit model is very simple. On the other hand, best fit

model is developed to provide a closer agreement with the experimental results, however, with an increase in complexity. The parameters used in each model were obtained from experimental data using the least squares curve fitting technique. These stress-strain models were divided into two branches: rising branch and falling branch.

The Acceptable Fit Model

The rising branch is formulated by a straight line from the origin up to the peak stress. The straight line is a function of two parameters f_{mtm} and ε_{mtm}, and can be written as in Eq. 2.44.

$$f_m(\varepsilon_m) = f_{mtm}\left(\frac{\varepsilon_m}{\varepsilon_{mtm}}\right) \quad \text{Eq. 2.44}$$

The falling branch is formulated by an exponential function, and can be written by Eq. 2.45.

$$f_m(\varepsilon_m) = f_{mtm}\, B e^{(-A\,\varepsilon_m)} \quad \text{Eq. 2.45}$$

By applying the boundary condition that $f_m = f_{mtm}$ at $\varepsilon_{mt} = \varepsilon_{mtm}$, the parameter B can be eliminated, thus Eq. 2.45 will be as Eq. 2.46.

$$f_m(\varepsilon_m) = f_{mtm}\, e^{\left[-A(\varepsilon_m - \varepsilon_{mtm})\right]} \quad \text{Eq. 2.46}$$

where, f_m = concrete masonry compressive strength, ε_m = concrete masonry compressive strain, f_{mtm} = maximum average measured compressive stress of masonry, ε_{mtm} = strain corresponding to maximum compressive stress, and A is the shape parameter.

The Best Fit Model

The rising branch is formulated by a second degree polynomial form and is given by Eq. 2.47.

$$f_m(\varepsilon_m) = A\varepsilon_m^2 + B\varepsilon_m \quad \text{Eq. 2.47}$$

By applying the boundary condition that $f_m = f_{mtm}$ at $\varepsilon_{mt} = \varepsilon_{mtm}$ and defining a new parameter $C = A / f_{mtm}$, the equation Eq. 2.47 can be written as Eq. 2.48.

$$f_m(\varepsilon_m) = f_{mtm}\left[C\varepsilon_m^2 + \left(\frac{1}{\varepsilon_{mtm}} - C\,\varepsilon_{mtm}\right)\varepsilon_m\right] \quad \text{Eq. 2.48}$$

The falling branch is formulated by an exponential function, and can be written by Eq. 2.49.

$$f_m(\varepsilon_m) = B + Ce^{(-E\,\varepsilon_m)} \quad \text{Eq. 2.49}$$

By applying the boundary condition that $f_m = f_{mtm}$ at $\varepsilon_{mt} = \varepsilon_{mtm}$ and defining a new parameter $D = B / f_{mtm}$, the equation can be written by Eq. 2.50:

$$f_m(\varepsilon_m) = f_{mtm}\ [D + (1-D)e^{[-E(\varepsilon_m - \varepsilon_{mtm})]} \qquad \text{Eq. 2.50}$$

To completely describe the stress-strain curve for the Best Fit Model, three shape parameters (A, D, and E) and two parameters f_{mtm} and ε_{mtm} must be defined.

2.3.4 SHEDID ET AL. (2010B)

Shedid et al. (2010b) tested rectangular and square half scale masonry prisms under compression that were four-blocks in height and grouted. This test was conducted to investigate the stress-strain relationship, the modulus of elasticity, and the effect of the vertical reinforcement and confinement on the compression stress-strain relationship. Twenty rectangular and square masonry specimens, made of standard and pilaster blocks, were tested to evaluate the effect of the presence of vertical reinforcement and confinement reinforcement, as shown in Figure 2.11.

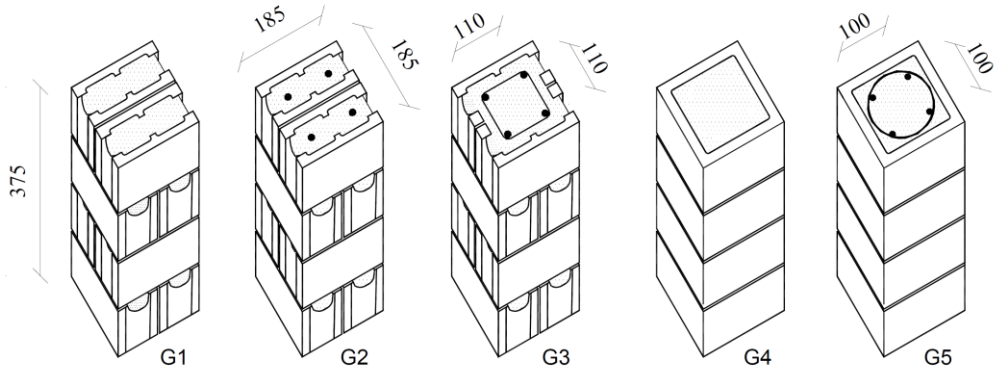

Figure 2.11 Confined reinforced prisms
(Adopted from Shedid et al., 2010b)

The axial strain was measured using two linear potentiometers placed on opposite faces of the prisms with a gauge length of 300 mm. The results showed that the rectangular prisms' failure was characterized by diagonal and/or horizontal cracks through their face shells. The modulus of elasticity for the tested masonry prisms was found with an average of 830 times f'_m. The failure of the unreinforced square masonry prisms was characterized by vertical cracks, after reaching a maximum load, followed by face shell spalling. The unconfined reinforced masonry prisms exhibited less damage compared to the unreinforced masonry prisms, however, they

exhibited an increase in strength due to the presence of vertical reinforcement. The confined reinforced masonry prisms with lateral reinforcement exhibited a slight increase in strength compared to the unconfined reinforced masonry prisms. The vertical cracks and face shell spalling were observed after reaching a maximum load, however, the buckling of vertical reinforcement was not observed. Additionally, confined reinforced masonry prisms produced more gradual post-peak stress-strain curves. Finally, the confined reinforced pilaster masonry prisms exhibited an increase in strength, moreover, exhibited an increase in strain, at 30% of the peak stress, by 50% higher than unreinforced pilaster masonry prisms.

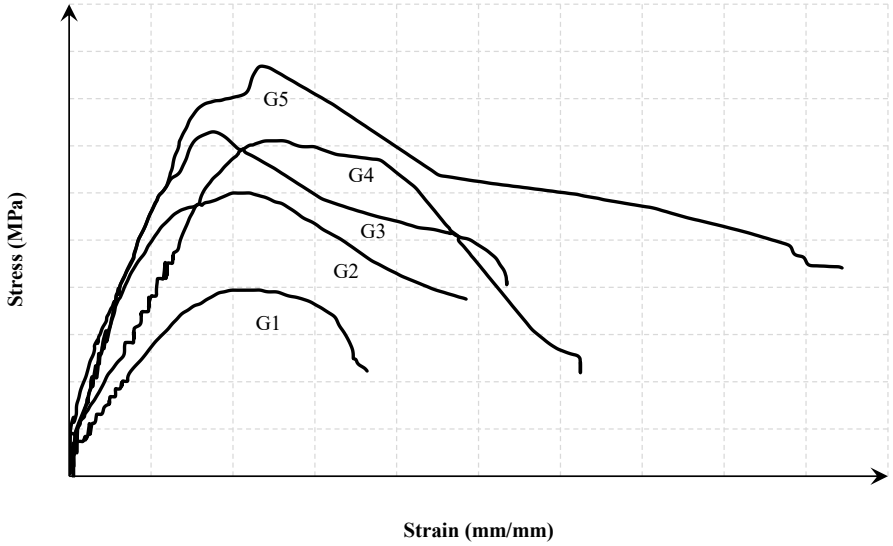

Figure 2.12 Stress-strain relationship for square prisms
(redrawn from Shedid et al., 2010b)

2.3.5 JOYAL (2014)

Joyal, M. (2014) employed a new technique of confinement called Self-Reinforced concrete block (SR Block) to improve the ductility of RM shear walls. The internal reinforcement devices are placed into concrete blocks during the standard masonry block manufacturing process (see Figure 2.13).

(a) (b)

Figure 2.13 SR block device: (a) Confining Device; and (b) Confining device exposed by removal of compacted exterior concrete
(Adopted from Joyal, 2014)

Figure 2.14 shows the adopted new prototype block with larger circular cells and a smaller block mass, compared to the traditional hollow block, to ease the placement of reinforcement and grout.

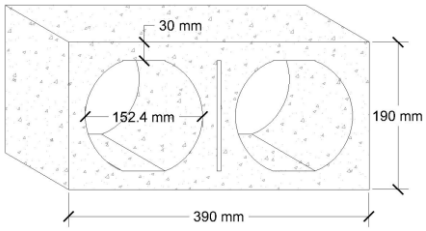

Figure 2.14 Prototype block design
(Adopted from Joyal, 2014)

Joyal, M. (2014) tested a total of 51 masonry prisms, including standard and prototype masonry unit blocks, in both ungrouted and grouted states. The prototype block was divided into two categories: Type I had 101.6 mm diameter cells and type II had 154.4 mm diameter cells. All prisms were constructed with a height of four courses and tested under compression using 2500 kN servo-hydraulically controlled testing machine (Rhiele). Axial strain was measured using eight 50 mm, draw-wire potentiometers. The first four potentiometers were placed on each face of the masonry prism and were mounted directly on the block. They had a gauge length of 600 mm from the mid-height of the bottom block to mid-height of the top block. The second four potentiometers were placed on each face of masonry prism, however, these had a gauge length equal to the full height of the prism.

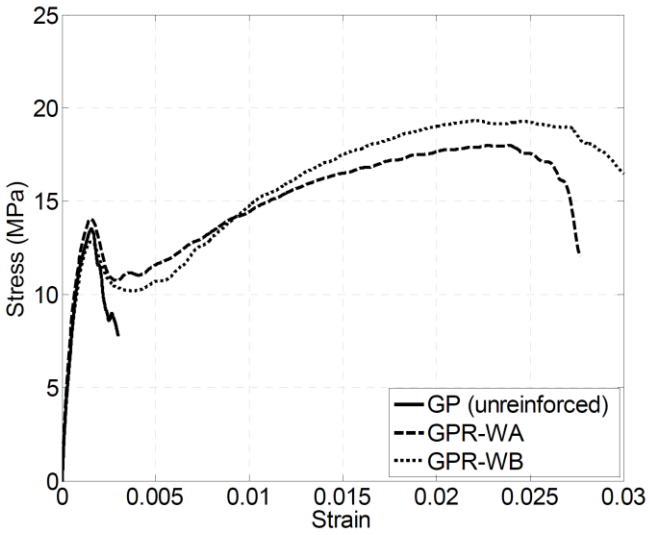

Figure 2.15 Stress-Strain Curves for Unreinforced and Self-Reinforced Prisms (Joyal, 2014)

It was found that all SR block prisms reached a peak capacity that was almost equal to the unreinforced counterpart's peak capacity. However, all SR block prisms reached a second peak capacity considerably more than the first peak, after spalling of the block and mortar. Additionally, the SR block prisms exhibited an increase in strength about six times and ten times compared to the unreinforced prisms at strain of 0.3% and 2% of peak stress, respectively (Figure 2.15). The presence of the SR block in the compression zones of the shear walls produced a significant increase in the lateral capacity and the ductility capacity of the shear wall.

2.3.6 ABO EL EZZ ET AL. (2015)

Abo El Ezz et al. (2015) experimentally and analytically investigated the compression behaviour of boundary elements with standard concrete blocks, considering the effects of the size and the spacing of the transverse reinforcement (seismic hoops). A simplified stress-strain model of unreinforced and confined reinforced boundary element was proposed. To achieve this objective, a total of 17 full scale, fully grouted concrete masonry boundary elements were tested, that represented the end zone of a RM shear wall. The boundary element specimens included; unreinforced, unconfined reinforced, and confined reinforced specimens that were confined with different lateral reinforcement in terms of hoops. The hoop diameters were 10M and 15M at vertical spacing's of 100 mm and 200 mm. The boundary element specimens were constructed using standard concrete block stretcher units with 15 MPa nominal compressive strength. Each

boundary element specimen consisted of 5 courses with two block units placed adjacent to each other in an alternating direction. The axial strain of the boundary element specimen was measured using four potentiometers. These potentiometers were attached to the embedded cross bars at each face of the specimen, with a gauge length of 600 mm, between the three middle blocks. The simplified stress-strain model is similar to the Kent and Park (1971) model with some modifications. For the unreinforced boundary element, the model is divided into three branchs as follows:

- A parabolic rising branch as in Eq. 2.51.

$$f_m = f_{max-u}\left(\frac{2\varepsilon_m}{\varepsilon_{max1}} - \left(\frac{\varepsilon_m}{\varepsilon_{max1}}\right)^2\right) \qquad \text{for } \varepsilon_m < \varepsilon_{max1} \qquad \text{Eq. 2.51}$$

- A plateau with constant stress as in Eq. 2.52.

$$f_m = f_{max-u} \qquad \text{for } \varepsilon_{max1} < \varepsilon_m < \varepsilon_{max2} \qquad \text{Eq. 2.52}$$

- A linear falling branch as in Eq. 2.53 and Eq. 2.54.

$$f_m = f_{max-u}\left(1 - Z\left(\varepsilon_m - \varepsilon_{max2}\right)\right) \quad \text{for } \varepsilon_m > \varepsilon_{max2} \qquad \text{Eq. 2.53}$$

$$Z = \frac{0.5}{\varepsilon_{50u} - \varepsilon_{max2}} \qquad \text{Eq. 2.54}$$

For the confined reinforced boundary element, the model is divided into two branchs as follows:

- The ascending branch is formulated by a second order parabola similar to Kent and Park (1971) as in Eq. 2.55.

$$f_m = f_{max-c}\left(\frac{2\varepsilon_m}{\varepsilon_{max-c}} - \left(\frac{\varepsilon_m}{\varepsilon_{max-c}}\right)^2\right) \qquad \text{for } \varepsilon_m < \varepsilon_{max-c} \qquad \text{Eq. 2.55}$$

Where, $f_{\max-c} = 1.15 f_{\max-r}$

- The descending branch is formulated by a straight line and modified based on the experimental results in this study as in Eq. 2.56 and Eq. 2.57.

$$f_m = f_{max-c}\left(1 - Z_c\left(\varepsilon_m - \varepsilon_{max-c}\right)\right) \qquad \text{for } \varepsilon_m > \varepsilon_{max-c} \qquad \text{Eq. 2.56}$$

$$Z = \frac{0.5}{\varepsilon_{50c} - \varepsilon_{max-c}} \qquad \text{Eq. 2.57}$$

f_m is the compression stress and ε_m is the corresponding compression strain, $f_{\max-c}$ is the peak compressive stress for the confined reinforced boundary element and $\varepsilon_{\max-c}$ is the corresponding strain, and $f_{\max-r}$ is the average strength of the unconfined reinforced boundary element.

It was concluded that adding confinement reinforcement improved the axial compression capacity and the strain ductility of the boundary elements. Moreover, the confinement reinforcement produced a more gradual post-peak stress-strain curve and had a significant effect on the compression stress-strain behaviour of masonry boundary elements. The proposed analytical model was in agreement with the experimental results.

2.4 Masonry Shear Walls With End Confined Zones

2.4.1 SAJJAD (1990)

Sajjad (1990) tested four masonry shear walls, at the University of California, Los Angeles, to study their behaviour while considering the effects of three confinements: hoop reinforcement (equivalent to the minimum confinement reinforcement required by 1988 UBC), confinement reinforcement Comb, and a spiral cage reinforcement. One of four the walls did not have confinement while the other three walls were confined with aforementioned confinement techniques. All four masonry walls had the same dimensions, horizontal reinforcement ratio, vertical reinforcement ratio, and applied axial load. Table 2.1 shows the test results from of unreinforced and confined reinforced shear masonry walls.

Table 2.1 Results from testing of unreinforced and confined reinforced shear walls (from Sajjad 1990)

		Unreinforced wall	Confined reinforced walls		
			Hoops spaced at 8"	Confining comb	Spiral cage
Ratio of confinement reinforcement (Volumetric)		-	0.0042	0.0022	0.0029
Max Force (kN)	**Mean**	352.7	374.1	403.0	374.5
	Ratio to Unreinforced	1.00	1.06	1.14	1.06
Drift (%) at Maximum Force	**Mean**	0.73	1.22	1.16	1.2
	Ratio to Unreinforced	1.00	1.66	1.58	1.64
Force (kN) at Maximum Drift	**Mean**	181.9	165.0	338.5	230.0
	Ratio to Unreinforced	1.00	0.91	1.86	1.26
Maximum Drift (%)	**Mean**	1.17	1.70	2.15	2.61
	Ratio to Unreinforced	1.00	1.45	1.83	2.24

It was concluded that the confined reinforced walls had increased maximum loads by 6% to 14% compared to the unreinforced wall. Wherein, the maximum load exists when the strain of concrete masonry at the extreme compression fiber is equal to the usable strain. The results show that the drift at the maximum load increased by 58% to 64% compared to the unreinforced wall. Finally, adding confinement to the wall increased the maximum drift by up to 123% as compared to the unreinforced wall.

2.4.2 SHEDID (2009)

Shedid (2009) tested seven half scale, fully grouted masonry walls to investigate the cyclic flexure response of the reinforced concrete masonry rectangular walls, walls with flanges, and walls with boundary elements. The purpose of the test was to investigate the influence of adding flanges or boundary elements on the stability of the compression zone (see Figure 2.16). The main goal of this study was to evaluate the effect of connecting flanges or boundary elements to the ends of the wall on the behaviour of the RM wall. All the walls had the same length, however, they had different end configurations and aspect ratios. All of the walls were subjected to identical axial loading. It was concluded that the flanged and end-confined reinforced masonry walls exhibited an increase in ductility of at least 39 and 106% higher than that of the rectangular walls, respectively.

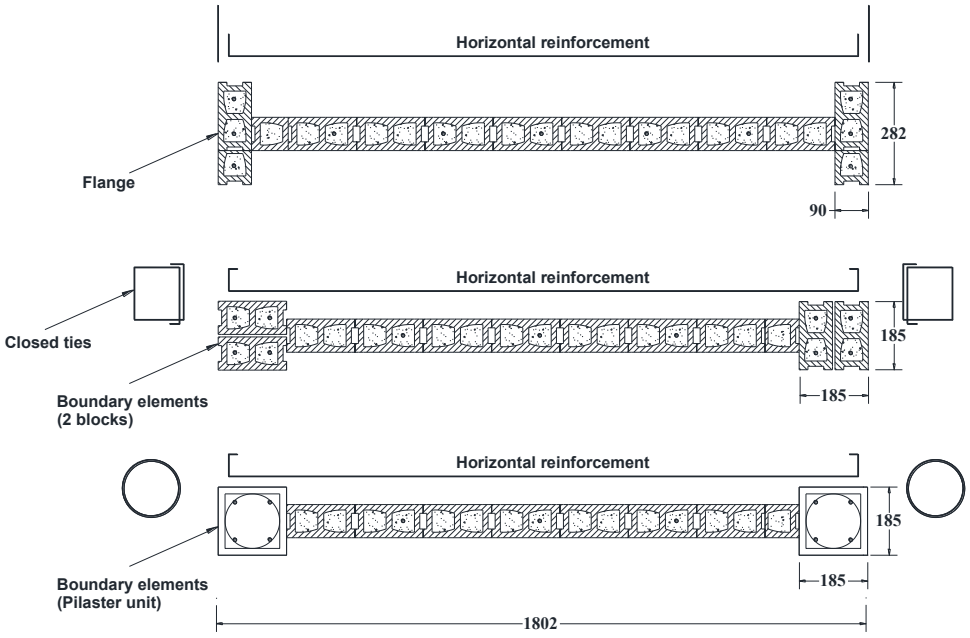

Figure 2.16 End-confined reinforced wall configurations
(Adopted from Shedid, 2009)

The rectangular, flanged, and end-confined reinforced walls produced a drift at 20% strength of at least 1.0, 1.5, and 2.0%, respectively. The test's results showed that all the walls provided the same capacity and elastic stiffness, hence, saving more than 40% in the amount of vertical reinforcement for the end-confined reinforced walls. Table 2.2 shows the results of the walls tested by Shedid (2009).

Table 2.2 Results from testing of unreinforced and end-confined reinforced shear walls (from Shedid, 2009)

		Unreinforced wall	Confined reinforced walls		
			Flanged	Two-block boundary elements	Pilaster boundary elements
Max Force (kN)	**Mean**	266	242	238	238
Drift at maximum Force	**Mean**	0.5	0.75	0.91	0.76
	Ratio to Unreinforced	1.00	1.50	1.82	1.52
Drift at 20% strength degradation	**Mean**	1.04	1.64	2.05	2.42
	Ratio to Unreinforced	1.00	1.58	1.97	2.33
Displacement ductility (idealized elastic-plastic)		4.8	6.6	9.8	9.7

2.4.3 BANTING (2013)

Banting (2013) tested nine half scale, fully grouted masonry walls integrated with boundary elements (BE). The objective of the study was to investigate the force-displacement behaviour and performance-based seismic design consideration for the RM walls containing BEs. For comparison purposes, two walls from Shedid (2009) were included in this study. The parameters that were considered for comparison in this study included the wall height, the wall length, the height to length aspect ratio, the number of inter-storey floor slabs, the discontinuity of confinement detailing above the plastic hinge, the axial load, and the vertical reinforcement ratio. Two out of the eleven walls had the same height to length ratio which matched the one of the walls tested by Shedid (2009). Each wall had the same boundary element, which in turn produced differing relative wall to BE lengths. Banting (2013) tested a series of four courses BEs composed of two block units under uniaxial compression, to investigate the compression stress-

strain behaviour. These BEs were constructed with blocks and grout that were consistent with those used for the walls. It was concluded that adding BE to the RM walls delayed the buckling of the vertical reinforcement and kept the inner core intact and stable, without a drop in resistance. It was observed that the mode of failure was characterized by buckling of the vertical reinforcement, crushing of the grouted core, and eventually fracturing of the reinforcement.

2.5 Summary of Literature Review

The majority of the literature review focused on the experimental and analytical investigations and evaluations of the compression behaviour of confined RC columns, including the quantification of the post-peak strain capacity. On the other hand, the majority of experimental, analytical, and numerical works that have been conducted on the structural behaviour of RM columns have focused on the evaluation of the ultimate compression strength rather than the evaluation of the post-peak strain capacity. A few researchers were focused on the investigation and evaluation of the compression stress-strain behaviour of masonry BEs. It can be seen that the standard blocks have been used in the construction of masonry BEs in previous studies. In addition, the open space within each cell is very restricted, hence, the volume of grout that can be confined will be limited. This in turn leads to leaving more than 50% of the cross-sectional area unreinforced and may be subjected to spalling under a compressing load. Moreover, the construction of boundary elements with standard concrete blocks requires the cutting of their webs and shells to make a seat that accommodates the confinement hoops. On the other hand, C-shaped concrete masonry blocks do not need to be cut. This alternative can be more practical in terms of constructability because a reinforcing steel cage is placed prior to the construction of the boundary element. As such, there is a need for experimental and numerical investigations on the compression stress-strain behaviour of confined reinforced boundary elements constructed with C-shaped concrete masonry blocks in order to determine their use in ductile RM walls with boundary elements.

Moreover, the majority of the analytical stress-strain model in literature describe the compression behaviour of RC columns. However, the analytical stress-strain model of the RM prisms and boundary element are scarce. For predicting the effect of different parameters (e.g. transverse reinforcement confinement), the analytical studies of analyzing the seismic response of the RMSW integrating with boundary element are implemented the stress-strain models

developed originally for concrete materials. Henceforth, there is a need for proposing an analytical stress-strain model focusing on the behaviour of RM boundary element because using stress-strain concrete material may or may not be true due to the anisotropic characteristics of reinforced masonry assemblage.

The objective of this research is to investigate the compression stress-strain behaviour of isolated unreinforced and confined reinforced RMBE, that represent a highly compressed end zone of a RM wall, experimentally, numerically, and analytically. Throughout this research, the effects of the following parameters on the stress-strain behaviour of RMBE are investigated;

1- Vertical reinforcement ratio, ρ_L
2- Volumetric ratio of transverse reinforcement, ρ_t
3- Strength of the grout, f_{gr}
4- Aspect ratio of boundary element (height to thickness), h/t, and
5- Proposed a compression stress-strain analytical model for the shaped masonry boundary element.

Chapter 3

Compression Behaviour of Confined Concrete Masonry Boundary Elements

3.1 Abstract

The seismic performance of reinforced masonry (RM) walls can be enhanced by integrating confined boundary elements at the end zones of the wall. The evaluation of the compression behaviour of the boundary elements is essential to the reliable assessment of displacement ductility and the seismic performance of the walls. Complementary to the experimental evaluation of the compression behaviour, finite element numerical simulations are particularly useful in assessing the influence and sensitivity of various design parameters. In this study, experimental and numerical investigations are conducted to evaluate the compression stress-strain behaviour of confined C-shaped reinforced concrete masonry block boundary elements (RMBEs). Compression tests are conducted on 16 full-scale confined RMBEs with different configurations of confinement reinforcement. A finite element modeling (FEM) procedure using the ABAQUS software is employed to simulate the compression behaviour of a RMBE. The FEM procedure is validated with experimental results on a full-scale confined RMBE. Comparative compression stress-strain curves and damage progression are presented and discussed. The study shows the significance of the confinement reinforcement in the improvement of the compression strain capacity of the RMBE. Moreover, the proposed FEM procedure provides a good approximation of the compression stress-strain behaviour in the elastic and inelastic regions and captures the influence of the confinement reinforcement ratio on the compression response of the RMBE.

Keywords: Reinforced Concrete Masonry Walls; Boundary Elements; Confinement; Finite Element; ABAQUS; Stress-Strain; Damage Plasticity.

3.2 Introduction

Reinforced masonry (RM) shear walls are commonly used in medium-rise and high-rise masonry buildings as the lateral load resisting system to provide the lateral strength, stiffness and energy dissipation capacity required to resist seismic loading. RM walls are expected to exhibit an inelastic response during severe ground motions. Furthermore, the end zones of the RM wall will be subjected to cycles of tension and compression, arising from seismic overturning moments, as seen in Figure 3.1. Therefore, ductile detailing of the horizontal and vertical reinforcements, especially at the end zones of the walls (toe region), is required. Typical rectangular RM walls would have only a single vertical reinforcement bar placed in the masonry block cells without violating the maximum reinforcement and spacing requirements specified in masonry design standards (e.g., MSJC-2013 and CSA-S304, 2014). Consequently, this single bar disallows the placement of confinement hoops at the end zones of the wall, which are subjected to high inelastic strains during earthquake-induced cyclic loading (Figure 3.1(a)). On the other hand, adding boundary elements at the wall ends allows the placement of at least four vertical reinforcing bars enclosed by hoops (Figure 3.1(b, c)), thus enhancing the wall performance by providing core confinement to the wall ends through the reinforcement cage. As such, RM walls constructed with boundary elements at the end zones ensure stability under high compression loading and demonstrate an enhanced curvature ductility for the wall. The compression strain capacity can be increased using confinement reinforcement (Paulay and Priestley, 1992). Therefore, compared to a rectangular wall, adding a confined boundary element will increase the width of the RM wall end. As such, the sustainable compression strain will be increased, and the compression zone depth will be decreased (Park et al. 2007). Hence, adding boundary elements will enhance the curvature capacity of the wall cross-section.

The use of ductile reinforced concrete masonry shear walls with column-like boundary elements has been introduced in recent North American codes and standards for the design of masonry structures to improve the ductility capacity of walls. The US Building Code Requirements and Specifications for Masonry Structures (MSJC, 2013) allows the use of confined boundary elements and only imposes some geometrical rules. The code requires testing to be conducted to verify that the detailing provided is capable of developing a strain capacity in

the boundary element that would be in excess of the maximum imposed strain. The most recent Canadian Standard for the Design of Masonry Structures (CSA S304, 2014) also allows for the use of confined boundary elements. However, this design standard does not provide a correlation between specific detailing for confinement reinforcement and the corresponding improvement in the strain capacity and required testing and analysis to satisfy the level of required strain. Experimental studies that quantify the compression strain ductility of concrete masonry boundary elements are scarce in the literature.

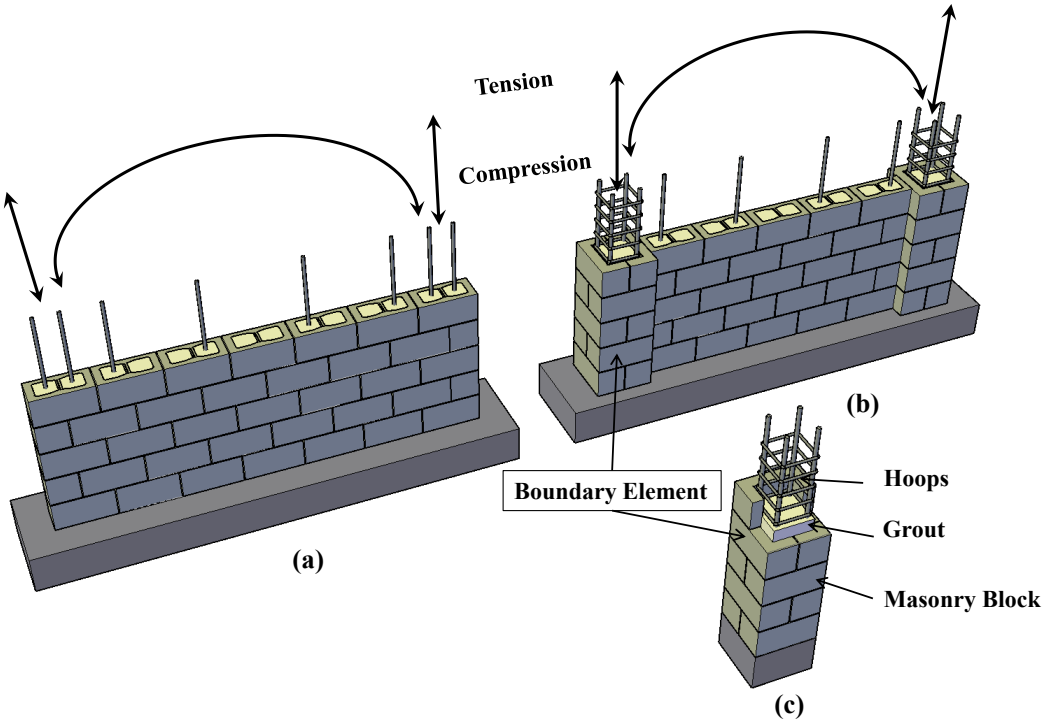

Figure 3.1 Schematics of a masonry building: (a) Rectangular RM wall; (b) RM wall connected with boundary elements; and (c) RM boundary element

The evaluation of the compression behaviour of the confined end zones of an RM wall is a key component in the assessment of the curvature and displacement ductility capacities of RM walls. Recent experimental investigations on RM shear walls with confined boundary elements (e.g., Shedid et al, 2010 and Banting et al. 2012) have concluded that the geometry of the boundary element allows for more than one layer of vertical reinforcement enclosed by hoops, which delays or prevents buckling of the vertical reinforcement, confines the compression zone, and limits the damage at the ends of the RM wall. Integrating the boundary element enhances the seismic performance of RM walls by improving the compression strain capacity and the

corresponding curvature and displacement capacities. Abo El Ezz et al. (2015) investigated the compression behaviour of boundary elements with standard concrete blocks experimentally. However, the construction of boundary elements with standard concrete blocks requires cutting of the webs and shells of the blocks to accommodate the placement of the confinement hoops (Figure 3.2 (a and c)). On the other hand, C-shaped concrete masonry blocks can provide a more attractive alternative in terms of constructability, with a reinforcing steel cage placed prior to the construction of the boundary element without the need to cut the blocks (Figure 3.2 (b and d)). As such, there is a need for experimental and numerical investigations on the compression stress-strain behaviour of confined boundary elements constructed with C-shaped concrete masonry blocks toward investigating their use in ductile RM walls with boundary elements.

The majority of experimental, analytical and numerical works that have been conducted on the structural behaviour of RM columns have focused on the evaluation of the ultimate compression strength rather than the evaluation of the post-peak strain capacity (e.g., Köksal et al, 2004, Feeg et al, 1979, Sturgeon et al, 1980, Khalaf et al, 1993, Hamid and Chuckwunenye, 1986, Ganesan and Ramamurthy, 1992, and Sayed-Ahmed and Shrive, 1996). On the other hand, considerable research has been conducted on the evaluation of the compression behaviour of confined reinforced concrete (RC) columns, including the quantification of the post-peak strain capacity. In addition, analytical stress-strain models for confined RC columns have been proposed (e.g., Sheikh and Uzumeri, 1980, Vallenas et al, 1977, and Mander et al, 1988). The compression behaviour of a confined RM column is not necessarily similar to that of RC columns since there are complex interactions between the mortar, grout, block and steel reinforcement.

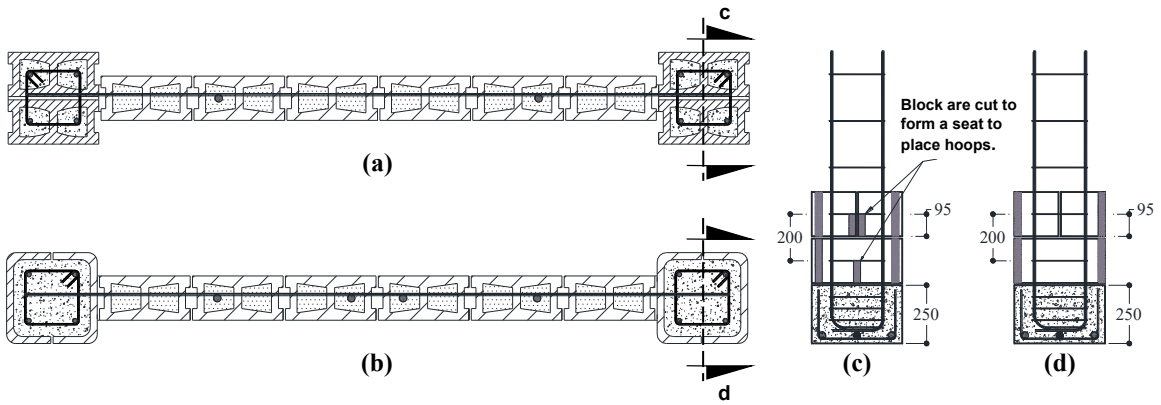

Figure 3.2 Horizontal cross-section of an RM wall with boundary elements using (a) standard blocks and (b) C-shaped block units. Vertical cross-section of a boundary element using (c) standard blocks and (d) C-shaped block units

Complementary to experimental investigations, a validated numerical model using a detailed FEM enables the investigation of the influence of the combination of different design parameters for the mortar, grout, masonry block, and steel reinforcement on the compression behaviour of RM boundary elements. This article presents experimental and numerical investigations on the compression stress-strain curve characteristics of isolated unconfined and confined reinforced RMBEs, representative of the highly compressed end zones of RM walls. Full-scale RMBEs were constructed and tested under axial compression loading until failure. A three-dimensional FEM was developed using the software ABAQUS, therein considering nonlinear constitutive material models for the mortar, steel, grout, and masonry block; then, the model was validated with experimental results. In this study, the influence of different configurations of the confinement reinforcement on the compression behaviour and a comparison between the experimental and numerical results, including the compression stress-strain curves and damage progression, are presented.

3.3 Experimental Work

3.3.1 Boundary element construction and design

A total of 16 full-scale fully grouted RMBEs were constructed and tested. All the unconfined and confined RMBEs were constructed by professional certified masons. Each specimen has an individual designation, where the first letter, BE, represents a boundary element. The second letter, R or U, denotes a reinforced or unreinforced specimen, respectively. The numbers following the letters refer to the hoop bar size and the spacing of the hoops, as shown in Figure 3.3. Typical dimensions of the unreinforced and reinforced RMBEs are shown in Figure 3.3. The total length of the test unit is 1250 mm, with an effective (gauge) length of 1000 mm. Each RMBE consists of five block layers placed on a concrete footing with dimensions of 400 mm x 400 mm x 250 mm (length x width x depth). Each course of the RMBE was composed of two block units placed together in alternating directions along its height. The blocks were joined together with 10 mm type-S mortar joints. The RMBE contained an internal vertical reinforcement of four bars of 20M (A_{sv}=300 mm^2) that extended continuously from the base of the footing to over the height of the RMBE without lap splices. The horizontal

reinforcement in the form of closed hoops was placed before the construction of the concrete blocks. The RMBEs had different volumetric reinforcing ratios, represented by the different diameters and spacings of the hoops. The hoop diameters were 10M and 15M at vertical spacing's of 100 mm and 200 mm (Table 3.1). The hoops were placed around a vertical reinforcement with outer dimensions of 230 mm x 230 mm. Figure 3.4 shows the sequence of the placement of the ties and C-shaped concrete blocks of the RMBEs. The RMBEs were filled with a standard coarse grout mixed in the lab. The confinement ratio C_f is calculated as $C_f = \rho_s \sqrt{(H/S)}$, as shown in Table 3.1, where ρ_s is the volumetric ratio of the confinement reinforcement (the volume of the confinement hoops to the volume of the core concrete at a spacing S), H is the width of the confined core (230 mm in this case), and S is the spacing between the confinement hoops.

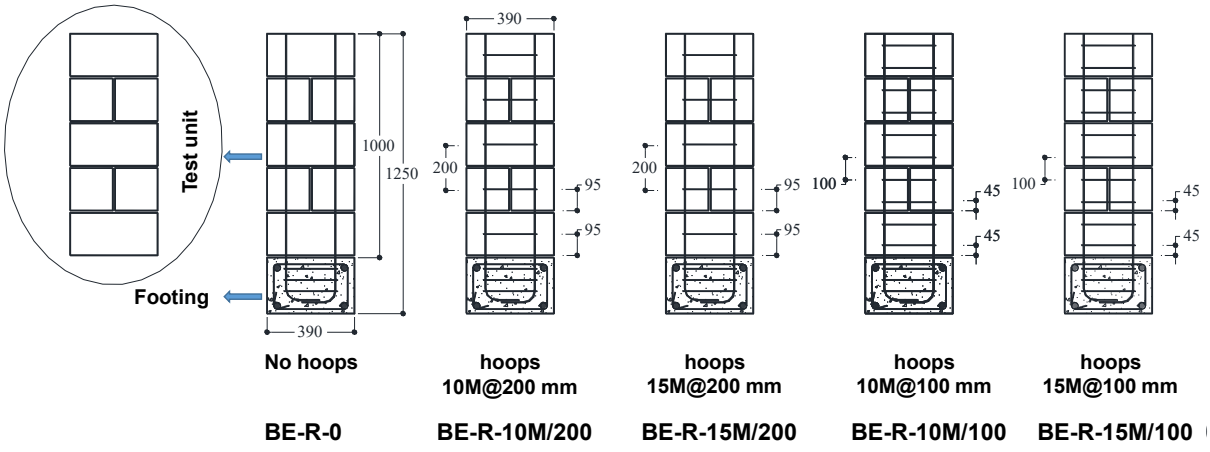

Figure 3.3 Construction details of unreinforced and reinforced concrete RMBEs

Figure 3.4 Construction sequence of placing steel bars and blocks in the RMBEs

Table 3.1 Test matrix of concrete RMBE

RMBE ID	Number of tested units	Vertical reinforcement	Transverse reinforcement (hoops)	ratio of transverse reinforcement	Confinement ratio C_f
BE-U-0	2	-	-	0	0
BE-R-0	3	4-20M	-	0	0
BE-R-10/200	3	4-20M	10M@200mm	0.0091	0.01
BE-R-15/200	2	4-20M	15M@200mm	0.0183	0.02
BE-R-10/100	3	4-20M	10M@100mm	0.0183	0.028
BE-R-15/100	3	4-20M	15M@100mm	0.0373	0.057

3.3.2 Material Properties

The properties of the materials used for the construction of the RMBEs are summarized in Table 3.2. Type-S mortar was used to join different courses with an average thickness of 10 mm, as shown in Figure 3.4. The proportions of the materials of the coarse grout mix are summarized in Table 3.3. Quasi-static tension tests were conducted on five 600-mm-long tensile specimens

for each diameter to determine the yield strength of the steel reinforcement used in the construction of the RMBE. The measured value of the yield strength was 420 MPa. The reinforcement characteristic stress-strain curves for three different diameters are shown in Figure 3.5. Full-scale 70-mm-thick shaped concrete blocks 190 mm x 190 mm x 390 mm (depth x width x length) were used in the RMBE construction, as shown in Figure 3.6. The average compressive strength based on the net area of three full-scale shaped concrete masonry block units was 15 MPa. The C-shaped concrete masonry block units were joined together with 10 mm of type-S mortar. Six 50 mm cubes were molded and tested under compression. The average compressive strength of the mortar at the beginning of testing of the RMBEs was 13.7 MPa. Course grout was used for grouting the RMBEs. The average grout compression strength of the six 100 mm x 200 mm (diameter x height) cylinders was 35 MPa when the RMBEs were tested. All materials used for the construction are available on the Montreal commercial market.

Table 3.2 Tested material properties

Material	**Property**	**Compressive strength (MPa)**	**C.O.V. %**
Masonry block	f_{bl}	15	3.5
Mortar	f_{mr}	13.7	10
Grout	f_{gr}	35	6.5
Reinforcement steel	f_y	420	7.5

C.O.V. (coefficient of variation)

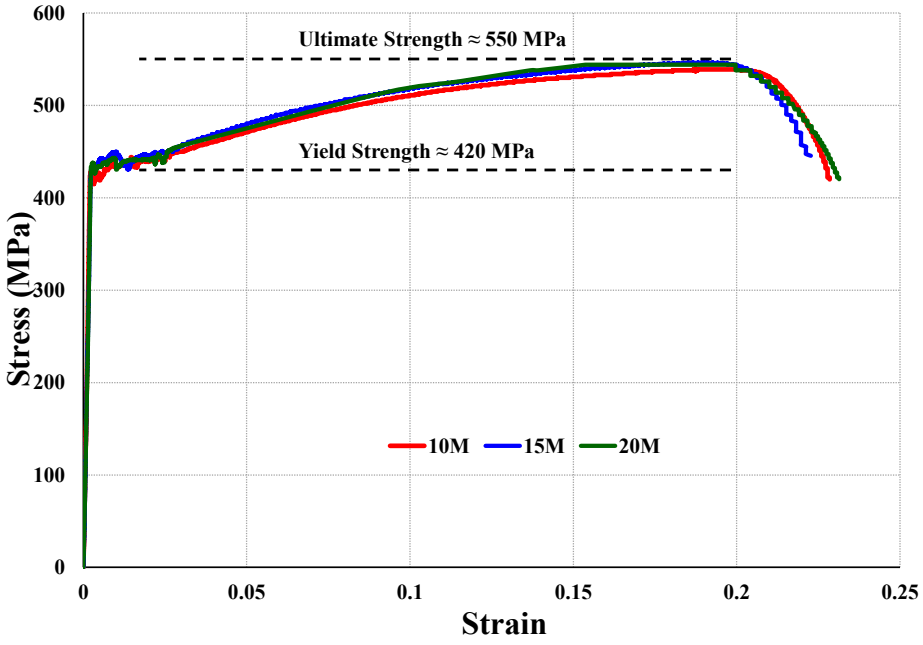

Figure 3.5 Stress-strain curves for the reinforcement steel used in the construction of the RMBEs

Table 3.3 Grout mix proportions

Element	Part
Portland	1
Fine aggregate	1.68
Coarse	1.68
Water	0.5

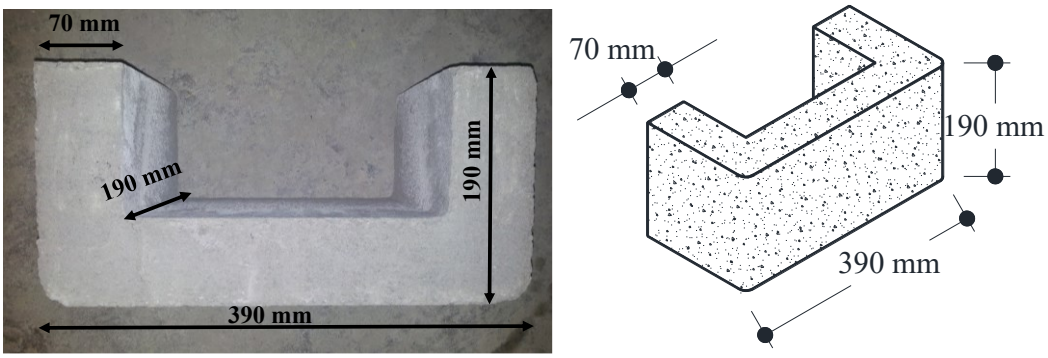

Figure 3.6 Full-scale C-shaped concrete masonry block unit

3.3.3 Test setup and instrumentation

The RMBE specimens were tested under compression using a displacement-controlled MTS machine (Figure 3.7) at École Polytechnique de Montréal. The displacement-controlled setting enabled capturing of the post-peak descending branch of the stress-strain curve, which is needed to quantify the influence of the confinement reinforcement on the strain capacity of the RMBEs. The test setup consisted of a steel frame transferring the load to the strong floor supporting the test unit, a 12000 kN hydraulic cylinder controlled by an MTS controller and a 50 mm rigid rectangular steel plate for transferring a uniformly distributed load to the test unit. High-strength gypsum was placed on the top and bottom of the RMBE to ensure that the top and bottom of the test unit were leveled and that the load was uniformly distributed on the specimen.

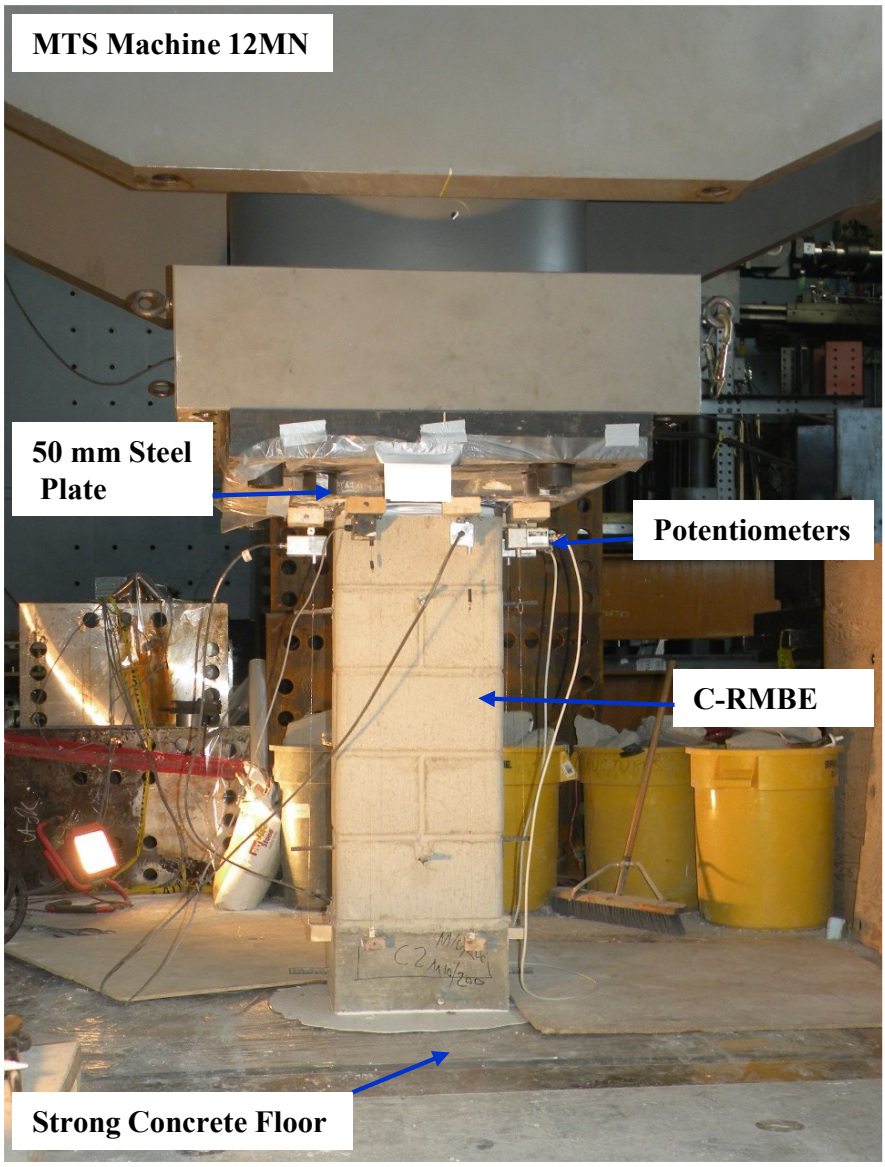

Figure 3.7 Test setup

The rate of displacement was 0.45 mm per minute, and the load was recorded from an MTS controller attached to a data acquisition system. To measure the continuous deformation of the RMBE, the vertical displacement of the RMBE was measured using four cable-extension transducers (potentiometers) attached at the centerline of each side of the unit while being fixed underneath the bearing plate and at the top of the concrete footing. The gauge length of the potentiometers was 1000 mm, measured from underneath the bearing plate to the top of the concrete footing.

3.4 Experimental Results

Figure 3.8 shows the observed compression stress–strain curves for all test units, including unreinforced, vertically reinforced and reinforced confined RMBEs.

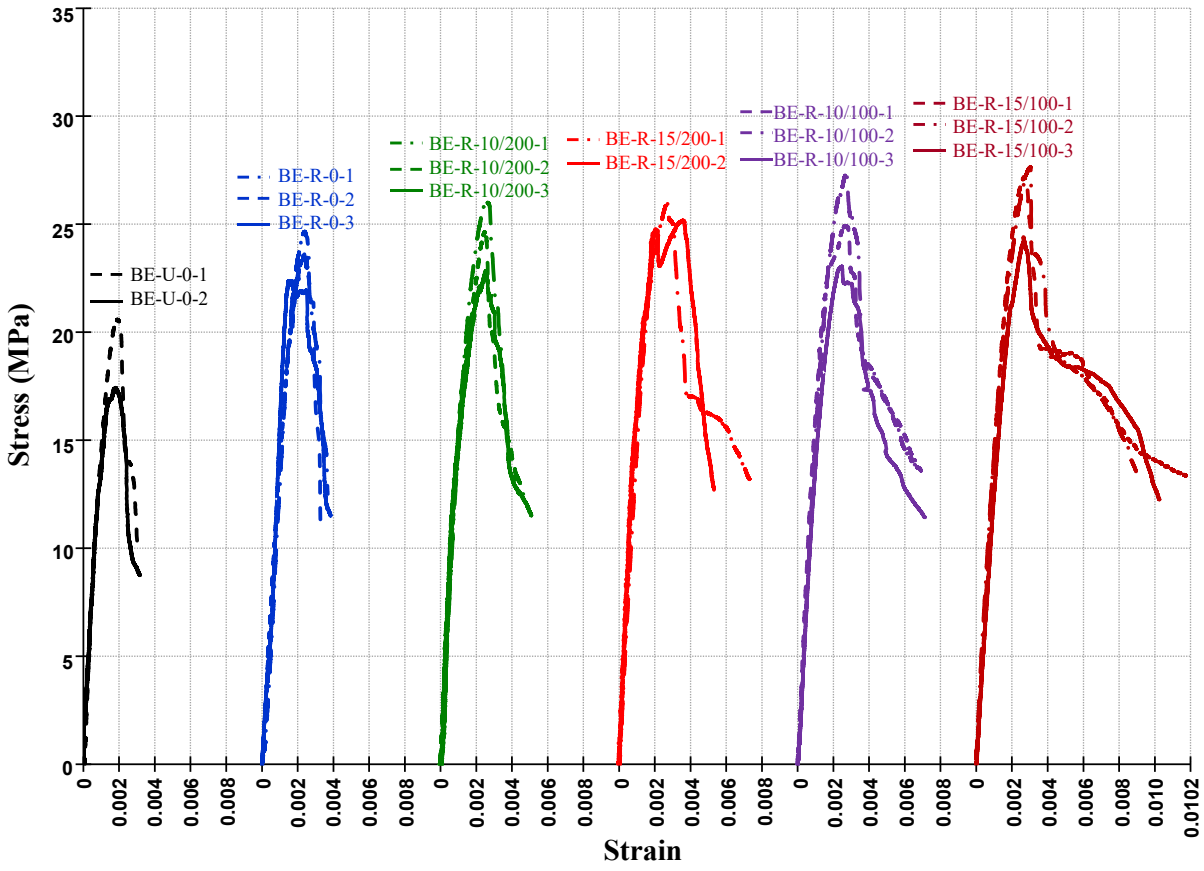

Figure 3.8 Observed stress-strain curves for all test units, including unreinforced, vertically reinforced and reinforced RMBEs

It can be seen that the vertically reinforced RMBE (BE-R-0) exhibited an increase in strength compared to the unreinforced RMBE (BE-U-0) due to the presence of the vertical reinforcement bars. The presence of the confinement horizontal reinforcement (hoops) produced a more gradual post-peak stress-strain behaviour and improved the strain capacity of the RMBE. As the horizontal confinement reinforcement increased, the strain capacity of the RMBE increased. For the test units BE-R-10/200 with $C_f = 0.01$, the test results indicated that post-peak strain at 75% and 50% of the strength an increase of 29% and 45%, respectively, compared to the test units BE-U-0 (the unreinforced units). The test units BE-R-15/200 with $C_f = 0.02$

exhibited an increase of 37.5% and 100% in the post-peak strain at 75% and 50% of the strength, respectively, compared to the test units BE-U-0. In contrast, the post-peak strains at 75% and 50% of the strength for the test units BE-R-10/100 with C_f = 0.028 were higher by 58.4% and 122.5%, respectively, compared to the test units BE-U-0. The highest increases in the post-peak strain at 75% and 50% of the strength were obtained with test units BE-R-15/100 with C_f = 0.057, which resulted in an increase of 83% and 232%, respectively, compared to the test units BE-U-0.

RMBEs BE-R-10/100 and BE-R-15/100 exhibited a milder post-peak strain softening behaviour compared to RMBEs BE-R-10/200 and BE-R-15/200 due to the presence of a higher confinement ratio. RMBEs with confinement reinforcement experienced an average drop in strength of 25% after reaching the RMBE's peak load. This is mainly attributed to the difference in the compressive strengths of the C-shaped concrete block (15 MPa) and the grout (35 MPa). The concrete block represents approximately 50% of the RMBE cross-sectional area that exhibits spalling after reaching the peak load.

3.5 Finite Element Analysis

The nonlinear finite element software package ABAQUS was employed for the numerical simulation of the compression stress-strain behaviour of the tested RMBEs. Details of the assumptions concerning the constitutive laws of the materials that are used in this FEM are discussed in the following subsections.

3.5.1 Constitutive models

For simulating the behaviour of grout, mortar, and masonry block, the damage plasticity model from ABAQUS was applied in this study. The plastic damage model requires the parameters of the concrete damage plasticity and the values of the modulus of elasticity, density and Poisson's ratio. Being cementitious material, the concrete damage plasticity parameters for the concrete block, grout and mortar were assumed to be the same (Alwathaf et al, 2012). The parameters of the concrete plastic damage that were used for the grout, mortar, and masonry block are the dilation angle (36°), the plastic potential eccentricity (0.1), the ratio of the strength in the biaxial state to the strength in the uniaxial state (1.16), the ratios of the distance between the hydrostatic axis and the compression meridian and the tension meridian, separately, in the

deviatoric cross section (0.667), and the viscosity parameter that defines viscoplastic regularization (0) (Kmiecik and Kaminski , 2011). A perfect bond between the steel reinforcement and grout was achieved using the embedded regions available in the ABAQUS library.

3.5.2 Grout, mortar and masonry block material model

The stress-strain behaviours of the grout and concrete blocks under uniaxial compression are modeled using the stress-strain relationship proposed by Saenz's (1964) equation (Obaidat et al, 2010, Ascione et al, 2005, Lam and Dai, 2010, and Sousa and Caldas, 2005).

$$f_c = \frac{E_c \varepsilon_c}{1 + (R + R_E - 2)\left(\frac{\varepsilon_c}{\varepsilon_{cc}}\right) - (2R - 1)\left(\frac{\varepsilon_c}{\varepsilon_{cc}}\right)^2 + R\left(\frac{\varepsilon_c}{\varepsilon_{cc}}\right)^3} \quad \text{Eq. 3.1}$$

$$R = \frac{R_E(R_\sigma - 1)}{(R_\varepsilon - 1)^2} - \frac{1}{R_\varepsilon}\ ,\ R_E = \frac{E_c}{E_0},\ \text{and}\ E_0 = \frac{f_c^{'}}{\varepsilon_0} \quad \text{Eq. 3.2}$$

$$\varepsilon_0 = 0.0014[2 - \exp(-0.024 f_c^{'}) - \exp(-0.140 f_c^{'})] \quad \text{Eq. 3.3}$$

where E_c is the initial modulus of elasticity, R is the ratio relation, R_E is the modular ratio, R_σ is the stress ratio, R_ε is the strain ratio, and E_0 is the secant modulus. The strain corresponding to the peak stress, ε_0, was calculated to be equal to 0.0028 and 0.0019 for the grout and masonry block, respectively, based on plotting the stress-strain curve equations using Eq. 3.3 , where $f_c^{'}$ is the average compressive strength, R_ε=4 , and R_σ=4, where the last two values are as reported in (Hu and Schnobrich , 1989). The fitted mortar stress-strain curve used in the numerical model in this study is captured graphically from Kaushik at al. 2007. Kaushik et al. 2007 obtained a compression stress-strain curve for mortar by testing mortar cubes 50 mm in size with a similar mortar strength that was used in this study. The stress-strain curve of the mortar was obtained by averaging the data from nine specimens. The stress-strain curve under uniaxial compression is shown in Figure 3.9. The ultimate compressive strengths of the grout, masonry block, and mortar are 35, 15, and 13.7 MPa, respectively, as recorded during the material testing.

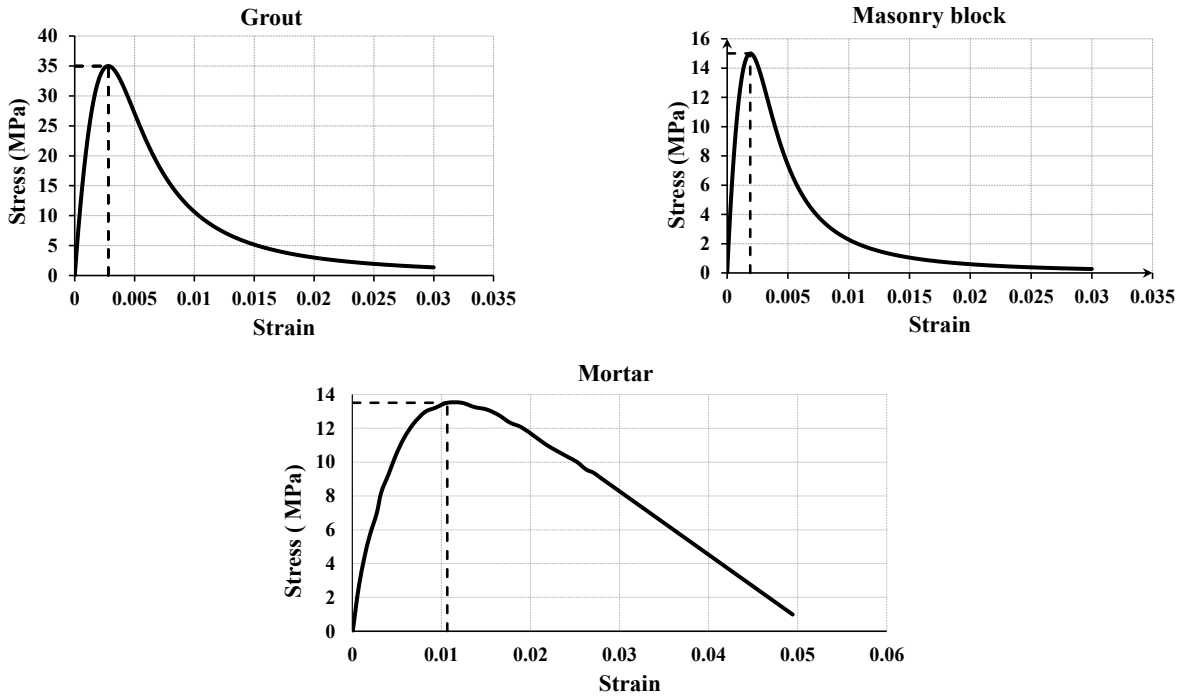

Figure 3.9 Stress-strain behaviour of concrete under uniaxial compression for the grout, masonry block, and mortar

3.5.3 Steel reinforcement

The plastic model from the ABAQUS software was applied to simulate the reinforcement stress-strain behaviour. The material constitutive model of the steel reinforcement bars is assumed to behave in tension, with multi-linear stress-strain curves for hoops and the longitudinal bars, which have a bar aspect ratio (*S/D*) of less than 8 (Yalcin and Saatcioglu, 2000), where *S* is the spacing between the hoops and *D* is the diameter of the longitudinal bar. In this case, the stress-strain behaviour in tension and compression is assumed to be similar (Feng, 2009) and was idealized from the as-tested curves shown in Figure 3.5. This curve consists of three segments and was idealized by three straight lines, as shown in Figure 3.10.a. The elastic and yield segments are linear. The strain hardening is also represented by a linear instead of parabolic curve. Whereas longitudinal bars have a bar aspect ratio (*S/D*) of greater than 8, the material constitutive model of steel reinforcement bars is assumed to behave in compression both linear elastically for buckling consideration and with the instability of the rebars, as shown in Figure 3.10b (Yalcin and Saatcioglu, 2000). In the figure, f_y, f_{sh}, and f_u represent the steel yield, strain-hardening, and ultimate stresses, respectively, and ε_y, ε_{sh}, and ε_u are the corresponding strains.

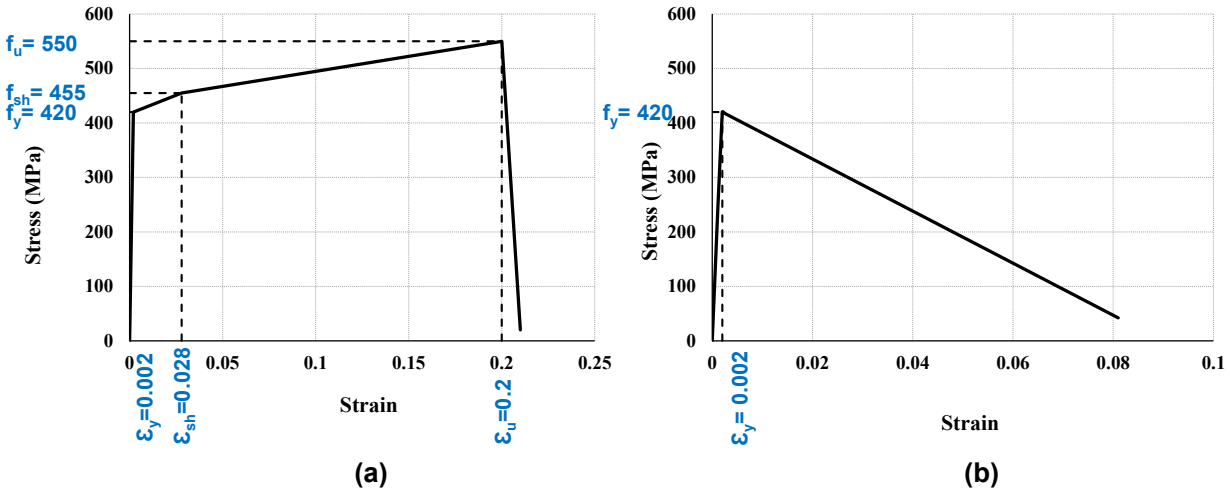

Figure 3.10 Stress-strain relationship for reinforcing steel rebars in a) Tension and compression for a bar aspect ratio (S/D) of less than 8 and in b) Compression for a bar aspect ratio (S/D) of greater than 8

In ABAQUS, the linear elastic portion of the steel stress-strain curve is defined by the modulus of elasticity. However, the non-linear portion requires the true stress, *f*, versus the plastic strain, ε^{pl}, relationship; this plastic strain must be calculated from the engineering stress-strain relationship. The steel reinforcement used in the FEM of the RMBE has a yielding stress of 420 MPa, modulus of elasticity of 200 GPa and Poisson's ratio of 0.3, as indicated in Figure 3.5. A perfect bond was assumed between the steel reinforcement and the grout (Wang et al, 2014 and Hassanein , 2010).

3.5.4 Geometry and boundary conditions

The FE models considered all the degrees of freedom of the nodes at the bottom of the RM RMBE to be restrained using the displacement and rotation commands available in the ABAQUS library, whereas the other nodes were considered to be free to rotate and translate in any direction. The boundary condition was applied at the top end of the RM RMBE geometry with a reference point at the middle to apply a concentrated load in increments using the static command available in the ABAQUS library (Figure 3.11.a).

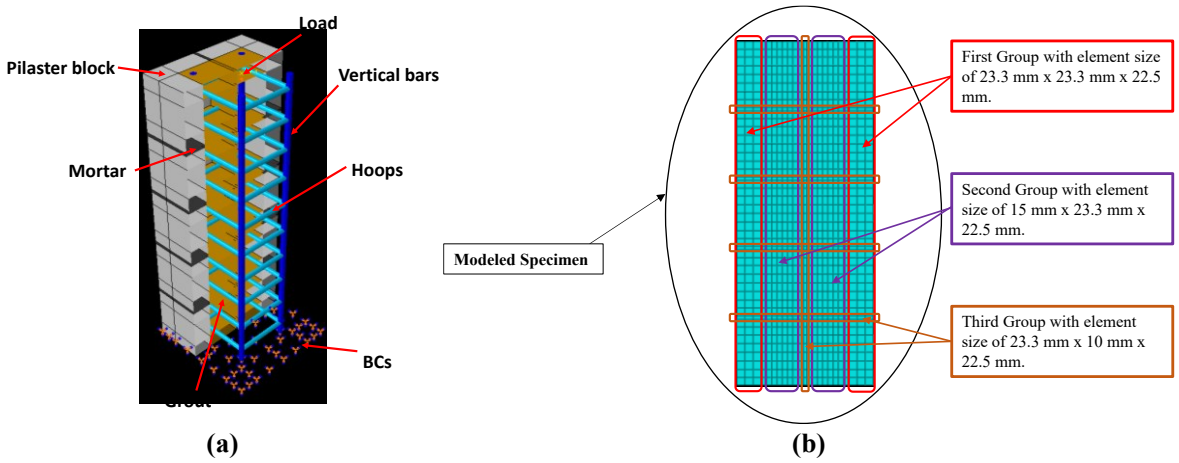

Figure 3.11 RM RMBE modeled specimen: (a) Typical geometry and finite element boundary conditions and (b) Element mesh sizes

To ensure that the nodes on the top of the geometry (i.e., all elements that are located at the top surface of the modeled specimen) have the same vertical displacement, and to ensure that the load is distributed uniformly, the multi-point connection (MPC) constraint commands available in the ABAQUS library were used.

3.5.5 Finite element type and mesh

3D simulations were conducted to obtain an accurate approximation of the overall compression behaviour of the RM RMBEs. Three-dimensional eight-node solid elements were used for the grout, mortar, and masonry block. A beam element was used for the reinforcement steel rebars. The perfect bond between the steel reinforcement and the grout was achieved using the embedded region available in the ABAQUS library. A fine mesh was used to provide more detailed recording of the elastic and inelastic behaviours (Hassanein , 2010), as shown in Figure 3.11.b. The RMBE has 28,800 solid elements and 32,435 nodes in total. Different element sizes were used within the single model (i.e., the model is discretized into small elements, and these elements are grouped into three groups based on element size). The first group, with an element size of 23.3 mm x 23.3 mm x 22.5 mm, is located at the corners of the masonry block along the height of the modeled specimen. The second group, with an element size of 15 mm x 23.3 mm x 22.5 mm, is located on the flange and web face of the masonry block along the height and depth of the modeled specimen. The third group, with an element size of 23.3 mm x 10 mm x 22.5 mm, is located on the bed and head mortar joints, as shown in Figure 3.11.b.

3.6 Validation of the Numerical Model

To verify the FEM approach of the RMBEs, six RMBE configurations, tested by the authors and as presented in the previous section, are modeled in this study using the ABAQUS software package. Table 3.4 shows the numerical and experimental results of the maximum stress f_{max}, strain at the peak stress ε_{max}, strain at 75% of the peak stress $\mathcal{E}_{75}$, strain at 50% of the peak stress $\mathcal{E}_{50,}$ and strain ductility μ of the RMBE. The strain ductility is defined as the ratio between the strain at 50% of the peak stress on the descending curve and the strain at the peak stress, as shown in Table 3.4. These results are based on the calculated and measured stress-strain behaviour of the RMBE. In the following subsections, a comparison of the experimental and numerical results of the compression stress-strain behaviour is presented.

3.6.1 Comparison of results

The compression stress-strain relationships of the RMBEs and the mechanisms of damage obtained from the FEM analysis, compared to the experimental results, are presented in this section. Figure 3.12 shows the average experimental compressive stress-strain curves and the FEM numerical curves of the RMBEs. It is clear that the initial elastic stage of the FEM calculated curves shows a good agreement with the experimentally measured curves. However, the FEM presents over-estimates in the post-peak behaviour, which can be attributed to the assumption of a perfect bond between the steel reinforcement and the grout and the perfect bond assumption between the block units, grout and mortar. However, the overall trends of the stress-strain curves obtained from the FEM show satisfactory agreement with the experimental results, and in general, the trends are quite similar.

Table 3.4 Numerical and experimental results of the RM RMBEs for the observed maximum stress, strains at the peak stress, strains at 75% and 50% of the peak stress, and strain ductility

RMBE ID	Maximum stress, f_{max} (MPa)			Strain at peak stress, ε_{max}			Strain at 75% of the peak stress, ε_{75}			Strain at 50% of the peak stress, ε_{50}			Strain ductility, μ	
	Experimental		FEM	Experimental		FEM	Experimental		FEM	Experimental		FEM	Experimental	FEM
	RMBE specimen	Ave. and COV. (%)		RMBE specimen	Ave. and COV. (%)		RMBE specimen	Ave. and COV. (%)		RMBE specimen	Ave. and COV. (%)			
BE-U-0-1	20.37	18.83 12%	18.81	0.0019	0.00195 4%	0.0018	0.0023	0.0024 3%	0.0024	0.0030	0.0031 5%	0.0033	1.59	1.83
BE-U-0-2	17.29			0.0020			0.0024			0.0032				
BE-R-0-1	25.60	23.80 8%	23.40	0.0022	0.0023 4%	0.0020	0.0031	0.0032 7%	0.0030	0.0036	0.0037 3%	0.0038	1.60	1.90
BE-R-0-2	24.00			0.0024			0.0035			0.0037				
BE-R-0-3	21.90			0.0023			0.0031			0.0038				
BE-R-10/200-1	27.50	25.32 13%	25.35	0.0028	0.0026 6%	0.0024	0.0033	0.0031 5%	0.0029	0.0044	0.0045 5%	0.0050	1.70	2.08
BE-R-10/200-2	24.62			0.0025			0.0030			0.0044				
BE-R-10/200-3	22.50			0.0026			0.0031			0.0048				
BE-R-15/200-1	26.15	25.53 3%	25.59	0.0028	0.0029 5%	0.0028	0.0032	0.0033 4%	0.0036	0.0067	0.0062 11%	0.0065	2.15	2.32
BE-R-15/200-2	24.90			0.0030			0.0034			0.0057				
BE-R-10/100-1	28.82	25.83 11%	25.85	0.0023	0.0026 12%	0.0027	0.0040	0.0038 5%	0.0039	0.0069	0.0069 4%	0.0080	2.71	2.97
BE-R-10/100-2	25.30			0.0029			0.0038			0.0066				
BE-R-10/100-3	23.40			0.0025			0.0036			0.0071				
BE-R-15/100-1	27.44	26.40 7%	26.46	0.0031	0.0029 5%	0.0030	0.0045	0.0044 2%	0.0048	0.009	0.0103 11%	0.0102	3.58	3.40
BE-R-15/100-2	27.35			0.0029			0.0044			0.011				
BE-R-15/100-3	24.30			0.0028			0.0043			0.011				

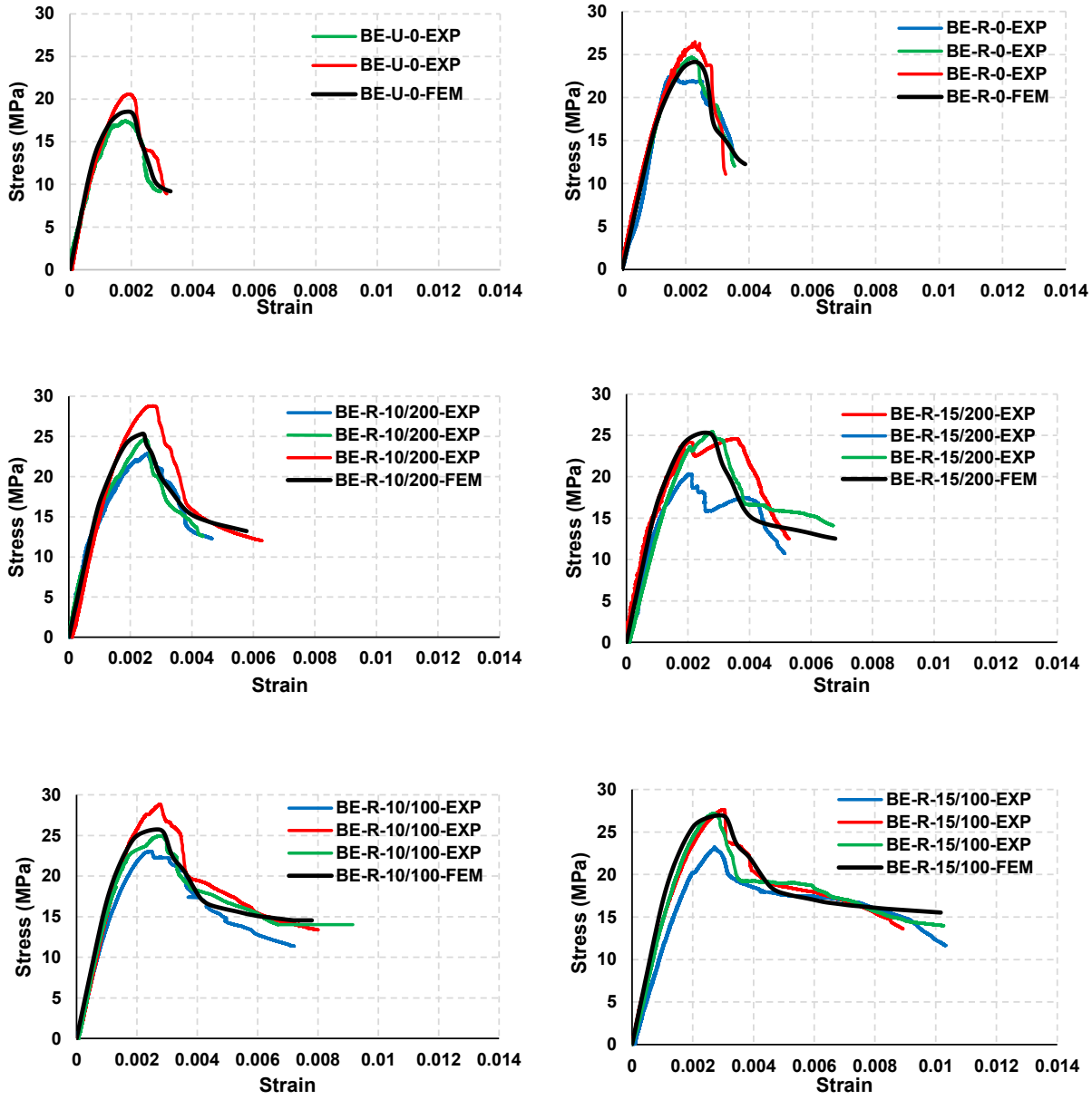

Figure 3.12 Average stress-strain curves of unreinforced and reinforced RMBE obtained by the numerical and experimental work

3.6.2 Definition of compression damage

The compression damage parameter, d_c, is shown in the output as DAMAGEC, which is used in the concrete damage plasticity model as a numerical indicator of material degradation in the post-peak range. The damage parameter values varied from zero, representing undamaged material, to one, which represents a total loss of strength. The damage variable, d_c, was computed using the following equation (Batikha and Alkam, 2015, Jankowiak and Lodygowski, 2005, and Yu et al. 2010):

$$d_c = (\sigma_{cu} - \sigma_c)/\sigma_{cu}$$ Eq. 3.4

where σ_{cu} is the compression ultimate strength and σ_c is the compression stress along the descending stress-strain curve. The attainment of a 50% reduction in the strength of the materials ($d_c > 0.5$) is used as an indicator of the extensive damage and spalling of the materials.

3.6.3 The unreinforced RMBE (Units BE-U-0)

As shown in Figure 3.13, the unconfined unit failed in a brittle manner, as initiated by vertical splitting cracks of the face shells of the C-shaped concrete blocks, with an increase in the density of cracking followed by spalling of the face shells. At the ultimate load, the strength of the test unit decreased quickly, and the cracking increased due to the crushing of the grouted core.

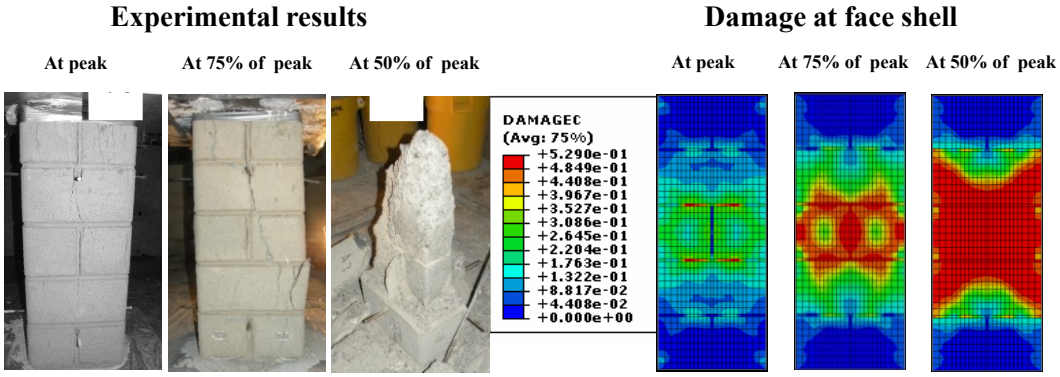

Figure 3.13 Comparison between the damage results from the FEM and experimental tests for the unreinforced RMBE

As shown in Figure 3.12, the average maximum compressive stress of the test unit was 18.83 MPa, and the corresponding maximum strain was 0.00195. It can be observed that the descending branch reached 50% of the strength with an average strain of 0.0031. Figure 3.13 shows the comparison of the damage result from the FEM analysis and the damage from the experimental tests, where the damage parameter (d_c) provides an indication of the damage propagation in the RMBE after the attainment of the peak load.

3.6.4 The vertically reinforced block RMBE (Units BE-R-0)

The vertically reinforced RMBE test units showed the first signs of failure immediately before experiencing the maximum compression load on the rising curve of the compressive stress-strain relationship. When the maximum load was reached, the vertically reinforced RMBE (BE-R-0) exhibited a similar cracking pattern as the unreinforced RMBE. However, the resulting 1.27-fold increase in strength compared to the unreinforced units (BE-U-0) was due to the presence of the vertical reinforcement, as shown in Figure 3.12. The post-peak behaviour was similar to that of the unreinforced units, with a steep slope after the peak load. Figure 3.14 shows the damage of the vertically reinforced RMBE and a comparison with the damage pattern recorded from the numerical simulation.

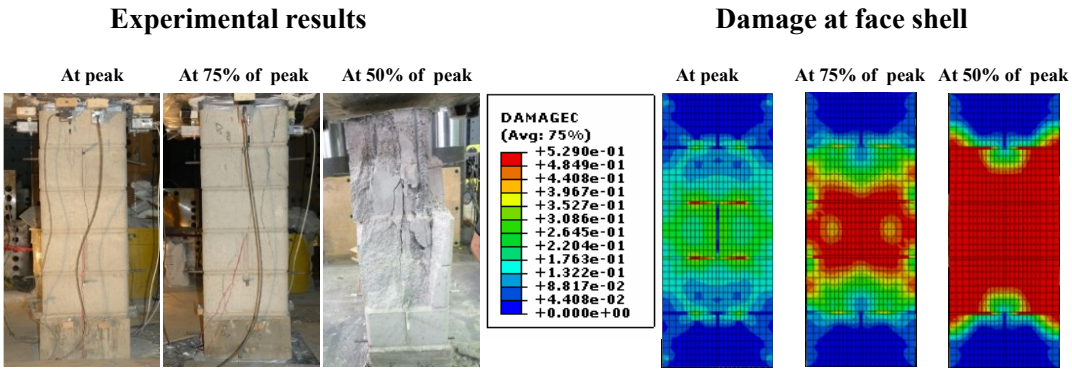

Figure 3.14 Comparison between the damage results from the FEM and the experimental tests for the vertically reinforced RMBE

The damage mechanisms of the units are as follows: vertical splitting cracks were observed at the peak loads, followed by spalling of the face shells and simultaneous core crushing and vertical bar buckling. Figure 3.14 shows the damage parameter, d_c, for the face shell of the concrete blocks. The extensive damage and spalling of the concrete blocks are indicated by the red color range, with an average value of d_c of 0.5. On the other hand, the post-yield stress in the longitudinal steel bars was used as an indicator for buckling. At the peak load, the yield stress was attained for the vertical bars. In the post-yield range, a reduction in the stress in the vertical bars was observed and provided an indication of bar buckling. This is compatible with the modeling assumptions shown in Figure 3.10.b for the stress-strain curves of the vertical bars in compression because the ratio of the spacing between the hoops and the diameter of the longitudinal bars is greater than 8. As seen in this figure, when the yield point is attained, the bars become unstable. Thus, the stress in the steel decreases linearly as the strain increases. Such a behaviour has been observed experimentally, as reported by Yalcin and Saatcioglu, 2000. The

average maximum compressive stress of the test unit was 23.80 MPa, and the corresponding maximum strain was 0.0022. As shown in Figure 3.12, the descending branch reached 50% of the strength, with an average strain of 0.0037.

3.6.5 The reinforced confined RMBE (BE-R-10/200 and BE-R-15/200)

Test units BE-R-10/200 and BE-R-15/200 were confined by hoops of 10M@200mm and 15M@200mm, respectively. As shown in Figure 3.12 and Table 3.4, the confinement reinforcement had a significant effect on the post-peak behaviour and produced a more gradual post-peak stress-strain curve. A slight 1.06-fold increase in the strength compared to the vertically reinforced units was observed. Figure 3.15 shows the comparison between the damage progression between the experimental and numerical results. In the experimental work, the damage mechanisms of the units were as follows: vertical splitting cracks at the peak load followed by spalling of the face shells and simultaneous core crushing and buckling of the vertical bars. The test unit BE-R-10/200 confined by hoops obtained a maximum strength of 25.32 MPa, resulting in a 34.5% higher strength compared to unreinforced RMBE test units BE-U-0 due to the presence of the confined reinforcement hoops. The strains at 75% and 50% of the strength were 0.0031 and 0.0045, respectively, which represent increases of 29% and 45%, respectively, compared to the unreinforced units (BE-U-0) due to the effects of the higher hoop confinement. For the unit BE-R15/200, the maximum strength of 25.53 MPa resulted in a maximum of 35.6% higher strength compared to test units BE-U-0. The strains at 75% and 50% of the strength were 0.0033 and 0.0062, respectively, resulting in an average increase in the strain of 37.5% and 100%, respectively, compared to the unreinforced units (BE-U-0) due to the effects of the higher hoop confinement.

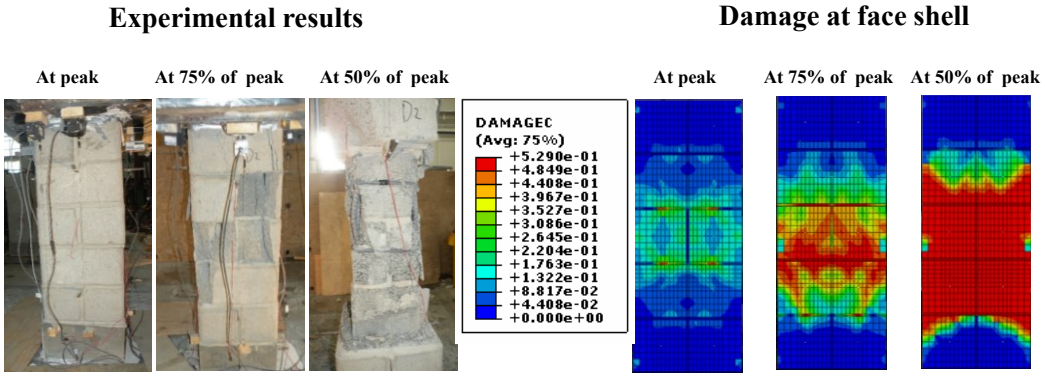

Figure 3.15 Comparison between the damage result from the FEM and the experimental tests for RMBE BE-R-10/200 and BE-R-15/200

3.6.6 The reinforced confined RMBE (BE-R-10/100 and BE-R-15/100)

The RMBE BE-R-10/100 and BE-R-15/100 behaved similarly to their counterparts RMBE BE-R-10/200 and BE-R-15/200, with a milder strain softening and gradual post-peak behaviour due to the presence of the higher confinement ratio. The strain ductility after obtaining the maximum strength was increased due to the closer spacing of the confinement transverse reinforcement (i.e., 100 mm instead of 200 mm). Figure 3.16 shows the comparison between the damage obtained from the FEM predictions and the experimental tests. From Figure 3.12, it can be observed that the test unit BE-R-10/100 confined by hoops obtained a maximum strength of 25.83 MPa, representing a 37.2% higher strength compared to test units BE-U-0 due to the presence of the confined reinforcement hoops. The strains at 75% and 50% of the strength were 0.0038 and 0.0069, respectively, representing increases of 58.4% and 122.5%, respectively. For the unit BE-R15/100, the maximum strength reached was 26.4 MPa, resulting in a 40% higher strength compared to test units BE-U-0. The strains at 75% and 50% of the strength were 0.0044 and 0.0103, respectively, representing average increases of 83% and 232% compared to the unreinforced units BE-U-0.

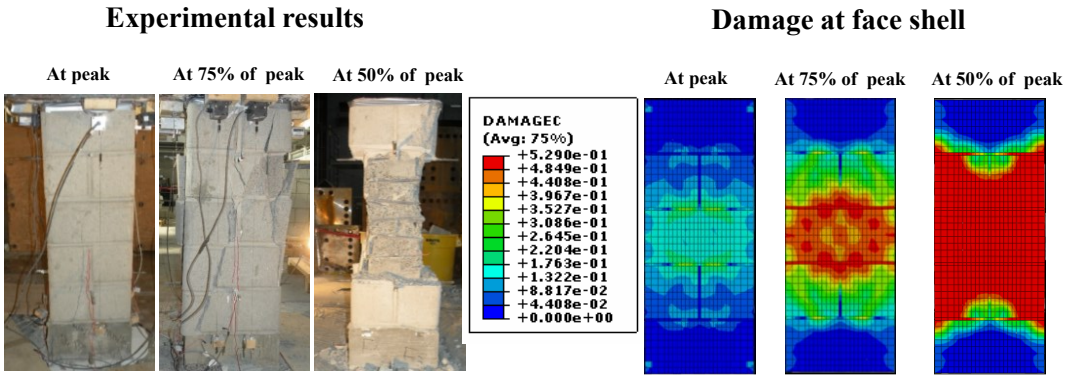

Figure 3.16 Comparison between the damage results from the FEM and the experimental tests for RMBE BE-R-10/100 and BE-R-15/100

3.7 Effect of Confinement Ratio

Figure 3.17 shows the correlation between the confinement ratio and the ratio of the maximum strength of the confined units to the unreinforced units based on the numerical and experimental results. For each unit, the peak stress of the confined unit is normalized by the peak stress of the unconfined unit, where $f_{max,c}$ is the average strength of the confined RMBE and $f_{max,u}$ is the average strength of the unreinforced RMBE. It can be observed that the confinement

introduces an increase in the axial strength in the range of 1.19 to 1.46 compared to the unreinforced units.

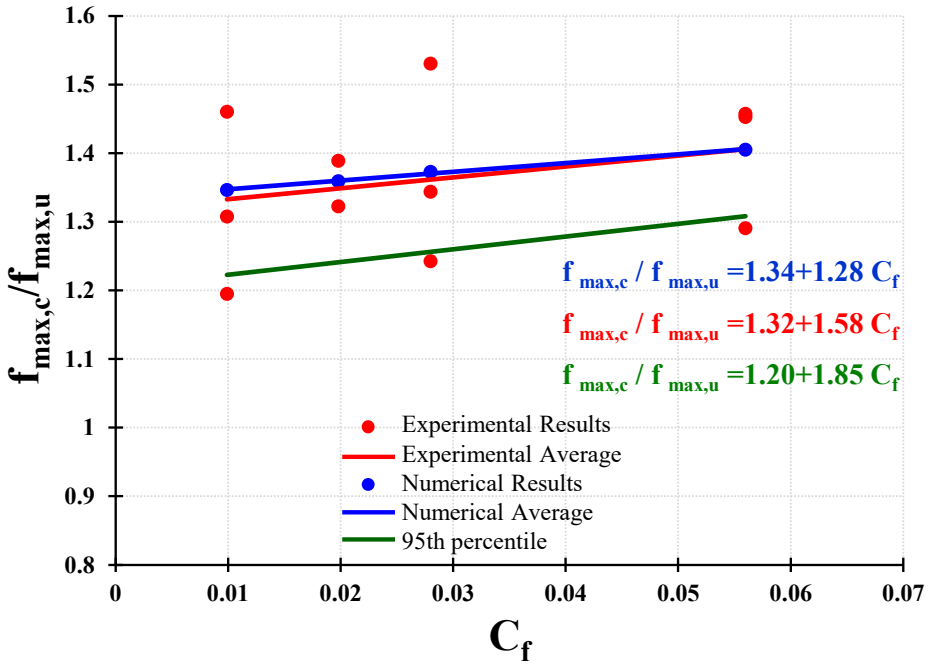

Figure 3.17 Correlation between the strength enhancement ratio and the confinement ratio based on experimental tests and numerical results

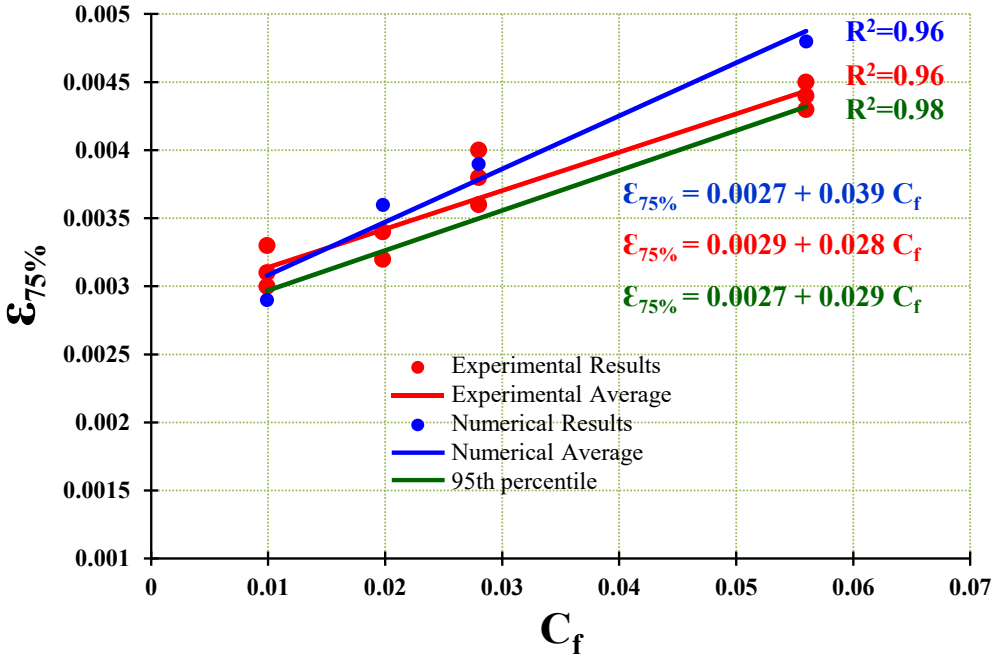

Figure 3.18 Correlation between the strain at 75% strength reduction and the confinement ratio based on the experimental tests and numerical results

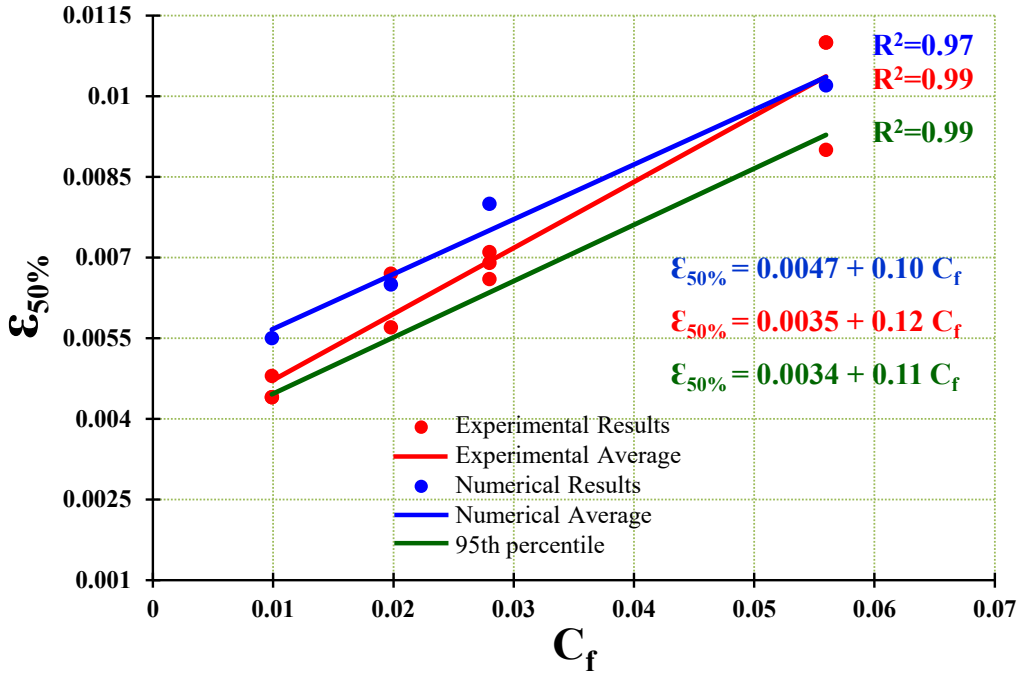

Figure 3.19 Correlation between the strain at 50% strength reduction and the confinement ratio based on the experimental tests and numerical results

On the other hand, an increase in the confinement reinforcement provided an increase in the range of 1.25 to 1.87 and 1.42 to 3.55 for the 75% and 50% strains, respectively, compared to the unreinforced units and had a significant effect on the post-peak behaviour, with softening of the descending branch of the stress-strain curve, as shown in Figure 3.18 and Figure 3.19.

The effect of the confinement ratio on the compressive strain is substantially more pronounced than that on the compression strength. In addition, the post-peak compressive strain behaviour of the confined RMBE depends on the confinement ratio of the transverse reinforcement. As the confinement ratio increases, the strains at 75% and 50% of the peak stress increase, and the severe deterioration of the RMBEs after the peak stress is reduced. Hence, the strain ductility increases, leading to an increase in the wall's curvature ductility. From the regression analysis presented in Figure 3.17, the observed trend representing the line of the value of $f_{max,c}$ compared to the $f_{max,u}$ based on the experimental average, the numerical results and 95% of the data above it, which is determined by subtracting 1.645 times the standard deviation from the experimental average, are given by the following equations:

$$f_{max,c} / f_{max,u} = 1.34 + 1.28\, Cf \qquad \text{for } C_f \geq 0.01 \text{ (Numerical results)} \qquad \text{Eq. 3.5}$$

$$f_{max,c} / f_{max,u} = 1.32 + 1.58\, Cf \qquad \text{for } C_f \geq 0.01 \text{ (Experimental average)} \qquad \text{Eq. 3.6}$$

$f_{max,c} / f_{max,u}$=1.20+1.85 Cf for $C_f \geq 0.01$ (95th percentile) Eq. 3.7

The values of the strains at 75% ($\mathcal{E}_{75\%}$) and 50% ($\mathcal{E}_{50\%}$) of the peak stress of the RMBEs are obtained from equations based on the regression analysis with the confinement ratio. Eq. 3.8 (R^2=0.96 and RMSE=4.71x10^{-8}) and Eq. 3.9 (R^2=0.97 and RMSE=1.12x10^{-7}) represent the numerical results, where R^2 is the coefficient of determination and the RMSE is the residual mean square error. Eq. 3.10 (R^2=0.96 and RMSE=3.67x10^{-8}) and Eq. 3.11 (R^2=0.99 and RMSE=3.81x10^{-4}) represent the experimental average. Eq. 3.12 (R^2=0.98 and RMSE=3.22x10^{-8}) and Eq. 3.13 (R^2=0.99 and RMSE=4.15x10^{-4}) represent the line that considers 95% of the experimental results above it, which is determined by subtracting 1.645 times the standard deviation from the experimental average, as shown in Figure 3.18 and Figure 3.19.

$\varepsilon_{75\%} = 0.0027+0.039\ C_f$ for $C_f \geq 0.009$ (Numerical results) Eq. 3.8

$\varepsilon_{50\%} = 0.0047+0.10\ C_f$ for $C_f \geq 0.009$ (Numerical results) Eq. 3.9

$\varepsilon_{75\%} = 0.0029+0.028\ C_f$ for $C_f \geq 0.009$ (Experimental average) Eq. 3.10

$\varepsilon_{50\%} = 0.0035+0.12\ C_f$ for $C_f \geq 0.009$ (Experimental average) Eq. 3.11

$\varepsilon_{75\%} = 0.0027+0.029\ C_f$ for $C_f \geq 0.009$ (95th percentile) Eq. 3.12

$\varepsilon_{50\%} = 0.0034+0.11\ C_f$ for $C_f \geq 0.009$ (95th percentile) Eq. 3.13

The current North American masonry codes apply a displacement-based method for the evaluation of the inelastic rotation demand and capacity of shear walls. CSA-S304 [2] estimates the rotation capacity of shear walls based on a maximum compression strain of 0.0025. If the rotation demand from seismic loading exceeds the rotation capacity, the compression region of the wall must be detailed to produce an increased compressive strain capacity in the masonry either by adding boundary elements or using another technique that can be demonstrated through testing. CSA-S304 [2] does not provide a correlation between the specific detailing for confinement reinforcement and the corresponding improvement in the strain capacity and thus requires testing and analysis to satisfy the strain demand requirements. Similarly, the MSJC-2013 [1] code requires testing to be conducted to verify that the provided confinement detailing is capable of ensuring a strain capacity in the boundary element that would be in excess of the maximum imposed strain. The conducted research in this paper provides a contribution to bridge the gap in knowledge on the correlation between the detailing of confinement reinforcement and the ratio to the increase in the compression strain. Such correlations were developed in this paper.

These correlations can be used to update the design methods in masonry standards by calculating the required confinement ratio based on the imposed strain demand corresponding to the earthquake-induced design inelastic rotation demand.

3.8 Conclusions

The prediction of the deformation and ductility capacity of RM walls with boundary elements requires an investigation of their compression behaviour. This article presented experimental and numerical investigations of the effects of the confinement ratio on the compression stress-strain behaviour of RM boundary elements at the ends of RM shear walls. Full-scale RMBE test units were constructed and tested under axial compression loading until failure. An FEM procedure was developed and validated with the experimental results. The FEM considered the specific stress-strain characteristics of the grout, mortar and concrete blocks. In this study, the influence of different configurations of the confinement reinforcement on the compression behaviour, as well as a comparison between the experimental and numerical results, including the compression stress-strain curves and damage progression, was presented. The results showed that increasing the confinement reinforcement ratio significantly affected the post-peak behaviour. This was indicated by a softening of the descending branch of the stress-strain curves resulting in an increase in the post-peak strain at 75% and 50% of the compressive strength of approximately 1.25 to 1.87 times and 1.42 to 3.55 times that of the unreinforced units, respectively. Regression equations were developed to correlate the confinement ratio with the corresponding improvement in the strain capacity. The proposed FEM procedure provided a good approximation of the compression stress-strain behaviour in the elastic and inelastic ranges and captured the influence of the confinement ratio on the compression response of the RMBE. The obtained results from this study provide greater insight into the complete compression stress-strain behaviour of confined concrete masonry boundary elements, an area with limited study in the literature. This is particularly important since recent masonry codes and standards in North America do not provide guidelines on how to correlate specific detailing for confinement reinforcement to the corresponding improvement in the compression strain capacity.

3.9 Recommendations for Future Research

The following lists some recommendations for future research toward improving the knowledge on the seismic behaviour and design of RM shear walls with boundary elements:

- Extending the experimental and numerical methodology developed in this paper to investigate the effects of design variables, such as the compressive strength of the constituent materials, and to update the proposed regression equations with additional data.
- Testing of full-scale shear walls with different configurations of boundary elements to develop recommendations for their seismic design.
- Developing numerical models for shear walls with boundary elements to evaluate the effects of confinement at the boundary elements on the ductility capacity of the wall. This can be performed using the validated FEM approach applied in this study.
- Based on these experimental and numerical studies, correlations between displacement ductility, inelastic rotation and the required compression strain at the boundary elements can be developed. These correlations will help in providing recommendations for confinement reinforcement for achieving a specific level of ductility.

3.10 Acknowledgments

This study was supported by the Natural Science and Engineering Research Council of Canada (NSERC) and was conducted in collaboration with the Canada Masonry Design Centre (CMDC) and the Canadian Concrete Masonry Producers Association (CCMPA). The authors would like to acknowledge the help of the technical staff at École Polytechnique de Montréal during the testing program.

Chapter 4

Stress-Strain Behaviour of C-Shape Confined Concrete Masonry Boundary Elements of RM Shear Walls

4.1 Abstract

Reliable material stress-strain relationship is the cornerstone of any analysis process. Unlike reinforced concrete, limited studies focused on the stress-strain behaviour of confined reinforced masonry. This could be due to the difficult reinforcement detailing in rectangular reinforced masonry shear walls (RMSWs), where they usually don't have enough space for placing confined reinforcement cage at the wall's ends. However, with the recent promotion of RMSWs with boundary elements there is a need for understanding the effect of different confinement levels in the boundary elements on the wall's behaviour. Reinforced C-shaped masonry boundary element (RMBE) allows placing of at least four vertical reinforcement bars confined by transverse hoops and thus introducing confinement to the wall's most stressed zone. Many studies highlighted the enhancement in the wall's lateral response (i.e. capacity and ductility) due to the introduction of RMBEs. However, predicting the improvement in the masonry response corresponding to different confinement ratios is yet to be investigated. This study presents the observed stress-strain relationship of thirty C-shape half-scale fully grouted unreinforced and reinforced masonry boundary element specimens tested under concentric compression loading up to failure. The effect of changing hoop spacing, vertical reinforcement ratio and the strength of grout on the axial stress-strain behaviour of RMBE is investigated. This study quantifies the effect of these parameters on the RMBE peak stress, strain corresponding to peak, and post-peak behaviour. In addition, this study presents linear correlations relationships that can be used by engineers to predict the RMBE stress and strain corresponding to peak, 75% and 50% of peak stress. Finally, this study investigates the capability of three existing stress-strain models in predicting the RMBE stress-strain relationship. Enhancement in both peak and post peak stress-strain behaviour were observed by decreasing the hoop spacing, increasing the vertical reinforcement ratio and increasing the grout strength. However, the hoop spacing had the most noticeable effect on the stress-strain relationship. None of the considered three material models was capable of capturing the drop in the RMBE strength that occurred due to the face shell spalling of the masonry block following the peak stress. Moreover, the studied models

overestimated the enhancement in the RMBE stress and significantly overestimated the enhancement in the RMBE strain. This study emphasizes the need for a new stress-strain model that can predict the RMBE response considering various confinement effects.

Keywords: Boundary elements, Concentric loading, Concrete block, C-shaped block, Confinement, Grout strength, Shear walls, Masonry prism, Reinforced masonry, Stress-strain behaviour.

4.2 Introduction

Reinforced masonry shear walls (RMSWs) are the main lateral force resisting system in reinforced masonry structures that are commonly used in low and mid-rise buildings. Adding confinement reinforcement cage at the wall extremities is a common practice in reinforced concrete (RC) structural shear walls to increase the wall's curvature and displacement ductilities as well as its lateral load capacity. This practice was recently adopted in RMSWs by introducing a boundary element column at the wall toes (e.g. Shedid et al. 2010, and Banting and El-Dakhakhni 2012). These boundary elements allow the placement of at least four vertical reinforcement bars that are enclosed by horizontal hoops; hence, enhancing the wall performance by providing core confinement to the wall ends through the reinforcement cage which was not attained in rectangular RMSW. Moreover, increasing the wall thickness in the most stressed zone in the wall (i.e. wall ends) decreases the compression stress block depth and thus enhance the wall curvature capacity (Park et al. 2007). Adding boundary elements to the RMSW improves the compression strain capacity and the displacement ductility, hence, improves the seismic performance of RMSW (Shedid et al. 2010).

Understanding the material stress-strain behaviour is key for reliable structural analysis and design. Recent numerical studies that focused on analyzing the lateral response of RMSW with boundary elements, (e.g. Ezzeldin et al. 2016, Hamzeh et al. 2015) implemented the available material stress-strain models that were originally developed for concrete materials (e.g. Mander et al. 1988) to estimate the effect of confinement on the reinforced masonry stress-strain behaviour. However, this approach may or may not be true due to the anisotropic characteristics of reinforced masonry assemblage. RMSW is composed of concrete masonry blocks that are connected with weak mortar joints and reinforced with vertical and horizontal steel bars, then filled with grout. The axial compressive stress-strain behaviour of RMSW boundary elements is

essential to predict the lateral wall response (see Figure 4.1), especially when having different confinement ratios in the boundary elements.

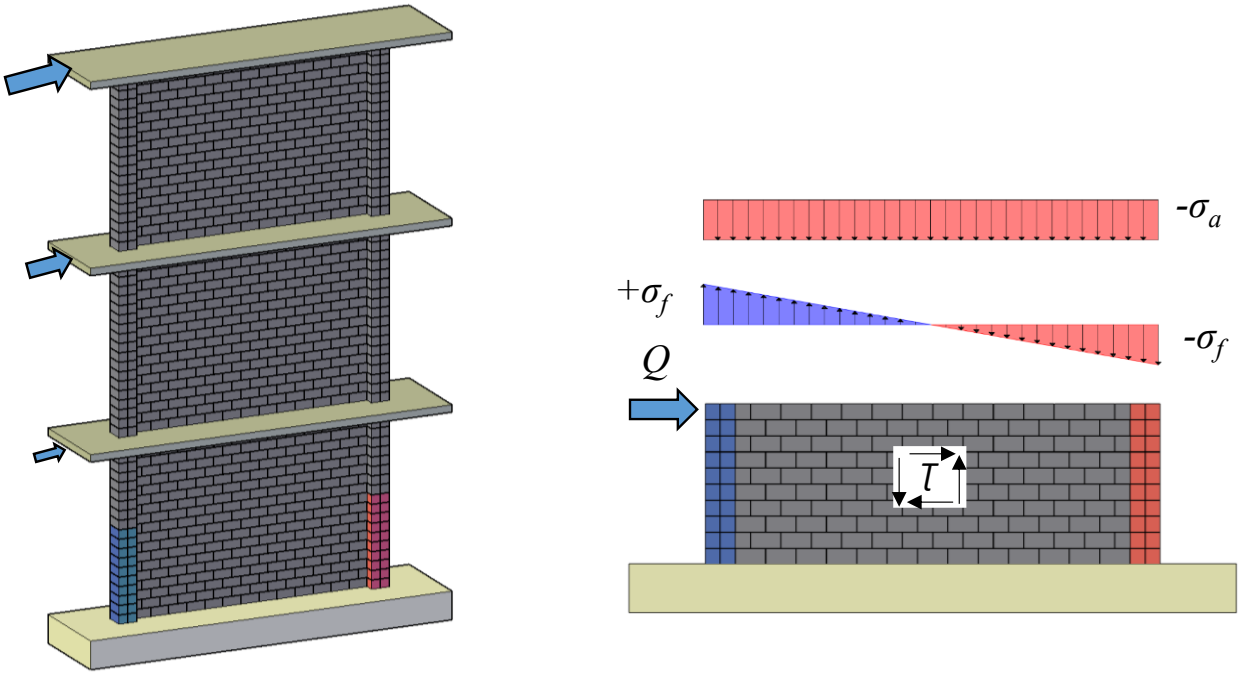

Figure 4.1 Internal stresses in reinforced masonry shear wall with boundary elements

Limited studies explored the behaviour of reinforced masonry boundary elements (RMBEs) considering different confinement ratios. Abo El Ezz et al. (2015) tested 17 full-scale fully-grouted concrete masonry boundary element columns utilizing standard concrete blocks (i.e. double cell stretchers). It was concluded that the confinement reinforcement enhances the strain ductility and has a noticeable effect on the post-peak behaviour. In addition, Abo El Ezz et al. (2015) proposed a smeared compression stress-strain model for confined boundary elements capable of predicting the RMBE stress-strain response. However, using standard stretcher concrete blocks to build the RMBEs introduce limitations on the hoop spacing, as the hoops can be placed only at the mortar bed joint. Therefore, Obaidat et al. (2017) introduced the use of C-shaped concrete masonry blocks in the RMBEs, which allows having any hoop spacing; thus enhancing the confinement effect. Obaidat et al. (2017) tested 16 full-scale fully grouted RMBE to evaluate the compression stress-strain behaviour considering different confinement ratios of lateral reinforcement (i.e. different hoop spacing). The results showed that as the confinement ratio increases, the compression strain capacity increases. Moreover, Obaidat et al. (2017) presented correlations between the confinement reinforcement ratio and the corresponding

enhancement in the compression peak stress and post peak strain, which can be used to calculate the required confinement ratio to achieve a specific strain demand.

The focus of the current study is to investigate the effect of changing confinement ratio (i.e. by changing the hoop spacing), vertical reinforcement ratio, and grout strength on the C-shaped RMBE compressive stress-strain behaviour. It should be noted that the C-shaped blocks introduced in this study are more slender than those used in Obaidat et al. (2017), thus increasing the confined core area within the RMBE. Thirty half-scale fully grouted RMBE specimens were tested under concentric loading up to failure. In the current study, three spacing were considered between the hoops, namely, 30, 45 and 60 mm. Moreover, two vertical reinforcement ratios were investigated: i.e. four #3 bars (with area of $71\ mm^2$ each) and #4 bars (with area of $129\ mm^2$ each), and two grout strengths: 15 and 45 MPa. The effect of these parameters on the peak stress, strain at the peak stress, post peak behaviour, ductility, and RMBE damage is investigated. Also, the current study aims at investigating the capability of the available stress-strain concrete model by Mander et al. (1988) in predicting the stress-strain behaviour of RMBE. Moreover, this study investigates the capability of stress-strain models proposed by Priestley and Elder (1983) and Abo El Ezz et al. (2015) for masonry assemblages in predicting the effect of the aforementioned parameters on the stress-strain behaviour.

4.3 Experimental Program

4.3.1 Test matrix

Thirty half-scale fully grouted RMBE specimens (see Figure 4.2) were constructed in Concordia University's structures laboratory and tested under concentric compression load up to failure. The specimens were divided into ten groups; each group consisted of three identical specimens to avoid the natural variability in masonry construction which may lead to wrong conclusions (Table 4.1). The identification of each group, e.g. BE15-R#3-D4/30-A, consisted of three parts: grout strength in MPa (i.e. BE15), vertical reinforcement bar size (i.e. R#3), and transversal reinforcement size and spacing in mm (i.e. D4/30). The letter A, B, or C that follows the group name identifies the sample in each group.

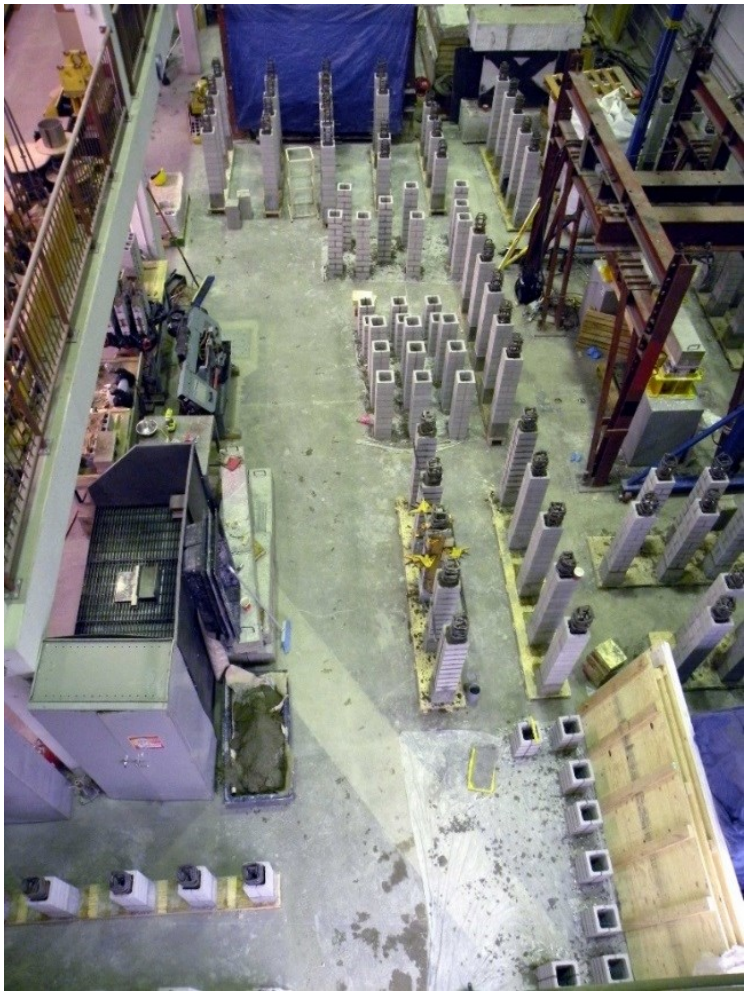

Figure 4.2 RMBE specimens during construction

The first two groups represent unreinforced boundary element prisms. On the other hand, the other eight groups represent the RMBE having two grout strengths, two vertical reinforcement ratios, ρ_v and various hoop spacing. All the reinforced specimens had four vertical reinforcement bars placed in each corner. Deformed wires D4 ($25.8\ mm^2$) were used as transverse reinforcement (i.e. hoops). It should be noted that the confinement ratio C_f is calculated according to Eq. 4.1 and presented in Table 4.1.

$$C_f = \rho_s \sqrt{(H / S)} \qquad \text{Eq. 4.1}$$

where; ρs is the volumetric ratio of the confinement reinforcement (the volume of confinement hoops to the volume of core concrete at spacing S); H is the width of the confined core and S is the spacing between the confinement hoops.

Table 4.1 Details of RMBE test specimens

Group #	RMBE ID	Number of tested specimens	Grout Strength (MPa)	Longitudinal Reinforcement		Transverse Reinforcement		Confinement ratio C_f
				Number-size of Bars	ρ_v%	Bar size (spacing mm)	ρ_h%	
1	**BE15-U-0**	3	15	-	-	-	-	-
2	**BE45-U-0**	3	45	-	-	-	-	-
3	**BE15-R#3-D4/30**	3	15	4#3	0.8	D4 (30)	3.15	0.062
4	**BE15-R#3-D4/45**	3	15	4#3	0.8	D4 (45)	2.1	0.034
5	**BE15-R#3-D4/60**	3	15	4#3	0.8	D4 (60)	1.57	0.022
6	**BE15-R#4-D4/30**	3	15	4#4	1.4	D4 (30)	3.15	0.062
7	**BE15-R#4-D4/45**	3	15	4#4	1.4	D4 (45)	2.1	0.034
8	**BE15-R#4-D4/60**	3	15	4#4	1.4	D4 (60)	1.57	0.022
9	**BE45-R#3-D4/60**	3	45	4#3	0.8	D4 (60)	1.57	0.022
10	**BE45-R#4-D4/60**	3	45	4#4	1.4	D4 (60)	1.57	0.022

Table 4.2 Materials compressive strength

Material	Notation	Average compressive strength (MPa)	C.V. %
Concrete cylinder (footings)	f_c	83.8	6.20
Masonry concrete block	f_b	22.0	13.80
Mortar cubes	f_{mc}	12.3	7.15
Grout cylinders	f_{gr}	15.0	8.70
		45.0	4.75

*C.V.: coefficient of variation

4.3.2 Construction of RMBE

The RMBE specimens were constructed by professional masons from Ontario and Québec following the Canadian construction practices. As shown in Figure 4.3(a to h), the construction started by assembling the reinforcement cage for each specimen. The reinforcement cage consisted of four reinforcement bars (#3 or #4), and deformed wire (D4) hoops tied at a specific spacing (30, 45 or 60 mm). All hoops were anchored with 135º bends extending 55 mm into the grout core. Each sample had 250 mm thick top and bottom reinforced concrete footings. The hoops size was increased to #4 (129 mm2) in the upper and lower transfer footings to avoid footing's failure. After assembling the reinforcement cage, each six RMBE were placed in a timber form to pour the bottom footing. After pouring the high strength concrete in the lower footing, the RMBE were cured for at least one week, and then the strain gauges were mounted on the mid-height of the four vertical reinforcement bars.

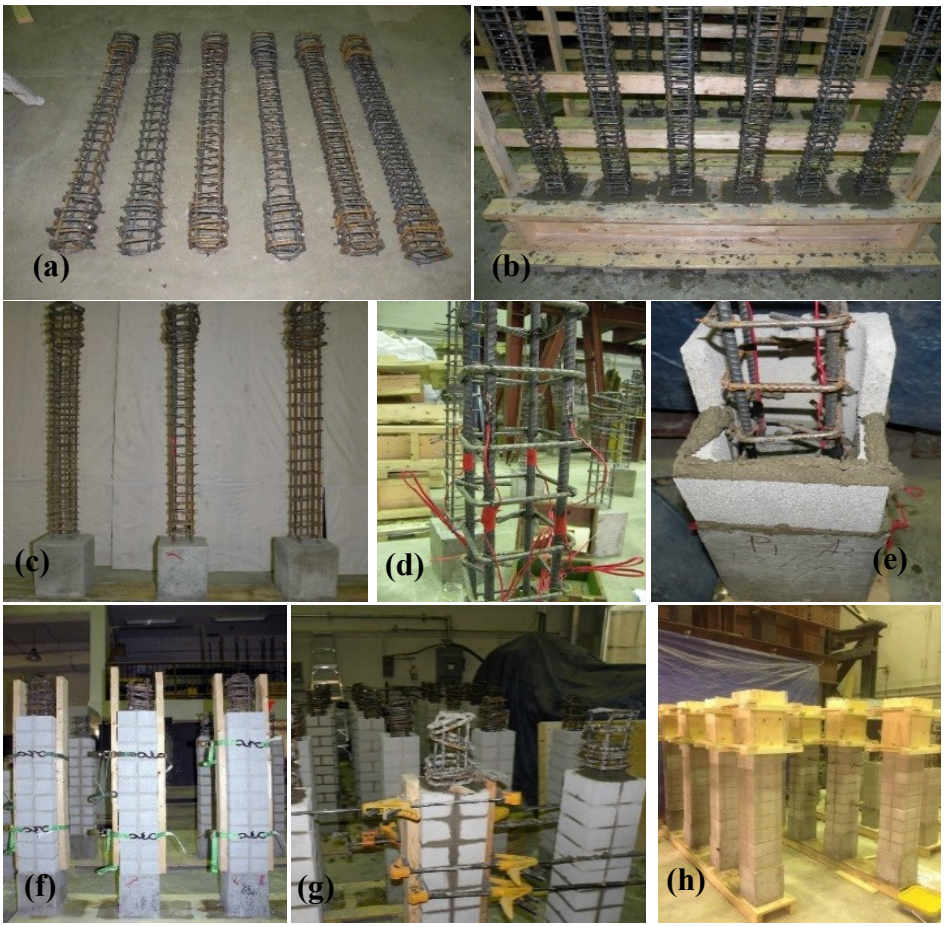

Figure 4.3 Construction sequence of RMBE

All RMBE specimens were constructed in a stacked bond pattern with two C-block units in each course. The stacked bond pattern represents the layout envisioned for RMSW with boundary elements. Each RMBE consisted of ten courses placed on a concrete footing with dimensions of 200 mm x 200 mm (length x width). Type S mortar was used to join the block units with 5 mm joints. The RMBE specimens had a height to thickness (aspect ratio A/R) of 5 to avoid any correction factor related to the specimen height as per CSA S304-14 (2014). The vertical reinforcement bars were extended continuously, over the height of the RMBE specimen, without splices from the base of the bottom footing to the top footing. Then the RMBE specimens were strapped before grouting to avoid any cracks in mortar head joints. Finally, the top footings were poured then cured in a preassembled formwork. The RMBE were stored for at least one month before testing.

4.3.3 Test Setup and Instrumentation

A newly upgraded 3000 kN servo controlled actuator was used to test the RMBE under constant displacement loading rate throughout the loading history up to failure. Consequently, this system allows capturing the stress-strain post-peak descending branch curve, which is essential to quantify the influence of different variables on the strain capacity of the RMBEs. The test was conducted at a displacement controlled rate of 0.003 mm/sec, and the corresponding load was recorded by a high precision load cell connected to control panel attached to a Vishay data acquisition system. The test was considered completed when the specimens reach 25% of its peak stress (75% stress degradation).

Figure 4.4(a) shows typical dimensions of the reinforced RMBE. It should be noted that the unreinforced RMBE specimens were constructed without the top and bottom footings. The total height of tested specimen is 1455 mm with an effective (gauge) length of 955 mm from the lower edge of the top footing to the upper edge of the bottom footing. Various precautions including a spherical head, two laser aligning devices, and two layers of high strength material at the top and bottom surfaces of the specimen, were taken to ensure the specimen leveling, verticality, alignment, and the uniform distribution of the applied load. Two rectangular steel plates, having high hardness coefficient, were used for transferring a uniformly distributed load from the actuator head to the test specimen.

At least one sample from each RMBE reinforced specimens was instrumented by strain gauges mounted on the vertical reinforcement bars at the specimen mid height. In all RMBE specimens, the load versus axial deformation behaviour of the tested region was measured using four Linear Variable Differential Transducers (LVDTs) that were attached (screwed) at the centerline of each side of the specimen as shown in Figure 4.4(b).

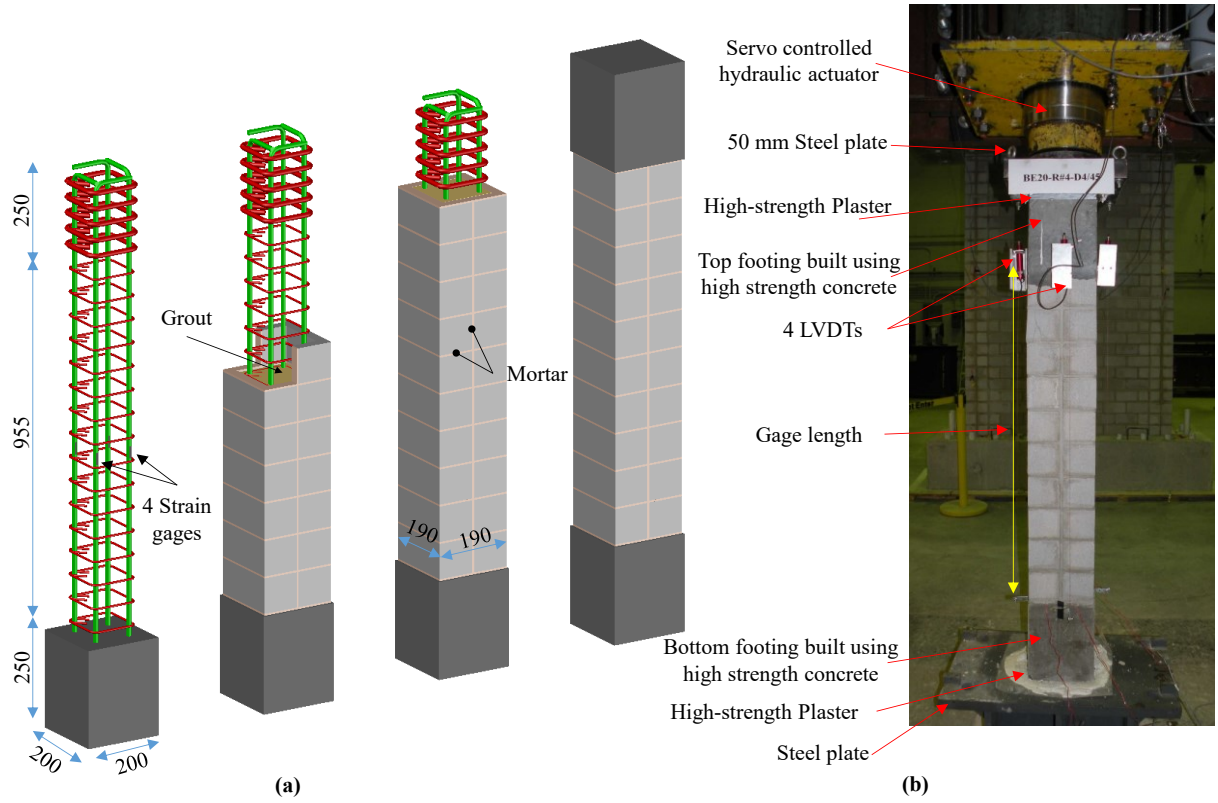

Figure 4.4 Schematic of the test set-up, RMBE components, and instrumentations (all dimensions are in mm)

4.3.4 Material Properties

The materials used for RMBE specimen's construction were: high strength concrete, steel reinforcement bar and deformed wires, C-shaped concrete masonry block, mortar, and grout (i.e. normal and high strength). All materials used for the construction are available in the Canadian market and were tested at the same time of testing the RMBE specimens. It should be noted that various pilot mixes have been conducted before the construction phase in order to adjust the concrete and grout strength. Moreover, various samples of the deformed wires and reinforcement

bars were tested to check the samples' yield stress and ductility. However, these data are not presented in the current study to avoid any confusion with the materials used in the construction.

Table 4.2 summarizes the compressive strength of the materials used for the construction of the RMBEs. The average of the concrete strength of the RC top and bottom footing was 83.8 MPa having a coefficient of variation (C.V. = 6.2%). C-shape half-scale concrete block units with 25 mm thickness 190 mm x 190 mm x 92.5 mm (width x length x depth) were used in RMBE specimens' construction. Fourteen coupons of half-scale concrete masonry blocks (100 mm x 50 mm x 25 mm) were tested under compressive loading as per ASTM C140 / C140M (2013). The average compressive strength of the 14 tested coupons was 22 MPa (C.V. = 13.8%). Pre-bagged type S mortar was used to join the masonry block units in the stacked bond as shown in Figure 4.4. An approximately 5 mm thickness mortar joints were used to meet the scaling requirements. A sample of 3 cubes was taken from each patch; fifteen mortar cubes in total were tested under compression at the time of the RMBE specimens testing. The average compressive strength of mortar cubes was 12.3 MPa (C.V. = 7.15%). All the RMBE specimens were fully grouted using two types of grout; pre-mixed fine grout and high strength grout having computed compressive strength of 15 MPa (C.V. = 8.7%) and 45 MPa (C.V. = 4.75%) according to CSA A179 (2004), respectively.

Standard deformed reinforcement steel bars, #3 and #4, were used for the vertical reinforcement and footing transversal reinforcement, whereas deformed wires D4 were used for hoops. Tension test was performed on steel samples of 600 mm long in order to measure the stress-strain of the tested samples. Figure 4.5 shows the stress-strain behaviour of the tested samples. An Epsilon extensometer having 200 mm gauge length and 50 mm stroke was used to measure the deformation. The observed average yield strength of #3 and #4 was 455 MPa and 482 MPa, respectively, whereas the computed proof yield strength of D4 was 600 MPa. A clear yield region did not exist for the steel deformed wire (D4). Therefore, for D4 tested samples the proof yield strength was defined corresponding to a 0.2% strain.

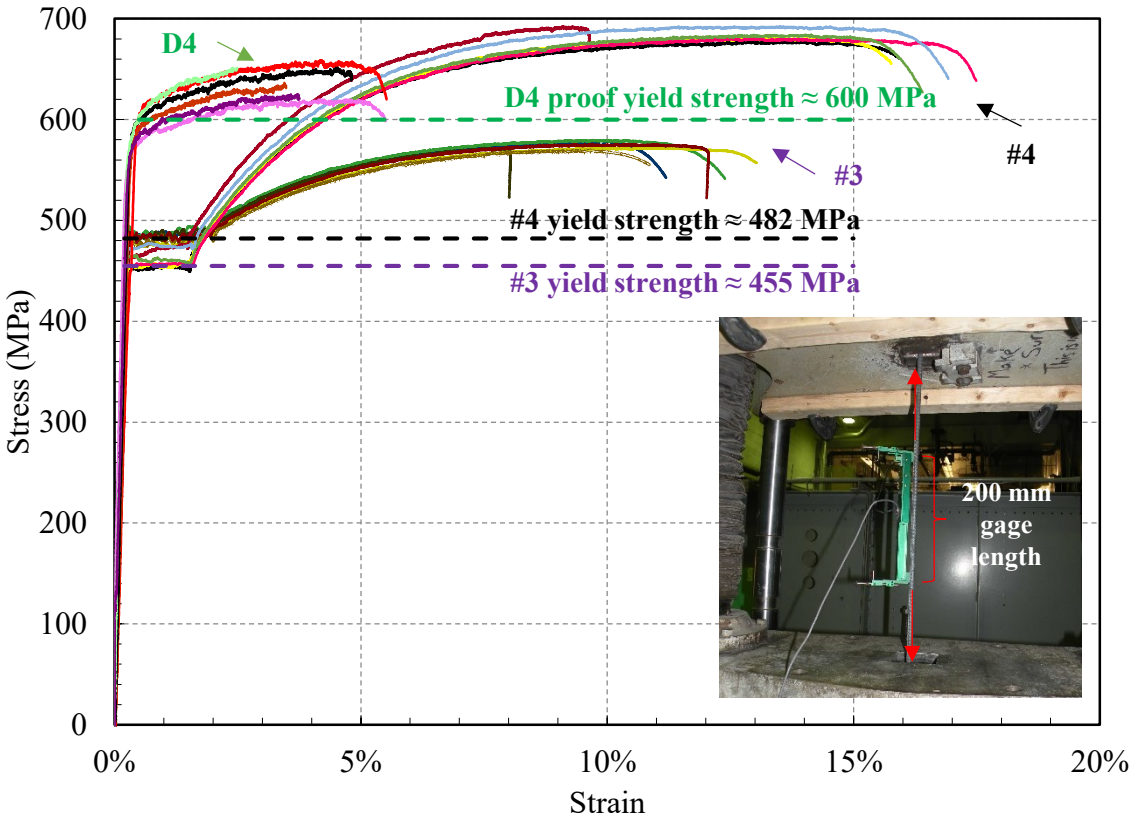

Figure 4.5 Stress-strain relationship for the reinforcement steel bars (#3 & #4) and deformed wire (D4) used in the construction of the RMBE

4.4 Experimental Results

The compression stress-strain curves for all RMBE specimens are presented in Figures 4.6, 4.7 and 4.8. It should be noted that the stress was computed by dividing the measured load by the RMBE gross cross-sectional area (190×190 mm^2). Also, the strain was calculated by dividing the average of the four LVDTs readings by the gauge length (i.e. 955 mm). Table 4.3 shows the experimental results of the peak stress (f_{max}), strain at the peak stress (ε_{max}), strain at 75% of the peak stress (ε_{75}), strain at 50% of the peak stress (ε_{50}), and strain ductility ($\mu_{\varepsilon 50}$) of the RMBE. The following paragraphs analyze the stress enhancement in RMBE to evaluate the effect of the studied parameters.

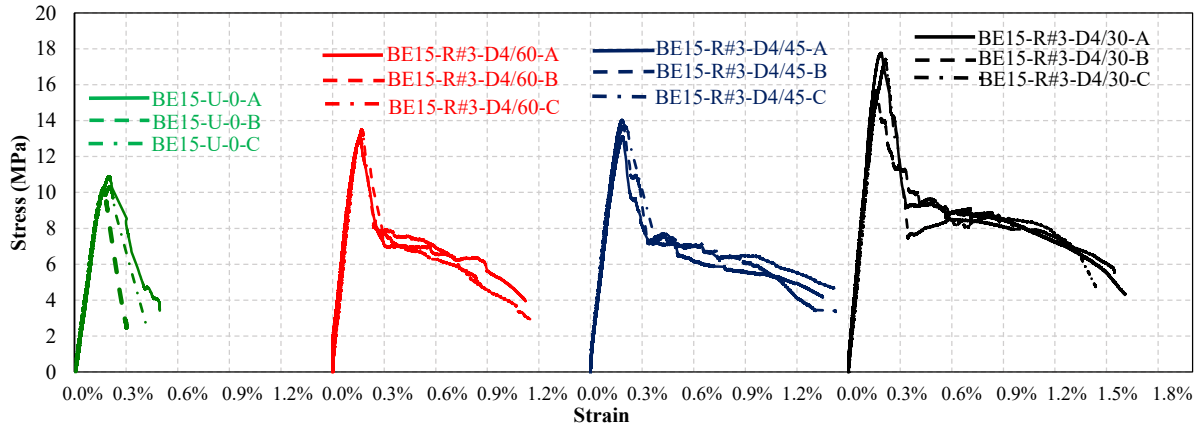

Figure 4.6 Observed compression stress–strain relationship for vertically reinforced units with #3 bars having different confinement ratios

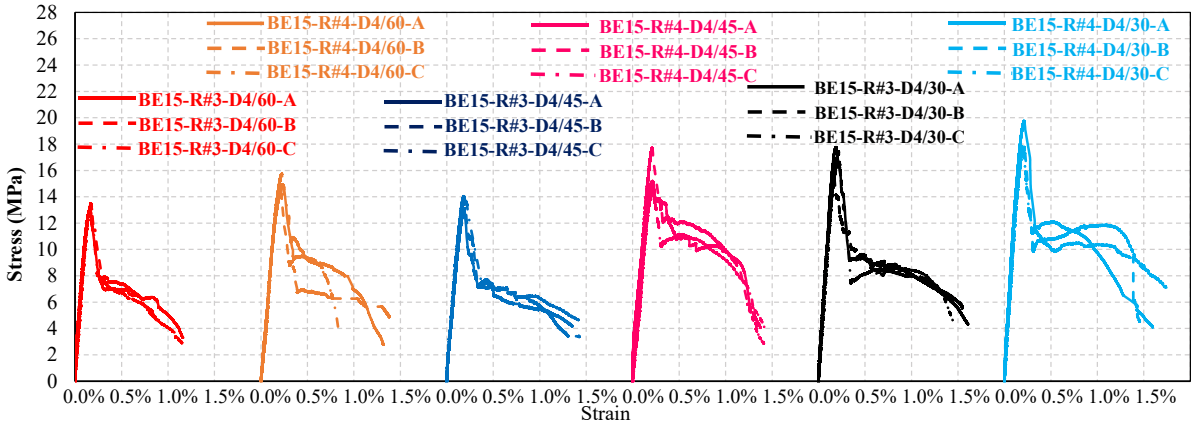

Figure 4.7 Observed compression stress–strain relationship for vertically reinforced units with #4 bars having different confinement ratios

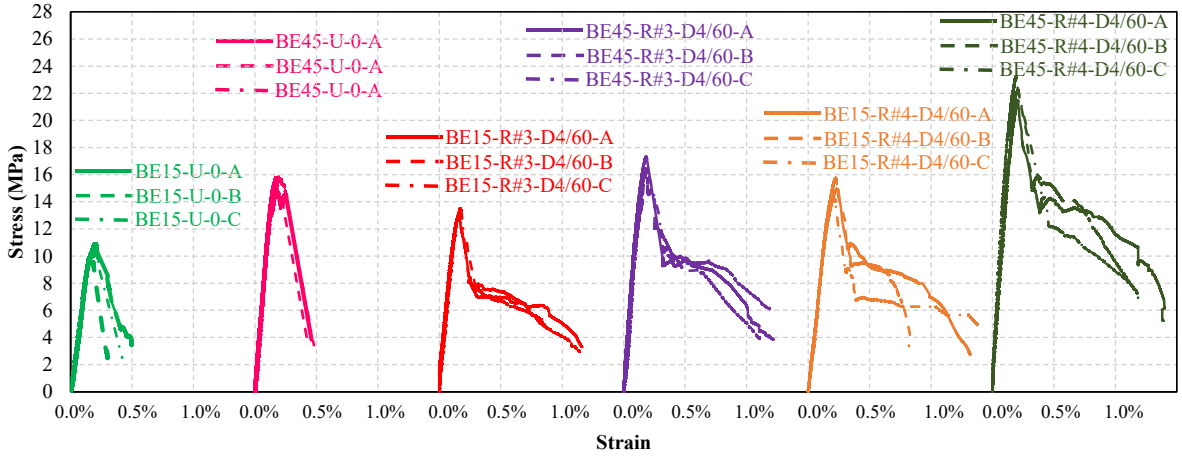

Figure 4.8 Observed compression stress–strain relationship for RMBE having same confinement ratio, vertically reinforced with #3, and constructed with grout having 15 and 45 MPa ultimate strength

4.4.1 RMBE stress results

Figure 4.6 shows the observed compression stress-strain curves of three specimens in four RMBE groups: BE15-U-0, BE15-R#3-D4/60, BE15-R#3-D4/45 and BE15-R#3-D4/30. The first group presents the compression stress-strain of un-reinforced un-confined RMBE grouted with normal strength grout. On the other hand, the other three groups present the stress-strain behaviour of RMBE specimens having #3 vertical reinforcement bars, grouted with normal strength grout, and having different spaces between transversal hoops (i.e. various confinement ratios). It can be observed from Figure 4.6 that the RMBE peak stress increased as the confinement ratio increased. The RMBE stress at peak increased by 25%, 29%, 61%, compared to BE15-U-0 peak stress, for BE15-R#3-D4/60, BE15-R#3-D4/45, and BE15-R#3-D4/30, respectively. As the hoop spacing decreased the lateral confinement imposed by the transverse reinforcement increased which postponed the vertical reinforcement bar buckling and thus increased the RMBE compressive capacity. However, it should be noted that the contribution of the vertical bars to the RMBE compression capacity is approximately 2.5 MPa if strain compatibility is assumed between the vertical reinforcement and the masonry. Therefore, the presence of vertical reinforcement increased the RMBE capacity by about 24% compared to un-reinforced boundary element. Subsequently, the RMBE stress at peak increased by 1%, 5%, 37%, compared to BE15-U-0 plus four #3 reinforcement bars, for BE15-R#3-D4/60, BE15-R#3-D4/45, and BE15-R#3-D4/30, respectively.

Moreover, it can be observed from Figure 4.6 that the stress-strain curve of the un-reinforced specimens, BE15-U-0, have two branches; rising curve up to the peak stress and descending post-peak curve. However, the reinforced groups, BE15-R#3-D4/60, BE15-R#3-D4/45, and BE15-R#3-D4/30, have three branches: rising curve up to the peak stress, followed by a sudden drop curve and a descending curve. The sudden drop in the RMBE was mainly attributed to the face-shell spalling of the C-shape concrete block which resulted in 40~50% loss of the RMBE peak stress. However, the RMBE lost at least 55% of the cross-sectional area after spalling of block face shell. Moreover, the vertical bar buckling could have also contributed to this sudden drop, especially in RMBE having large hoop spacing.

Figure 4.7 shows the observed compression stress-strain curves of six RMBE groups: BE15-R#3-D4/60, BE15-R#4-D4/60, BE15-R#3-D4/45, BE15-R#4-D4/45, BE15-R#3-D4/30, and BE15-R#4-D4/30. All groups had similar grout strength. The effect of changing the vertical

reinforcement ratio was investigated for three hoop spacing. It can be observed that the RMBE peak stress increased by 42%, 51%, 75%, compared to BE15-U-0 peak stress, for BE15-R#4-D4/60, BE15-R#4-D4/45, and BE15-R#4-D4/30, respectively. However, it should be noted that the vertical bars increased the RMBE capacity by approximately 4.5 MPa assuming strain compatibility (i.e. 42% enhancement compared to unreinforced boundary element). Subsequently, the RMBE stress at peak increased by 0%, 9%, 33%, compared to BE15-U-0 plus four #4 reinforcement bars, for BE15-R#4-D4/60, BE15-R#4-D4/45, and BE15-R#4-D4/30, respectively. Therefore, increasing the vertical reinforcement bar size from #3 to #4 did not boost the enhancement in the stress due to the confinement of the transverse hoops. The same finding could be obtained by comparing the RMBE reinforced with #4 to those reinforced with #3 vertical bars.

Figure 4.8 shows the observed compression stress-strain curves of three specimens in six RMBE groups: BE15-U-0, BE45-U-0, BE15-R#3-D4/60, BE45-R#3-D4/60, BE15-R#4-D4/60, and BE45-R#4-D4/60. The first and second groups present the compression stress-strain of un-reinforced un-confined RMBE grouted with normal and high strength grout, respectively. The third and fifth groups show the compression stress-strain of RMBE specimens having #3 vertical reinforcement bars and grouted with normal and high strength grout, respectively. Whereas, the fourth and sixth groups present the compression stress-strain of RMBE specimens having #4 vertical reinforcement bars, and grouted with normal and high strength grout, respectively. It can be observed from Figure 4.8 that as the grout strength increased, the RMBE peak stress increased. As such, the BE45-U-0, BE45-R#3-D4/60, and BE45-R#4-D4/60 RMBE specimens exhibited an increase in peak stress by 48%, 27%, 49%, compared to BE15-U-0, BE15-R#3-D4/60, and BE15-R#4-D4/60, respectively. It should be noted that the RMBE capacity did not increase proportionally to the grout strength based on the grout area and this observation was clearly reported by Drysdale and Hamid (2005).

4.4.2 Damage propagation

The damage propagation of un-reinforced specimens, i.e. BE15-U-0 and BE45-U-0, was characterized by surface hair cracks followed by sudden splitting in the RMBE at the onset of the peak-load [see Figure 4.9(a)]. On the other hand, the reinforced RMBE damage propagation was characterized by the formation of surface hair cracks, these cracks increased in size and length,

followed by spalling of RMBE face shell, yielding and buckling of longitudinal bars and finally crushing the grout core [see Figure 4.9 (b,c)].

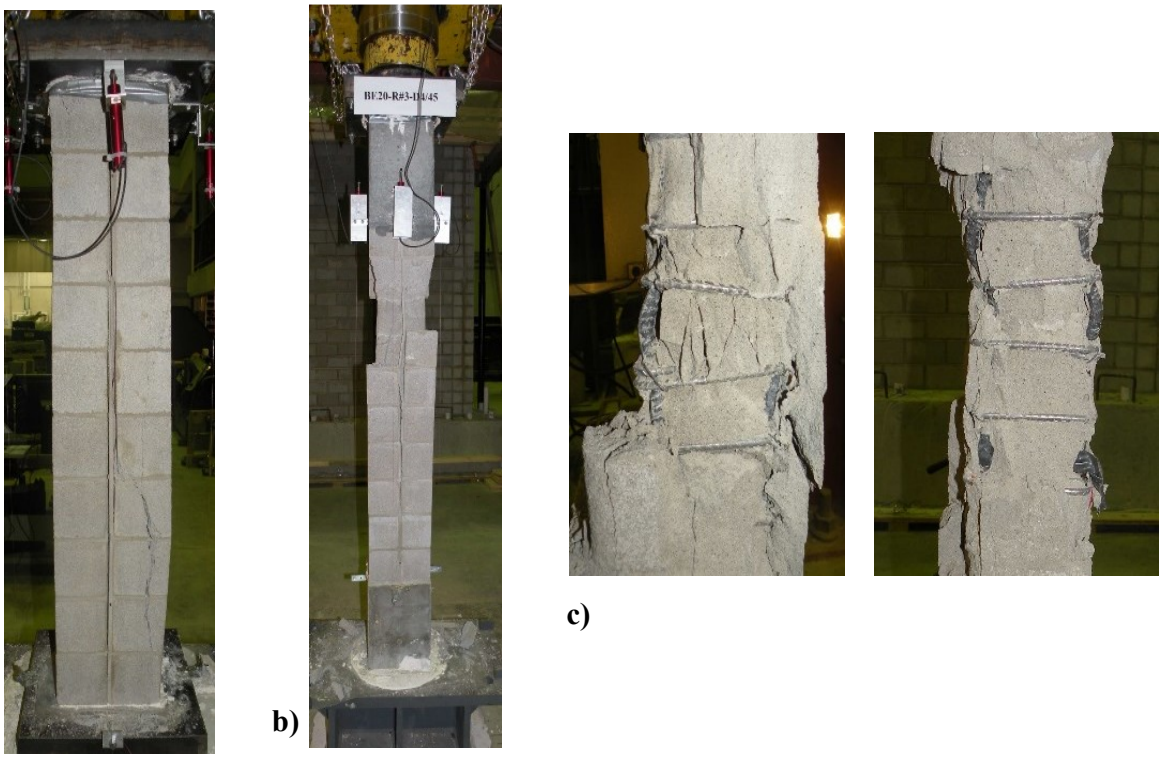

Figure 4.9 RMBE boundary elements damage: a) splitting of un-reinforced specimen, b) face shell spalling RMBE at 25% stress degradation, c) buckling of reinforcement bars

4.4.3 Reinforcement-strain Readings

Figure 4.10 presents a sample of the recorded strain in the longitudinal bars versus the axial strain computed from the four LVDTs that were externally mounted on the RMBE specimens. It can be observed that concrete-reinforcement strain compatibility was achieved up to approximately 0.2% axial strain, which corresponds to the RMBE peak stress. Beyond the strain at the RMBE peak stress, the axial strain computed from the LVDT was not similar to the strain in the longitudinal bars. This could be a result of initiation of partial debonding between the longitudinal bars and the surrounding grout. Buckling of longitudinal reinforcement was observed in RMBE specimens with widely spaced hoops after 50% of peak stress (see Figure 4.9). On the other hand, the RMBE specimens with closely spaced hoops show longitudinal reinforcement bars buckling at higher axial strain values. Hoops rupture was not observed in any of the RMBE specimens over the complete loading history.

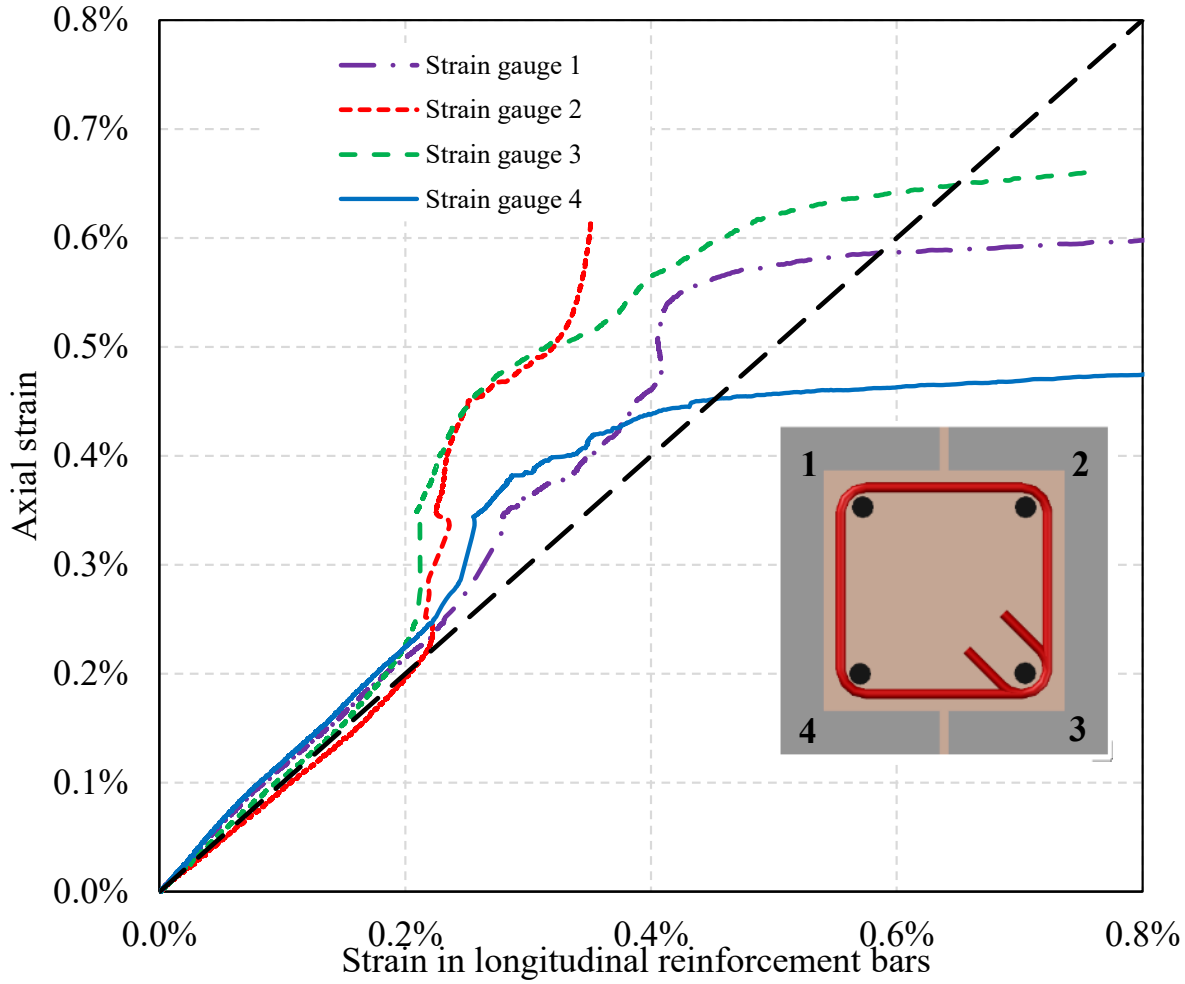

Figure 4.10 Strain in vertical reinforcement bars versus the RMBE axial strain computed from the LVDTs

4.4.4 RMBE axial strain ductility

Ductility is the ability of a material, a component or a system to sustain plastic deformations without an appreciable loss of strength. The RMBE compression strain ductility is defined as the ratio between the strain at 50% of the peak stress on the descending curve (ε_{50}) and the strain at the peak stress (ε_{max}), as shown in Table 4.3. The normalized stress-strain relationship presented in Figure 4.11 shows clearly that the RMBE ductility and the post peak slope enhances by decreasing the hoop spacing, increasing the grout strength and increasing the vertical reinforcement ratio.

Table 4.3 Summary of the experimental results of the RMBEs

RMBE ID	Maximum stress (MPa)		Strain at peak stress, ε_{max}		Strain at 75% of the peak stress, ε_{75}		Strain at 50% of the peak stress, ε_{50}		Strain ductility, $\mu_{\varepsilon 50}$
	f_{max}	Average (C.V. %)	ε_{max}	Average (C.V. %)	ε_{75}	Average (C.V. %)	ε_{50}	Average (C.V. %)	$\varepsilon_{50}/\varepsilon_{max}$
BE15-U-0-A	10.88	10.55 (2.77%)	0.00195	0.00180 (7.91%)	0.0022	0.00210 (4.30%)	0.0037	0.0030 (19.05%)	1.62
BE15-U-0-B	10.26		0.00171		0.0023		0.0027		
BE15-U-0-C	10.35		0.00200		0.0023		0.0032		
BE15-U-0-D	10.7		0.00174		0.0021		0.0024		
BE45-U-0-A	15.17	15.61 (2.44%)	0.00180	0.00175 (6.10%)	0.0027	0.00220 (3.57%)	0.0030	0.0032 (6.25%)	1.81
BE45-U-0-B	15.83		0.00170		0.0028		0.0034		
BE45-U-0-C	15.83		0.00192		0.0029		0.0032		
BE15-R#3-D4-30-A	17.78	16.97 (6.57%)	0.00195	0.0020 (6.61%)	0.0029	0.00280 (3.57%)	0.0080	0.0090 (11.11%)	4.50
BE15-R#3-D4-30-B	15.7		0.00190		0.0027		0.0100		
BE15-R#3-D4-30-C	17.44		0.00215		0.0028		0.0090		
BE15-R#3-D4-45-A	13.14	13.64 (3.38%)	0.00180	0.00179 (2.01%)	0.0025	0.00250 (4.00%)	0.0060	0.0069 (11.18%)	3.82
BE15-R#3-D4-45-B	14.05		0.00182		0.0026		0.0070		
BE15-R#3-D4-45-C	13.73		0.00175		0.0024		0.0075		
BE15-R#3-D4-60-A	13.08	13.2 (2.12%)	0.00156	0.00162 (4.45%)	0.0022	0.00233 (6.55%)	0.0066	0.0061 (7.51%)	3.77
BE15-R#3-D4-60-B	13		0.00160		0.0025		0.0057		
BE15-R#3-D4-60-C	13.52		0.00170		0.0023		0.0060		
BE15-R#4-D4-30-A	19.76	18.45 (6.15%)	0.00220	0.00218 (3.50%)	0.0031	0.00310 (3.23%)	0.0130	0.0124 (9.36%)	5.65
BE15-R#4-D4-30-B	17.78		0.00210		0.0030		0.0110		
BE15-R#4-D4-30-C	17.81		0.00225		0.0032		0.0130		
BE15-R#4-D4-45-A	15.21	15.92 (9.84%)	0.00214	0.00208 (3.47%)	0.0030	0.00290 (3.45%)	0.0090	0.0096 (6.30%)	4.60
BE15-R#4-D4-45-B	17.72		0.00200		0.0029		0.0095		
BE15-R#4-D4-45-C	14.84		0.00210		0.0028		0.0102		
BE15-R#4-D4-60-A	14.95	15.02 (4.61%)	0.00200	0.00201 (4.74%)	0.0028	0.00272 (2.81%)	0.0085	0.0075 (11.13%)	3.76
BE15-R#4-D4-60-B	14.37		0.00191		0.0027		0.0070		
BE15-R#4-D4-60-C	15.75		0.00210		0.0026		0.0071		
BE45-R#3-D4-60-A	17.32	16.72 (3.13%)	0.00181	0.00181 (3.04%)	0.0023	0.00260 (11.54%)	0.0076	0.0079 (13.23%)	4.33
BE45-R#3-D4-60-B	16.42		0.00176		0.0026		0.0070		
BE45-R#3-D4-60-C	16.41		0.00187		0.0029		0.0090		
BE45-R#4-D4-60-A	21.48	22.31 (3.81%)	0.00210	0.00213 (2.71%)	0.0032	0.00307 (4.98%)	0.0110	0.0095 (14.03%)	4.45
BE45-R#4-D4-60-B	22.26		0.00220		0.0031		0.0090		
BE45-R#4-D4-60-C	23.18		0.00210		0.0029		0.0085		

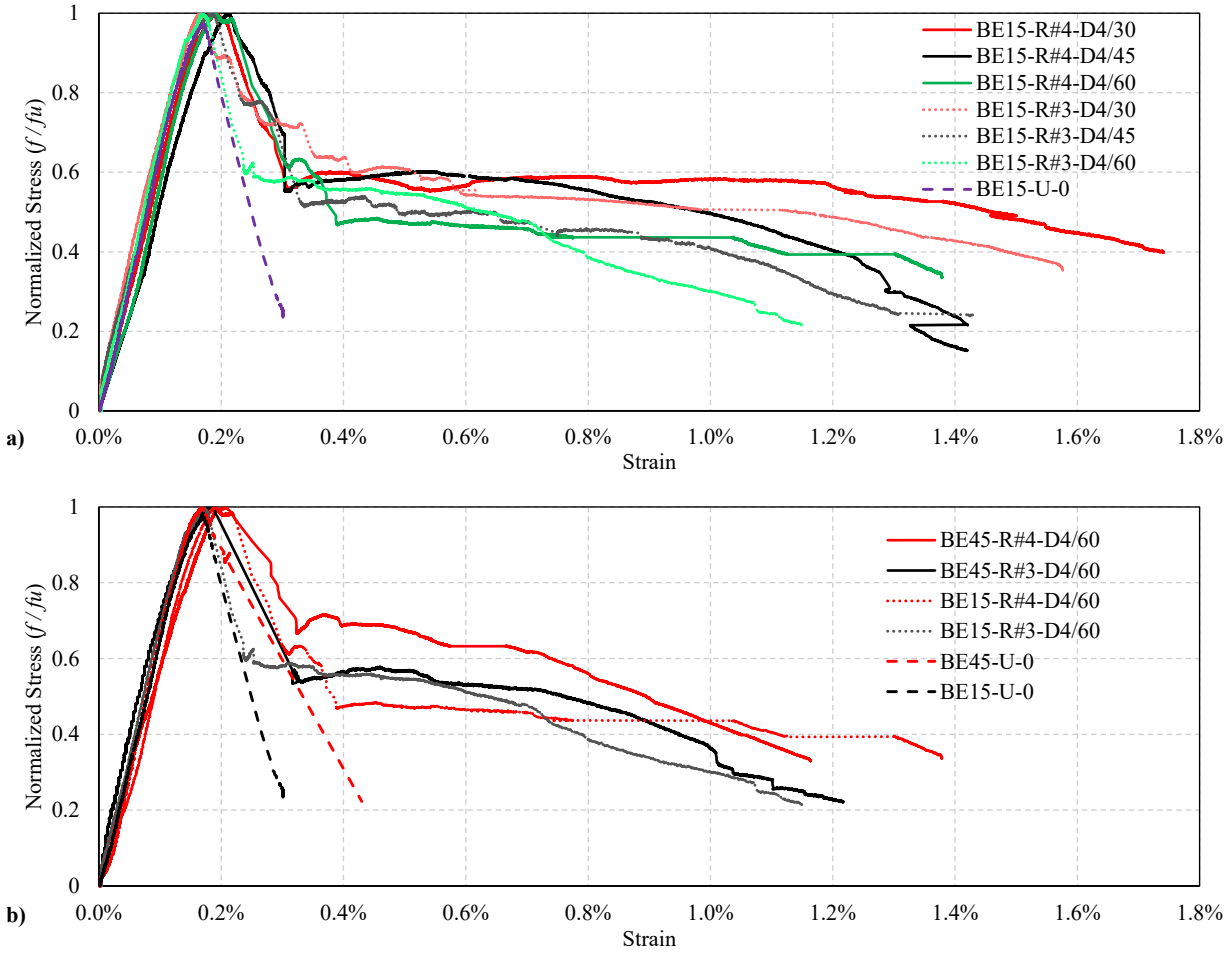

Figure 4.11 Normalized compression stress-strain curves RMBE

4.5 Influence of Test Variables on the RMBE Response

4.5.1 Confinement Ratio of Transverse Reinforcement

The effect of the amount of transverse confining steel on the compression stress-strain behaviour of the RMBE is well observed in the post peak branch as shown in Figure 4.11(a). The RMBE specimens with high confinement ratio exhibited more gradual post-peak stress-strain curve compared to those with low confinement ratio. It can be seen that the confinement ratio of lateral reinforcement had a slight effect on the stress-strain curve in the elastic stage. An increase in the RMBE peak stress was observed by decreasing the hoop spacing. As such, the average RMBE peak stress increased from 13.2 to 16.9 MPa and from 15.0 to 18.4 MPa when decreasing the hoop spacing from 60 to 30 mm for RMBE reinforced with #3 and #4 vertical bars,

respectively. Decreasing the hoop spacing, for samples reinforced with #3 and #4 vertical bars, from 60 to 30mm resulted in corresponding increase in the RMBE strain ε_{75} by 20 and 14%, respectively. Moreover, an increase in the strain ε_{50} by 48 and 65% was observed when decreasing the hoop spacing from 60 to 30, for RMBE reinforced with #3 and #4 vertical bars, respectively.

4.5.2 Amount of Longitudinal Reinforcement

The increase in the longitudinal reinforcement had no effect on the strength of the confined core, however it increased the capacity of the RMBE in proportion to the added vertical steel area. On the contrary, it enhanced the post-peak strain capacity of the RMBE. Figure 4.11(a) presents the three different pairs of RMBE specimens having different vertical reinforcement ratio and same hoop spacing and grout strength. From the figure, it can be seen that RMBEs having #4 bars as vertical reinforcement showed an increase in the strain capacities by 11% to 16% and 23% to 38% more than that of the RMBEs having #3 bars at 75% and 50% of peak stress, respectively. Comparing BE45-R#4-D4-60 to BE45-R#3-D4-60 [Figure 4.11(b)], it could be concluded that the aforementioned enhancement in strain capacities slightly increases with the increase in the grout strength.

4.5.3 Grout Compressive Strength

Increasing the grout strength, for a given hoop spacing (i.e. 60mm), from 15 to 45 MPa resulted in a corresponding increase in the RMBE peak stress by 27 and 49% for samples having #3 and #4 vertical bars, respectively. The stress-strain behaviour of RMBE specimens having the same confinement ratio and the amount of longitudinal reinforcement ratio but different grout strength is presented in Figure 4.11(b). It can be observed from Figure 4.11(b) that as the vertical reinforcement ratio increases the grout strength had more noticeable effect on the RMBE stress-strain response.

4.6 Correlation between the Test Parameters and Stress-Strain Response

Figure 4.12 presents the relation between the confinement ratio, vertical reinforcement ratio, and grout strength, versus the "confined RMBE peak stress normalized to the unreinforced unconfined RMBE peak stress ratio, $f_{max\text{-}c}/f_{max\text{-}un}$". Figure 4.12(a) shows that the confinement

ratio increases the axial peak stress of the RMBEs reinforced by #3 and #4 in the range of 1.23 to 1.69 and 1.36 to 1.87 times, respectively, compared to the unreinforced unconfined boundary elements. In contrast, the vertical reinforcement ratio introduces an increase in axial peak stress of the RMBEs constructed with 15 MPa and 45 MPa strength in the range of 1.24 to 1.49 and 1.58 to 2.20 times, respectively, compared to the unreinforced unconfined boundary elements as shown in Figure 4.12(b). Finally, Figure 4.12(c) shows that increasing the grout strength from 15 MPa to 45 MPa exhibited an increase in axial peak stress of the RMBEs reinforced by #3 and #4 in the range of 1.23 to 1.64 and 1.36 to 2.20 times, respectively, compared to the unreinforced unconfined RMBEs.

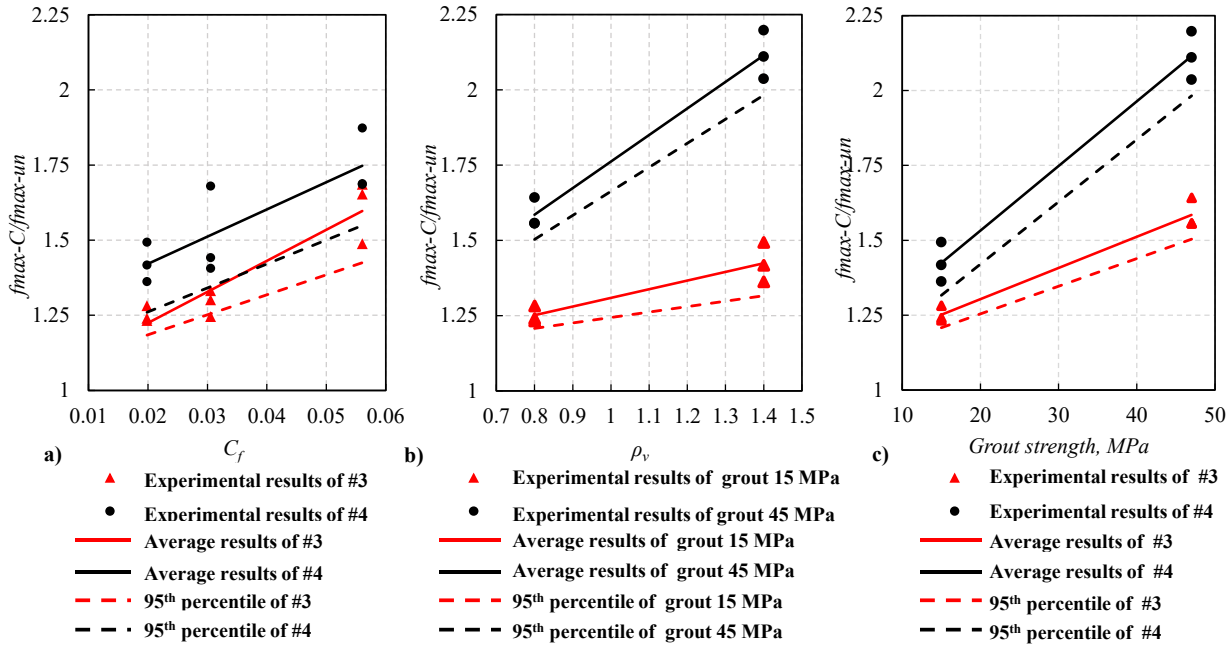

Figure 4.12 Correlation between the strength enhancement ratio and the: a) confinement ratio b) vertical reinforcement ratio, and c) grout strength

Figure 4.13 presents the relation between the confinement ratio of lateral reinforcement and the strain at peak stress, strain at 75% of peak stress, and strain at 50% of peak stress for the RMBEs constructed with 15 MPa grout strength. The effect of confinement reinforcement is more pronounced on the post peak behaviour. An increase in the confinement reinforcement provided a slight increase in the strain at peak stress of the RMBEs reinforced by #3 and #4 in the range of 1 to 1.2 and 1.06 to 1.25 times, respectively, compared to the unreinforced unconfined boundary elements as shown in Figure 4.13(a). However, an increase in the strain at 75% of peak stress was in the range of 1.05 to 1.38 and 1.26 to 1.53 times for the RMBE

reinforced by #3 and #4 due to the confinement compared to the unreinforced unconfined boundary elements as shown in Figure 4.13(b). Figure 4.13(c) shows that the confinement reinforcement increases the strain at 50% of peak stress of the RMBE reinforced by #3 and #4 in the range of 1.9 to 3.33 and 2.33 to 4.33 times, respectively, compared to the unreinforced unconfined boundary elements.

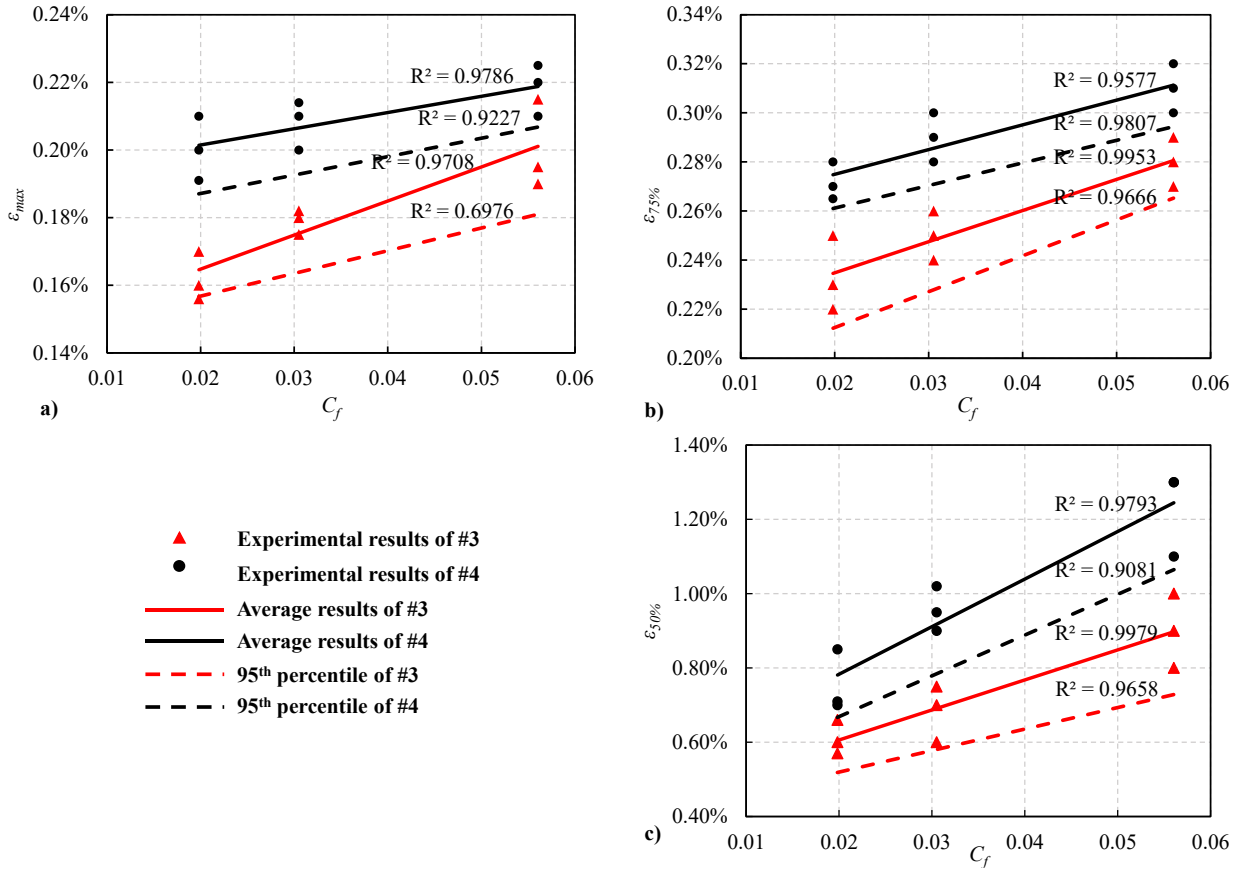

Figure 4.13 Correlation between the confinement ratio for the specimens reinforced vertically by #3 and #4, constructed with normal strength grout and the strain at: a) maximum, b) 75%, and, c) 50% of maximum stress

Figure 4.14 presents the relation between the vertical reinforcement ratio and the strain at peak stress, strain at 75% of peak stress, and strain at 50% of peak stress for the RMBEs constructed with 15 MPa and 45 MPa grout strength. The vertical reinforcement ratio provides an increase in strain at peak stress of the RMBE built with 15 MPa and 45 MPa strength in the range of 1 to 1.16 and 1.01 to 1.26 times, respectively, compared to the unreinforced unconfined RMBEs as shown in Figure 4.14(a). Whereas, an increase in strain at 75% of peak stress due to

the increase in vertical reinforcement ratio was in the range of 1.05 to 1.34 and 1.05 to 1.45 times for the RMBE constructed with 15 MPa and 45 MPa strength compared to the unreinforced unconfined boundary elements as shown in Figure 4.14(b). Figure 4.14(c) indicates that the strain at 50% peak stress gain increases for the RMBE constructed with 15 MPa and 45 MPa strength in the range of 1.66 to 2.83 and 2.18 to 3.44 times, respectively, compared to the unreinforced unconfined boundary elements. It can be observed from Figures 4.13 and 4.14 that the confinement ratio, vertical reinforcement ratio, and grout strength have a more pronounced effect on the post peak behaviour, however, have slightly effect on the ascending curve.

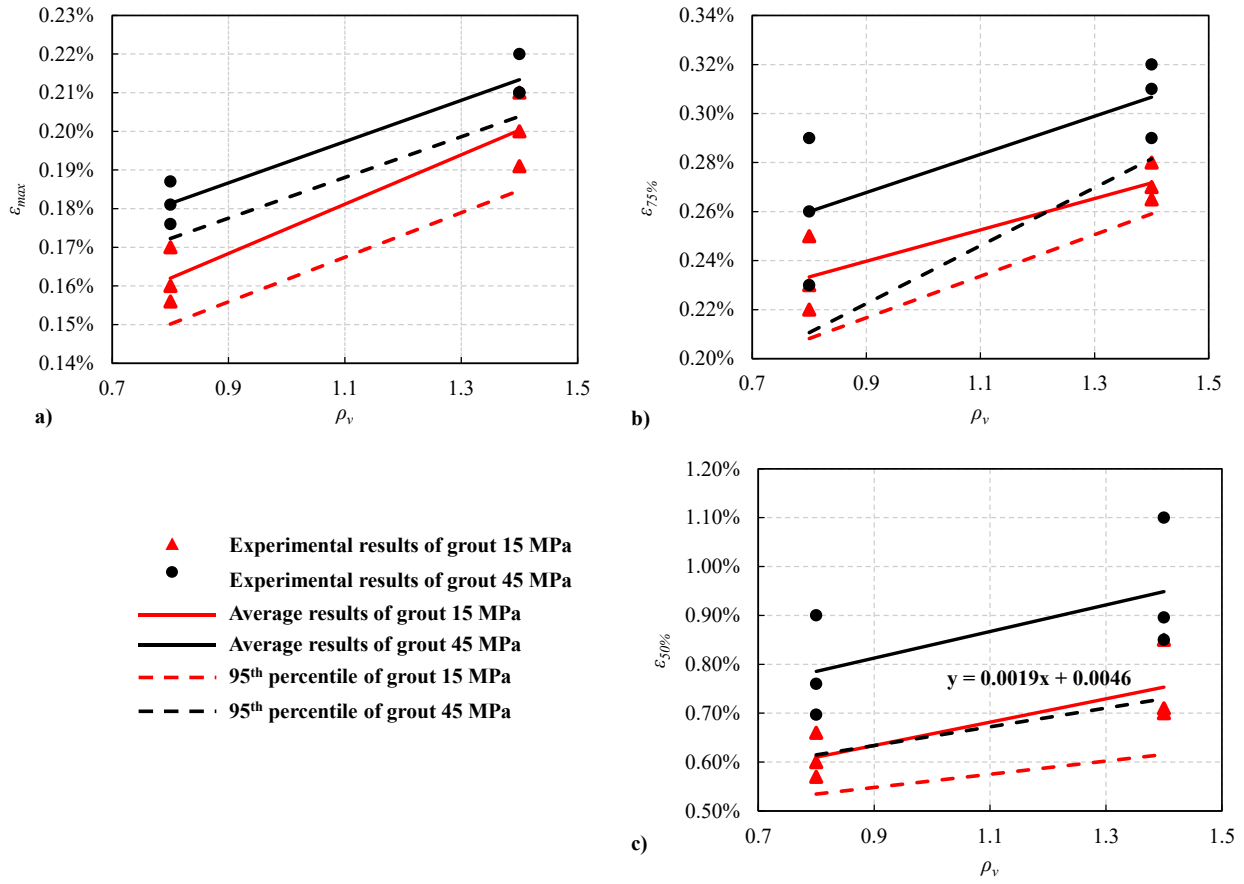

Figure 4.14 Correlation between the vertical reinforcement ratio for the specimens constructed with normal and high strength grout and the strain at: a) maximum, b) 75%, and, c) 50% of maximum stress

4.7 Comparisons with Existing Predictive Models

In this section, three stress-strain predictive models, proposed by Mander et al. (1988), Priestley and Elder (1983), and Abo El Ezz et al. (2015), are presented and compared to the observed stress-strain response of the tested RMBEs. It should be noted that for the models proposed by Mander et al. (1988), and Priestley and Elder (1983), the vertical reinforcement bars contribution to the RMBE resistance was considered by assuming elastic-perfect plastic response. Therefore, by assuming strain compatibility the reinforcement stress-strain curve was superimposed to the confined and unconfined masonry models, then it was compared with the experimental data. However, this was not the case for the model proposed by Abo El Ezz et al. (2015) where the reinforcement contribution and the effect of confinement is smeared over the RMBE cross-section.

4.7.1 Mander et al. model

Mander et al. (1988) proposed a stress-strain model for unconfined and confined concrete material. The effective lateral confinement pressure is computed and presented by effective confinement coefficient, k_e. Mander et al. (1988) model is a function of the confined area between longitudinal bars, the confined area between hoops, dimensions of the confined core, the number of vertical bars, and the volumetric ratio of lateral reinforcement to concrete core. Mander et al. (1988) proposed an expression representing both ascending and descending branches of the stress-strain curve and which is presented in Eqs. 4.2 to 4.10 as follows:

$$f_c = \frac{f'_{cc}\, x\, r}{r - 1 + x^r} \qquad \text{Eq. 4.2}$$

$$x = \frac{\varepsilon_c}{\varepsilon_{cc}} \qquad \text{Eq. 4.3}$$

$$\varepsilon_{cc} = \varepsilon_{co}\left[1 + 5\left(\frac{f'_{cc}}{f'_{co}} - 1\right)\right] \qquad \text{Eq. 4.4}$$

$$r = \frac{E_c}{E_c - E_{sec}} \qquad \text{Eq. 4.5}$$

$$E_c = 5{,}000\sqrt{f'_{c0}} \qquad \text{Eq. 4.6}$$

$$E_{sec} = f_{cc}^{'} / \varepsilon_{cc} \qquad \text{Eq.4.7}$$

$$f_{cc}^{'} = f_{co}^{'}\left(-1.254 + 2.254\sqrt{1 + \frac{7.94 f_i^{'}}{f_{co}^{'}}} - 2\frac{f_i^{'}}{f_{co}^{'}}\right) \qquad \text{Eq. 4.8}$$

for the rectangular sectional column; $f_{l\,y}^{'} = \frac{1}{2} k_e \, \rho_s \, f_{yh}$ Eq. 4.9

$$k_e = \frac{\left(1 - \sum_{i=1}^{n} \frac{\left(w_i^{'}\right)^2}{6 b_c d_c}\right)\left(1 - \frac{s'}{2 b_c}\right)\left(1 - \frac{s'}{2 d_C}\right)}{1 - \rho_{cc}} \qquad \text{Eq. 4.10}$$

Where; f_c is the longitudinal compressive concrete stress; ε_c is the longitudinal compressive concrete strain; $f_{cc}^{'}$ is the maximum concrete stress; ε_{cc} is the strain corresponding to the maximum concrete stress; $f_{c0}^{'}$ is the unconfined concrete peak stress; ε_{c0} is the strain corresponding to the unconfined concrete peak stress; $f_i^{'}$ is the effective lateral confining pressure; ρ_s is the ratio of volume of transverse confining steel to volume of confined concrete core; f_{yh} is the yield strength of the transverse reinforcement; k_e is the confinement effectiveness coefficient; ρ_{cc} is the ratio of longitudinal reinforcement area to area of core of section; $s^{'}$ is the clear vertical spacing between spiral or hoop bars; b_c and d_c are the core dimensions to centerlines of perimeter hoop in x and y directions, respectively, where $b_c \geq d_c$; n is the number of longitudinal bars; and $w_i^{'}$ is the closest clear space between adjacent longitudinal bars.

4.7.2 Priestley and Elder model

Priestley and Elder (1983) built on the modified Kent–Park model proposed by Scott et al. (1982) to investigate the compression stress-strain relationship of the unconfined and confined grouted concrete masonry block. The unconfined curve consists of two branches; a parabolic rising curve and a linear falling branch and are presented in Eqs. 4.11 to 4.13 as follows;

- Parabolic rising curve

$$f_m = 1.067 f_m^{'}\left[\frac{2\varepsilon_m}{0.002} - \left(\frac{\varepsilon_m}{0.002}\right)^2\right] \text{ for } \varepsilon_m \leq 0.0015 \qquad \text{Eq. 4.11}$$

- Falling branch

$$f_m = f_m^{'}\left[1 - Z_m\left(\varepsilon_m - 0.0015\right)\right] \text{ for } \varepsilon_m > 0.0015 \quad \text{Eq. 4.12}$$

$$\text{where, } z_m = \frac{0.5}{\frac{3 + 0.29 f_m^{'}}{145 f_m^{'} - 1000} - 0.002} \quad \text{Eq. 4.13}$$

On other hand the confined curve consists of three branches; a parabolic rising curve, a linear falling branch, and a final horizontal plateau and are presented in Eqs. 4.14 to 4.17 as follows:

- Parabolic rising curve

$$f_m = 1.067 K f_m^{'}\left[\frac{2\varepsilon_m}{0.002K} - \left(\frac{\varepsilon_m}{0.002K}\right)^2\right] \text{ for } \varepsilon_m \le 0.002\text{K} \quad \text{Eq. 4.14}$$

$$\text{where, } K = 1 + \left(\frac{\rho_s f_{yh}}{f_m^{'}}\right) \quad \text{Eq. 4.15}$$

- Falling branch

$$f_m = K f_m^{'}\left[1 - Z_m\left(\varepsilon_m - 0.002K\right)\right] \quad \text{Eq. 4.16}$$

$$\text{Where, } z_m = \frac{0.5}{\frac{3 + 0.29 f_m^{'}}{145 f_m^{'} - 1000} + \frac{3}{4}\rho_s\sqrt{\frac{h^{''}}{s_h}} - 0.002K} \quad \text{Eq. 4.17}$$

- Horizontal plateau

f_m is assumed equivalent to 0.2 $f_m^{'}$

Where f_m is the compressive stress of the masonry; $f_m^{'}$ is the peak stress of unconfined masonry; ε_m is the axial compressive strain of the masonry; f_{yh} is the yield strength of hoop reinforcement; Z_m is the slope of the post-peak part of the stress-strain curve; ρ_s is the volumetric ratio of the confining steel; $h^{''}$ is the lateral dimension of confined core; and s_h is the longitudinal spacing of confining steel.

4.7.3 Abo El Ezz et al. model

Abo El Ezz et al. (2015) proposed a simplified smeared compression stress-strain relationship of fully grouted unconfined and confined RMBE built using standard concrete blocks. The simplified stress-strain model is based on the Kent and Park (1971) model. It should be noted that this model smear the effect of confinement and vertical reinforcement bar contribution to the RMBE stress-strain response over the RMBE cross-section. The model predictions were computed using Eqs. 4.18 to 4.19 as follows:

- Ascending curve for $\varepsilon_m \leq \varepsilon_{max-c}$

$$f_m = f_{(max-c)}\left(\frac{2\varepsilon_m}{\varepsilon_{max-c}} - \left(\frac{\varepsilon_m}{\varepsilon_{max-c}}\right)^2\right), f_{\max-c} = 1.15 f_{\max-r} \quad \text{Eq. 4.18}$$

- Descending curve for $\varepsilon_m > \varepsilon_{max-c}$

$$f_m = f_{max-c}\left(1 - Z_c\left(\varepsilon_m - \varepsilon_{max-c}\right)\right), Z = \frac{0.5}{\varepsilon_{50c} - \varepsilon_{max-c}} \quad \text{Eq. 4.19}$$

Where ε_m is the axial compressive strain of the masonry; $f_{\max-c}$ is peak stress for confined reinforced boundary element; $\varepsilon_{\max-c}$ is the strain at peak stress for confined reinforced boundary element; $\varepsilon_{\max-r}$ is the average peak stress of the vertically RMBEs; Z_c is the slope of the post-peak part of the stress-strain curve; and ε_{50c} is the strain at 50% of peak stress for the confined boundary element.

4.7.4 Stress-strain model predictions versus the experimental results

Mander et al. (1988) model was developed based on the experimental data of reinforced concrete columns, however, Priestley and Elder (1983) and Abo El Ezz et al. (2015) are computed based on the experimental results of masonry members constructed using standard blocks. Figure 4.15 shows that the above models overestimate the peak stress the strain at peak. Moreover, all the models significantly overestimated the strain corresponding to 75% (ε_{75}) and 50% (ε_{50}) of peak stress compared to the experimental results. It should be noted that the stress-strain model predictions, proposed by Abo El Ezz et al. (2015) were the closest to the

experimental observations, although this model does not account for changing the confined zone dimensions and the vertical bars effect on the core confinement. Figure 4.15 shows that none of the models was capable of predicting the drop in the stress-strain curve due to the face shell spalling. As such, these models should be used with caution when predicting the seismic response of RMSW with boundary elements.

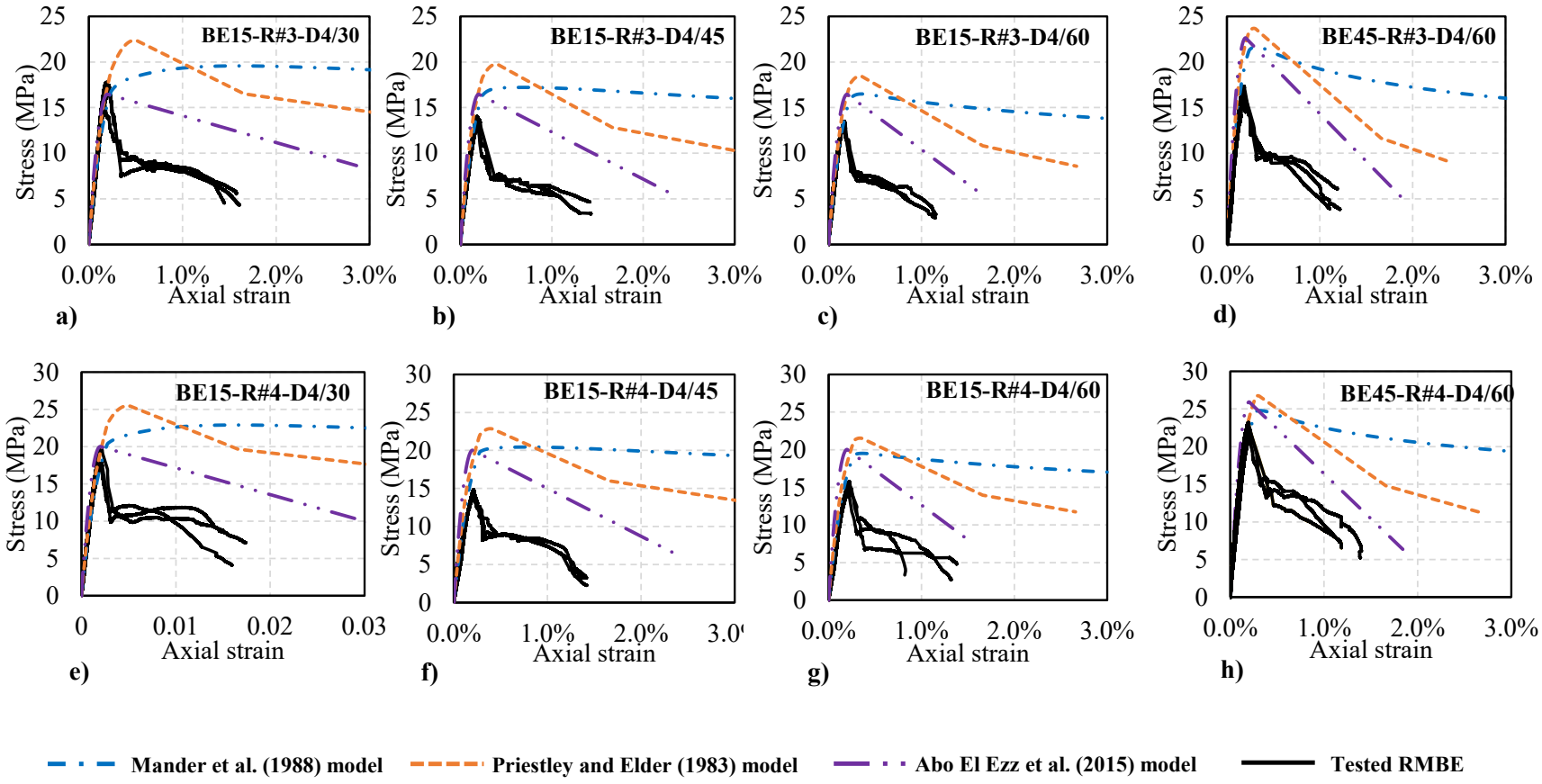

Figure 4.15 Comparison between the observed stress-strain relationship and three predictive models for RMBE: a) BE15-R#3-D4/30, b) BE15-R#3-D4/45, c) BE15-R#3-D4/60, d) BE45-R#3-D4/60, e) BE15-R#4-D4/30, f) BE15-R#4-D4/45, g) BE15-R#4-D4/60, and h) BE45-R#3-D4/60

4.8 Conclusions

This study presents the observed compressive stress-strain response of thirty half-scale C-shape reinforced masonry boundary elements (RMBEs) simulating the end zones of reinforced masonry shear walls. The influence of changing hoop spacing, vertical reinforcement ratio, and grout compressive peak stress was investigated by testing ten different RMBEs groups. The aim of this study is to provide the essential experimental data that quantifies the effect of these parameters on the compressive stress-strain response towards bridging the knowledge gap in this area.

The stress-strain curve of the un-reinforced boundary elements specimens was categorized by two zones, a rising curve until the peak stress followed by almost a linear decay up to failure. However, the stress-strain curve of the confined RMBE is characterized by three zones: a rising curve up to the peak stress, a sudden drop in the stress due to face shell spalling, and gradual failing curve up to failure. Enhancement in the RMBE was observed as the hoop spacing decreased and the grout strength increased. As the hoop spacing decreased from 60 to 30 mm, the RMBE peak stress enhanced by about 25%. On the other hand, the RMBE peak stress increased by approximately 38% as the grout strength increased from 15 to 45 MPa. Significant enhancement in the RMBE strain capacity was observed especially beyond the 50% of the peak stress. The strain at 50% peak stress increased for the RMBE constructed with 15 MPa and 45 MPa strength by approximately 1.66 to 2.83 and 2.18 to 3.44 times, respectively, compared to the unreinforced unconfined specimens. Adding vertical reinforcement to the RMBE enhanced the RMBE post peak strain.

Linear correlations between the hoop spacing, vertical reinforcement ratio, and grout strength, versus the RMBE peak stress and strain corresponding to 75% and 50% of the peak stress are presented. These correlations are quantified herewith to serve as design aids for practical engineers aiming at computing a value for the peak stress and strain enhancement due to different design parameters.

Finally, three stress-strain predictive models were compared to the observed stress-strain relationship of the tested RMBEs. All the considered models overestimated the RMBE stress enhancement at different confinement levels. Moreover, the presented models overestimated the strain enhancement corresponding to different confinement ratios significantly. However, none

of the predictive models was able to capture the sudden stress drop following the peak stress due to the face shell spalling. This study clearly highlighted the need for a new stress-strain material model for reinforced masonry boundary elements.

4.9 Acknowledgments

The Authors acknowledge the support from the Natural Science and Engineering Research Council of Canada (NSERC), l'Association des Entrepreneurs en Maçonnerie du Québec (AEMQ), the Canadian Concrete Masonry Producers Association (CCMPA) and Canada Masonry Design Centre (CMDC). The authors would like to acknowledge the help of the technical staff at Concordia University and Khalid S. Alotaibi during the testing program.

4.10 NOTATION

f_{max} = peak stress

ε_{max} = strain at the peak stress

ε_{75} = strain at 75% of the peak stress

ε_{50} = strain at 50% of the peak stress

μ = strain ductility of the RMBE

$f_{max\text{-}c}$ = the average peak stress of confined RMBE

$f_{max\text{-}un}$ = the average peak stress of unreinforced unconfined RMBE

E_c = tangent modulus of elasticity of the concrete

E_{sec} = secant modulus of elasticity of the concrete

Chapter 5

Stress-Strain Model for C-Shape Confined Concrete Masonry Boundary Elements of RM Shear Walls

5.1 Abstract

Reinforced masonry (RM) shear walls with boundary elements have been recently presented as a more ductile alternative to RM rectangular shear walls. Increasing the wall thickness and introducing confining hoops in the wall most stressed zone enhances the overall wall performance. Consequently, the evaluation of the complete (i.e. including the post-peak branch) compression stress-strain behaviour of the confined and unconfined masonry become an essential step for predicting the seismic response of the RM walls. Recently, the authors investigated the effect of various volumetric ratios of transverse reinforcement, vertical reinforcement ratios, and grout strength on the axial stress-strain behaviour of reinforced masonry boundary elements (RMBEs). However, all the specimens had a specific height to thickness ratio (i.e., AR=5). This study presents the observed stress-strain relationship of seventeen C-shape half-scale fully grouted unreinforced and RMBE specimens tested under concentric compression loading up to failure. The effect of changing the aspect ratio (height to thickness) for RMBEs having different confinement ratios is presented in this study. This study quantifies the effect of these parameters on the RMBEs peak stress, strain corresponding to peak, and post-peak behaviour. The results indicate that, as the hoop spacings and/or aspect ratio decreases, the peak stress and post-peak strains increase. As such, for samples having 60 mm hoops spacing, as the aspect ratio decreased from 5 to 2 the peak stress increased by 28% and post-peak strain at 75% and 50% of the peak stress enhanced by 83%, and 28%, respectively. Moreover, this study presents a stress-strain empirical model capable of predicting the RMBE stress-strain response by computing the confined and unconfined masonry stress-strain behaviour. The model is calibrated using the experimental data of thirty-three RMBE specimens, tested in this study and reported by the authors in the literature. The model considers the effect of different parameters, namely, confinement ratio of lateral reinforcement, vertical reinforcement ratio, grout strength, and aspect ratio on the RMBE stress-strain response. This model presents

an efficient tool that can be implemented in different numerical packages aiming at a better seismic prediction of RM shear walls with boundary elements.

KEYWORDS: Aspect ratio, Boundary elements, Concrete block, Confinement, Shear walls, C-shape, Reinforced masonry, Stress-strain behaviour, stress-strain masonry model.

5.2 Introduction

Understanding the compressive stress-strain behaviour of reinforced masonry boundary elements (RMBEs) is essential for predicting the lateral response of reinforced masonry (RM) shear walls with boundary elements. Limited studies, to date, focused on the confinement effect on the stress-strain response of reinforced masonry assemblages. RMBE is a kind of masonry column added towards the wall ends to increase the wall thickness in the wall's most stressed zone, subsequently allowing a reinforcement confinement cage to be added at the wall extremities and thus enhance the wall curvature ductility and lateral response (e.g., Shedid et al 2010, Banting and El-Dakhakhni 2012, and FEMA 2006). Unlike reinforced concrete (RC) structural elements, the cover to confined core ratio in masonry assemblage is much higher. Moreover, the cover in the reinforced masonry assemblage consists of masonry blocks, mortar and grout cover to the hoops. All these discrepancies are questioning the ability of the stress-strain models that are originally developed to predict the confined RC component response, to predict the stress-strain axial response of RMBE.

Abo El Ezz et al. 2015 investigated the effect of hoops spacing on the axial compressive response of RMBEs built using standard concrete stretcher blocks. Unlike stretchers, C-shaped blocks allow placing the confinement hoops at any desired spacing. Thus, choosing the hoops spacing gives Engineers more control over the confinement level in the wall boundaries. Therefore, Obaidat et al. 2017 investigated the effect of changing the confinement ratio introduced by transversal hoops on the axial stress-strain behaviour of full-scale RMBEs built using C-shaped concrete block masonry. Moreover, Obaidat et al. 2017b investigated the effect of changing grout strength, vertical and transversal reinforcement ratio on the axial stress-strain behaviour of half-scale RMBEs built using C-shaped block.

The CSA 2014 and ASTM 2014 material testing standards specify different height to thickness ratios, i.e. 5 and 2, respectively, in order to obtain the stress-strain relationship of masonry prisms. On the other hand, each standard presents a different correction factors to

account for changing the aspect ratio. Therefore, this implies that the sample aspect ratio has a direct effect on the resulting compressive stress-strain response. As such, this study investigates the effect of changing the aspect ratio (height to thickness) and confinement ratio (i.e. by changing the hoop spacing) on the compression stress-strain behaviour of half-scale RMBE. Two aspect ratios will be investigated, namely, 2 and 3. Moreover, for each aspect ratio two hoops spacing will be utilized, namely, 30 and 60 mm. Also, unreinforced masonry boundary elements (BEs) with the same aspect ratios will be tested. Therefore, six groups of RMBEs and masonry BEs were tested, each had at least two samples. A total of seventeen RMBE and BE specimens were tested under concentric axial loading up to failure in the structural laboratory at Concordia University. Furthermore, the experimental results will be compared to two other groups of RMBEs and one group of masonry BEs having an aspect ratio of 5 and similar hoops spacing tested by Obaidat et al. 2017b. Therefore by investigating the RMBE aspect ratio, this experimental and numerical study complements the parameters experimentally tested by Obaidat et al. 2017b (i.e. vertical reinforcement ratio, the volumetric ratio of transverse reinforcement, and grout strength).

Although unconfined masonry numerical models are available in the literature (e.g. Lourenço 1996 and Hunt and Sherwood 2017), limited research was conducted for establishing the complete stress-strain relationship for confined masonry members. Priestley and Elder 1983 proposed numerical model capable of predicting the compression behaviour of unconfined and confined masonry prisms. However, Priestley and Elder 1983 model was conducted using standard blocks considering (Priestly and Bridgeman 1974) 3mm confining steel plate. Abo El Ezz et al. 2015 proposed a simplified stress-strain model for fully grouted unconfined and confined reinforced masonry boundary element built using standard concrete blocks. However, this model predicts the compression stress-strain curve of RMBE over the whole cross section smearing the transversal and the vertical reinforcement contributions. Obaidat et al. 2017b investigated the ability of three existing stress-strain models (Abo El Ezz et al. 2015, Priestley and Elder 1983, and Mander et al. 1988) in predicting the compression stress-strain behaviour of RMBEs built using C-shaped concrete blocks. It was concluded that these three models were not capable of capturing the post-peak response and the drop occurred due to the face shell spalling at the RMBE peak stress. Moreover, the available models were insensitive to the changing of

aspect ratio and highly overestimated the enhancement in the RMBE peak stress and corresponding strain (Obaidat et al. 2017b).

Based on the experimental data presented in this study and the data reported by Obaidat et al. 2017b a stress-strain empirical model is developed. The proposed model was calibrated to best fit the experimental results of a total of thirty-three RMBEs using polynomial and linear regression techniques. The model used a similar mathematical formulation as proposed by Mander et al. 1988. At a given strain value, the corresponding stress of the RMBE was computed by adding the stress in the vertical reinforcement bars to the unconfined and confined masonry zones, each weighted to its cross-sectional area. Proposing only one equation to generate a smooth curve for the confined zone adds to the simplicity of this model. This model aims at bridging the existing gap of computing the effect of different design parameters on the compressive stress-strain behaviour of RMBEs.

5.3 Experimental Program

5.3.1 Test matrix

Table 5.1 presents the nine test groups considered in this study, where each group consisted of at least two samples. A total of seventeen RMBEs having a various aspect (i.e. height to thickness) and confinement ratios and nine unreinforced BE (see Figure 5.1) were tested under concentric axial compressive loading up to failure. It should be noted that all groups having an aspect ratio equal to 5 were tested earlier by Obaidat et al. 2017b. For each group, the specimens were labeled with four terms of letters and numbers, e.g. BE-D4/60-AR2-A. The first term, BE, represents a boundary element. The second term (i.e. D4/60) is used to describe the transversal reinforcement size and spacing in mm. The third term (i.e. AR2) represent the sample's aspect ratio (i.e. height to thickness = 2 in this group). The letters A, B, or C follow the group name to identify the sample within each group. It should be noted that the confinement ratio, C_f, is calculated according to Eq. 5.1 and presented in Table 5.1.

$$C_f = \rho_l \sqrt{(H / S_h)} \qquad \text{Eq. 5.1}$$

where; ρ_l is the volumetric ratio of the confinement reinforcement (i.e., the volume of confinement hoops to the volume of core concrete at spacing, S_h), H is the width of the confined core, and S is the spacing between the confinement hoops.

Figure 5.1 RMBE specimens during construction

All samples were grouted with normal strength grout (i.e. 15 MPa). As shown in Table 5.1, the first three groups represented unreinforced BEs having aspect ratios of 2, 3 and 5. These three groups were tested to compare their stress-strain behaviour with the corresponding RMBEs, and thus to quantify the vertical and transversal reinforcement influence on the RMBE stress-strain behaviour. All the RMBE reinforced specimens had four vertical reinforcement #3 bars (71 mm^2). The vertical bars were placed in each corner and confined with transverse reinforcement (i.e., hoops) of deformed D4 wires (25.8 mm^2) having two different hoop's spacing of 60 or 30 mm. Groups 4 and 7 had the same aspect ratio of 2 and were confined with D4/60 mm and D4/30 mm hoops, respectively. Similarly, the remaining groups (5 and 8; 6 and 9) had aspect ratios of 3 and 5 and confined with D4/60 mm and D4/30 mm hoops, respectively. Therefore, this test matrix was designed to investigate the effect of different confinement levels and aspect ratios on the RMBE's compressive stress-strain behaviour.

5.3.2 Construction of RMBEs

The construction of the RMBE specimens was performed by experienced masons following the Canadian construction practices. Half-scale concrete C-shaped blocks were used in all samples. Figure 5.2 (a to e) illustrates the RMBEs construction sequence. First, the rebars were cut and bent, then the reinforcement cage for each RMBE specimen was assembled. The cage consisted of four #3 (71 mm2) reinforcement bars, and deformed wire (D4) hoops tied at a particular spacing (30 or 60 mm). All hoops were anchored with 135º bends extending 55 mm into the grout's core. The reinforcement cage of each RMBE specimen was placed in a preassembled formwork to pour the bottom reinforced concrete footing with dimensions of 200 mm x 200 mm x 250 mm (length x width x height). However, the unreinforced BE specimens were placed on solid templates to provide equal elevation, and they did not have a top or a bottom footing. It should be noted that the hoops' size was increased to #4 (129 mm2) with 40 mm spacing to avoid any local failure in the bottom and top footing. The vertical reinforcement bars were continuous along the height of the RMBE specimen. There were no splices from the base of the bottom footing to the top footing. High strength concrete was poured in the wooden formwork; then the samples were permitted, approximately, one week to cure. Before laying the C-shaped concrete blocks, four strain gauges were mounted on the mid height of the vertical reinforcing steel bars to track the axial strain on the vertical bars. A stacked bond pattern was utilized for each RMBE specimen. Each course had two C-block units placed face to face. The stacked bond pattern represented the layout envisioned for RMSW with boundary elements. All RMBE and unreinforced specimens had cross-sectional dimensions of 190 mm x 190 mm (length x width). Samples were assembled in four, six, and ten courses high for samples having aspect ratios of 2, 3, and 5, respectively. The RMBE specimens were strapped before grouting to avoid any cracks in the mortar head joints. Finally, once the masonry process was complete, a top footing, similar to the bottom one, was poured and left to cure in a preassembled formwork.

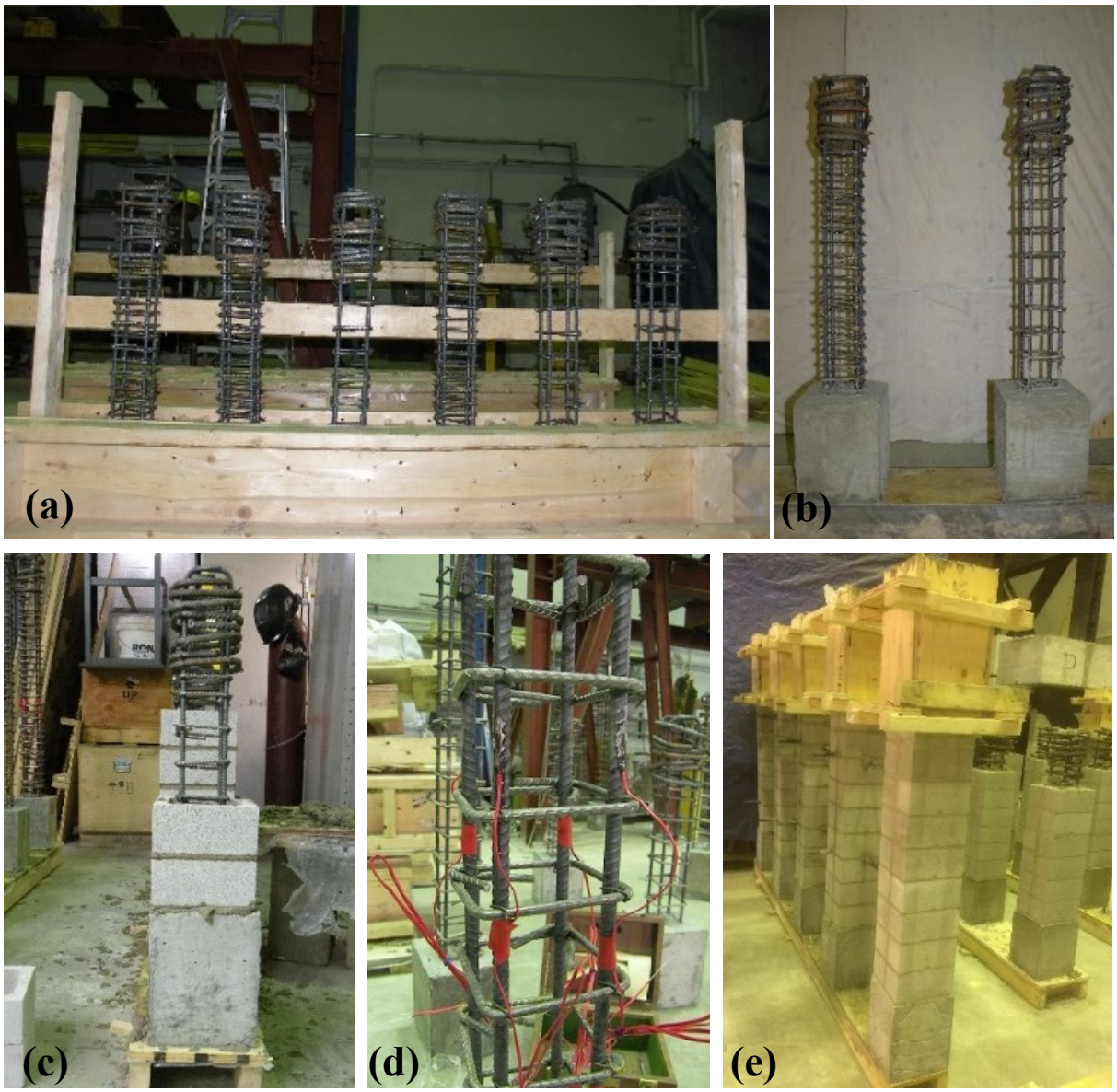

Figure 5.2 Construction sequence of RMBEs

5.3.3 Material Properties

RMBE's bottom and top footings were constructed using high strength concrete to eliminate any local failure and to ensure that failure occurs within the test region. Table 5.2 summarizes the materials' compressive strength used for the construction of the RMBEs. The footings' strength was 83.8 MPa with a coefficient of variation (C.V.) of 6.2%. These results were based on the testing of twelve concrete cylinders. All RMBE specimens were constructed with C-shape half-scale concrete block units. Their nominal dimensions were 25 mm x 190 mm x 92.5 mm x

90 mm (thickness x length x width x height). According to the ASTM C140 / C140M [14], fourteen coupons of half-scale concrete masonry blocks (100 mm x 50 mm x 25 mm) were tested under compressive loading. The average compressive strength, of the 14 tested coupons, was 22 MPa (C.V. = 13.8%). The C-shaped block units were joined in a stacked bond with an approximate thickness of 5 mm mortar joints (i.e., to meet the scaling requirements). Pre-bagged type S mortar was used for each specimen tested. From each batch, three 50 mm x 50 mm x 50 mm cubes were molded and cured. A total of fifteen mortar cubes were tested under compression. The average compressive strength of the mortar cubes was 12.3 MPa (C.V. = 7.15%). Fine grout was used for the construction of all specimens. The pre-mixed fine grout air treated in cylinders had an average compressive strength of 15 MPa (C.V. = 8.7%) tested according to CSA A179, 2014.

Standard deformed reinforcement steel bars, sizes #3 and #4, were used for the vertical reinforcement and footing transversal reinforcement, respectively. On the other hand, deformed wire, D4, was utilized for the hoops. An average tensile yield strength of #3 and #4 was 455 MPa and 482 MPa, respectively. A clear yield region did not exist for the steel deformed wire (D4). Therefore, the proof yield strength corresponding to a 0.2% strain for D4 tested samples was 600 MPa.

Table 5.1: RMBE test specimen details

Group #	RMBE ID	Number of tested specimens	Grout Strength (MPa)	Longitudinal Reinforcement		Transverse Reinforcement		Confinement ratio C_f
				Number-size of Bars	ρ_v%	Bar size (spacing mm)	ρ_l%	
1	**BE-0-AR2**	2	15	-	-	-	-	-
2	**BE-0-AR3**	3	15	-	-	-	-	-
3	**BE-0-AR5***	4	15	-	-	-	-	-
4	**BE-D4/60-AR2**	3	15	4 - #3	0.79	D4 (60)	1.57	0.022
5	**BE-D4/60-AR3**	3	15	4 - #3	0.79	D4 (60)	1.57	0.022
6	**BE-D4/60-AR5***	3	15	4 - #3	0.79	D4 (60)	1.57	0.022
7	**BE-D4/30-AR2**	3	15	4 - #3	0.79	D4 (30)	3.15	0.062
8	**BE-D4/30-AR3**	3	15	4 - #3	0.79	D4 (30)	3.15	0.062
9	**BE-D4/30-AR5***	3	15	4 - #3	0.79	D4 (30)	3.15	0.062

*Tested by Obaidat et al. [6]

Table 5.2: Materials properties

Material	Notation	Average compressive strength (MPa)	C.V. %
Concrete cylinder (footings)	f_c	83.8	6.20
Masonry concrete block	f_b	22.0	13.8
Mortar cubes	f_{mc}	12.3	7.15
Grout cylinders	f_g	15.0	8.70

*C.V.: coefficient of variation

5.3.4 Test Setup and Instrumentation

All RMBE specimens were tested under compressive concentric loading until failure. The test setup is illustrated in (Figure 5.3). The compressive concentric loading was applied by a newly upgraded 3000 kN servo controlled actuator operated at a constant displacement rate (i.e., 0.003 mm/sec). Using a displacement control loading enables the capturing of the post-peak stress-strain curve branch. This is essential to quantify the influence of the studied parameters on the behaviour of the RMBE's post-peak behaviour. The termination of the tests occurred when the specimens reach approximately 25% of its ultimate load (75% strength degradation).

Two 50 mm thick rectangular steel plates and a spherical steel head were placed between the specimen and the actuator head. To ensure that the specimen's extreme ends remained parallel to one another and that the loads would be distributed uniformly, two layers of high strength plaster were added between the specimen's top and bottom surfaces and the steel plates. Figure 5.3 displays typical dimensions of the RMBE specimens with different aspect ratios. The total height of the tested specimen having four courses (AR=2), six courses (AR=3), and ten courses (AR=5) was 880, 1070, and 1455 mm, respectively, with an effective (gauge) length of 380, 570, and 955 mm, respectively.

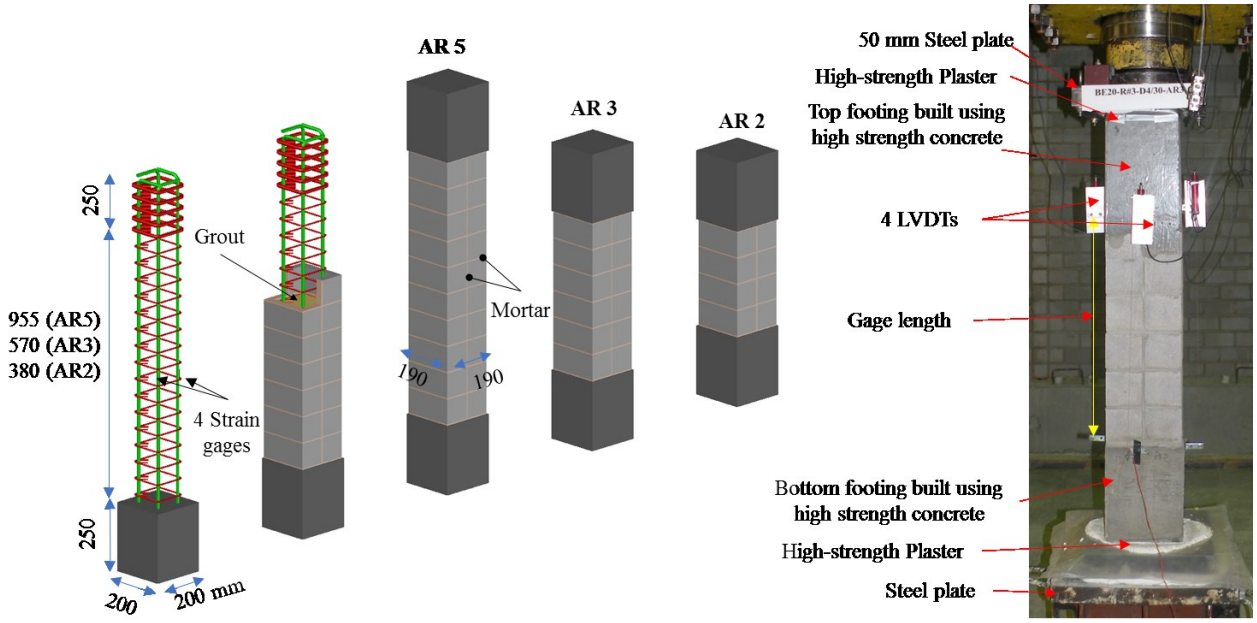

Figure 5.3 Schematic of the test set-up, RMBE components, and instrumentations

The effective gauge length was measured from the lower edge of the top footing to the upper edge of the bottom footing. In all RMBE specimens, four Linear Variable Differential Transducers LVDTs were used to measure the axial strain over the tested region.

5.4 Experimental Results and Discussion

Figure 5.4 presents the compression stress-strain curves for all RMBE specimens. It should be noted that the stress was computed by dividing the reported load by the RMBE's cross-sectional area (190 mm × 190 mm). Also, the strain was calculated by dividing the average of the four LVDTs readings by the corresponding effective gauge length. It can be noticed that the compressive stress-strain curve of confined RMBEs consists of three branches: rising curve up to the peak load, followed by a sudden drop, and gradually descending curve. However, the stress-strain curve of the unreinforced specimens has two branches: rising curve up to the peak load and descending post-peak curve. The sudden drop in the RMBE's stress was mainly attributed to the face-shell spalling of the concrete block, which resulted in a 40~50% loss of the RMBE strength, where the RMBE lost at least 55% of the cross-sectional area. Table 5.3 presents the experimental results of the peak stress (f_{max}), strain at the peak stress (ε_{max}), strain at 75% of the peak stress (ε_{75}), strain at 50% of the peak stress (ε_{50}), and strain ductility ($\mu_{50\%}$) of the RMBE. The strain ductility is defined as the ratio between the strain at 50% of the peak stress on the descending curve (ε_{50}) and the strain at the peak stress (ε_{max}).

5.4.1 Effect of changing aspect ratio (height to thickness) on the stress-strain response of RMBEs

The compressive stress-strain curves of three specimens, in three different groups having the same aspect ratio 2, 3, and 5, with various confinement ratios of transverse reinforcement ratios, can be seen in Figure 5.4. It should be noted that the effect of the aspect ratio on the initial stiffness of the RMBE specimen was minimal. Figure 5.4 shows that as the aspect ratio decreases, the peak stress increases. However, this was not the case for RMBEs having the highest confinement ratio (i.e., 30 mm hoops spacing). As such, as the aspect ratio decreased the confinement effect introduced by the specimen's capping resulted in increasing the RMBE peak stress. However, this confinement effect could be minimized in the RMBEs having the highest ratio of transversal

reinforcement (i.e. RMBE become well confined). On average, as the aspect ratio decreased from 5 to 2, the peak stress increased by 20%, 28%, and 2% for unreinforced BEs, RMBEs having 60 and 30 mm hoops spacing, respectively.

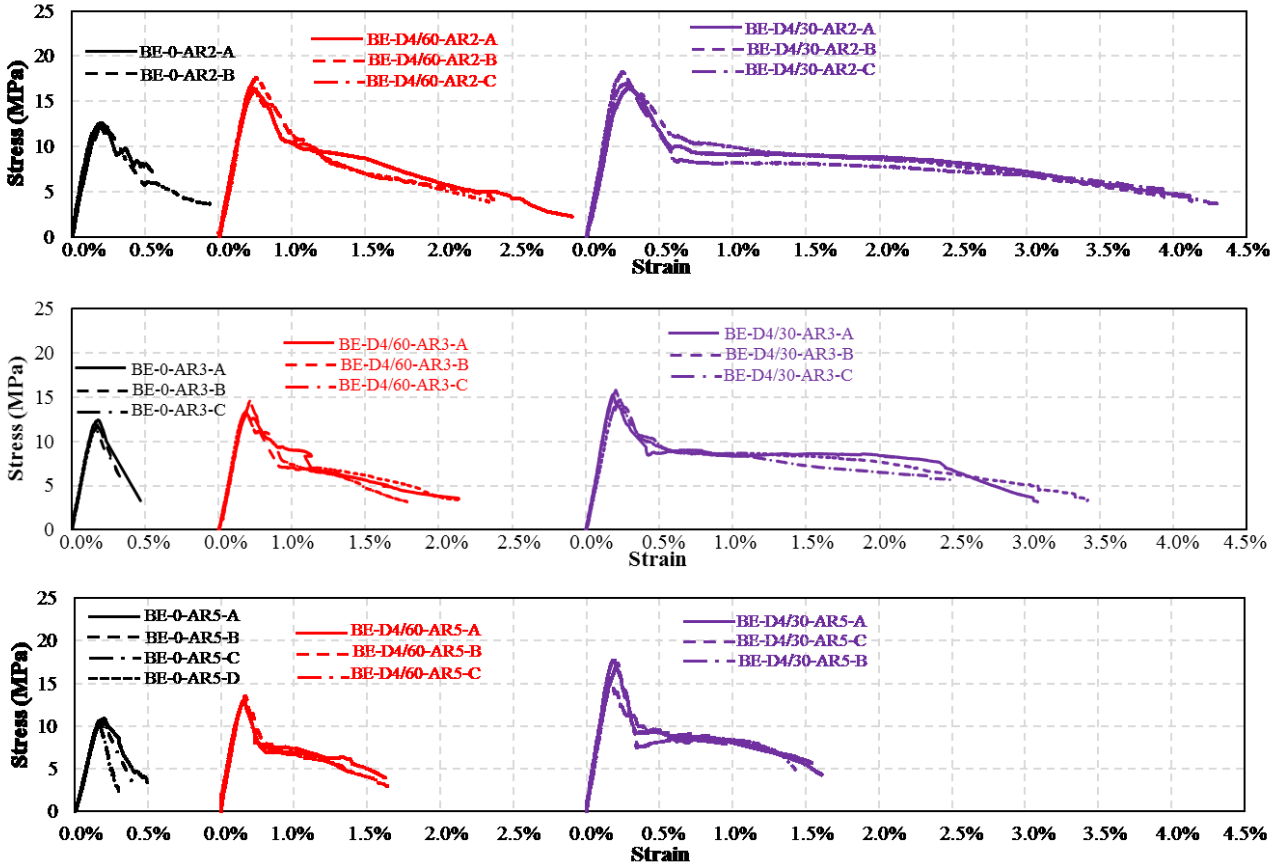

Figure 5.4 Observed compression stress–strain curves for RMBE specimens having different height to thickness and confinement ratios

Figure 5.5 presents the RMBEs stress-strain results each normalized to its maximum stress in order to visualize the effect of the different parameters on the RMBEs post-peak response and ductility. As shown in Figure 5.5, as the aspect ratio decreases the RMBEs developed a more gradual post-peak stress degradation. On average, as the aspect ratio decreased from 5 to 2, the strain corresponds to the peak strength increased by 14%, 46%, and 29% for unreinforced BEs, RMBEs having 60 and 30 mm hoops spacing, respectively. Moreover, the strain ductility (i.e. ratio of the strain at 50% of peak stress to strain at peak stress) increased as the aspect ratio decreased from 5 to 2 by 46%, and 69% for unreinforced BEs, RMBEs having 30 mm hoops spacing, respectively. However, the last observation was not the consensus of all, where for RMBEs having

60 mm hoops spacing as the aspect ratio decreased from 5 to 2 the displacement ductility decreased by 12%.

5.4.2 Effect of confinement ratio on the stress-strain response of RMBEs

Figure 5.4 shows that, as the confinement ratio of transverse reinforcement increases, the peak stress increases. The increase in peak stress is more noticeable in the RMBE specimens having an aspect ratio of 5. On average, as the confinement ratio of transverse reinforcement increased from 0.022 (i.e. 60 mm hoops spacing) to 0.062 (i.e. 30 mm hoops spacing), the peak stress increased by 2%, 12%, and 29% for RMBEs with AR of 2, 3 and 5, respectively.

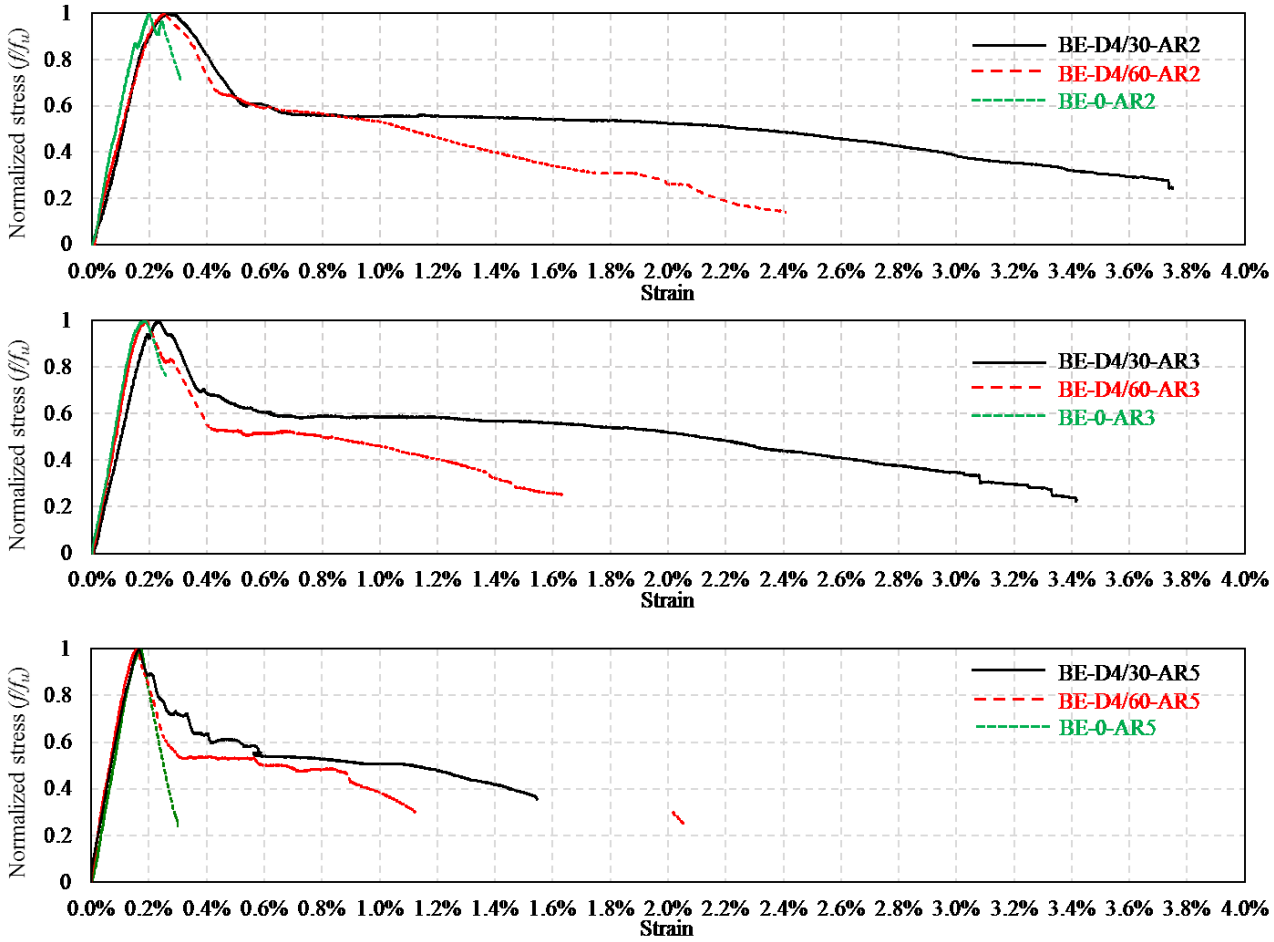

Figure 5.5 Normalized compression stress–strain curves of RMBE having different confinement ratios

The RMBEs developed a more gradual post-peak stress degradation as the confinement ratio of transverse reinforcement increases (Figure 5.5). On average, as the confinement ratio of transverse reinforcement increased from 0.022 to 0.062, the strain corresponds to the peak stress, ε_{max},

increased by 9%, 8%, and 23% for RMBEs with AR of 2, 3 and 5, respectively. Moreover, the strain ductility, $\mu_{50\%}$, increased by 130%, 131%, and 19%, as the confinement ratio of transverse reinforcement increased from 0.022 to 0.062, for RMBEs with AR of 2, 3 and 5, respectively.

5.4.3 RMBEs damage propagation

Figure 5.6 shows the typical failure modes of the unreinforced BE and RMBE specimens with various aspect ratios. Prior to the peak strength, both unreinforced BE and RMBE specimens showed similar damage characterized by surface hair cracks. However, the unreinforced BEs failed in a brittle manner, and sudden splitting occurred at the onset of the peak stress. On the other hand, face shell spalling was observed in RMBE following the peak stress. This was followed by vertical reinforcement bars buckling outwards at high strains. It should be noted, no fracture in the transversal hoops was observed in any of the tested samples. Steel-masonry strain compatibility was observed up to the peak-stress as observed by Obaidat et al. 2017b. Subsequently, vertical reinforcement bars yielding was observed following the RMBE's peak stress. Finally, failure occurred when the grout between the hoops was crushed, as seen in (Figure 5.6).

Figure 5.6 Observed damage of BE specimens with various aspect ratios: a) unreinforced BEs, and b) RMBEs

Table 5.3 Experimental results of the RMBEs.

RMBE ID	Maximum stress (MPa)		Strain at peak stress		Strain at 75% of the peak stress, ε_{75}		Strain at 50% of the peak stress, ε_{50}		Strain ductility, $\mu_{50\%}$
	f_{max}	Average (C.V. %)	ε_{max}	Average (C.V. %)	ε_{75}	Average (C.V. %)	ε_{50}	Average (C.V. %)	$\varepsilon_{50}/\varepsilon_{max}$
BE-0-AR2-A	12.62	12.64 (0.17%)	0.00209	0.002045 (3.11%)	0.0034	0.0032 (9.25%)	0.0047	0.0049 (4.37%)	2.37
BE-0-AR2-B	12.65		0.00200		0.0030		0.0050		
BE-0-AR3-A	12.41	11.91 (4.16%)	0.00180	0.001757 (2.30%)	0.0026	0.0025 (3.03%)	0.0037	0.0034 (7.33%)	1.95
BE-0-AR3-B	11.88		0.00175		0.0025		0.0032		
BE-0-AR3-C	11.42		0.00172		0.0025		0.0034		
BE-0-AR5-A*	10.88	10.55 (2.77%)	0.00195	0.00180 (7.91%)	0.0022	0.0021 (4.30%)	0.0037	0.0030 (19.05%)	1.62
BE-0-AR5-B*	10.26		0.00171		0.0023		0.0027		
BE-0-AR5-C*	10.35		0.00200		0.0023		0.0032		
BE-0-AR5-D*	10.70		0.00174		0.0021		0.0024		
BE-D4/60-AR2-A	16.39	16.88 (3.86%)	0.00250	0.002367 (6.45%)	0.0039	0.0042 (7.65%)	0.0090	0.0078 (12.91%)	3.31
BE-D4/60-AR2-B	17.62		0.00240		0.0042		0.0072		
BE-D4/60-AR2-C	16.63		0.00220		0.0045		0.0073		
BE-D4/60-AR3-A	13.00	13.65 (6.15%)	0.00210	0.00210 (4.76%)	0.0038	0.0035 (8.07%)	0.0075	0.0074 (10.41%)	3.50
BE-D4/60-AR3-B	13.36		0.00200		0.0032		0.0080		
BE-D4/60-AR3-C	14.60		0.00220		0.0034		0.0065		
BE-D4/60-AR5-A*	13.08	13.2 (2.12%)	0.00156	0.00162 (4.45%)	0.0022	0.0023 (6.55%)	0.0066	0.0061 (7.51%)	3.77
BE-D4/60-AR5-B*	13.00		0.00160		0.0025		0.0057		
BE-D4/60-AR5-C*	13.52		0.00170		0.0023		0.0060		
BE-D4/30-AR2-A	16.45	17.25 (5.53%)	0.00260	0.002587 (6.97%)	0.0044	0.0041 (6.45%)	0.0220	0.0197 (12.80%)	7.61
BE-D4/30-AR2-B	18.30		0.00240		0.0040		0.0200		
BE-D4/30-AR2-C	16.98		0.00276		0.0039		0.0170		
BE-D4/30-AR3-A	15.28	15.25 (3.45%)	0.00220	0.002267 (2.55%)	0.0035	0.0034 (2.94%)	0.0180	0.0184 (8.33%)	8.09
BE-D4/30-AR3-B	14.70		0.00230		0.0034		0.0200		
BE-D4/30-AR3-C	15.75		0.00230		0.0033		0.0170		
BE-D4/30-AR5-A*	17.78	16.97 (6.57%)	0.00195	0.0020 (6.61%)	0.0029	0.0028 (3.57%)	0.0080	0.0090 (11.11%)	4.50
BE-D4/30-AR5-B*	15.70		0.00190		0.0027		0.0100		
BE-D4/30-AR5-C*	17.44		0.00215		0.0028		0.0090		

*Tested by Obaidat et al. [6]

5.5 Empirical Compressive Stress-Strain Relationship for RMBEs

5.5.1 Model overview

Based on the experimental data of the current study and the study by Obaidat et al. 2017b an empirical stress-strain relationship is proposed for the confined and unconfined masonry zones considering different grout strength, aspect ratio, vertical, and transversal reinforcement ratios. As shown in Figure 5.7, at a given strain the RMBE total stress is computed by adding the stress of the unconfined masonry, confined masonry and the vertical reinforcement each weighted to its cross-sectional area according to Eq. 5.2. Therefore, this model provides the flexibility of predicting the stress-strain relationship for RMBEs built using various reinforcement bar sizes, block, and core dimension combinations.

$$f = f_{mu}\frac{A_{mu}}{A_t} + f_{mc}\frac{A_{mc}}{A_t} + f_s\frac{A_s}{A_t} \qquad \text{Eq. 5.2}$$

where f is the compressive stress, f_{mu} is the unconfined stress, f_{mc} is the confined stress, f_s is the vertical steel reinforcement stress, A_{mu} is the unconfined zone area, A_{mc} is the confined zone area, A_s is the vertical reinforcement steel area, and A_t is the total cross section area.

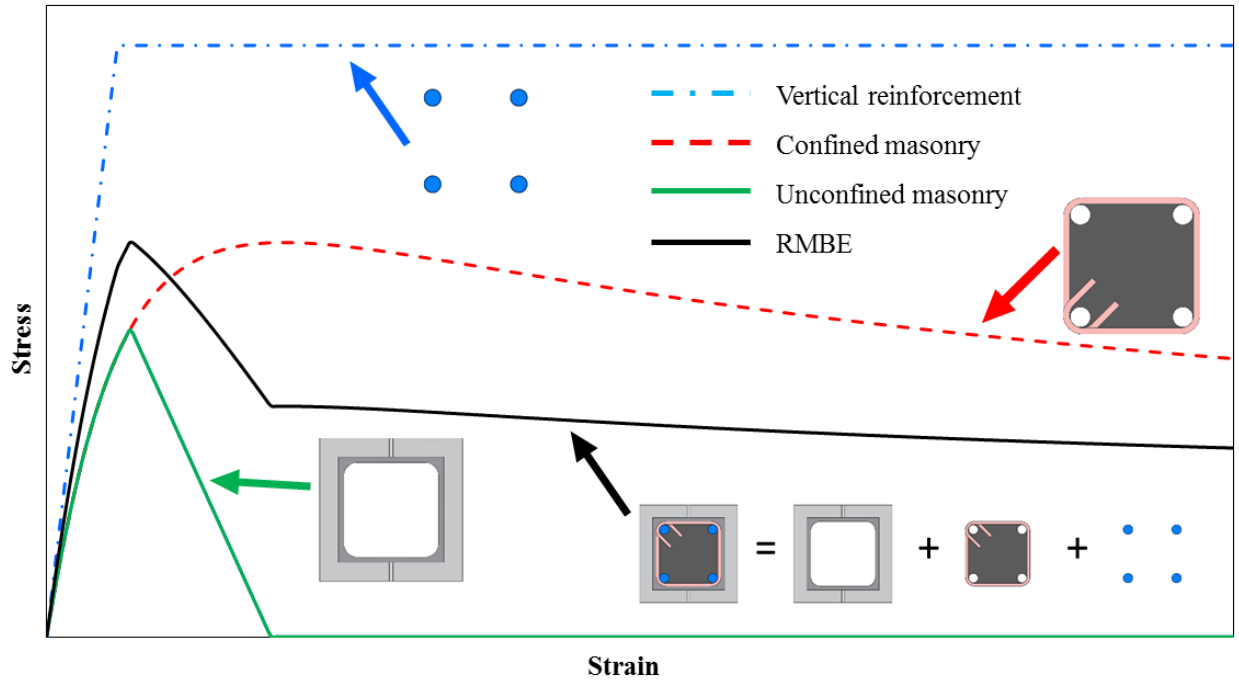

Figure 5.7 Stress-strain relationship of RMBE components

In this study, a mathematical expression similar to the one proposed by Mander et al. 1988 is utilized to produce a smooth continuous curve for the compression stress-strain behaviour of RMBE unconfined and confined masonry zones. This expression was calibrated with the experimental results of thirty-three RMBEs having a different aspect ratio, grout strength, vertical and transversal reinforcement ratios. The specimens' details are presented in Table 5.4. The following sections introduce the calibration process, the computed model, and the model predictions compared to the experimental data.

5.5.2 Model calibration

In the first two curves in the legend of Figure 5.8, the contribution of the vertical bars to the RMBE's stress-strain behaviour was subtracted assuming steel-masonry strain compatibility (Obaidat et al. 2017b). The load carried by the vertical reinforcement, P_s, was subtracted from the total load, P_{exp}, considering an elastic-perfect plastic response. The elastic modulus and the yield stress for the two studied vertical bar sizes (i.e. #3 and #4) were measured experimentally. The resulting load ($P_{exp} - P_s$) is divided once by the total area of the RMBE, A_t, and once by only the core area, A_c, as shown in Figure 5.8. As discussed earlier, the sudden stress drop was mainly attributed to the spalling of the block face shell which represent approximately 55% of RMBE specimen cross section. Hence, the applied load was resisted by the whole RMBE cross-section up to the peak stress.

Figure 5.8 shows the technique used to calibrate the proposed stress-strain model to the experimental results. It is assumed that both the confined and unconfined masonry models will have the same stress up to the ultimate stress that corresponds to $\varepsilon_{mu\text{-}max}$, where the strain in the confined hoops is not high enough to confine the core as explained by Yong et al. 1988. Following the face shell spalling at strain ε_{sp}, the load will be totally carried by the confined core. Consequently, the transition zone between the strain corresponding to maximum stress, $\varepsilon_{mu\text{-}max}$, and the spalling strain, ε_{sp}, is assumed to have a linear decay in the unconfined masonry model and a smooth transition curve for the confined masonry model, as shown in the last two curves in the legend of Figure 5.8. This calibration process was conducted for each RMBE and the required parameters that will be defined in the following section for the unconfined and confined models were computed for different grout strength, aspect ratio, vertical and horizontal reinforcement ratios.

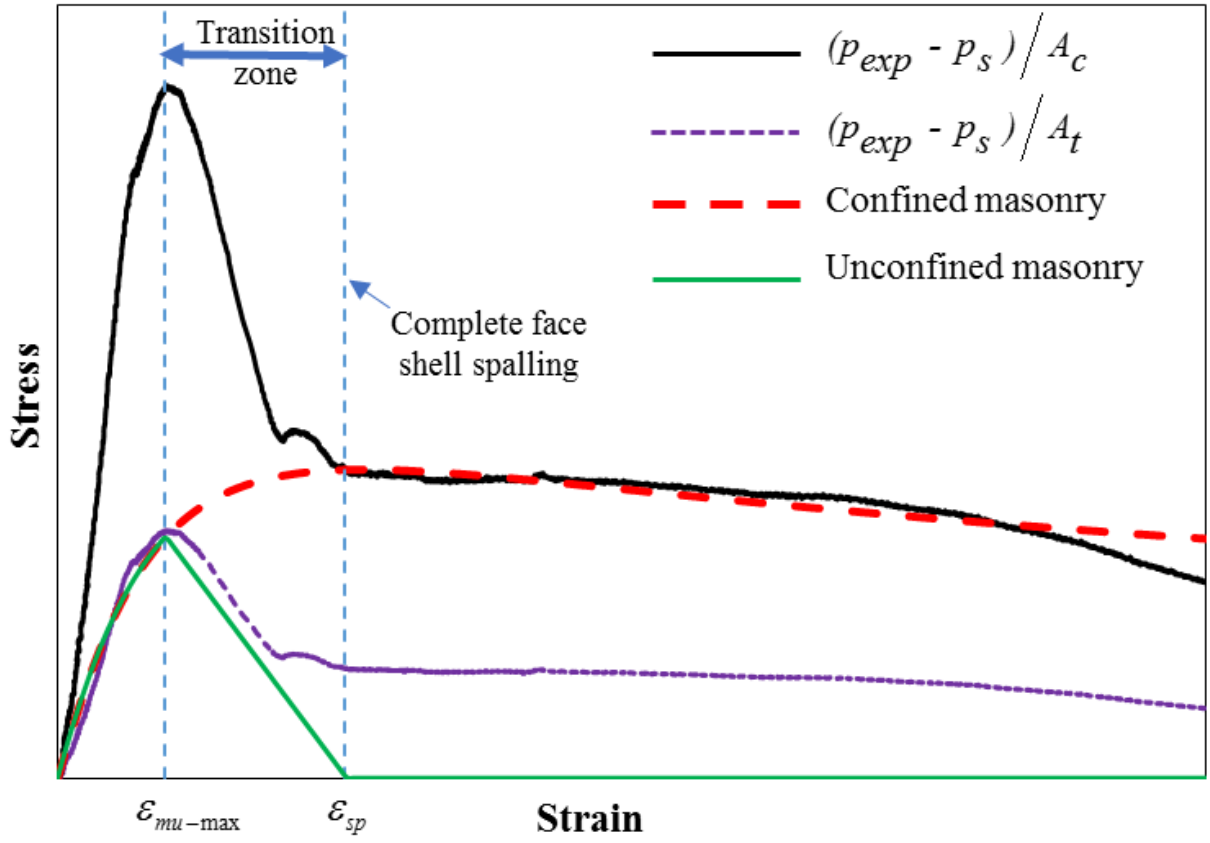

Figure 5.8 Calibration of the proposed model with the experimental data

5.5.3 Model formulation

The complete compressive stress-strain relationship of the ***confined masonry*** is computed using Eq. 5.3 (see Figure 5.9).

$$f_{mc} = \frac{f_{mc-\max}\left(\varepsilon_{mc}/\varepsilon_{mc-\max}\right)S}{S-1+\left(\varepsilon_{mc}/\varepsilon_{mc-\max}\right)^{S}} \qquad \text{Eq. 5.3}$$

where, f_{mc} is the confined compressive stress corresponding to a particular strain ε_{mc}, $f_{mc-\max}$ is the confined masonry peak stress, $\varepsilon_{mc-\max}$ is the strain corresponding to the confined masonry peak stress, and S is a parameter guiding the degradation slope.

Computing $f_{mc-\max}$, $\varepsilon_{mc-\max}$, and S requires four RMBE's properties, namely: (1) the compressive strength of the corresponding unreinforced unconfined masonry prism, f_{prism}; (2) the

aspect ratio of the RMBE (height to thickness), AR; (3) the vertical reinforcement ratio, ρ_v; and (4) the volumetric ratio of transverse reinforcement (hoops), ρ_l. It should be noted that f_{prism} can be estimated experimentally or by using available numerical models (e.g. Hunt and Sherwood 2017). These models are capable of predicting f_{prism} from the characteristics of masonry prism components (i.e. block, grout, mortar, prism pattern, and mortar bedding). Based on the model calibration, empirical best-fit equations have been generated for $f_{mc-\max}$, $\varepsilon_{mc-\max}$, and S, where two sets of empirical equations are proposed for each parameter. As such, the first equation is high order polynomial equation with a higher R-squared (coefficient of determination) value. On the other hand, the second equation is a simple linear regression relationship with R-squared value lower than their counterparts. Therefore, $f_{mc-\max}$ is calculated using Eqs. 5.4 and 5.7, $\varepsilon_{mc-\max}$, is calculated using Eqs. 5.5 and 5.8, and S is calculated using Eqs. 5.6 and 5.9, for polynomial regression and linear regression, respectively.

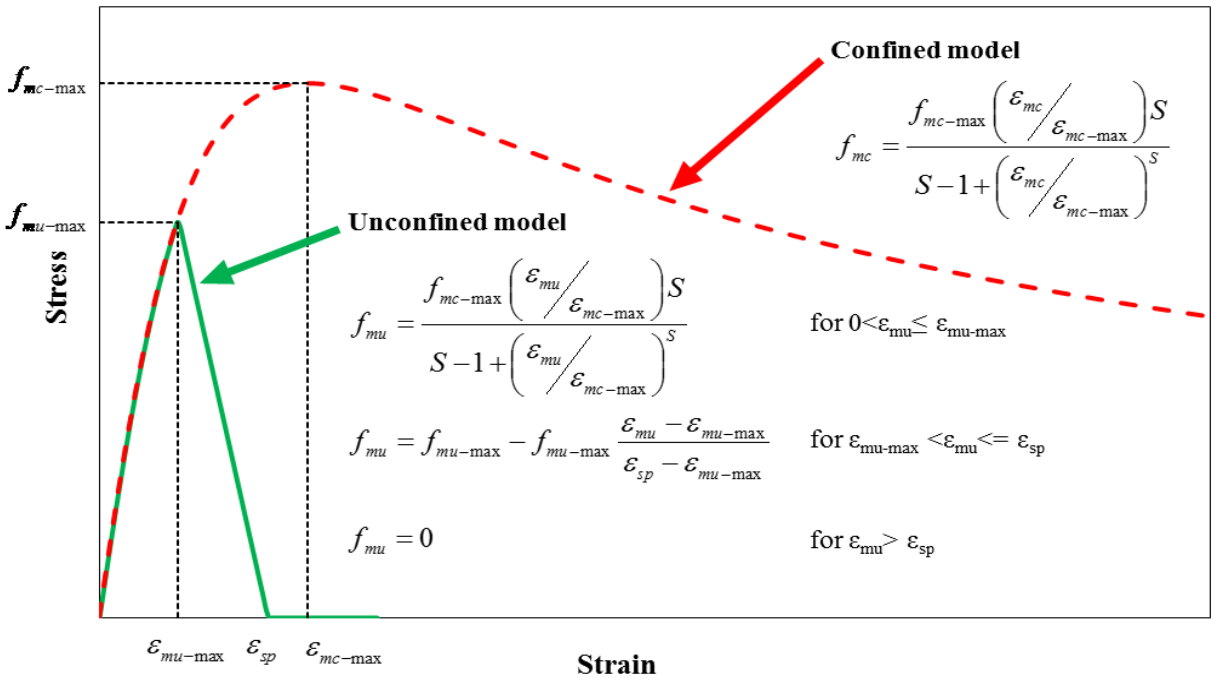

Figure 5.9 Proposed empirical stress-strain model formulations

Polynomial regression:

- $f_{mc\text{-}max} = a + bx_1 + c/x_2 + dx_1^2 + e/x_2^2 + fx_1/x_2 + gx_1^3 + h/x_2^3 + ix_1/x_2^2 + jx_1^2/x_2$ Eq. 5.4

  $R^2 = 94.3\%$

  a = 619.011, b = -328.425, c = -2727.636, d = -16.984, e = 1477.570, f = 1797.299, g = 1.386, h = 1679.370, i = -1827.581, j = -0.1055.

  $x_1 = f_{prism}/AR$, $x_2 = \rho_l$

- $\varepsilon_{mc\text{-}max} = \left(a + bx_1 + cx_1^2 + dx_1^3 + ex_2 + fx_2^2 + gx_2^3 + hx_2^4 + ix_2^5\right)/10000$ Eq. 5.5

  $R^2 = 92.8\%$

  a = -3769.319, b = 66.500, c = -15.247, d = 1.185, e = 10003.658, f = -10328.925, g = 5103.408, h = -1204.992, and i = 108.509.

  $x_1 = f_{prism}/AR$, $x_2 = \rho_l/\rho_v$

- $S = a + bx_1 + cx_2 + dx_1^2 + ex_2^2 + fx_1x_2 + gx_1^3 + hx_2^3 + ix_1x_2^2 + jx_1^2x_2$ Eq. 5.6

  $R^2 = 86.3\%$

  a = 21.158, b = -18.376, c = 2.175, d = 5.788, e = 0.100, f = -1.952, g = -0.498, h = -0.062, i = 0.189, j = 0.095

  $x_1 = f_{prism}/AR$, $x_2 = \rho_l/\rho_v$.

Linear regression:

- $f_{mc\text{-}max} = ax_1 + bx_2 + cx_3 + dx_4 + e$ Eq. 5.7

  $R^2 = 74.3\%$

  a = 1.530, b = -0.640, c = 1.775, d = 0.891, e = -5.329

  $x_1 = f_{prism}$, $x_2 = AR$, $x_3 = \rho_l$, and $x_4 = \rho_v$

- $\varepsilon_{mc\text{-}max} = \left(ax_1 + bx_2 + cx_3 + dx_4 + e\right)/10000$ Eq. 5.8

  $R^2 = 91.5\%$

  a = 2.336, b = -7.139, c = 10.020, d = 1.691, e = 16.488

  $x_1 = f_{prism}$, $x_2 = AR$, $x_3 = \rho_l$, and $x_4 = \rho_v$

- $S = exp\left(ax_1 + bx_2 + cx_3 + dx_4 + e\right)$ Eq. 5.9

  $R^2 = 68.0\%$

  a = -0.014, b = -0.088, c = -0.302, d = 0.323, e = 1.575

  $x_1 = f_{prism}$, $x_2 = AR$, $x_3 = \rho_l$, and $x_4 = \rho_v$

The complete compressive stress-strain relationship of the ***unconfined masonry*** is computed using Eqs. 5.10 to 5.12 (see Figure 5.9).

$$f_{mu} = \frac{f_{mc-\max}\left(\varepsilon_{mu} \big/ \varepsilon_{mc-\max}\right)S}{S - 1 + \left(\varepsilon_{mu} \big/ \varepsilon_{mc-\max}\right)^S} \qquad \text{for } 0 < \varepsilon_{mu} \leq \varepsilon_{mu\text{-}max} \qquad \text{Eq. 5.10}$$

$$f_{mu} = f_{mu-\max} - f_{mu-\max}\frac{\varepsilon_{mu} - \varepsilon_{mu-\max}}{\varepsilon_{sp} - \varepsilon_{mu-\max}} \qquad \text{for } \varepsilon_{mu\text{-}max} < \varepsilon_{mu} \leq \varepsilon_{sp} \qquad \text{Eq. 5.11}$$

$$f_{mu} = 0 \qquad \text{for } \varepsilon_{mu} > \varepsilon_{sp} \qquad \text{Eq. 5.12}$$

where, f_{mu} is the unconfined compressive stress corresponding to specific strain ε_{mu}; $\varepsilon_{mu-\max}$ is the strain at peak stress of unconfined RMBE; and ε_{sp} is the strain corresponding to the end of face shell spalling. Similar to the confined model, two regression techniques were utilized; polynomial regression and linear regression. The $f_{mc-\max}$, $\varepsilon_{mc-\max}$, and S are calculated as discussed above. $\varepsilon_{mu-\max}$ is calculated by Eqs. 5.13 and 5.15 and ε_{sp} is calculated by Eqs. 5.14 and 5.16, for polynomial regression and linear regression, respectively.

Polynomial regression:

- $\varepsilon_{mu\text{-}max} = (a + b/x_1 + c/x_1^2 + d/x_1^3 + e/x_2 + f/x_2^2 + g/x_2^3 + h/x_2^4 + i/x_2^5)/10000$ Eq. 5.13

  $R^2 = 77.3\%$

  a = 1108.230, b = -14.055, c = -229.929, d = 415.095, e = -11954.400, f = 50626.963, g = -102380.018, h = 98965.561, i = -36608.490.

  $x_1 = f_{prism} / AR$, $x_2 = \rho_l / \rho_v$

- $\varepsilon_{sp} = \left(a + bx_1 + cx_2 + dx_1^2 + ex_2^2 + fx_1x_2 + gx_1^3 + hx_2^3 + ix_1x_2^2 + jx_1^2x_2\right) / 10000$ Eq. 5.14

  $R^2 = 95.1\%$

  a = 119.108, b = -36.576, c = -81.598, d = 9.136, e = 33.409, f = 5.676, g = -0.894, h = -3.752, i = -2.257, j = 0.908.

  $x_1 = f_{prism} / AR$, $x_2 = \rho_l / \rho_v$

Linear regression:

- $\varepsilon_{mu-\max} = exp\left(ax_1 + bx_2 + cx_3 + dx_4 + e\right) / 10000$ Eq. 5.15

  $R^2 = 65.5\%$

  a = 0.0052, b = -0.102, c = 0.0401, d = 0.298, e = 2.976

  $x_1 = f_{prism}$, $x_2 = AR$, $x_3 = \rho_l$, and $x_4 = \rho_v$

- $\varepsilon_{sp} = exp\left(ax_1 + bx_2 + cx_3 + dx_4 + e\right) / 10000$ Eq. 5.16

  $R^2 = 85.8\%$

  a = 0.026, b = -0.178, c = 0.041, d = 0.052, e = 3.848

  $x_1 = f_{prism}$, $x_2 = AR$, $x_3 = \rho_l$, and $x_4 = \rho_v$

5.5.4 Model results

Figures 5.10 to 5.13 show the comparison of the proposed empirical model with the experimental results. The model provides overall good results for both the ascending and descending branches of the compressive stress-strain curves. The model was able to simulate the most relevant characteristics of the RMBE stress-strain response, including the initial stiffness, peak load, strain corresponding to peak, stiffness and stress degradation at different strain levels. Table 5.5 shows the percentage of difference between the proposed model and the experimental data at $f_{\max}$, $\varepsilon_{\max}$, and ε_{75} using the two regression approaches. A difference range between the model predictions using polynomial regression and the experimental results of (-6 to +17%), (-8 to +19%), and (-20 to +9%), was computed for $f_{\max}$, $\varepsilon_{\max}$, and ε_{75}, respectively. Similarly, a difference range of (-10 to +21%), (-8 to +19%), and (-18 to +12%) was observed when using linear regression. Although this model fits the analyzed experimental data well, further calibration against larger set of experimental data, when available, is recommended to generalize the model.

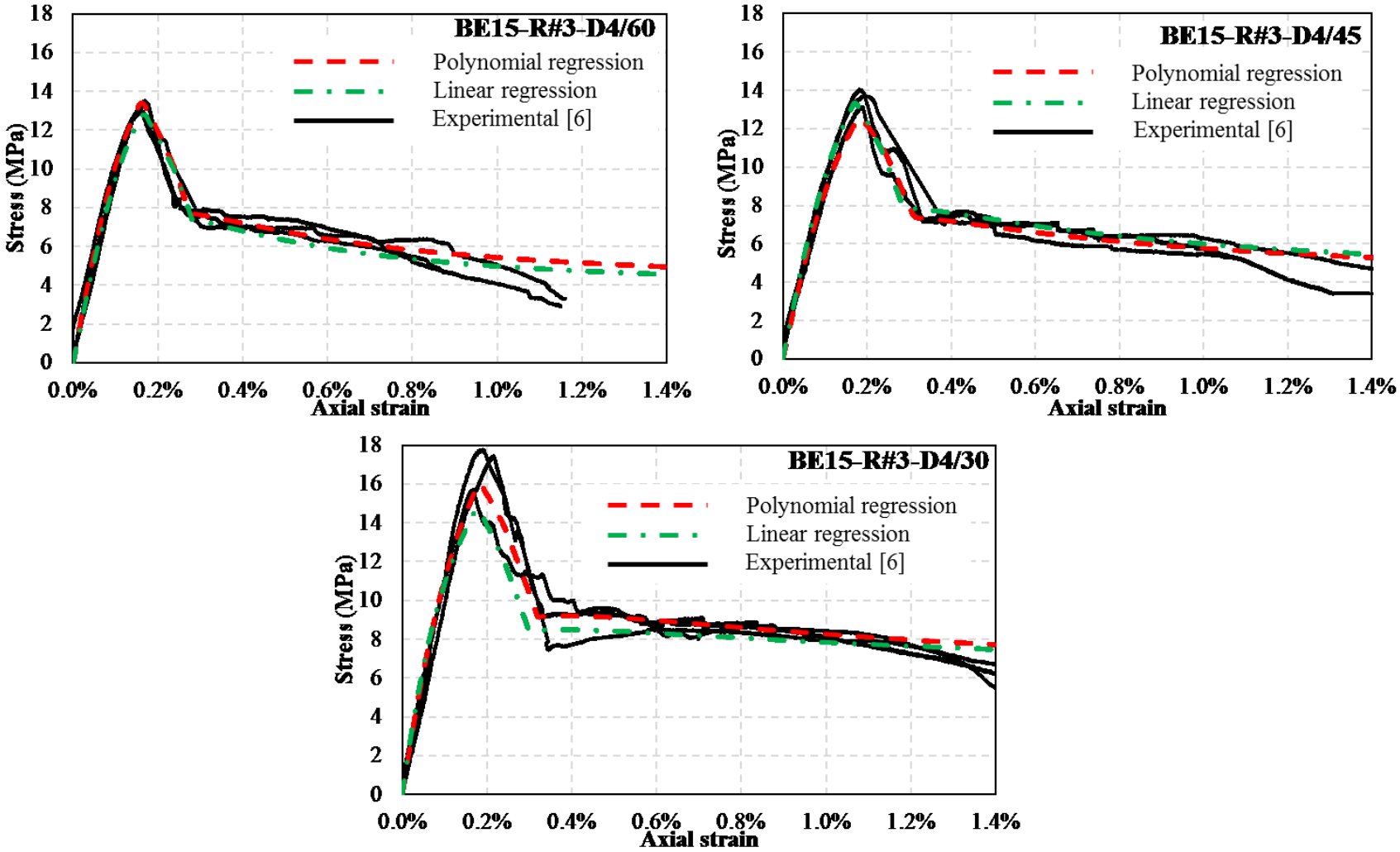

Figure 5.10 Model predictions versus the experimental results for RMBE built using #3 vertical bars

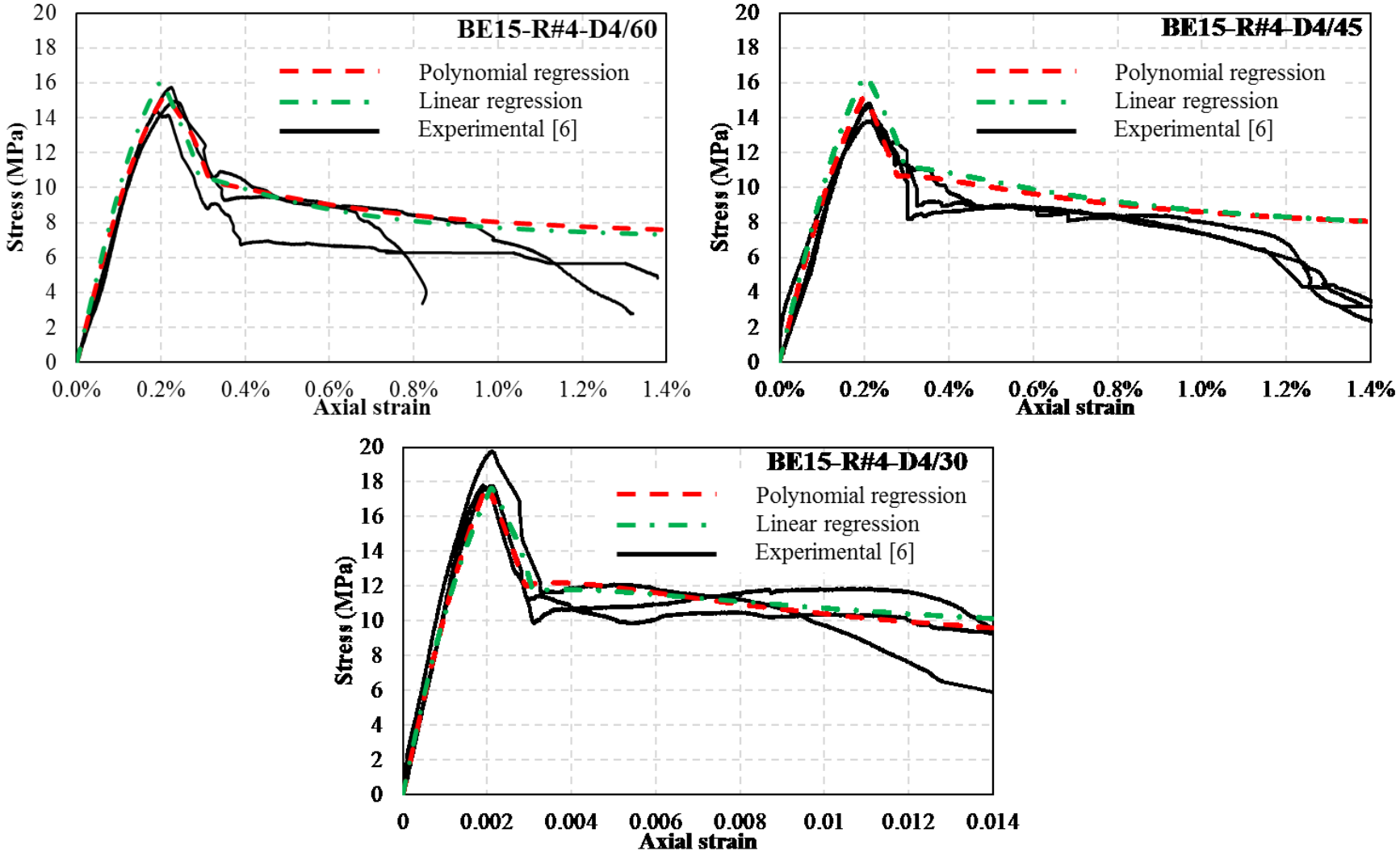

Figure 5.11 Model predictions versus the experimental results for RMBE built using #4 vertical bars

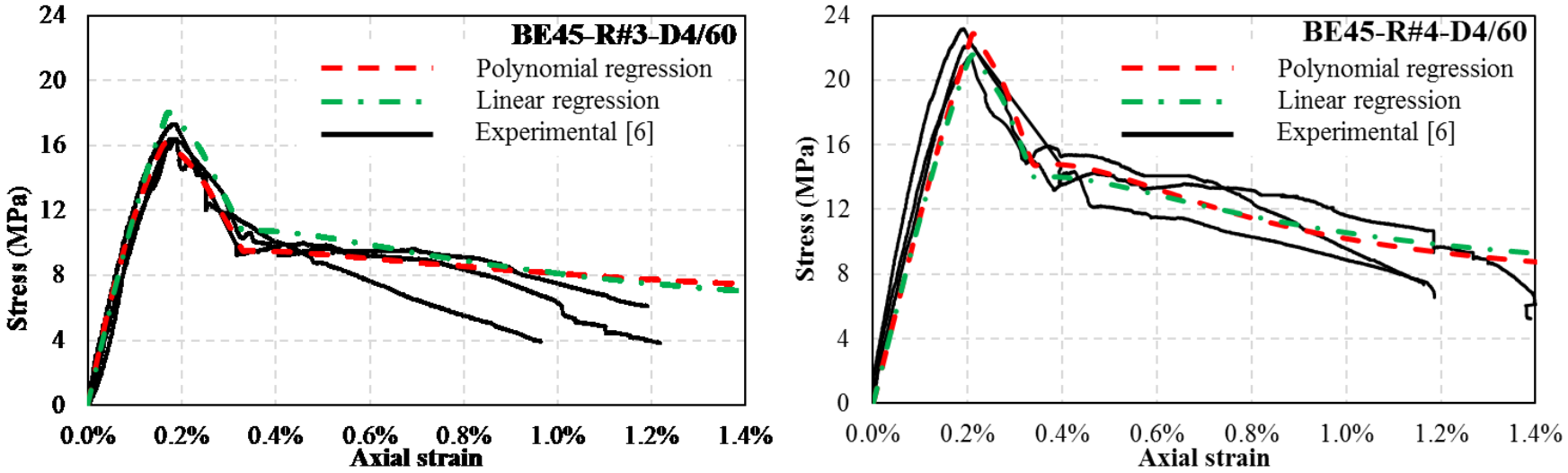

Figure 5.12 Model predictions versus the experimental results for RMBE built using 45 MPa grout

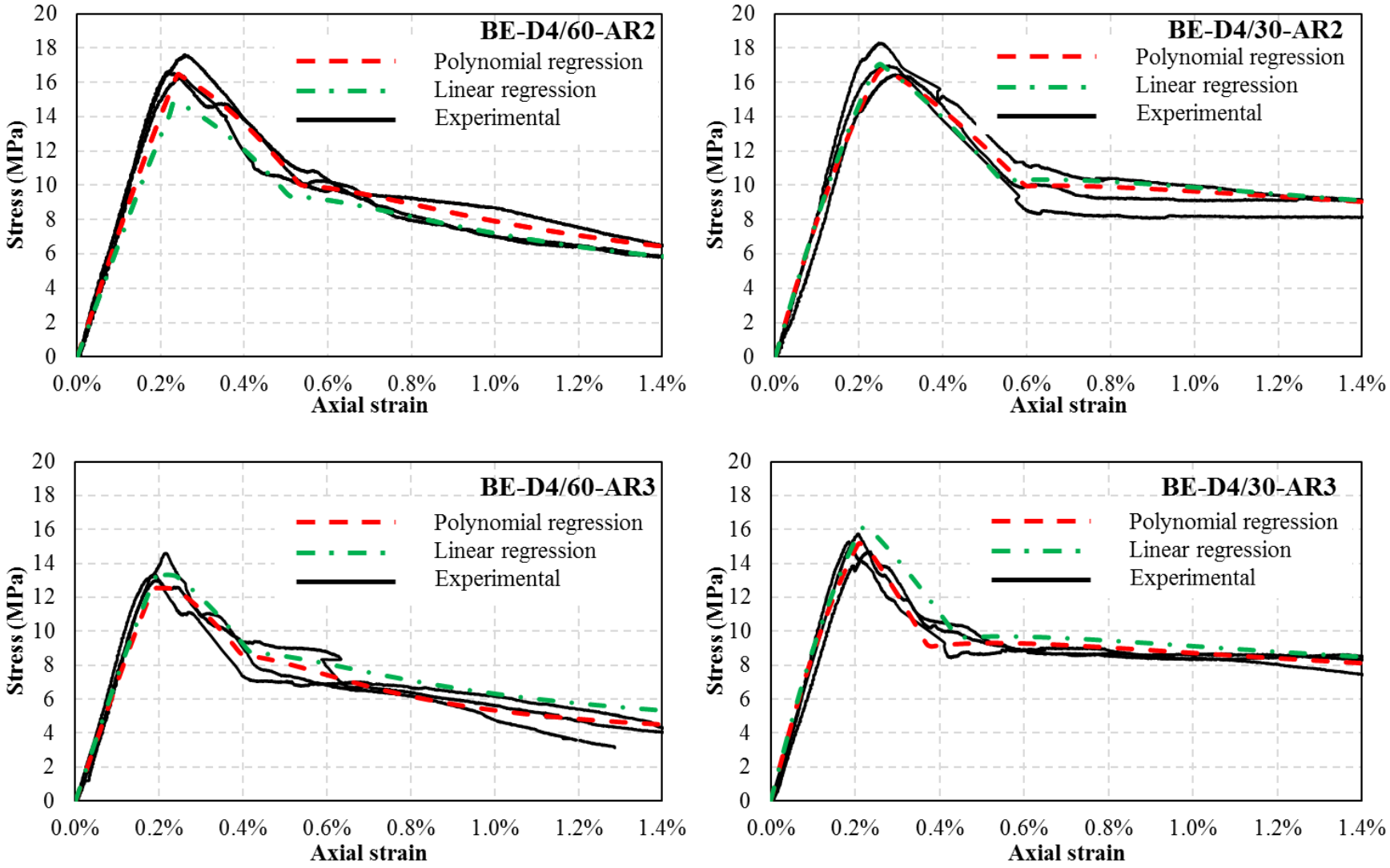

Figure 5.13 Model predictions versus the experimental results for RMBE built using different aspect ratios

Table 5.4: RMBE specimen details used for calibrating an empirical model

RMBE #	RMBE ID	Grout Strength (MPa)	Longitudinal Reinforcement		Transverse Reinforcement		Aspect ratio AR
			Number-size of Bars	ρ_v%	Bar size (spacing mm)	ρ_l%	
1	**BE15-R#3-D4/60-A***	15	4 - #3	0.79	D4 (60)	1.57	5.03
2	**BE15-R#3-D4/60-B***	15	4 - #3	0.79	D4 (60)	1.57	5.03
3	**BE15-R#3-D4/60-C***	15	4 - #3	0.79	D4 (60)	1.57	5.03
4	**BE15-R#3-D4/45-A***	15	4 - #3	0.79	D4 (45)	2.1	5.03
5	**BE15-R#3-D4/45-B***	15	4 - #3	0.79	D4 (45)	2.1	5.03
6	**BE15-R#3-D4/45-C***	15	4 - #3	0.79	D4 (45)	2.1	5.03
7	**BE15-R#3-D4/30-A***	15	4 - #3	0.79	D4 (30)	3.15	5.03
8	**BE15-R#3-D4/30-B***	15	4 - #3	0.79	D4 (30)	3.15	5.03
9	**BE15-R#3-D4/30-C***	15	4 - #3	0.79	D4 (30)	3.15	5.03
10	**BE15-R#4-D4/60-A***	15	4 - #4	1.40	D4 (60)	1.57	5.03
11	**BE15-R#4-D4/60-C***	15	4 - #4	1.40	D4 (60)	1.57	5.03
12	**BE15-R#4-D4/45-A***	15	4 - #4	1.40	D4 (45)	2.1	5.03
13	**BE15-R#4-D4/45-B***	15	4 - #4	1.40	D4 (45)	2.1	5.03
14	**BE15-R#4-D4/45-C***	15	4 - #4	1.40	D4 (45)	2.1	5.03
15	**BE15-R#4-D4/30-A***	15	4 - #4	1.40	D4 (30)	3.15	5.03
16	**BE15-R#4-D4/30-B***	15	4 - #4	1.40	D4 (30)	3.15	5.03
17	**BE45-R#3-D4/60-A***	45	4 - #3	0.79	D4 (60)	1.57	5.03
18	**BE45-R#3-D4/60-C***	45	4 - #3	0.79	D4 (60)	1.57	5.03
19	**BE45-R#4-D4/60-A***	45	4 - #4	1.40	D4 (60)	1.57	5.03
20	**BE45-R#4-D4/60-B***	45	4 - #4	1.40	D4 (60)	1.57	5.03
21	**BE45-R#4-D4/60-C***	45	4 - #4	1.40	D4 (60)	1.57	5.03
22	**BE-D4/60-AR2-A**	15	4 - #3	0.79	D4 (60)	1.57	2.00
23	**BE-D4/60-AR2-B**	15	4 - #3	0.79	D4 (60)	1.57	2.00
24	**BE-D4/60-AR2-C**	15	4 - #3	0.79	D4 (60)	1.57	2.00
25	**BE-D4/60-AR3-A**	15	4 - #3	0.79	D4 (60)	1.57	3.00
26	**BE-D4/60-AR3-B**	15	4 - #3	0.79	D4 (60)	1.57	3.00
27	**BE-D4/60-AR3-C**	15	4 - #3	0.79	D4 (60)	1.57	3.00
28	**BE-D4/30-AR2-A**	15	4 - #3	0.79	D4 (30)	3.15	2.00
29	**BE-D4/30-AR2-B**	15	4 - #3	0.79	D4 (30)	3.15	2.00
30	**BE-D4/30-AR2-C**	15	4 - #3	0.79	D4 (30)	3.15	2.00
31	**BE-D4/30-AR3-A**	15	4 - #3	0.79	D4 (30)	3.15	3.00
32	**BE-D4/30-AR3-B**	15	4 - #3	0.79	D4 (30)	3.15	3.00
33	**BE-D4/30-AR3-C**	15	4 - #3	0.79	D4 (30)	3.15	3.00

*Tested by Obaidat et al. [6]

Table 5.5: Percentage of difference between the proposed model and the experimental results

RMBE #	RMBE ID	Polynomial regression Difference %			Linear regression Difference %		
		f_{max}	ε_{max}	ε_{75}	f_{max}	ε_{max}	ε_{75}
1	**BE15-R#3-D4/60-A**	-2.39	-2.50	-8.33	2.19	-8.24	-10.20
2	**BE15-R#3-D4/60-B**	-2.99	0.00	4.17	1.56	-5.88	2.04
3	**BE15-R#3-D4/60-C**	0.90	6.25	-4.17	5.62	0.00	-6.12
4	**BE15-R#3-D4/45-A**	4.29	0.00	-7.41	-1.20	5.88	0.00
5	**BE15-R#3-D4/45-B**	11.51	1.11	-3.70	5.64	7.06	4.00
6	**BE15-R#3-D4/45-C**	8.97	-2.78	-11.11	3.23	2.94	-4.00
7	**BE15-R#3-D4/30-A**	11.13	8.33	7.41	20.95	8.33	11.54
8	**BE15-R#3-D4/30-B**	-1.88	5.56	0.00	6.80	5.56	3.85
9	**BE15-R#3-D4/30-C**	9.00	19.44	3.70	18.64	19.44	7.69
10	**BE15-R#4-D4/60-A**	-2.29	-4.76	-6.67	-7.14	0.00	1.82
11	**BE15-R#4-D4/60-C**	2.94	0.00	-13.33	-2.17	5.00	-5.45
12	**BE15-R#4-D4/45-A**	0.07	7.00	13.21	-7.26	7.00	5.26
13	**BE15-R#4-D4/45-B**	16.58	0.00	9.43	8.05	0.00	1.75
14	**BE15-R#4-D4/45-C**	-2.37	5.00	5.66	-9.51	5.00	-1.75
15	**BE15-R#4-D4/30-A**	10.39	10.00	16.98	12.27	4.76	8.77
16	**BE15-R#4-D4/30-B**	-0.67	5.00	13.21	1.02	0.00	5.26
17	**BE45-R#3-D4/60-A**	6.91	6.47	-17.86	-3.78	6.47	-17.86
18	**BE45-R#3-D4/60-C**	1.30	10.00	3.57	-8.83	10.00	3.57
19	**BE45-R#4-D4/60-A**	-6.20	0.00	3.23	-0.09	0.00	3.23
20	**BE45-R#4-D4/60-B**	-2.79	4.76	0.00	3.53	4.76	0.00
21	**BE45-R#4-D4/60-C**	1.22	0.00	-6.45	7.81	0.00	-6.45
22	**BE-D4/60-AR2-A**	-0.67	4.17	-13.33	10.74	4.17	-11.36
23	**BE-D4/60-AR2-B**	6.79	0.00	-6.67	19.05	0.00	-4.55
24	**BE-D4/60-AR2-C**	0.79	-8.33	0.00	12.36	-8.33	2.27
25	**BE-D4/60-AR3-A**	4.00	-12.50	2.70	-5.11	5.00	5.56
26	**BE-D4/60-AR3-B**	6.88	-16.67	-13.51	-2.48	0.00	-11.11
27	**BE-D4/60-AR3-C**	16.80	-8.33	-8.11	6.57	10.00	-5.56
28	**BE-D4/30-AR2-A**	-2.08	0.00	-9.28	-3.80	4.00	-2.22
29	**BE-D4/30-AR2-B**	8.93	-7.69	-17.53	7.02	-4.00	-11.11
30	**BE-D4/30-AR2-C**	1.07	6.15	-19.59	-0.70	10.40	-13.33
31	**BE-D4/30-AR3-A**	0.53	4.76	9.38	-5.09	0.00	-5.41
32	**BE-D4/30-AR3-B**	-3.29	9.52	6.25	-8.70	4.55	-8.11
33	**BE-D4/30-AR3-C**	3.62	9.52	3.12	-2.17	4.55	-10.81

5.5.5 Model Limitations

This study presents an empirical stress-strain model for RMBEs. The proposed model takes into account the effect of different grout strength, aspect ratio, vertical reinforcement ratio and the volumetric ratio of transversal reinforcement. Moreover, the model can predict the stress-strain response of RMBEs having different vertical reinforcement area and different confined core dimensions. Therefore, this model presents an effective tool that can be utilized in various numerical analysis packages. However, this model, similar to any empirical model, has limitations and still open for further enhancements. Considering the limited available experimental data, this model is calibrated with limited data of RMBEs. The considered experimental data consisted of half-scale RMBEs built using C-shaped concrete blocks. The model predictions are reliable within the range of each calibrated parameter, AR (2–5), f_g (15–45 MPa), ρ_v (0.79–1.4), and ρ_l (1.53–3.11). It should be noted that two regression techniques were implemented in this model. The polynomial regression is well suited for samples having similar properties to the calibrated RMBEs, however, it could result in out of range predictions for other RMBEs. On the other hand, the linear regression equations are applicable for a wider range of RMBEs, however, with a lower coefficient of determination. This model presents an essential tool to engineers that can predict the compressive stress-strain response of confined and unconfined masonry zones, which will result in a better prediction of RM shear walls with boundary elements seismic response.

5.6 Conclusions

This study presents the second phase of a research project conducted at Concordia University aiming at investigating the axial stress-strain response of reinforced masonry boundary elements (RMBEs). The first phase investigated, experimentally, the effect of changing grout strength, vertical and horizontal reinforcement ratio on the stress-strain response of thirty RMBEs and unreinforced masonry boundary elements (BEs) (Obaidat et al. [6]). Moreover, the first phase tested the capability of existing stress-strain models in predicting the stress-strain response of RMBEs where none of the examined models was capable of capturing the overall response of the RMBEs. On the other hand, the second phase of this project, which is the focus of the current study, investigated the effect of changing the RMBE's height to thickness ratio (i.e. aspect ratio) on the stress-strain behaviour considering different confinement ratios by testing seventeen RMBEs and unreinforced BEs. Finally, this study was concluded by presenting a stress-strain empirical model calibrated using the experimental data of the two phases.

The current study investigated the effect of three different aspect (AR) ratios and two confinement ratios of transverse reinforcement (i.e. by changing the hoop spacing) on the compression stress-strain behaviour of RMBE. The results showed that increasing the confinement ratio of transverse reinforcement and decreasing the AR enhanced the RMBE peak stress. On average, as the AR decreased from 5 to 2, the peak stress increased by 20%, 28%, and 2% for unreinforced BEs, RMBEs having 60 and 30 mm hoops spacing, respectively. On the other hand, as the confinement ratio of transverse reinforcement increased from 0.022 (i.e. 60 mm hoops spacing) to 0.062 (i.e. 30 mm hoops spacing), the peak stress increased by 2%, 12%, and 29% for RMBEs with AR of 2, 3 and 5, respectively. It was also observed that decreasing the aspect ratio did not affect the RMBE peak stress in specimens having highest confinement ratio of transverse reinforcement (i.e. 30 mm hoops spacing).

In general, decreasing the hoop spacing and/or the AR exhibited an increase in the corresponding RMBE post-peak strain. The strain ductility, $\mu_{50\%}$, increased as the aspect ratio decreased from 5 to 2 by 46%, and 69% for unreinforced BEs and RMBEs having 30 mm hoops spacing, respectively. Moreover, the strain ductility, $\mu_{50\%}$, increased by 130%, 131%, and 19%, as the confinement ratio of transverse reinforcement increased from 0.022 to 0.062, for RMBEs with aspect ratio of 2, 3 and 5, respectively.

An empirical stress-strain model was proposed for half-scale C-shape RMBE simulating the end zones of reinforced masonry shear walls with BEs. The proposed model considered different parameters, namely, aspect ratio, the volumetric ratio of transverse reinforcement, the vertical reinforcement ratio, and the grout strength. This model was calibrated with the experimental data of thirty-three RMBEs. Two regression approaches were implemented to calibrate this model; polynomial and simple linear regression. The model results fitted well with the experimental stress-strain relationships. The proposed model was capable of capturing the descending part of the compressive stress-strain curve including the sudden stress drop after the peak stress due to the face shell spalling. A maximum difference varies from -20 to +21% was observed when comparing the model predictions with the experimental results at RMBE peak stress (f_{max}), strain at the peak stress (ε_{max}) and strain at 75% of the peak stress (ε_{75}). Although this model is still open for more enhancement considering more experimental results, it presents a simple and effective tool that can be used in different numerical analyses.

5.7 Acknowledgments

The Authors acknowledge the support from the Natural Science and Engineering Research Council of Canada (NSERC), l'Association des Entrepreneurs en Maçonnerie du Québec (AEMQ), the Canadian Concrete Masonry Producers Association (CCMPA) and Canada Masonry Design Centre (CMDC). The authors would like to acknowledge the help of the technical staff at Concordia University during the testing program.

Chapter 6

Summary, Conclusions, and Recommendations for Future Work

6.1 Summary

The purpose of the current research project was to investigate the compression stress-strain behaviour of reinforced C-shaped masonry boundary elements (RMBE) considering the effects of the following parameters:

1- Vertical reinforcement ratio, ρ_L

2- Volumetric ratio of transverse reinforcement, ρ_l

3- Grout strength, f_g

4- Aspect ratio of boundary elements (height to thickness), h/t.

In addition to the aforementioned objective, this study presents an empirical analytical compression stress-strain model, capable of computing the reinforced C-shaped RMBE axial response considering the above parameters.

This dissertation consists of experimental, numerical, and analytical work. The experimental program included a total of 16 full-scale RMBE with square sections of 390 mm x 390 mm (length x width) and 47 half-scale RMBE with square sections of 190 mm x 190 mm (length x width). Each specimen was tested under a concentric loading up to failure. The experimental test results focused on the: stress-strain relationships, ultimate stress, mode of failure and damage propagation, axial strains (i.e., the strain corresponding to peak and post-peak behaviour), and ductility. The numerical work was performed on the full-scale RMBEs. The nonlinear finite element software package, ABAQUS, was employed for the numerical simulation of the compression stress-strain behaviour of the tested RMBEs. The FE model was able to capture key RMBE response including; ultimate stress, and post peak behavior. Finally, this study concludes by presenting a compressive stress-strain analytical model capable of predicting the RMBE overall response by computing the stress-strain relationship of the confined and unconfined zones. The model formulations were calibrated against thirty-three tested RMBE and consider the effect of: the vertical reinforcement ratio, the volumetric ratio of transverse reinforcement, grout strength, and the aspect ratio of a RMBE (height to thickness). This model present a simple, yet reliable, tool that can be implemented in different analysis packages.

6.2 Conclusions

To predict the deformation and ductility capacities of a RM wall integrated with boundary elements, research of the boundary element is essential. This study presents observed compressive stress-strain behaviours for a total of 16 full-scale RMBEs and 47 half-scale RMBEs. They simulated the high stress zones of RMSWs. The influence of changing hoop spacing, vertical reinforcement ratio, grout compressive strength, and aspect ratio (height to thickness) were investigated. This research richens the knowledge in this study area by providing experimental evidence of the influences the previously mentioned parameters on the compressive stress-strain response. The following points were concluded based on the experimental, numerical, and empirical results:

6.2.1 Conclusions Based on the Experimental Results

This section presents the conclusions drawn from the experimental results considering each investigated parameter.

Transverse reinforcement ratio

- As the confinement ratio of transverse reinforcement increases, the strength of the RMBE increases. The full-scale C-RMBE's results showed that the confinement ratios of 0.01, 0.02, 0.028, and 0.057, increased the peak stress excluding the vertical reinforcement's contribution by 8.1%, 9.2%, 10.8%, and 13.81%, respectively, compared to unconfined specimens. On the other hand, in the half-scale RMBE with an aspect ratio, AR of 5, which were reinforced with #3 bars, the confinement ratios 0.022, 0.034, and 0.062 increased the peak stress, excluding the vertical reinforcement's contribution by 1%, 4%, and 37%, respectively, upon the comparison to unconfined specimens. However, the peak stress increased by 1%, 9%, and 33% for the half-scaled RMBEs with an AR of 5 which reinforced with #4 bars. On other hand, the strength of the RMBE for samples BE-D4/60-AR2 and BE-D4/60-AR3 increased by 22.77% and 0.5% compared to BE-D4/60-AR5 strength, respectively. Therefore, Based on the previous conclusion, it was derived that the RMBE's peak stress did not increase proportionally to the confinement ratio. The enhancement in the RMBE peak stress was only noticeable for specimens that had a 30 mm hoop spacing.

- The confinement reinforcement ratio affected the post peak behaviour significantly and produced a post-peak stress-strain curve that was less steep. In the full-scale specimens, using confinement ratios of 0.01, 0.02, 0.028, and 0.057 increased the strains, at 75% of the peak stress, by 29%, 37.5%, 58.4%, and 83% respectively, compared to the unreinforced units. However, the strain, at 50% gain, increased by 45%, 100%, 122.5%, and 232%, respectively, higher than unreinforced specimens. On other hand, the half-scale specimens confined by 0.022, 0.034, and 0.062confinement reinforcement ratios and reinforced with #3 bars exhibited an increase in strain, at 75% of peak stress, of 11%, 19%, and 33%, respectively, compared to unreinforced specimens. However, the strain, at 50% of peak stress, increased by 103, 130, and 200%, respectively, compared to unreinforced specimens. The half-scale specimens confined by 0.022, 0.034, and 0.062 confinement reinforcement ratios and reinforced with #4 bars, experienced an increase in strain, at 75% of peak stress, of 30%, 38%, and 48%, respectively, compared to unreinforced specimens. Moreover, the strain at 50% of peak stress increased by 147%, 150%, and 220% when increasing the corresponding confinement reinforcement ratios from 0.022 to 0.034 to .062, respectively. On other hand, the specimens of BE-D4/60-AR2 and BE-D4/30-AR2 exhibited an increase in the strain at 50% of peak stress of 61.65% and 306.19%, respectively, compared to BE-0-AR2. However, the specimens of BE-D4/60-AR3 and BE-D4/30-AR3 exhibited an increase in the strain at 50% of peak stress of 115.74% and 436.44%, respectively compared to BE-0-AR3.

Vertical reinforcement ratio

- The presence of vertical reinforcement enhanced the strength and, therefore, less damage was exhibited for such specimens, contrary to those that were unreinforced.
- After removing the vertical reinforcement contribution to the RMBE strength, the RMBE specimens vertically reinforced with #3 bars experienced a strength increase of 1%, 4%, and 37% with corresponding hoop spacing of 30 mm, 45 mm, and 60 mm. Whereas, the #4 vertically reinforced specimen revealed a strength increase of 1%, 9%, and 33% for the corresponding hoop spacing of 30 mm, 45 mm, and 60 mm. Therefore, the increase in the longitudinal reinforcement had no effect on the strength of the confined core, however it increased the capacity of the RMBE in proportion to the added vertical steel area.

- Decreasing hoops from 60 to 45 to 30mm for RMBE specimens having #4 vertical rebar, resulted in a corresponding increase in the RMBE strain, at 75% of peak stress of 9.7%, 13.8%, and 15.5%, respectively, compared to the RMBE specimens with #3 vertical bars. Moreover, the increases in the strain at 50% of peak stress, were 27.5%, 28.2%, and 18.7%, respectively, for the RMBE specimens with #4 vertical bars, with decreasing hoops from 60 to 45 to 30mm, compared to the RMBE specimens with #3 vertical bars. An increase in strain capacity of over 25% was revealed for the specimens reinforced with #4 vertical bars, as compared to those reinforced with #3 bars.
- The concrete-reinforcement strain compatibility was achieved up to approximately 0.2% of axial strain, which corresponds to the RMBE peak stress. However, following the RMBE peak stress, the axial strain, computed from the LVDT, was not similar to the strain in the longitudinal bars. The longitudinal steel bars yielded after the peak stress was reached (i.e., at the stage of block face shell spalling). Buckling of the longitudinal reinforcement was observed in RMBE specimens, with widely spaced hoops, after 50% of peak stress.

Grout strength

- As the grout strength increases, the RMBE peak stress increased. The unreinforced specimens, confined specimens reinforced, with #3, and confined specimens reinforced with #4 that were constructed with high strength grout of 45 MPa exhibited an increase in peak stress by 48%, 27%, and 49%, respectively compared to those RMBE specimens constructed with normal strength grout of 15 MPa. On another hand, the strain at 75% of peak stress increased in the RMBE specimens constructed with grout 45 MPa strength and reinforced with #3 and #4 about 13% and 21%, respectively, compared to those specimens constructed with grout 15 MPa. However, the RMBE specimens constructed with grout 45 MPa strength and reinforced with #3 and #4 exhibited increase in strain at 50% of peak stress about 14% and 55%, respectively.
- Based on the grout area, the RMBE capacity did not increase proportionally to the grout strength.
- The effect of the grout strength was more noticeable on the peak and post-peak behaviour.

Aspect ratio

- As the aspect ratio decreases, the peak stress, strain at peak stress, and post peak strain increases, however, the sudden drop following the peak decreases,
- By comparing the specimens having AR of 5 to those of 2 and 3, an increase in RMBE strength of 23%, and 0.5%, respectively was observed. On the other hand, the strain at peak stress increased by 34% and 19.5%, respectively.
- Furthermore, decreasing the height to thickness ratio from AR 5 to 2 and 3, exhibited a strain increase, at 75% of peak stress, of 55% and 28%, respectively. However, the strain, at 50% of peak stress, increased by 13% and 6%, respectively.
- Therefore decreasing the aspect ratio from 5 to 3 had less effect on the RMBE overall stress-strain response. This was not the case for AR 2 which exhibited more gradual post-peak stress-strain descending curves compared to the specimens having AR of 5.

6.2.2 Conclusions based on the Numerical model

- The compression stress-strain behaviour of the tested C-RMBEs was numerically simulated with the nonlinear finite element software package, ABAQUS. The damage plasticity model from ABAQUS was applied in this study for simulating the behaviour of grout, mortar, and masonry block. The stress-strain relationship proposed by Saenz's was used to model the stress-strain behaviours of the grout and the concrete blocks under uniaxial compression. The plastic model from the ABAQUS software was applied to simulate the reinforcement stress-strain behaviour. The proposed FEM procedure provided a respectable approximation for the compression stress-strain behaviour in the elastic and inelastic ranges. In addition, the proposed FEM procedure expressed the influence of the confinement ratio on the compression response of the C-RMBEs.

6.2.3 Conclusions based on the Empirical compressive stress-strain model

- Based on the experimental data an empirical stress-strain model is proposed for the confined and unconfined masonry zones considering different grout strength, aspect ratio, vertical, and transversal reinforcement ratios. The model was calibrated against the experimental results of thirty-three RMBE. The RMBE stress-strain relationship is computed by adding

the unconfined masonry, confined masonry and the vertical reinforcement contribution. Consequently, the model provide a flexibility in changing the vertical bar size and the core area. Therefore this model can be utilized in different analysis packages.

- The model was calibrated with RMBE that have varying grout strength (15-45 MPa), hoops spacing (30-60 mm), Aspect ratio (2-5), vertical reinforcement ratio (0.8-1.4) and transversal reinforcement ratio (1.53-3.057). Therefore, this model cover a wide range of different parameters. The proposed model captures the descending part of the compressive stress-strain curve including the sudden stress drop after the peak stress due to the face shell spalling. It should be noted, that this model is an emperical model caliberated over a limited number of specimens. Therefore this model is open for more enhancement by considering more specimens and more parameters.

6.3 Recommendations for Future Research

The investigation of the compression stress-strain behaviour of unconfined and confined masonry boundary elements was the main objective of this study. The conclusions of this study were limited to the parameters that were being tested. However, in order to further expand the knowledge in this field, other parameters may be considered. Therefore, the following is a list of some recommendations for future research.

- Additional experimental work on boundary elements constructed with special masonry blocks that have different compressive strengths. This can be done to eliminate the sudden drop in strength and enhance the compression behaviour of boundary elements.
- The results of the masonry boundary elements are limited to square cross-section. Consequently, it is recommended to perform experimental tests on boundary elements with rectangular cross-sections.
- Each test was performed under concentric loading, therefore, experimental tests for the response of masonry boundary elements subjected to different loads, such as eccentric compression and cyclic loads, needs to be investigated.
- Validation of the proposed analytical model can be completed with additional testing of reinforced boundary elements.

- The arrangement of vertical reinforcement and the configuration of the hoops can to be considered in future research.
- It is recommended to test full-scale shear walls, with differing configurations of boundary elements, to investigate the effect of changing specific parameters in the RMBE on the wall response.
- Extending the experimental and numerical methodology developed in this study to investigate the effects of design variables, such as the compressive strength of the constituent materials.
- Finally, this dissertation presents a wealth of experimental data that can be used to calibrate/validate numerical and analytical models.

References

Abrams, D. P. (1986). “Lateral resistance of a two-story block building.” Proc., Advances in Analysis of Structural Masonry, ASCE, Reston, VA,41–57.

ABAQUS. (2011). Analysis user’s manual 6.11, Dassault Systems Simulia Corp., Providence, RI, USA.

Abo El Ezz A, Eldin H, Galal K. (2015). “Influence of confinement reinforcement on the compression stress–strain of grouted reinforced concrete block masonry boundary elements.” Structures Journal, Vol. 2, pp. 32-43.

Alwathaf H, Thanoon WA, Jaafar MS, Noorzaei J. (2012). “Mathematical modelling of stress-strain curves of masonry materials.” Australian Journal of Structural Engineering; 13 (3): 219-229.

Ascione L, Berardi VP, Feo L, Mancusi G. (2005). “A numerical evaluation of the international stress state in externally FRP plated RC beams.” Composites Part B; 36: 83-90.

ASTM, ASTM C140 / C140M - 13a, Standard Test Methods for Sampling and Testing Concrete Masonry Units and Related Units, 2013, ASTM International.

Banting B, El-Dakhakhni W. (2012). “Force-and Displacement-Based Seismic Performance Parameters for Reinforced Masonry Structural Walls with Boundary Elements.” Journal of Structural Engineering, Vol. 138, No. 12, pp 1477-1491.

Batikha M, Alkam F. (2015). “The effect of mechanical properties of masonry on the behaviour of FRP-strengthened masonry-infilled RC frame under cyclic load.” Composite Structures; 134: 513-522.

Bertero V, Popov E. (1977). “Concrete confined by rectangular hoops and subjected to axial loads.” Report No. UCB/EERC-77/13, Earthquake Engineering Research Center, University of California, Berkeley, California.

CSA (Canadian Standards Association). (2004). “Mortar and grout for unit masonry.” CSA A179-04, CSA, Mississauga, Canada.

CSA S304-14. (2014). “Design of masonry structures.” Mississauga, Ontario, Canada: Canadian Standards Association.

Dhanasekar M, Shrive NG. (2002). “Strength and deformation of confined and unconfined grouted concrete masonry.” American Concrete Institute (ACI) Journal, Vol. 99, No. 6, pp. 819–26.

Drysdale, R.G. and Hamid A.A. (1979) “Behaviour of Concrete Block Masonry under Axial Compression”. ACI Journal, pp. 707-721.

Drysdale, R.G. and Hamid, A. (2005). “Masonry Structures-Behaviour and Design.” 3 ed., Canada Masonry Design Centre, Mississauga, Canada.

Ezzeldin, M., Wiebe, L., Shedid, M., and El-Dakhakhni, W. (2014). “Numerical modelling of reinforced concrete block structural walls under seismic loading.” 9th Int. Masonry Conf., International Masonry Society, Surrey, U.K.

Federal Emergency Management Agency (FEMA). (2006). NEHRP Recommended Provisions: Design Examples. FEMA 451, Applied Technology Council, Redwood City, CA.

Feeg C, Longworth J, Warwaruk J. (1979). “Effects of reinforcement detailing for concrete masonry columns.” Department of Civil Engineering, University of Alberta, Edmonton, Alberta. Technical report 76.

Feng F. (2009). “Progressive collapse analysis of high-rise building with 3-D finite element modelling method.” Journal of Constructional Steel Research; 65: 1269-1278.

Ganesan T, Ramamurthy K. (1992). “Behaviour of concrete hollow-block masonry prisms under axial compression.” Journal of Structural Engineering; 118(7): 1751–1769.

Hamid A, Chuckwunenye A. (1986). “Compression behaviour of concrete masonry prisms.” Journal of Structural Engineering; 112(3): 605–613.

Hamzeh, L., Abo ElEzz, A., and Galal, K. (2015). "Numerical simulation of the seismic behaviour of reinforced concrete masonry structural walls". 11th Canadian Conference on Earthquake Engineering, Victoria, BC, Canada.

Hart G, Noland J, Kingsley G, Englekirk R, Sajjad NA. (1988). “The use of confinement steel to increase the ductility in reinforced concrete masonry shear walls.” The Masonry Society Journal, Vol. 7, No. 2, pp. 19–42.

Hart, G. C., Sajjad, N., Kingsley, G. R., and Noland, J. L. (1989). “Analytical stress-strain curves for grouted concrete masonry.” Masonry Soc. J., 8(1), pp. 21-34.

Hassanein M. (2010). “Numerical modeling of concrete filled lean duplex slender stainless steel tubular stub columns.” Journal of Constructional Steel Research; 66(8-9): 1057-1068.

Hognestad, E. (1951). "A study on combined bending and axial load in reinforced concrete members." Univ. of Illinois Engineering Experiment Station, Univ. of Illinois at Urbana-Champaign, IL, pp.43-46.

Hoshikuma, J., Kawashima, K., Nagaya, K., and Taylor, A. W. (1997). "Stress–strain model for confined reinforced concrete in bridge piers." Journal of Structural Engineering, 123(5), pp.624–633.

Hu H-T, Schnobrich WC. (1989). "Constitutive modelling of concrete by using non-associated plasticity." Journal of Materials in Civil Engineering; 1(4): 199-216.

Hunt BR, Sherwood EG. Simplified smeared area compression model for calculating compression strength of hollow concrete block masonry. 13th Canadian masonry symposium 2017.

Jankowiak T. Lodygowski T. (2005). "Identification of parameters of concrete damage plasticity constitutive model." Foundations of Civil and Environmental Engineering; 6: 53-69.

Joyal, M. (2014). "Enhanced ductility of masonry shear walls using laterally confined (Self-reinforced) concrete block." Master of applied science, McMaster University, Hamilton, Canada.

Kaushik H, Rai D, Jain S. (2007). "Stress-strain characteristics of clay brick masonry under uniaxial compression. Journal of Materials in Civil Engineering: Vol. 19(9): 728-739.

Kent, D.C. and Park, R. (1971). "Flexural Members with Confined Concrete." ASCE, Journal of the Structural Division, 97(7), pp.1969-1990.

Khalaf F, Hendry A, Fairbairn D. (1993). "Reinforced blockwork masonry columns." American Concrete Institute (ACI) Journal, 90(5), No. 5, pp. 496–504.

Kmiecik P, Kaminski M. (2011). "Modelling of reinforced concrete structures and composite structures with concrete strength degradation taken into consideration." Archives of Civil and Mechanical Engineering; 11(3): 623-636.

Köksal H, Doran B, Ozsoy A, Alacali S. (2004). "Nonlinear modelling of concentrically loaded reinforced blockwork masonry columns." Canadian Journal of Civil Engineering, Vol. 31, No. 6, pp. 1012-1023.

Lam D, Dai X. (2010). "Numerical modelling of the axial compressive behaviour of short concrete-filled elliptical steel columns." Journal of Constructional Steel Research; 66(7):931-942.

Lourenço PB. (1996). “Computational strategies for masonry structures.” Ph.D. thesis, Delft Univ. of Technology, Delft.

MacGregor, J.G. and Wight, J.K. (2004). “Reinforced Concrete: Mechanics and Design,” 4 ed. Prentice Hall.”

Malmquist, K.J. (2004). “Influence of Confinement Reinforcement on the Compressive Behavior of Concrete Block Masonry and Clay Brick Masonry Prisms.” M.S. Thesis, Washington State University, Washington, U.S.A.

Mander, J.B., Priestley, M.J.N. and Park, R. (1988b). “Observed Stress-Strain Behaviour of Confined Concrete”, Journal of Structural Engineering, 114(8), pp.1827-1849.

Mander, J. B., Priestley, M. J. N., and Park, R. J. T. (1988a). "Theoretical stress-strain model for confined concrete." Journal of structural engineering, ASCE, 114(8), pp.1804-1826.

Masonry Standards Joint Committee (MSJC). (2013). “Building code requirements for masonry structures.” TMS 402/ACI 530/ASCE 5. American Concrete Institute, Farmington Hills, MI., American Society of Civil Engineers, Reston, VA and The Masonry Society, Boulder, CO.

Obaidat, A., Abo El Ezz, A., and Galal, K. (2017a). "Compression behaviour of confined concrete masonry boundary elements". Engineering Structures, 132, 562-575.

Obaidat, A., Ashour, A., and Galal, K. (2017b). “Stress-Strain Behaviour of C-Shape Confined Concrete Masonry Boundary Elements of RM Shear Walls". Journal of structural engineering, submitted.

Obaidat Y, Heyden S, Dahlblom O. (2010). “The effect of CFRP and CFRP/concrete interface models when modelling retrofitted RC beams with FEM.” Composite Structures; 92: 1391-1398.

Park H, Kang SM, Chung L, Lee DB. (2007). “Moment-curvature relationship of flexure dominated walls with partially confined end-zones.” Engineering Structures, Vol. 29, No. 1, pp. 33–45.

Park, R., and Paulay, T. (1975). “Reinforced concrete structures.” John Wiley and Sons, New York, N.Y.

Paulay T, Priestley MJN. (1992). “Seismic design of reinforced concrete and masonry buildings.” New York, Wiley.

Priestley M.J.N. and Bridgeman, D.O. (1974). “Seismic Resistance of Brick Masonry Walls.” Bulletin of the New Zealand National Society for Earthquake Engineering, 7(4), pp.167-187.

Priestley, M., and Elder, D. (1983). "Stress-strain curves for unconfined and confined concrete masonry". ACI Journal Proceedings, 80(3), 192-201.

Saenz LP. (1964) Discussion of ‘‘Equation for the stress-strain curve of concrete” by Desayi P, Krishnan S. ACI Journal; 61:1229–35.

Sajjad, N.A. (1990). “Confinement of Concrete Masonry.” Ph.D. Thesis, University of California, Los Angeles, USA.

Sayed-Ahmed E, Shrive N. (1996). “Nonlinear finite element model of hollow masonry.” Journal of Structural Engineering; 122(6): 683–690.

Scott, B.D., Park, R., and Priestley, M.J.N. (1982). "Stress-strain behaviour of concrete confined by overlapping hoops at low and high strain rates." American Concrete Institute Journal, 79, pp.13-27.

Seible, F., Priestley, M.J.N., Kingsley, G.T., and Kurkchubasche,A.G. (1994b). “Siesmic response of a five-story full-scale RM research building.” ASCE Journal of Structural Engineering, Vol. 120, No. 3.

Shedid M, El-Dakhakhni W, Drysdale R. (2010). “Alternative Strategies to Enhance the Seismic Performance of Reinforced Concrete-Block Shear Wall Systems.” Journal of Structural Engineering, Vol. 136, No. 6, pp. 676-689.

Shedid, M. T., El-Dakhakhni, W. W., and Drysdale, R. G. (2010b). “Characteristics of confined and unconfined masonry prisms for seismic performance enhancement of structural walls.” Masonry Int., 23(2), pp.69–78.

Shedid, M.T. (2009). “Strategies to Enhance Seismic Performance of Reinforced Masonry Shear Walls.” Ph.D. Thesis, McMaster University, Hamilton, Canada.

Sheikh SA, Uzumeri SM. (1980). “Strength and Ductility of Tied Concrete Columns.” Journal of Structural Engineering; 106(5): 1079-1102.

Sousa J, Caldas Jr. (2005). “Numerical analysis of composite steel concrete columns of arbitrary cross-section.” Journal of Structural Engineering; 131(11): 1721-1730.

Sturgeon G, Longworth J, Warwaruk J. (1980). “An investigation of reinforced concrete block masonry columns.” Department of Civil Engineering, University of Alberta, Edmonton, Alberta. Technical report 91.

Vallenas J, Bertero V, Popov E. (1977). “Concrete confined by rectangular hoops and subjected to axial loads.” Report No. UCB/EERC-77/13, Earthquake Engineering Research Center, University of California, Berkeley, California.

Wang X, Su Y, Yan L. (2014). “Experimental and numerical study on steel reinforced high-strength concrete short-leg shear walls.” Journal of Constructional Steel Research; 101: 242-253.

Yalcin C, Saatcioglu M. (2000). “Inelastic analysis of reinforced concrete columns.” Journal of computers and structures; 77(5): 539-555.

Yong, Y. K., Nour, M. G., and Nawy, E. G. (1988). “Behaviour of laterally confined high-strength concrete under axial loads.” Journal of structural engineering, ASCE, 114(2), 332 – 351.

Yu T, Teng JG, Wong YL, Dong SL. (2010). “Finite element modeling of confined concrete-II: plastic-damage model.” ASCE Journal Engineering Structures; 32(3):680–691.

Appendix A

Experimental Work

A.1 Construction of C-Shape Reinforced Masonry Boundary Element

The C-shape reinforced masonry boundary elements (RMBEs) were constructed in the structural laboratory of the Concordia University. First, all the vertical reinforcement bars and hoops including cutting and bending were prepared. Then, all the masonry block units were cut into C-shapes. Followed by preparing the reinforcement cages for all RMBE specimens. All the RMBE specimens were constructed in two stages: 1) the footing, and 2) the masonry boundary elements.

A.1.1 Reinforced concrete footing

All the tested units of RMBEs were constructed on a RC footing. For full-scale RMBE, fourteen RC footing with dimensions of 400 mm x 400 mm x 250 mm (length x width x height) were constructed with a compressive strength of 35 MPa (see Figures A.1). Moreover, for the half-scale RMBE specimens, forty-two reinforced footing concrete with dimensions of 200 mm x 200 mm x 250 mm (length x width x height) were constructed with a compressive strength of 84 MPa. For the full-scale RMBE specimens, the concrete footing was reinforced longitudinally with 4-20M and transversally by hoops with 4-10M. However, for the half-scale RMBE specimens, the concrete footing was reinforced longitudinally either with 4-#3 or 4-#4 or transversally by hoops with 4-#4 (Figure A.2). After assembling the reinforcement cage, each six or eight RMBE were placed in a timber form to pour the bottom footing as shown in Figure A.3. RC bottom footing was poured prior the construction of RMBE specimens. The concrete was mixed at the Concordia University's structures laboratory at the. After pouring the high strength concrete in the lower footing, the RMBE were cured for at least one week (see Figure A.4).

Figure A.1 Bottom RC footing formwork for full-scale RMBE

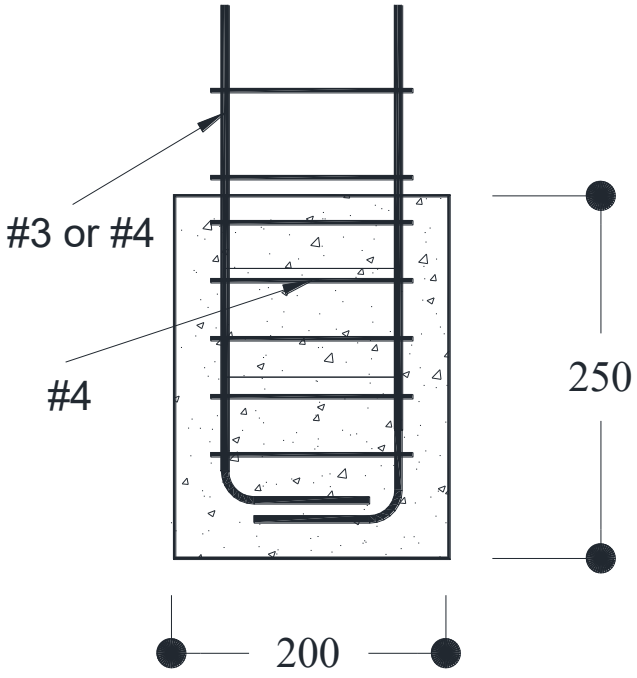

Figure A.2 Cross section with reinforcement layout of half-scale RC footing

Figure A.3 Bottom RC footing formwork

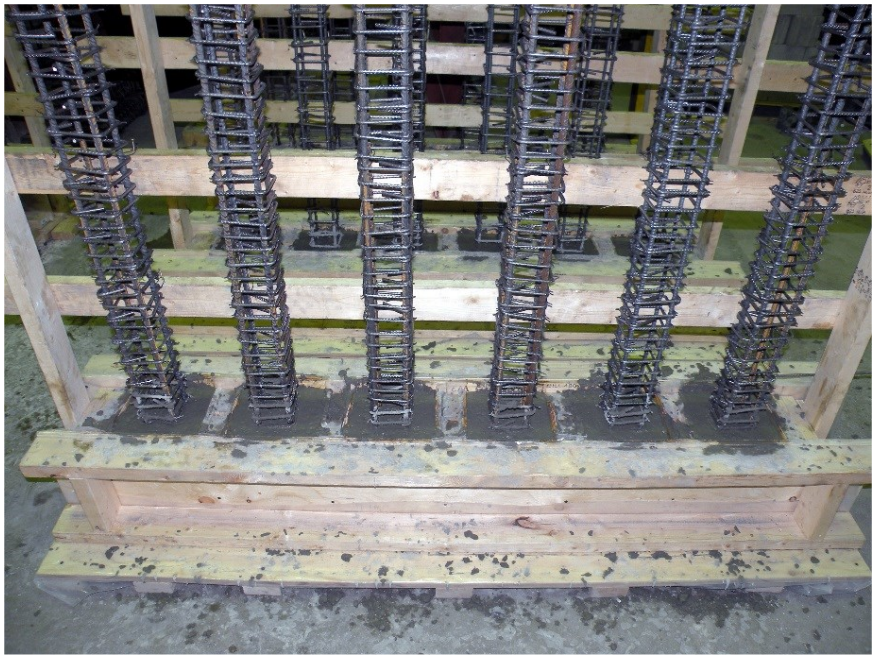

Figure A.4 Casting of RC footing

A.1.2 RMBE specimens

All full-scale and half scale fully grouted RMBE specimens were constructed at the structural laboratory of Concordia University. All the unconfined and confined C-RMBEs were constructed by professionally certified masons. Each full-scale specimen consists of five block courses. Whereas, the half-scale specimens consisted of four, six, and ten block courses placed on a concrete footing. Each course of the RMBE was composed of two block units. The blocks were joined together in full scale and half scale with 10 mm and 5 mm type-S mortar joints, respectively (see Figures A.5 to A.7). The construction of RMBE started off by assembling the reinforcement cage for each specimen (Figure A.8). The reinforcement cage consisted of four reinforcement bars (20M or #3 or #4), and deformed bars hoops (D4 or 10M, or 15M) at different spacings. The hoops size was increased to #4 (129 mm^2) in the upper and lower transfer footings to avoid failure in the footing. The vertical reinforcement bars were extended continuously, over the height of the RMBE specimen, without splices from the base of the bottom footing to the top footing. After that, each six RMBE specimens were inserted in a wooden formwork to pour the bottom footing (Figure A.9 and A.10). After pouring RC footing, the RMBE specimens were stored two weeks for the RC footing to cure (Figure A.11). Figures A.12 to A.15 show the reinforcemnt cage for the RMBE specimens. Then, the strain gauges were installed on the vertical reinforcement bars (Figure A.16). Followed by the construction of the RMBE specimens process (Figure A.17), the RMBE specimens were strapping before grouting to avoid any cracks in mortar head joints. (Figure A.18). The full-scale RMBE specimens were grouted with coarse grout and the half scale RMBE specimens with fine grout (Figure A.19). Finally, top footing was constructed on the RMBE and poured with high strength concrete (Figure A.20). Figures A.28 to A30 show most of Full-scale and half-scale RMBE specimens during constructions.

Figure A.5 Full-scale RMBE with five courses

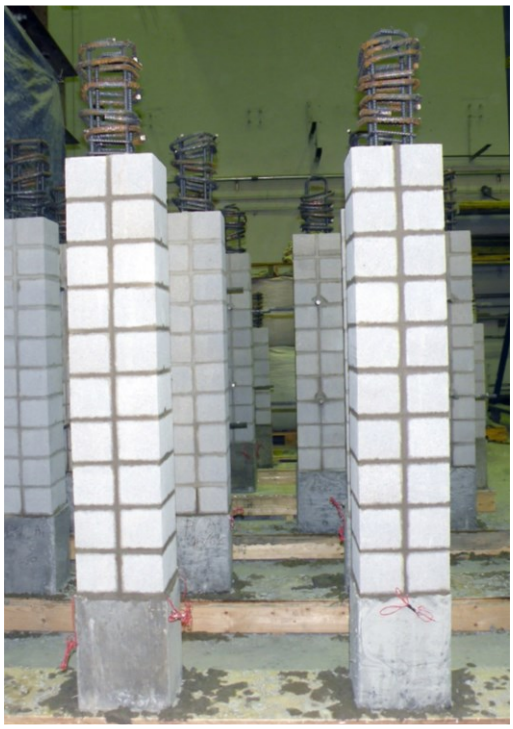

Figure A.6 Half scale RMBE with ten courses

Figure A.7 Half scale RMBE with six courses

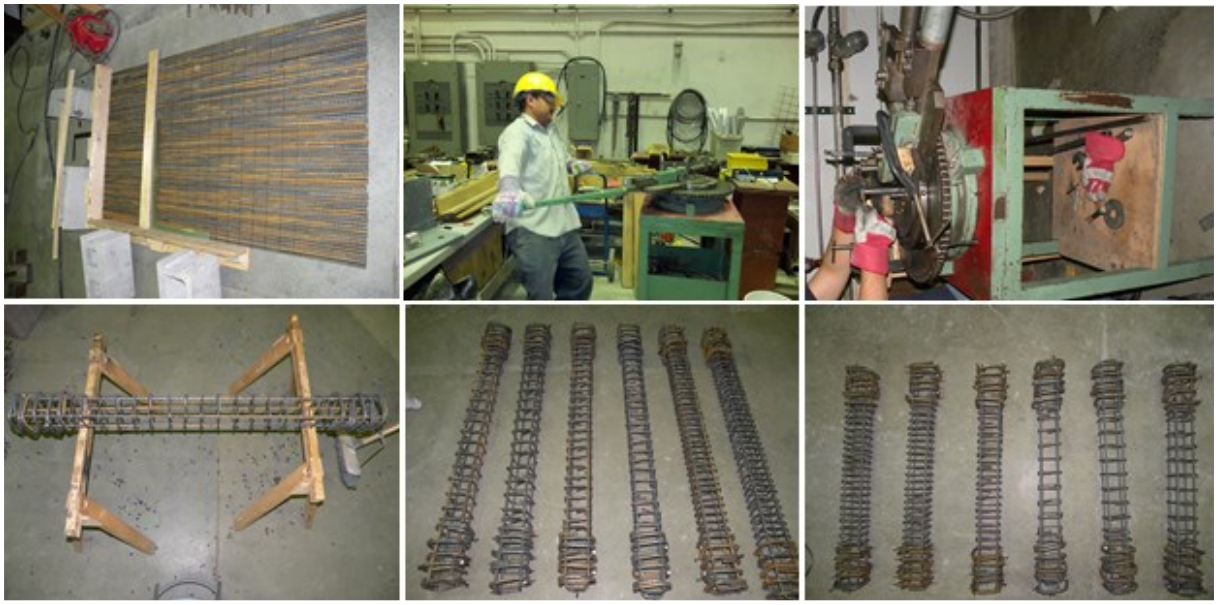

Figure A.8 Assemblage sequence of reinforcement steel cage for RMBE specimens

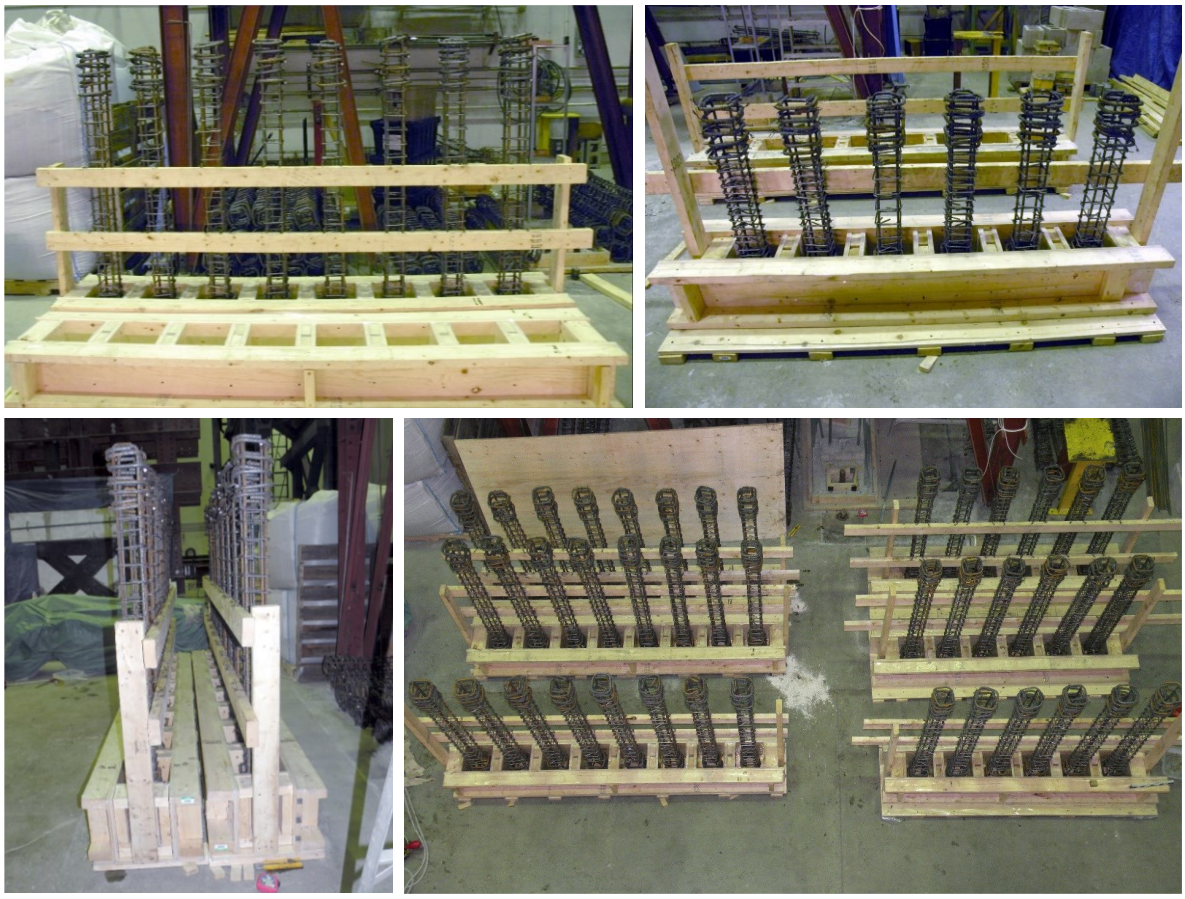

Figure A.9 Inserting the RMBE specimens in the timber

Figure A.10 Pouring the RC footing of the RMBE specimens in the timber

Figure A.11 Curing of the RC footing of the RMBE specimens

Figure A.12 RMBE specimens with ten courses, vertically reinforced with #3, and confined with D4/60, D4/45, and D$/30

Figure A.13 RMBE specimens with ten courses, vertically reinforced with #4, and confined with D4/60, D4/45, and D$/30

Figure A.14 RMBE specimens with six courses, vertically reinforced with #3, and confined with D4/60 and D$/30

Figure A.15 RMBE specimens with four courses, vertically reinforced with #3, and confined with D4/60 and D$/30

Figure A.16 Installation of the strain gauges on the vertical reinforcement bars

Figure A.17 Building blocks in the RMBE specimens

Figure A.18 Strapping of the RMBE specimens

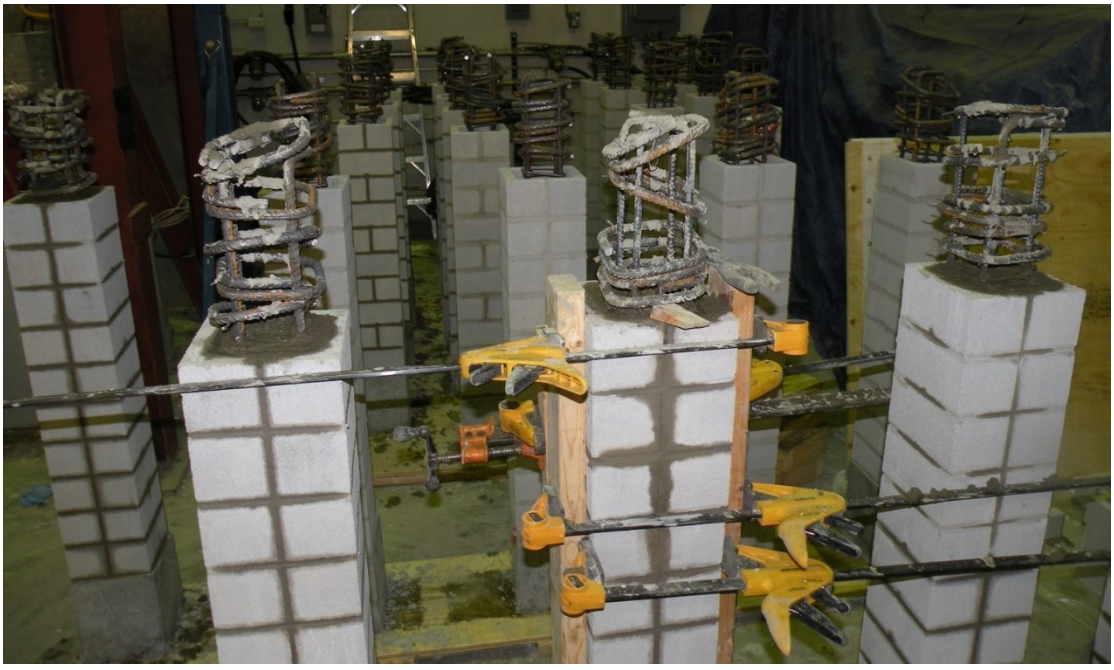

Figure A.19 Grouting of the RMBE specimens

Figure A.20 Construction of the top RC footing

A.2 Material Properties

A.2.1 Masonry block units

All RMBE specimens were constructed with C-shape block. The block units were manufactured as a whole rectangular unit with a dimension of 390 mm x 190 mm x 90 mm (length x width x depth) as shown in Figure A.21. The block units were cut with saw to obtain C-shape block unit with a dimension of 190 mm x 92.5 mm x 90 mm (length x width x height) as shown in Figure A.22 and A.23. A small groove was made in some block units to place the embedded cross bars that mount the LVDTs (Figure A.24).

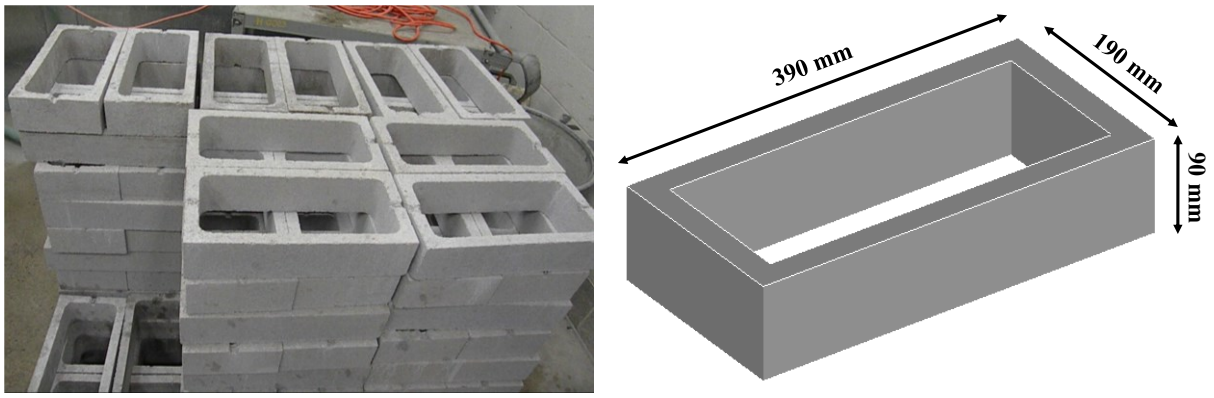

Figure A.21 Whole rectangular half-scale concrete masonry block

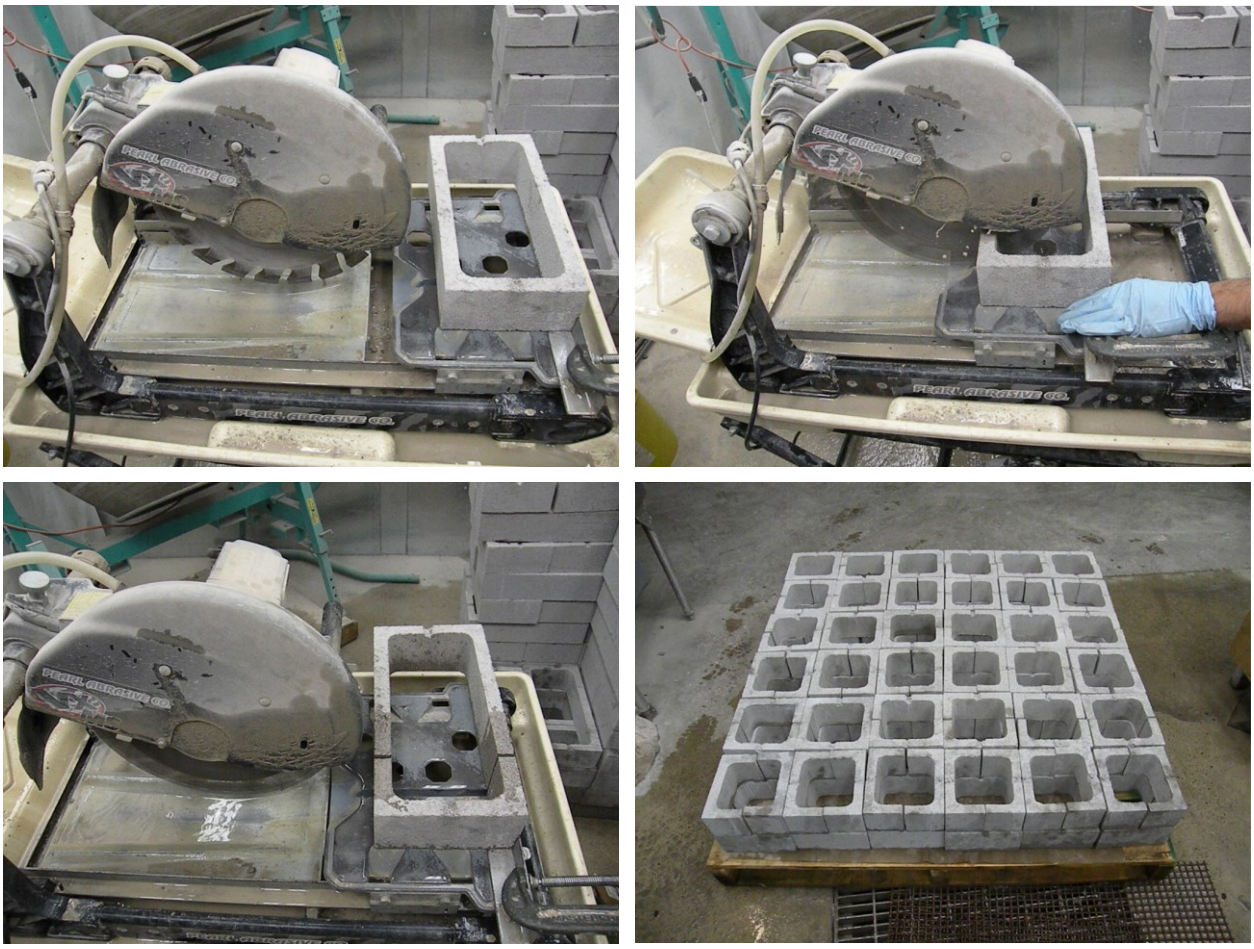

Figure A.22 Cut sequence of rectangular concrete masonry block

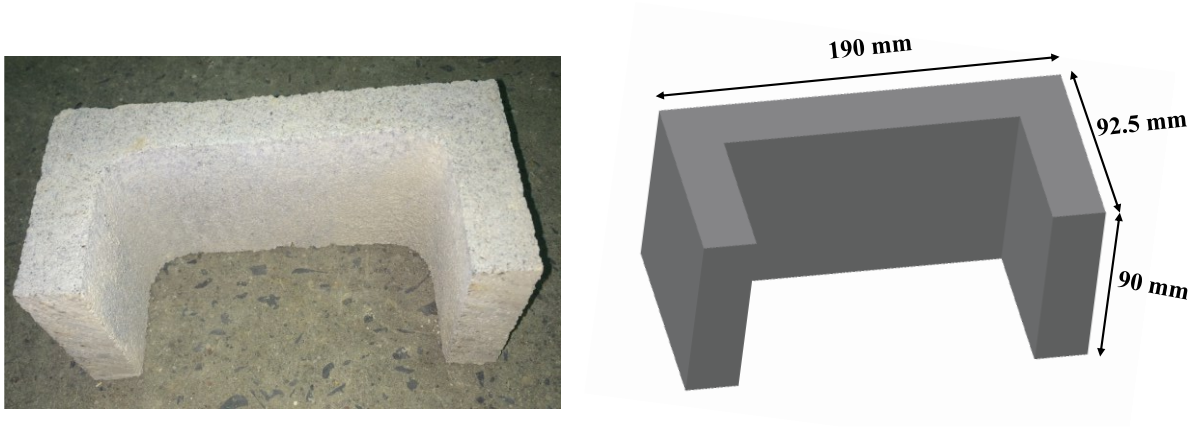

Figure A.23 Half scale C-shaped concrete masonry block unit

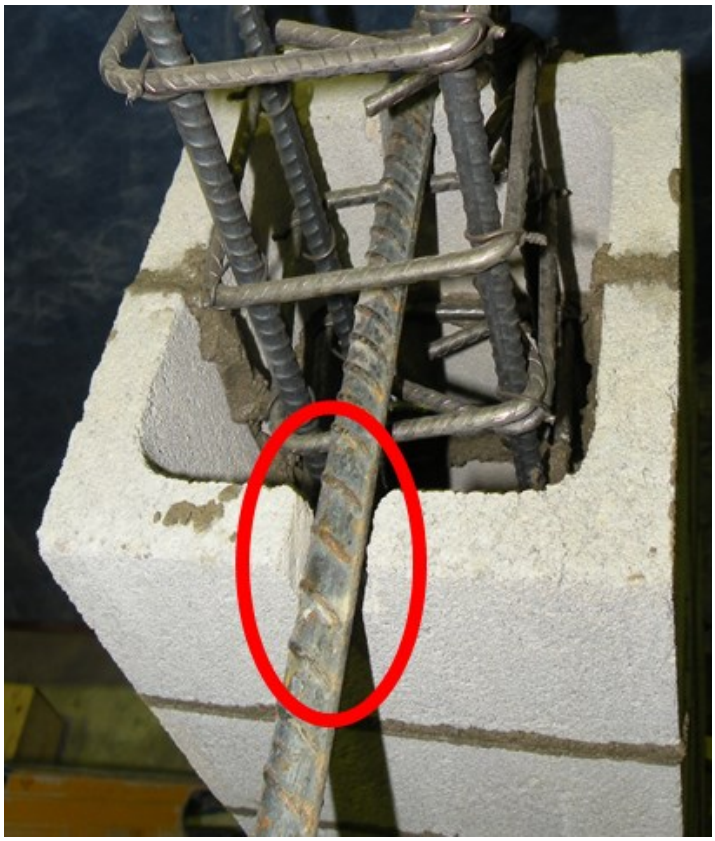

Figure A.24 Grooves in the masonry block units

A.2.2 Mortar

Type S mortar was used to join different courses with an average thickness of 5 mm and 10 mm in the half-scale and full-scale RMBE specimens, respectively. The mortar moulded into 50 mm cubes as shown in Figure A.25.

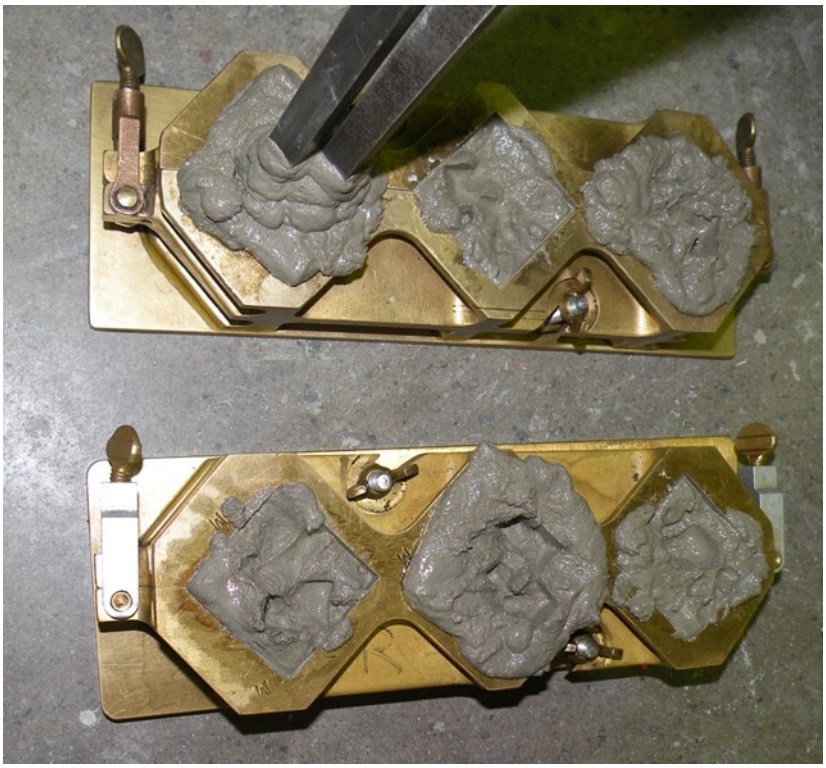

Figure A.25 Moulding of mortar cubes

A.2.3 Grout

Coarse aggregate was used in the construction of full-scale RMBE specimens. However, fine grout was used in the construction of half-scale RMBE specimens because the fine grout can flow between the steel reinforcement cage in half scale block unit to encase the reinforcement without segregation. Some of the C-RMBE specimens were grouted and some of them are not grouted. Two fine grout strengths, of 45 MPa and 15 MPa, were used in this experimental work. The 45 MPa fine grout was mixed in the structural laboratory at Concordia University. Table A.1 presents the mix proportions used in the 45 MPa grout mix. For the 15 MPa fine grout, pre-mixed bags of grout were used. Each pre-bag fine grout weighed 30 kg and was mixed in structure lab at Concordia University by adding 5.4 liters to each bag. The slump test of the fine grout was conducted and the average slump for 45 MPa and 15 MPa were 210 mm and 290 mm,

respectively (see Figure A.26). The C-RMBE specimens were strapped to avoid the grout blowout since the stacking bond was used which provides a weeker mortar joint. The strapping was done using two 2 x 4 wood pieces and two straps one at the top half and the other at the bottom half as shown in Figure A.14.

Table A.1 Proportions of 45 MPa fine aggregate

Constituent material	Cement	Sand	Water	Total
kg/batch	40 kg	104 kg	20 kg	164 kg
Part by weight	1.00	2.6	0.5	4.1

Figure A.26 Slump test for 15 MPa fine grout

A.2.4 Steel reinforcement

The longitudinal and horizontal reinforcement used in the construction of the half-scale RMBE specimens were scaled to represent the rebars used in full-scale RM construction. For vertical reinforcement, the deformed steel rebar #3, #4, and 20M with nominal diameters of 9.525 mm, 12.7 mm, and 19.5 mm, respectively, were used. On other hand, the deformed wire and a deformed bar of D4, 10M, and 15M were used for horizontal reinforcement (hoops) with nominal diameters of 5.73 mm, 11.3 mm, and 16 mm, respectively. Figure A.27 shows the details of D4 hoops which made at the structures laboratory at Concordia University. All the

reinforcement rebars of each diameter were ordered from the same batch at the same time. Quasi-static tension tests were conducted on five 600-mm-long tensile specimens for each diameter to determine the yield strength of the steel reinforcement used in the construction of the RMBE.

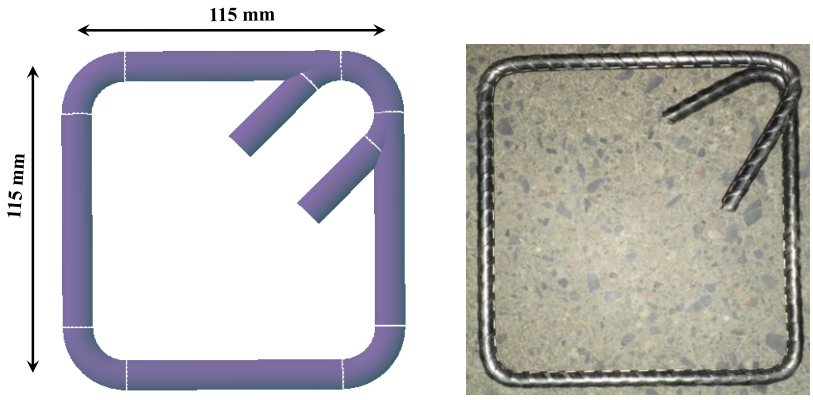

Figure A.27 Details of a D4 hoop

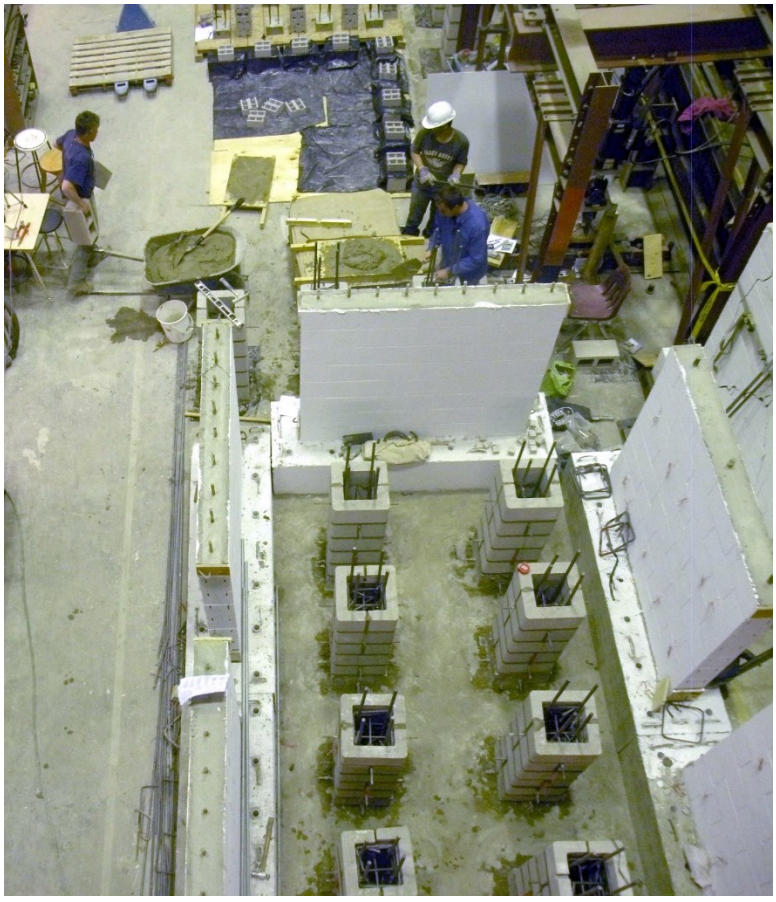

Figure A.28 Full-scale specimens during construction

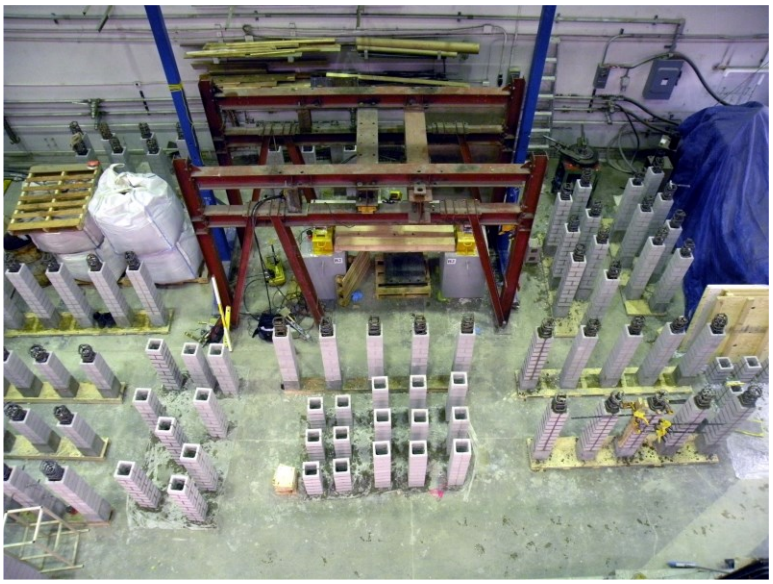

Figure A.29 Half-scale specimens during construction

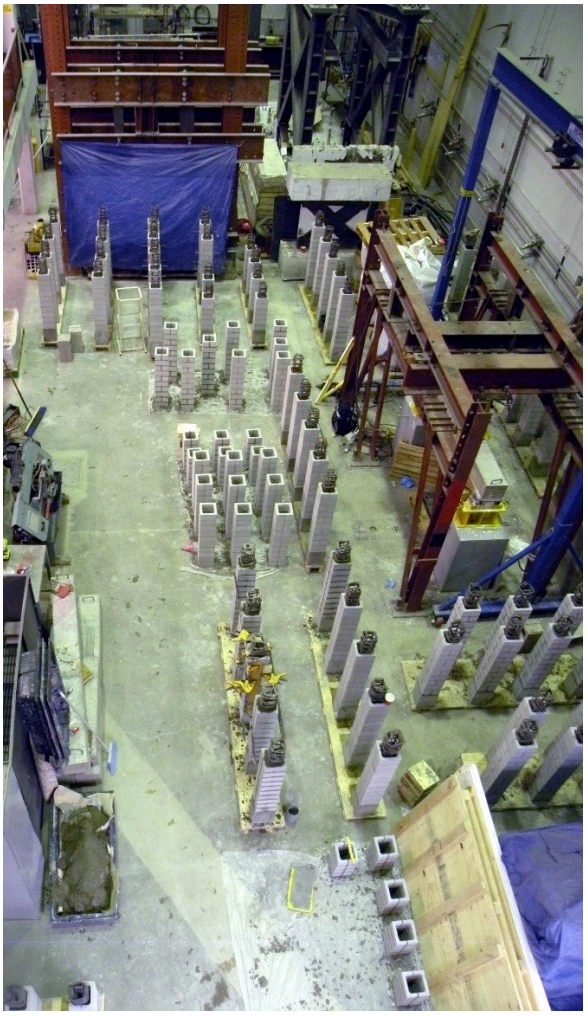

Figure A.30 Half-scale specimens during construction

Appendix B

Testing of RMBE Specimens

B.1 Instrumentation

The RMBEs were instrumented with Linear Variable Differential Transducers (LVDTs), strain gauges, and load cells.

B.1.1 Axial displacement measurement

The axial displacement of the RMBE specimens was measured using LVDTs. Four LVDTs were attached (screwed) at the centerline of each side of the specimen. These LVDTs gauge length went from the lower edge of the top footing to the upper edge of the bottom footing (Figure B.1). The LVDTs used to measure relative displacement between the lower edge of the top footing to the upper edge of the bottom footing had a stroke of 50 mm and range from +/- 0.15% to +/- 0.25% of stroke. However, the LVDTs used to measure the axial displacement in the middle of the RMBE specimen had a stroke of 25 mm and range from +/- 0.15% to +/- 0.25% of the stroke.

B.1.2 Longitudinal strain in vertical reinforcement

One specimen of each configuration was instrumented with strain gauges. Four strain gauges were installed on the vertical reinforcement to measure longitudinal strain. The strain gauges had an effective gauge length of 5 mm. Figure B.2 illustrates the locations of the strain gauges on the vertical reinforcement bars.

B.1.3 Load measurement

A newly upgraded 3000 kN servo controlled actuator was used to test the RMBE under constant displacement loading rate throughout the loading history, until failure occurred. The corresponding loads were measured with a high precision load cell connected to a control panel that attached to the Vishay data acquisition system. The readings of the LVDTs and strain gauge results versus the axial load values were recorded to the computer's hard disk.

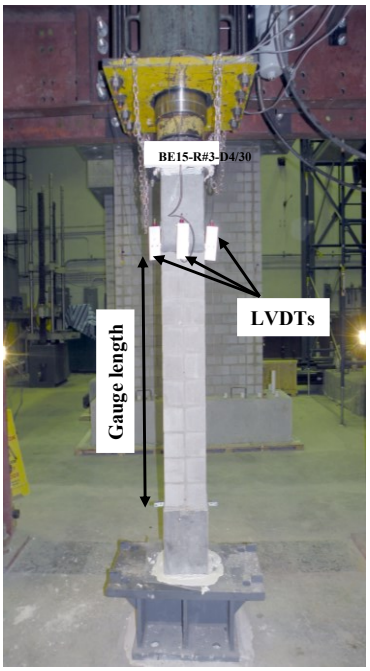

Figure B.1 Linear Variable Differential Transducers (LVDTs) on RMBE specimen with one gauge length equal to the height of the specimen

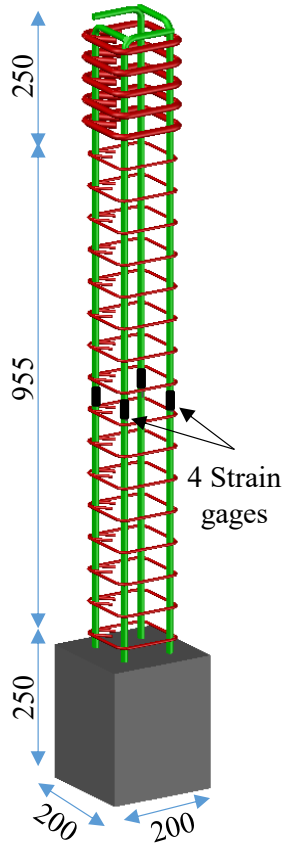

Figure B.2 Strain gauges on vertical reinforcement bars of RMBE specimen

B.2 Placing of RMBE Specimen

The test RMBE specimen was positioned in the testing machine using clamps and a forklift as shown in Figure B.3.

Figure B.3 Transport and positioning of RMBE specimen

Appendix C

Test Results

C.1 Damage at the RMBE

The observed stress-strain relationship and damage pattern of each configuration of the RMBE specimens at peak stress, 75% and 50% of peak stress is illustrated in Figure C.1 to Figure C.28. Figure C.29 shows the appearance of all RMBE specimens after testing.

C.1.1 BE15-R#3-D4/60 configuration

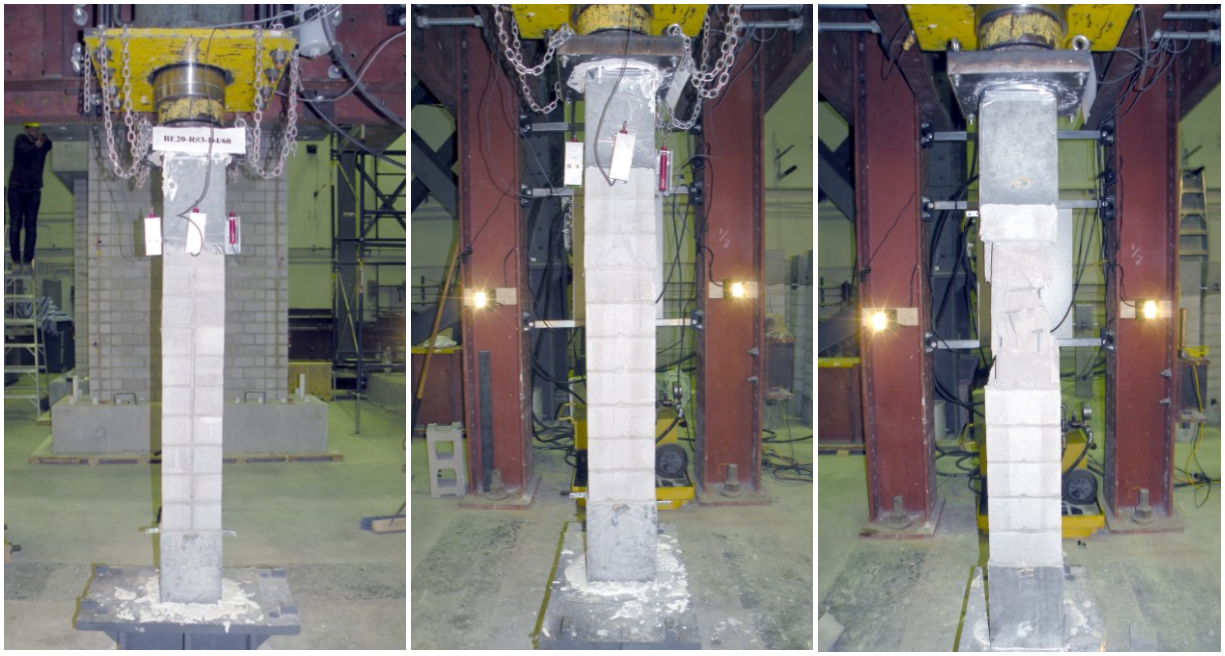

a) b) c)

Figure C.1 BE15-R#3-D4/60 damage pattern; a) at peak stress; b) at 75% of peak stress; and c) at 50% of peak stress

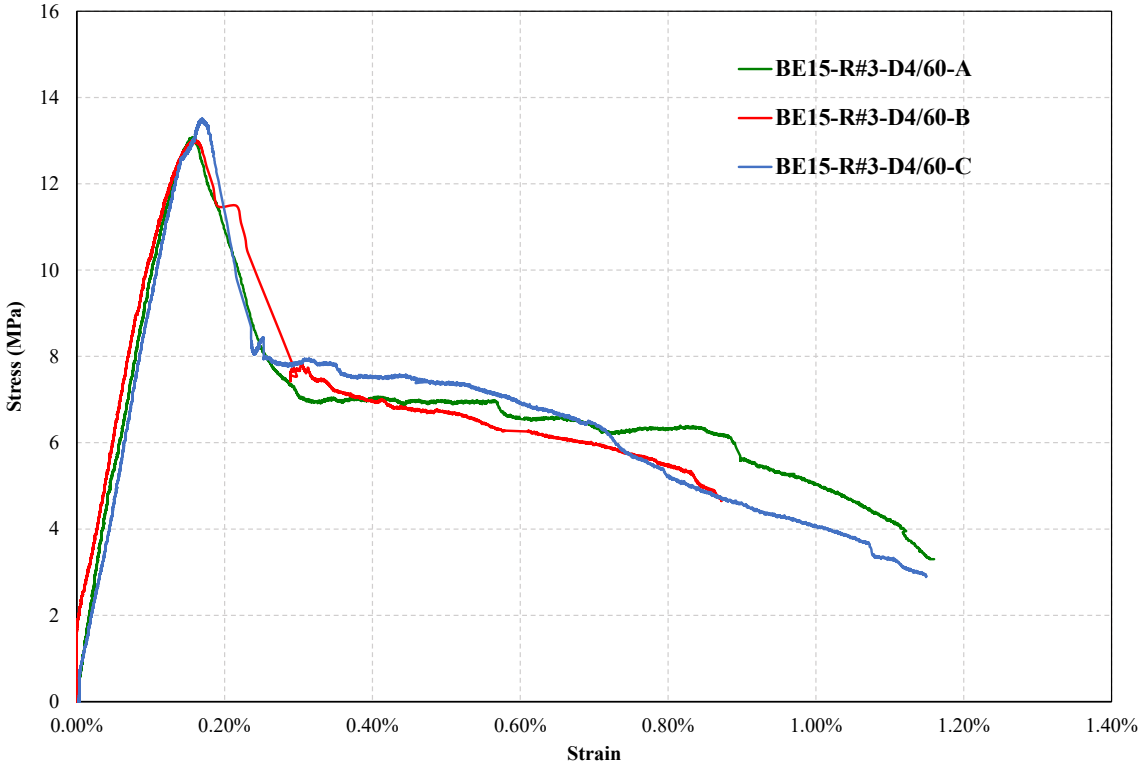

Figure C.2 Observed stress-strain relationship for the BE15-R#3-D4/60

C.1.2 BE15-R#3-D4/45 configuration

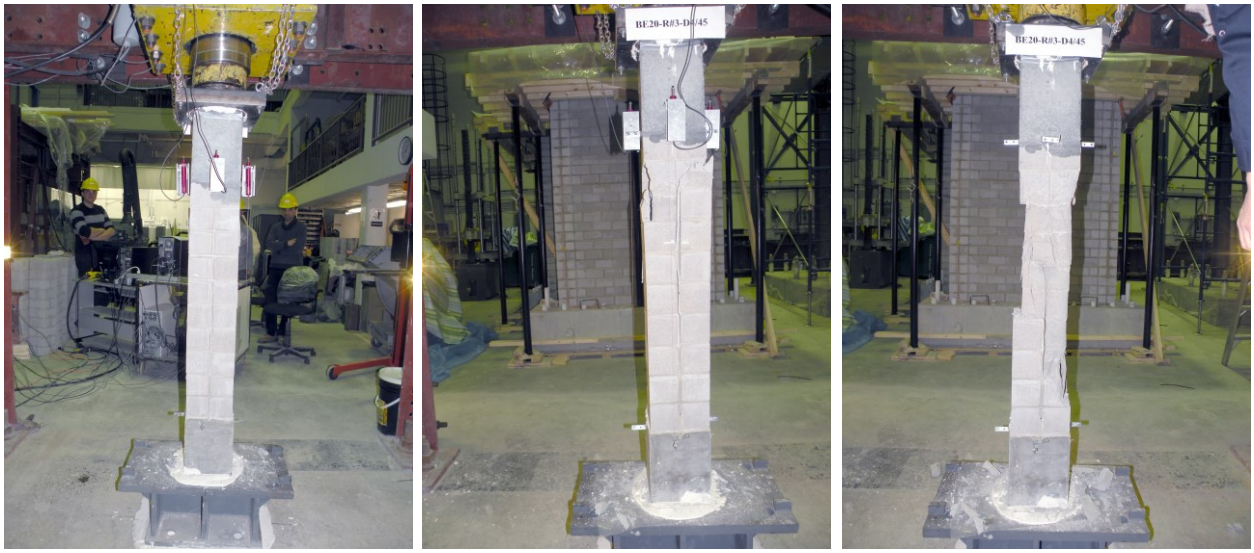

a) **b)** **c)**

Figure C.3 BE15-R#3-D4/45 damage pattern; a) at peak stress; b) at 75% of peak stress; and c) at 50% of peak stress

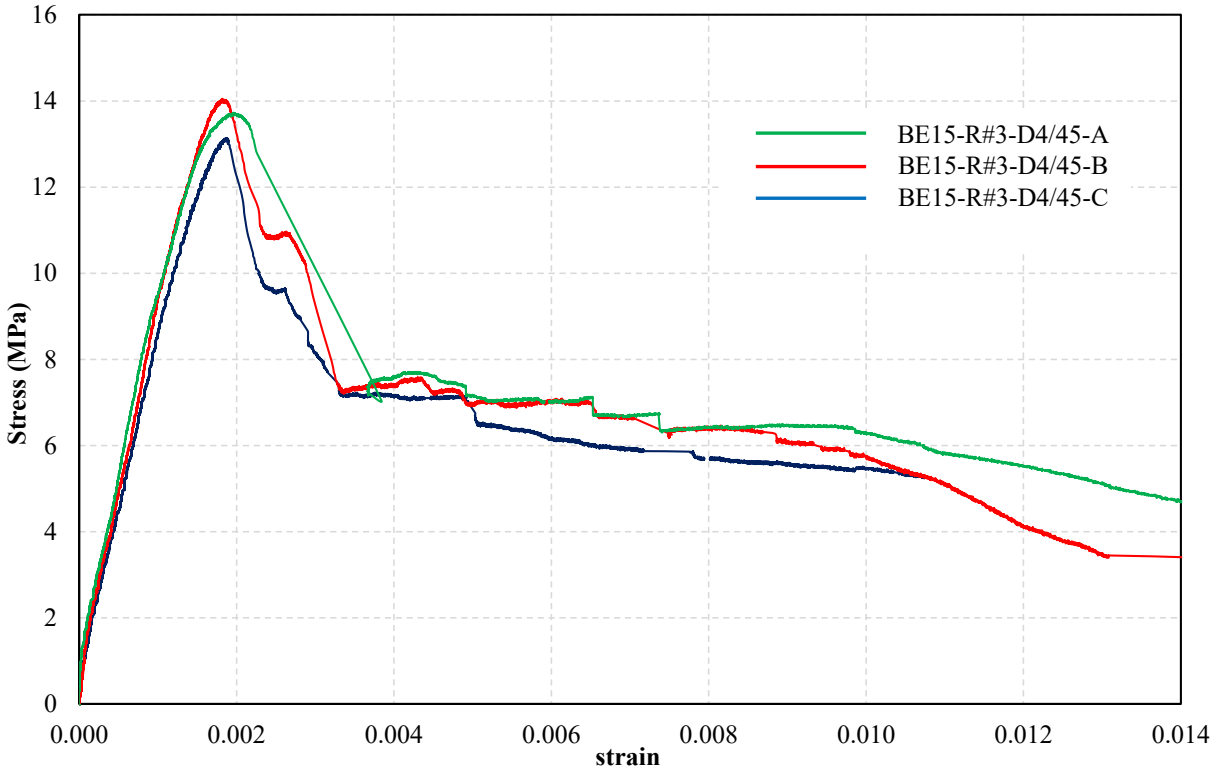

Figure C.4 Observed stress-strain relationship for the BE15-R#3-D4/45

C.1.3 BE15-R#3-D4/30 configuration

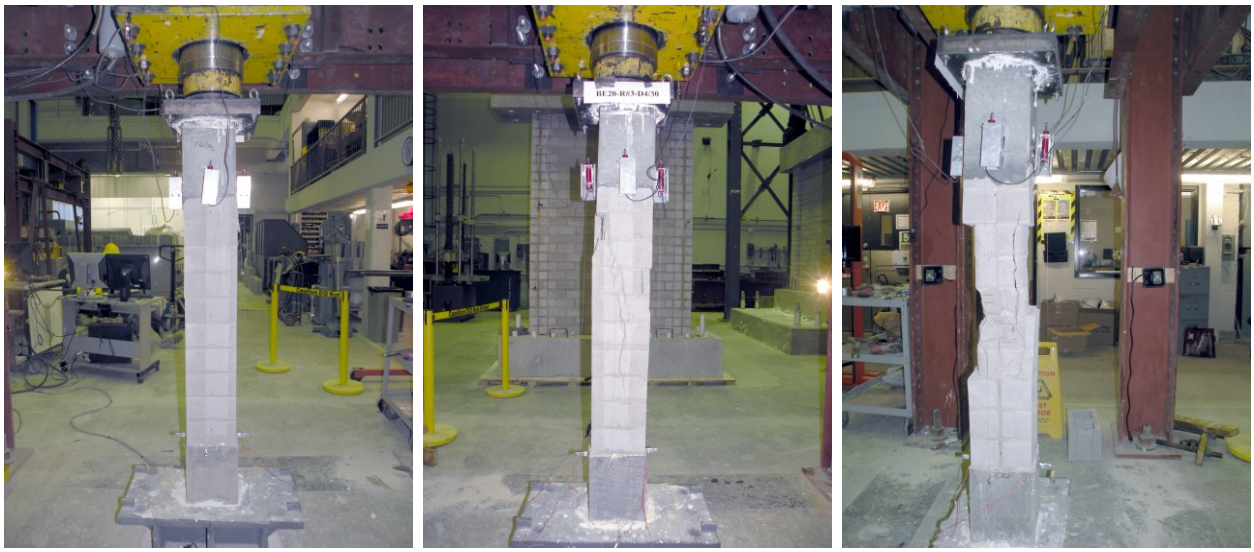

a) **b)** **c)**

Figure C.5 BE15-R#3-D4/30 damage pattern; a) at peak stress; b) at 75% of peak stress; and c) at 50% of peak stress

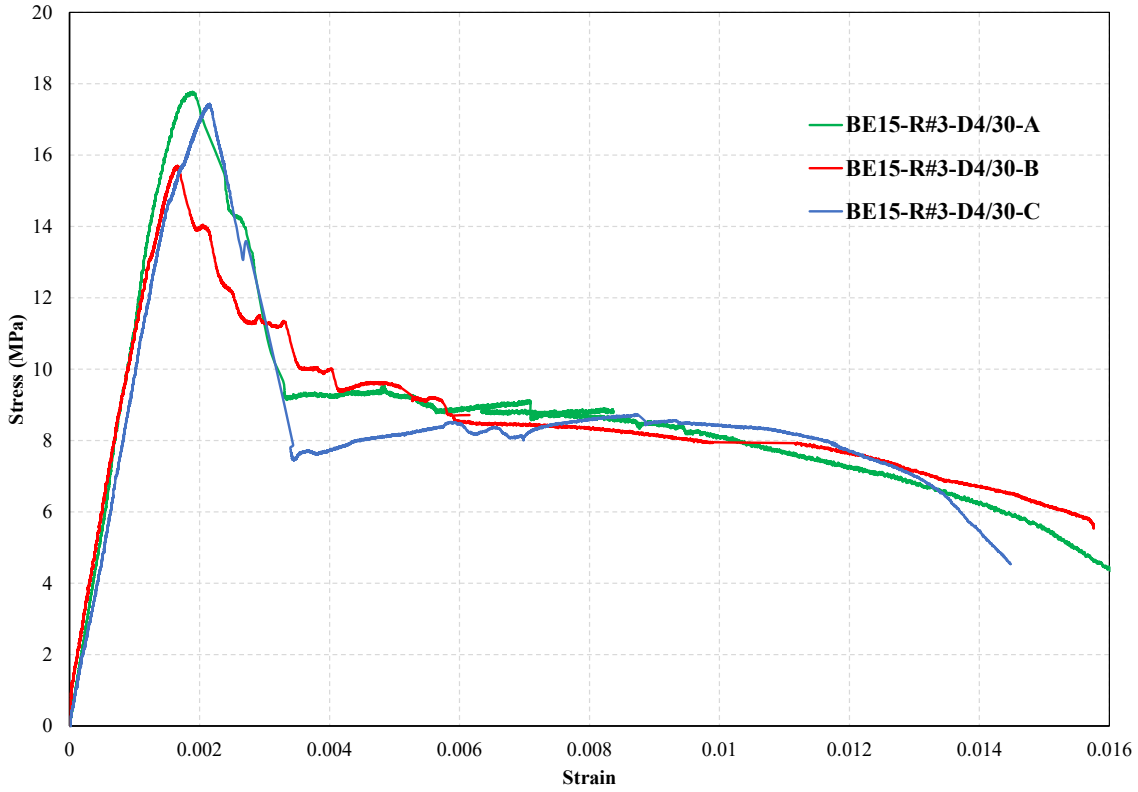

Figure C.6 Observed stress-strain relationship for the BE15-R#3-D4/30

C.1.4 BE15-R#4-D4/60 configuration

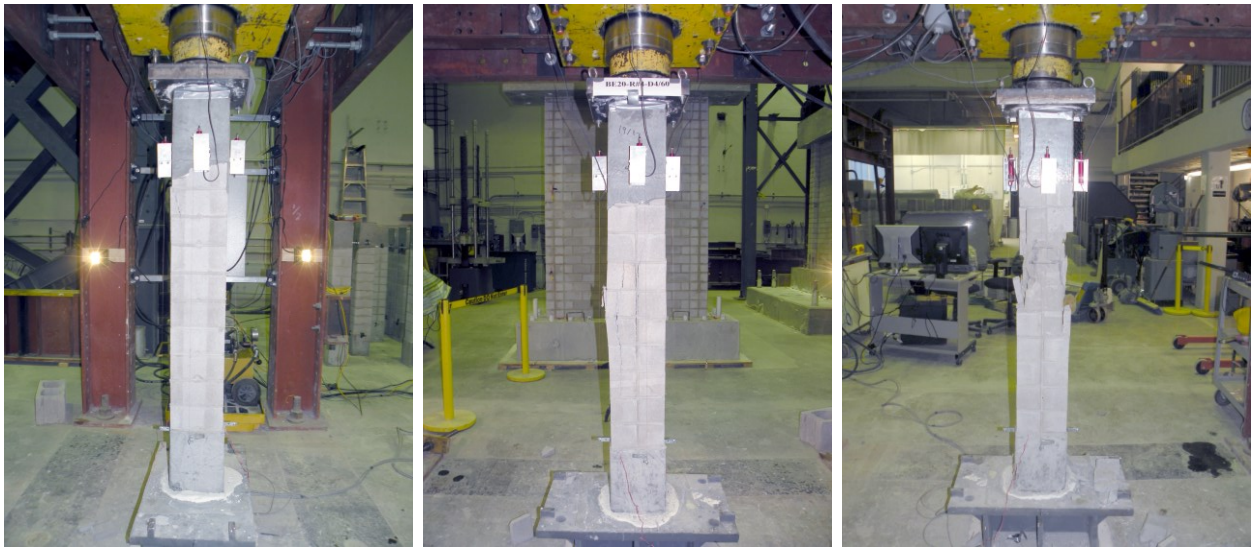

a) **b)** **c)**

Figure C.7 BE15-R#4-D4/60 damage pattern; a) at peak stress; b) at 75% of peak stress; and c) at 50% of peak stress

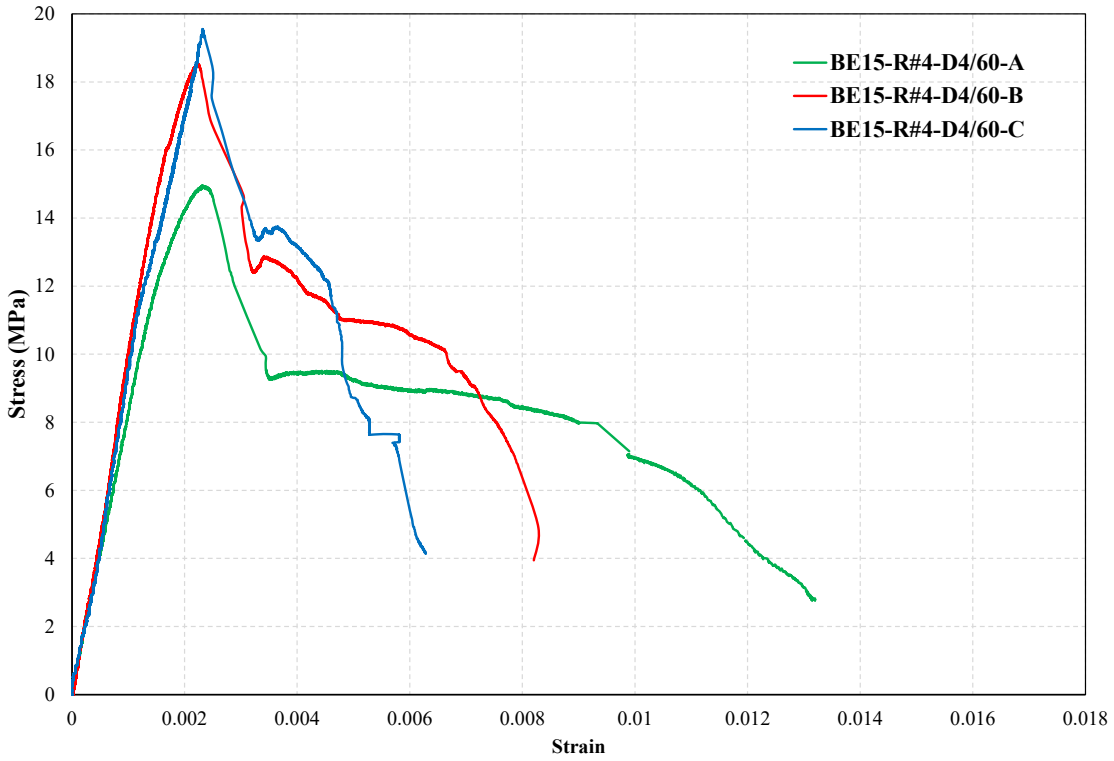

Figure C.8 Observed stress-strain relationship for the BE15-R#4-D4/60

C.1.5 BE15-R#4-D4/45 configuration

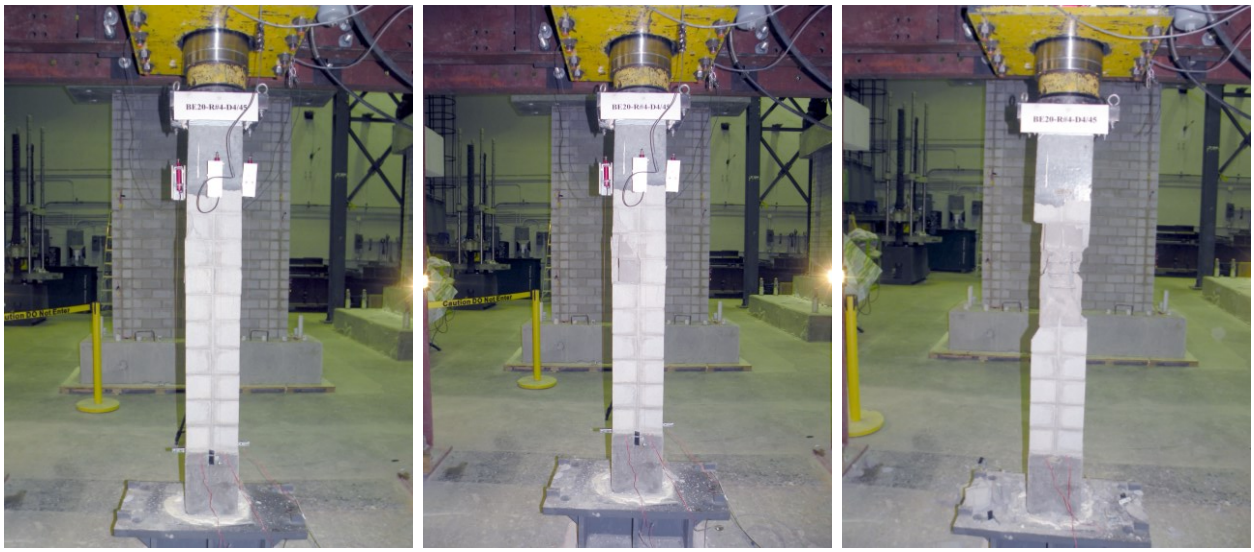

a) **b)** **c)**

Figure C.9 BE15-R#4-D4/45 damage pattern; a) at peak stress; b) at 75% of peak stress; and c) at 50% of peak stress

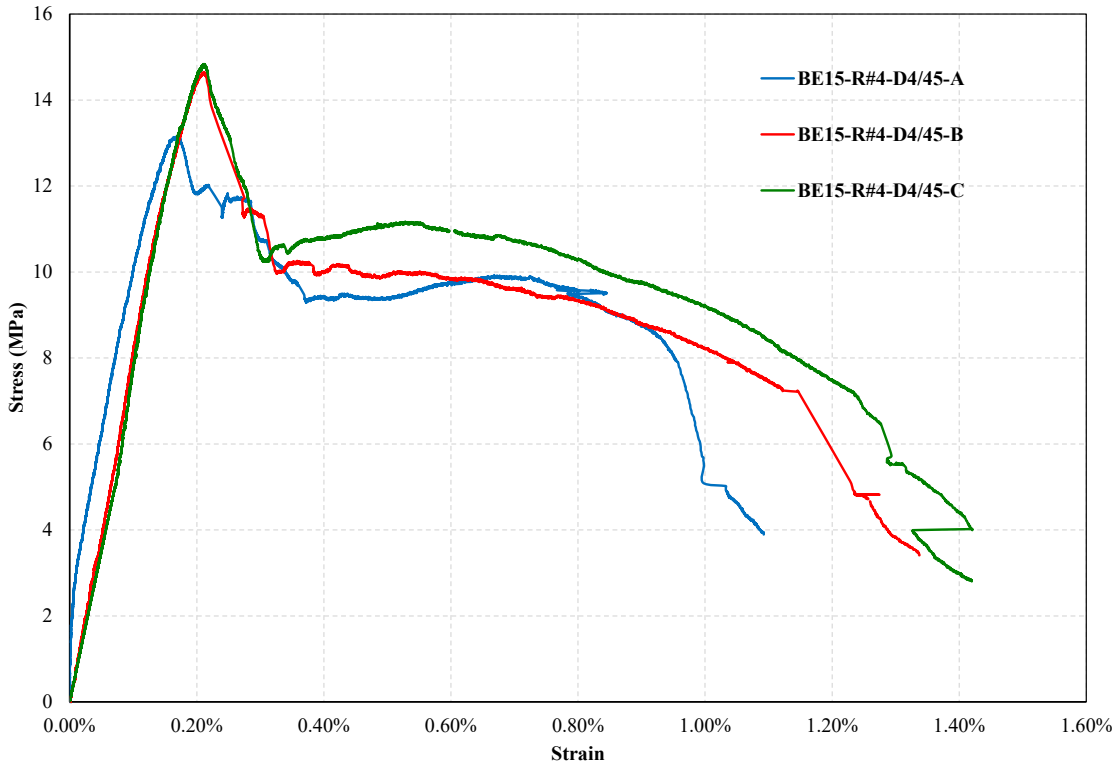

Figure C.10 Observed stress-strain relationship for the BE15-R#4-D4/45

C.1.6 BE15-R#4-D4/30 configuration

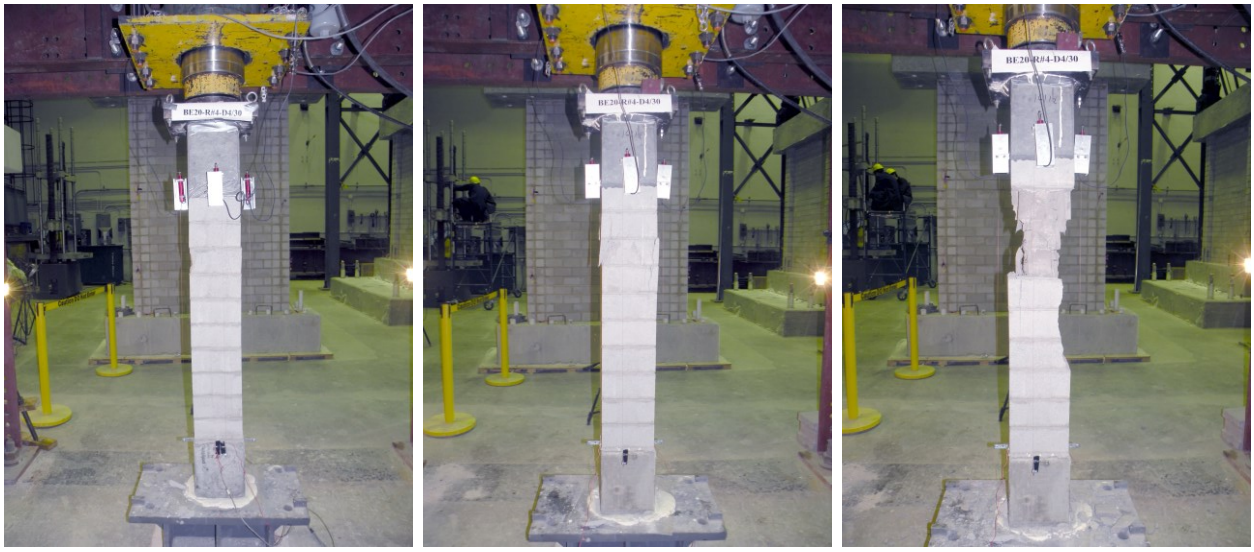

a) **b)** **c)**

Figure C.11 BE15-R#4-D4/30 damage pattern; a) at peak stress; b) at 75% of peak stress; and c) at 50% of peak stress

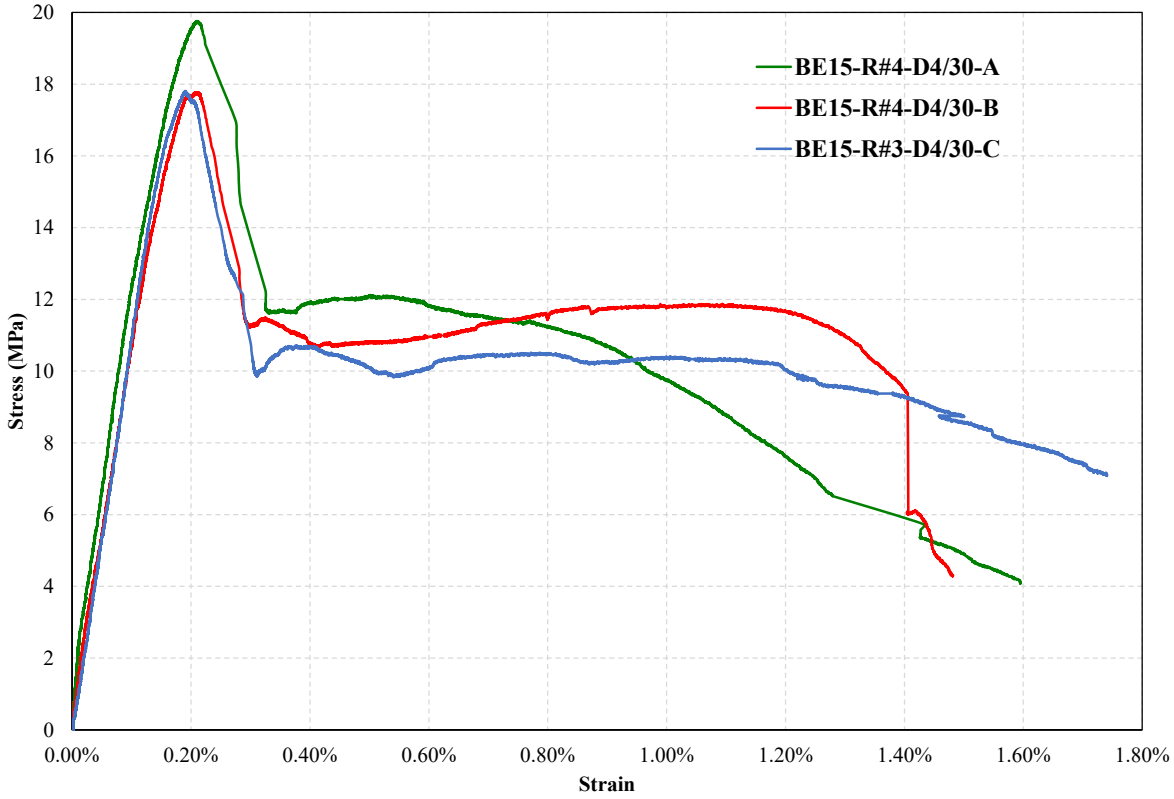

Figure C.12 Observed stress-strain relationship for the BE15-R#4-D4/30

C.1.7 BE45-R#3-D4/60 configuration

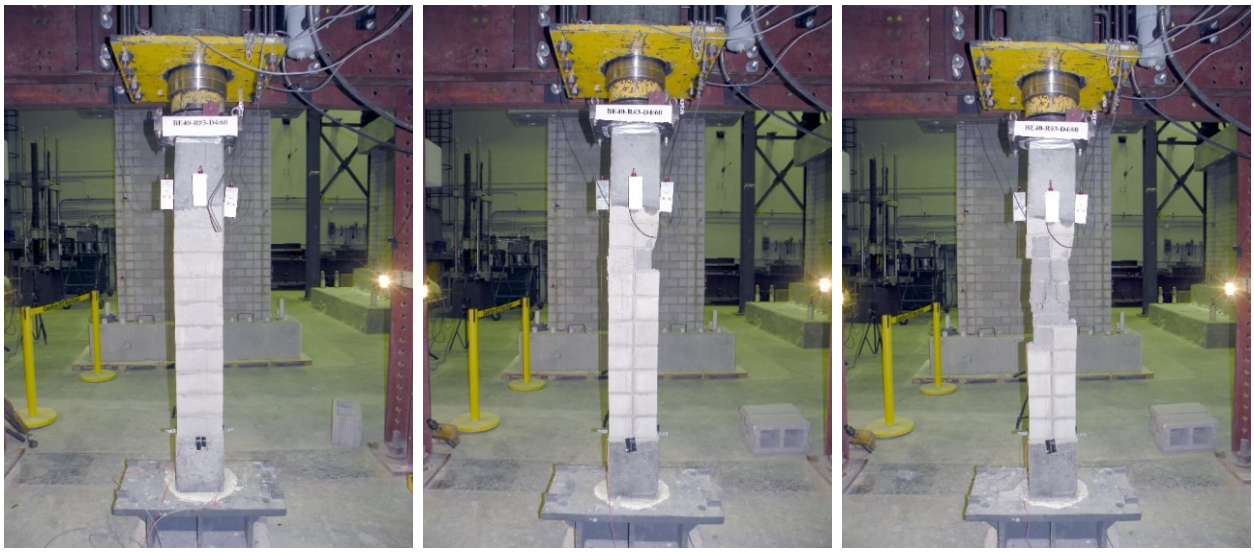

a) **b)** **c)**

Figure C.13 BE45-R#3-D4/60 damage pattern; a) at peak stress; b) at 75% of peak stress; and c) at 50% of peak stress

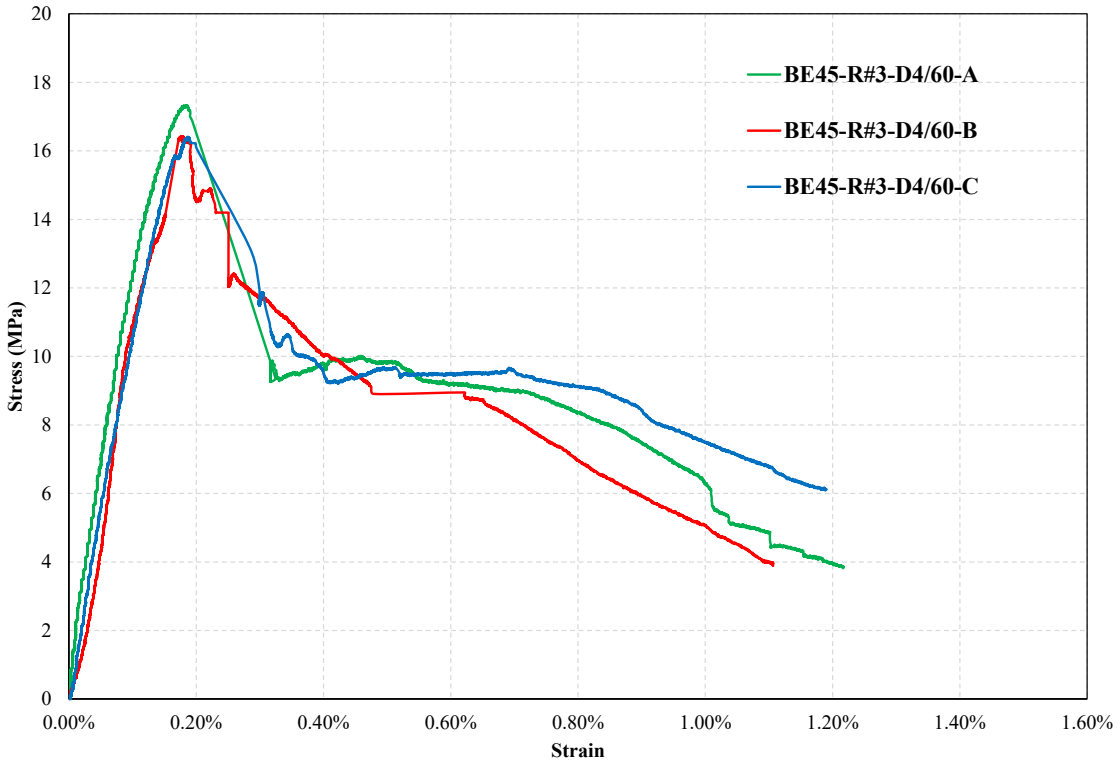

Figure C.14 Observed stress-strain relationship for the BE45-R#3-D4/60

C.1.8 BE45-R#4-D4/60 configuration

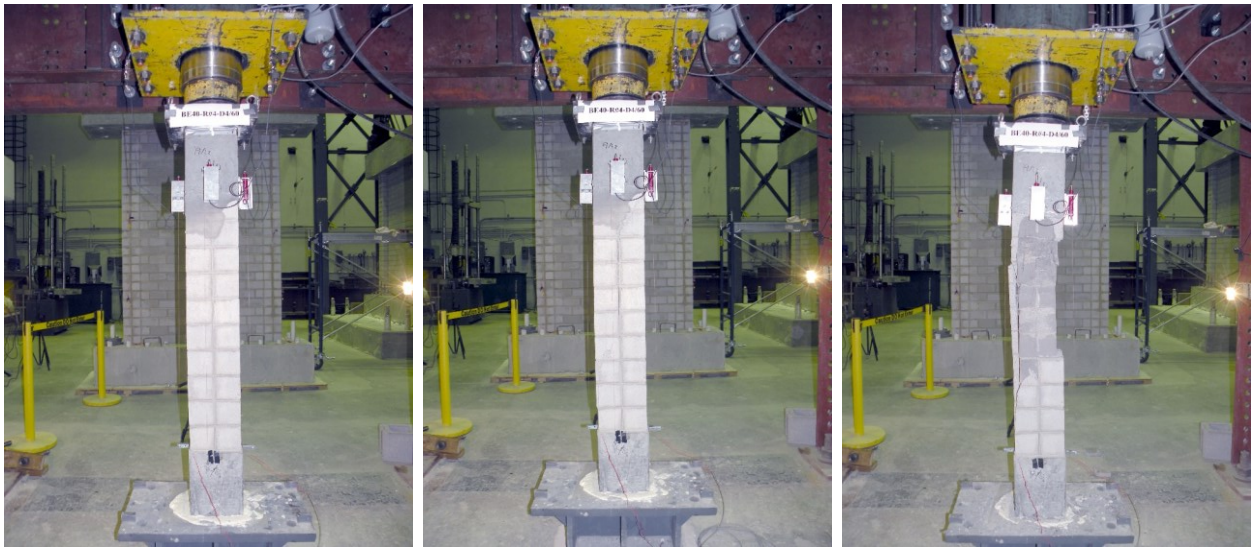

a) **b)** **c)**

Figure C.15 BE45-R#4-D4/60 damage pattern; a) at peak stress; b) at 75% of peak stress; and c) at 50% of peak stress

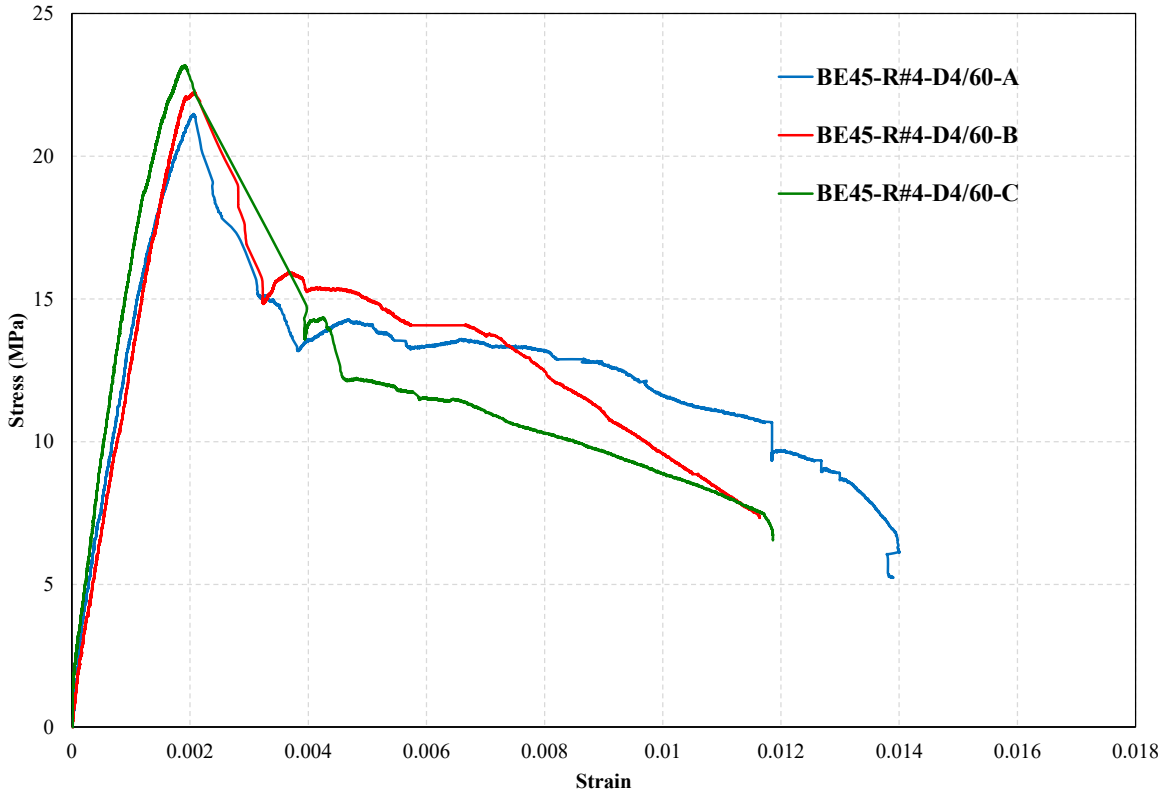

Figure C.16 Observed stress-strain relationship for the BE45-R#4-D4/60

C.1.9 BE-D4/60-AR2 configuration

a) b) c)

Figure C.17 BE-D4/60-AR2 damage pattern; a) at peak stress; b) at 75% of peak stress; and c) at 50% of peak stress

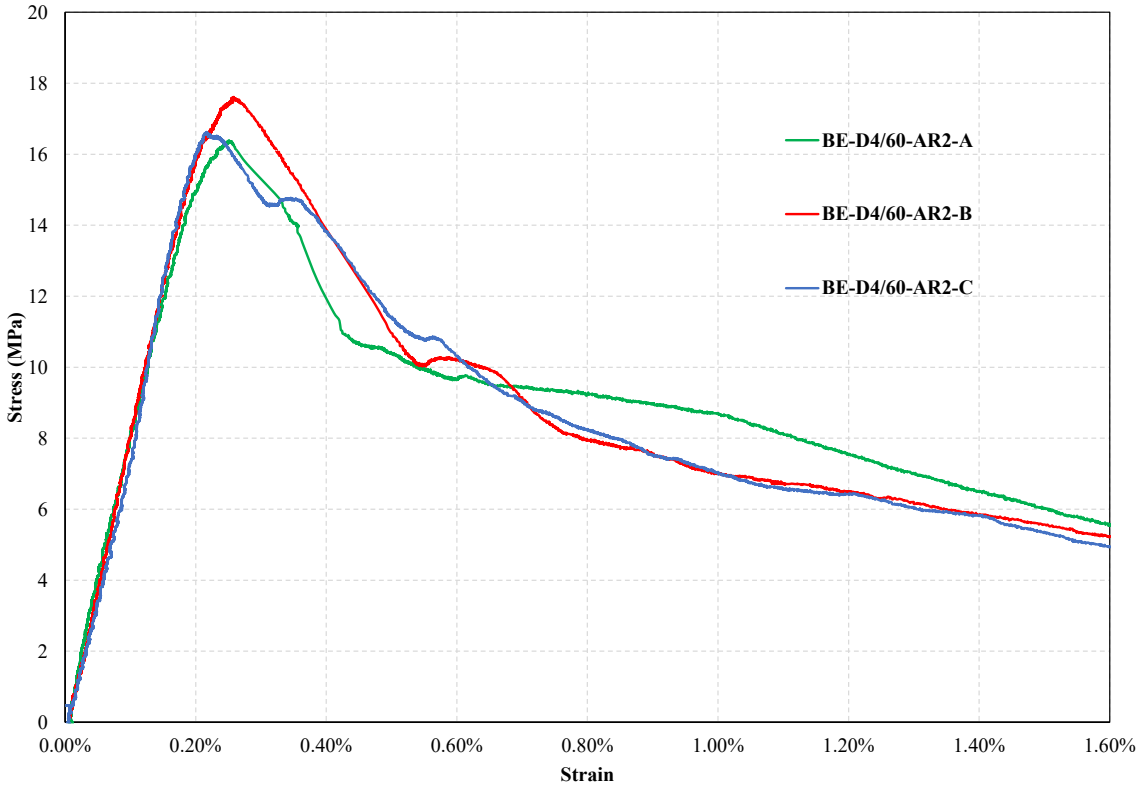

Figure C.18 Observed stress-strain relationship for the BE-D4/60-AR2

C.1.10 BE-D4/30-AR2 configuration

a) **b)** **c)**

Figure C.19 BE-D4/30-AR2 damage pattern; a) at peak stress; b) at 75% of peak stress; and c) at 50% of peak stress

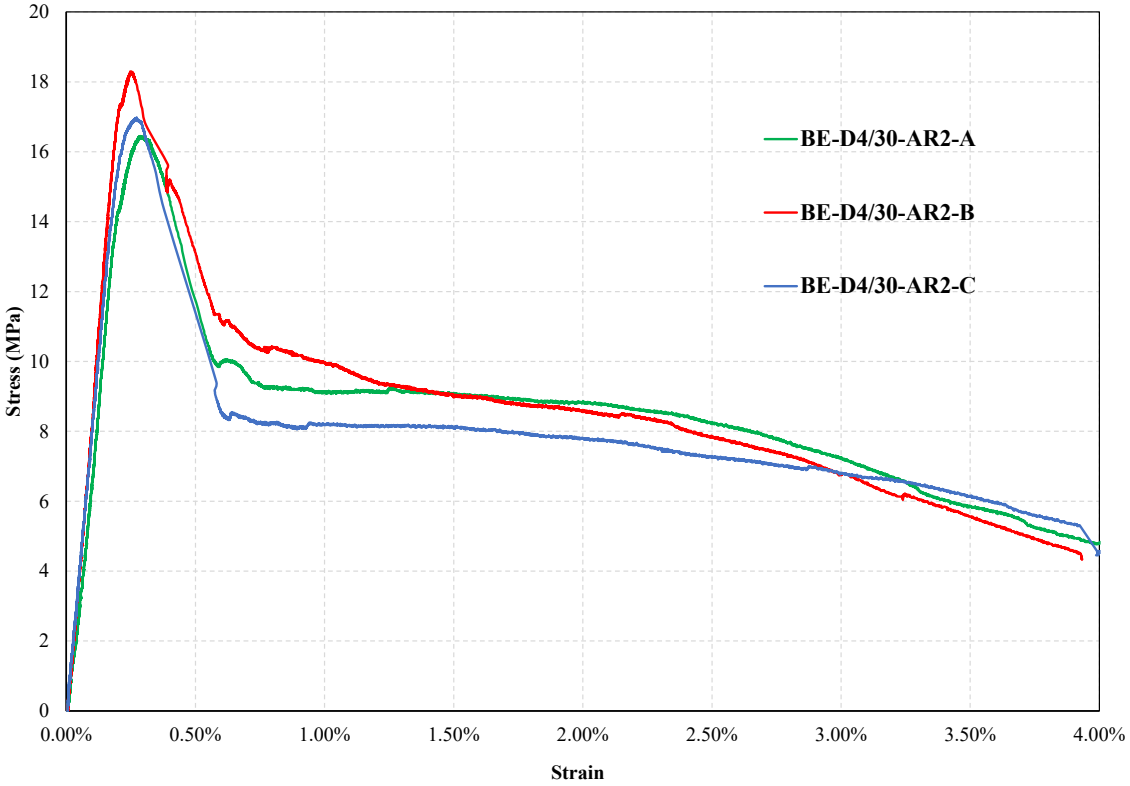

Figure C.20 Observed stress-strain relationship for the BE-D4/30-AR2

C.1.11 BE-D4/60-AR3 configuration

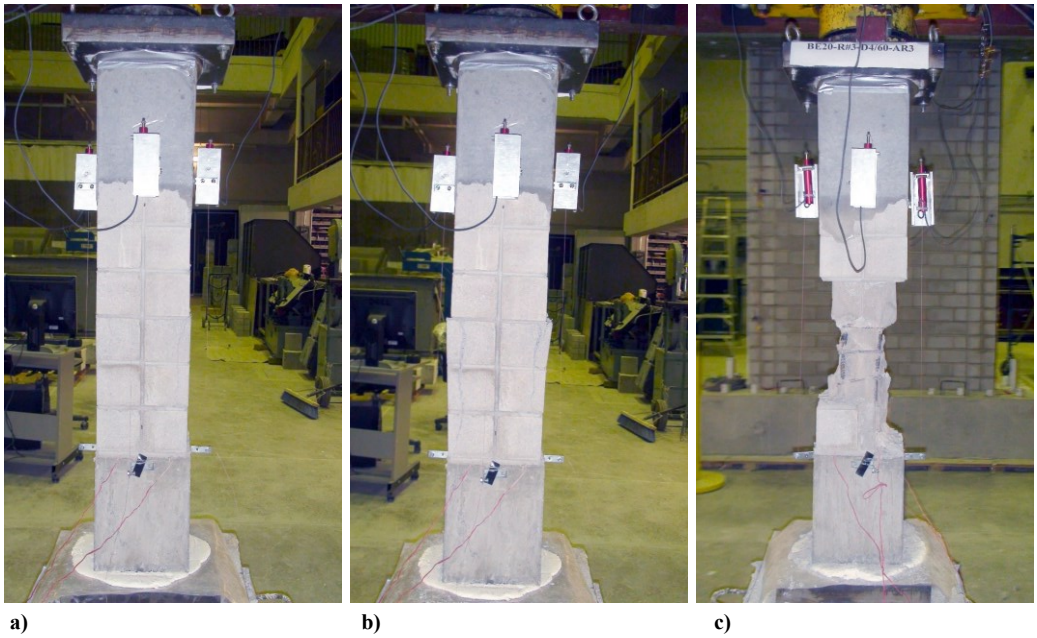

Figure C.21 BE-D4/60-AR3 damage pattern; a) at peak stress; b) at 75% of peak stress; and c) at 50% of peak stress

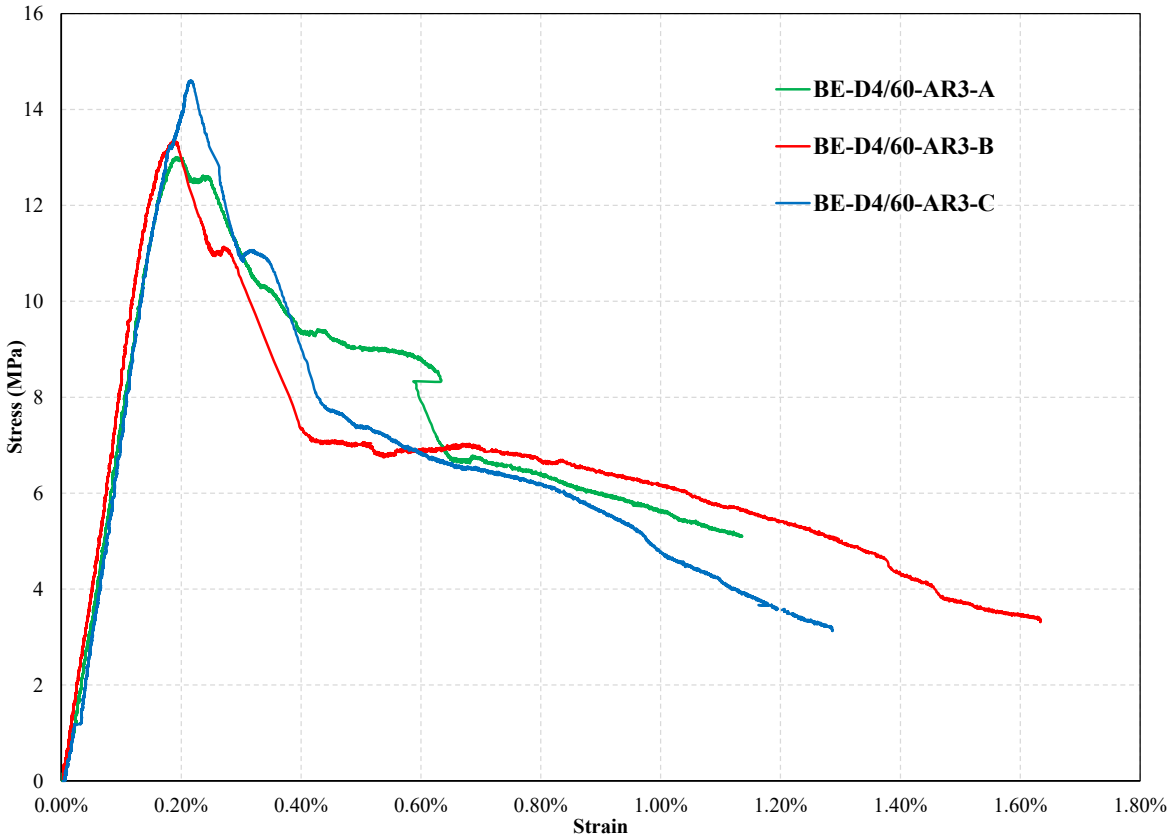

Figure C.22 Observed stress-strain relationship for the BE-D4/60-AR3

C.1.12 BE-D4/30-AR3 configuration

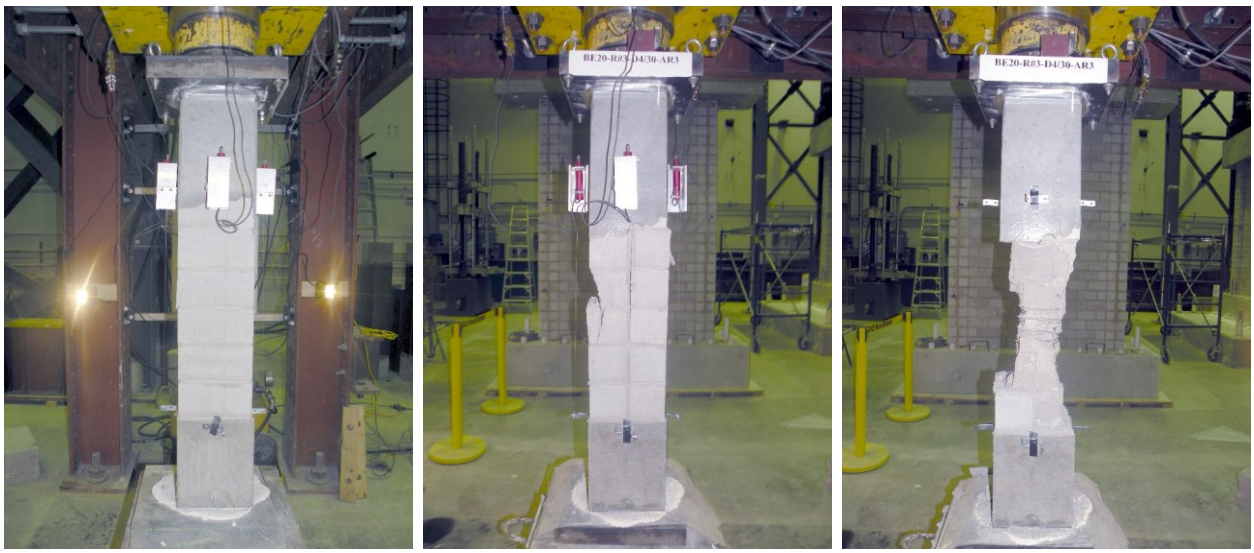

a) **b)** **c)**

Figure C.23 BE-D4/30-AR3 damage pattern; a) at peak stress; b) at 75% of peak stress; and c) at 50% of peak stress

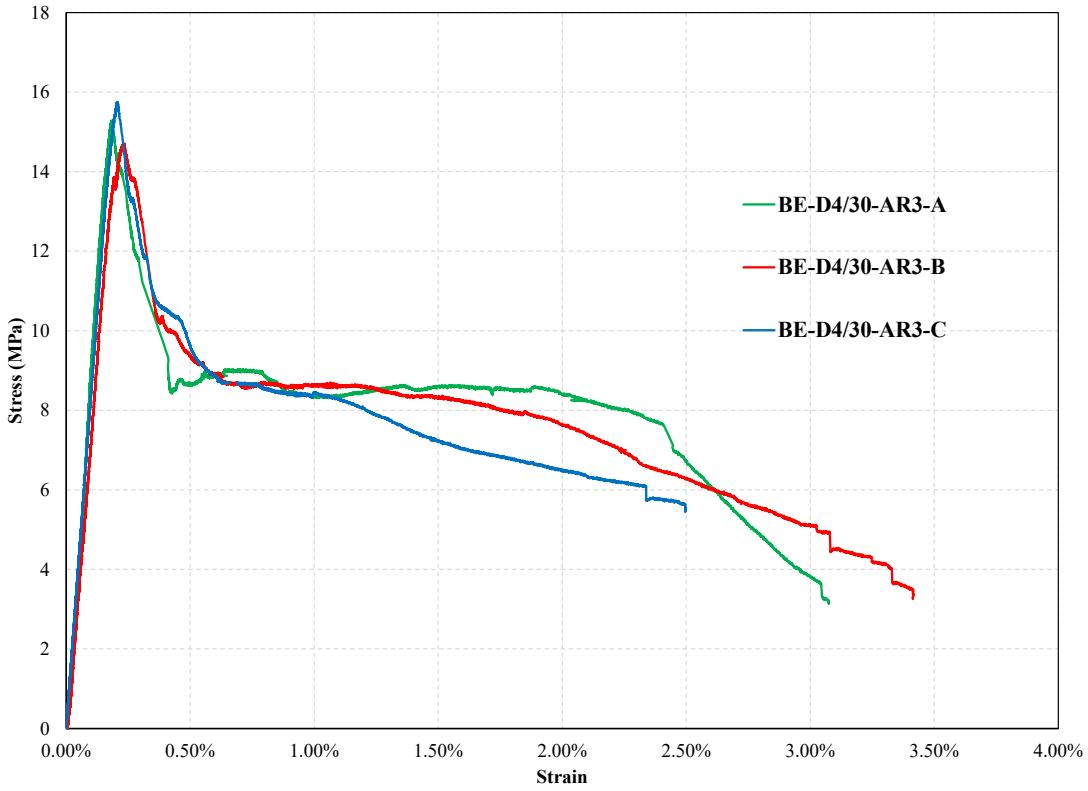

Figure C.24 Observed stress-strain relationship for the BE-D4/30-AR3

C.1.13 All RMBE specimens after testing

Figure C.25 Appearance of all RMBE specimens after testing

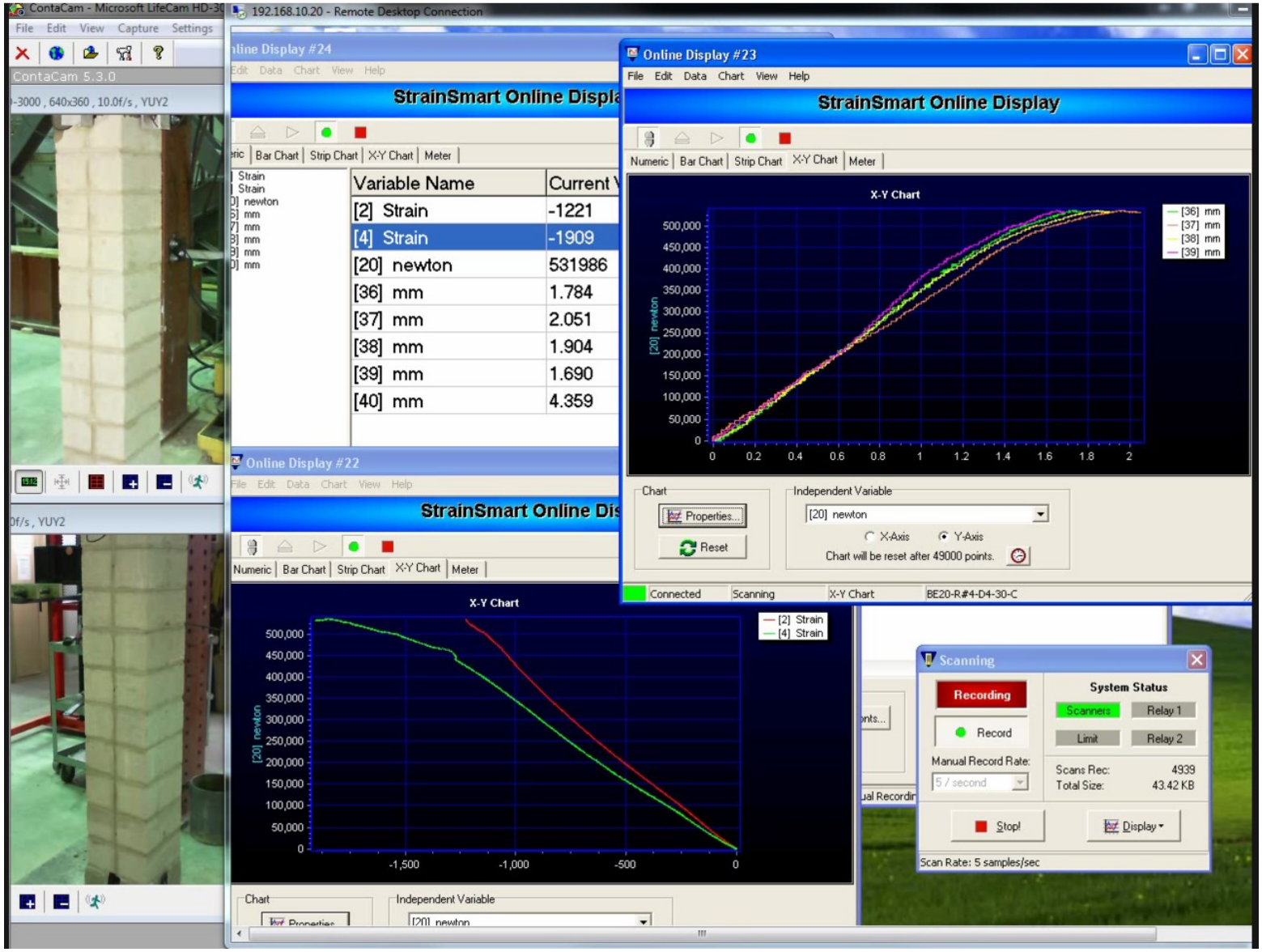

Figure C.26 Observed stress-stress relationship and the damage propagation of the RMBE specimen at the peak stress

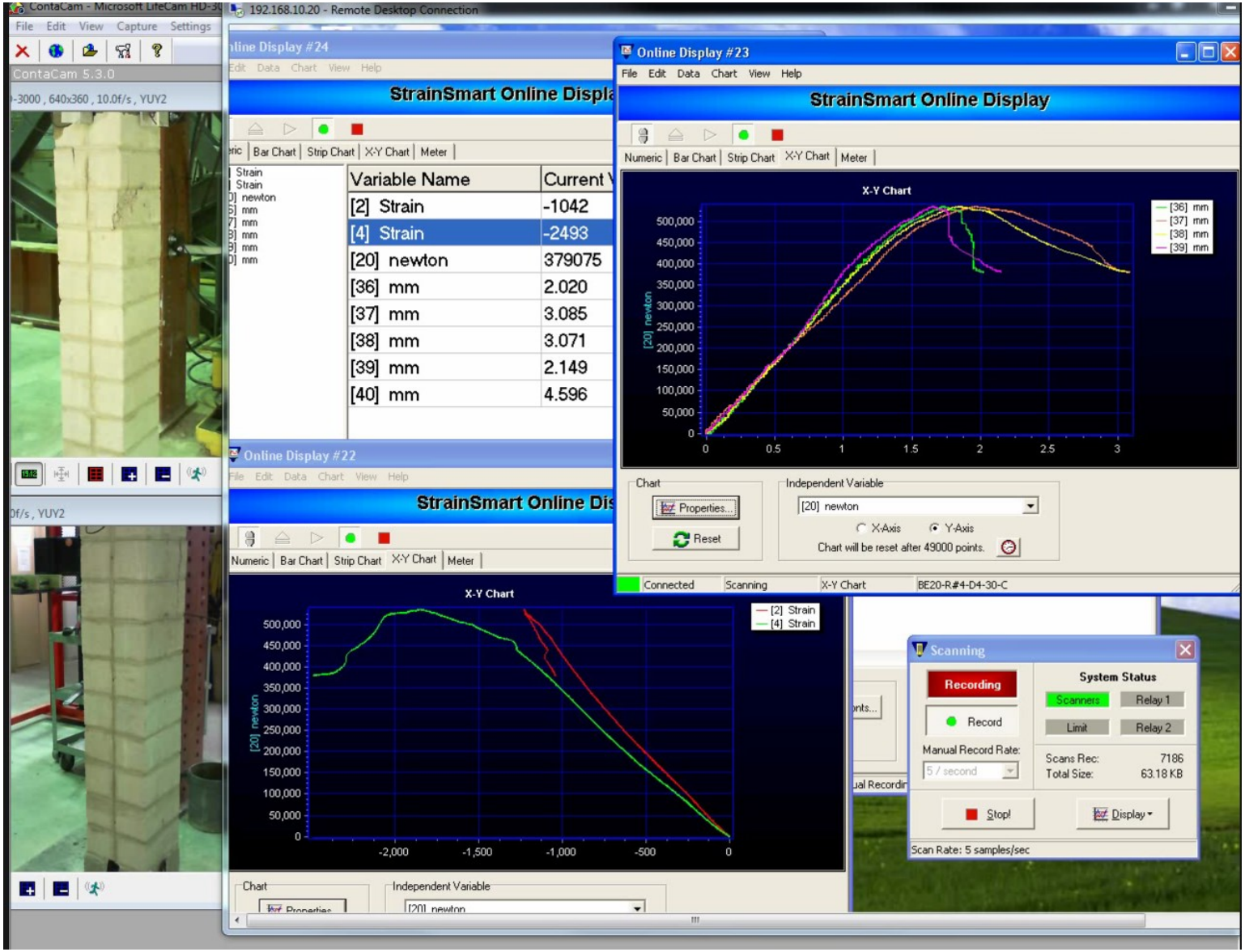

Figure C.27 Observed stress-stress relationship and the damage propagation of the RMBE specimen at the 75% of peak stress

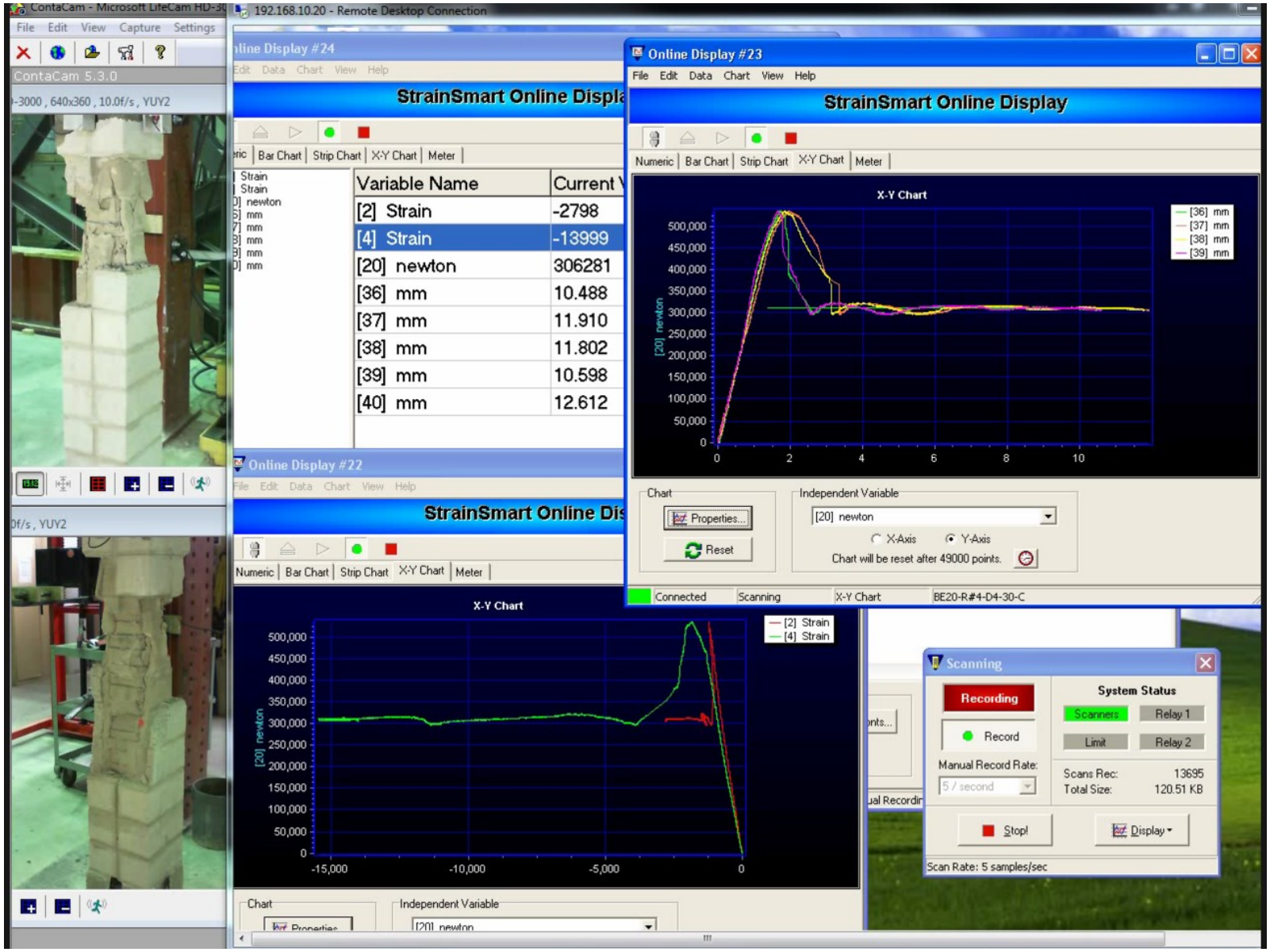

Figure C.28 Observed stress-stress relationship and the damage propagation of the RMBE specimen at the 50% of peak stress

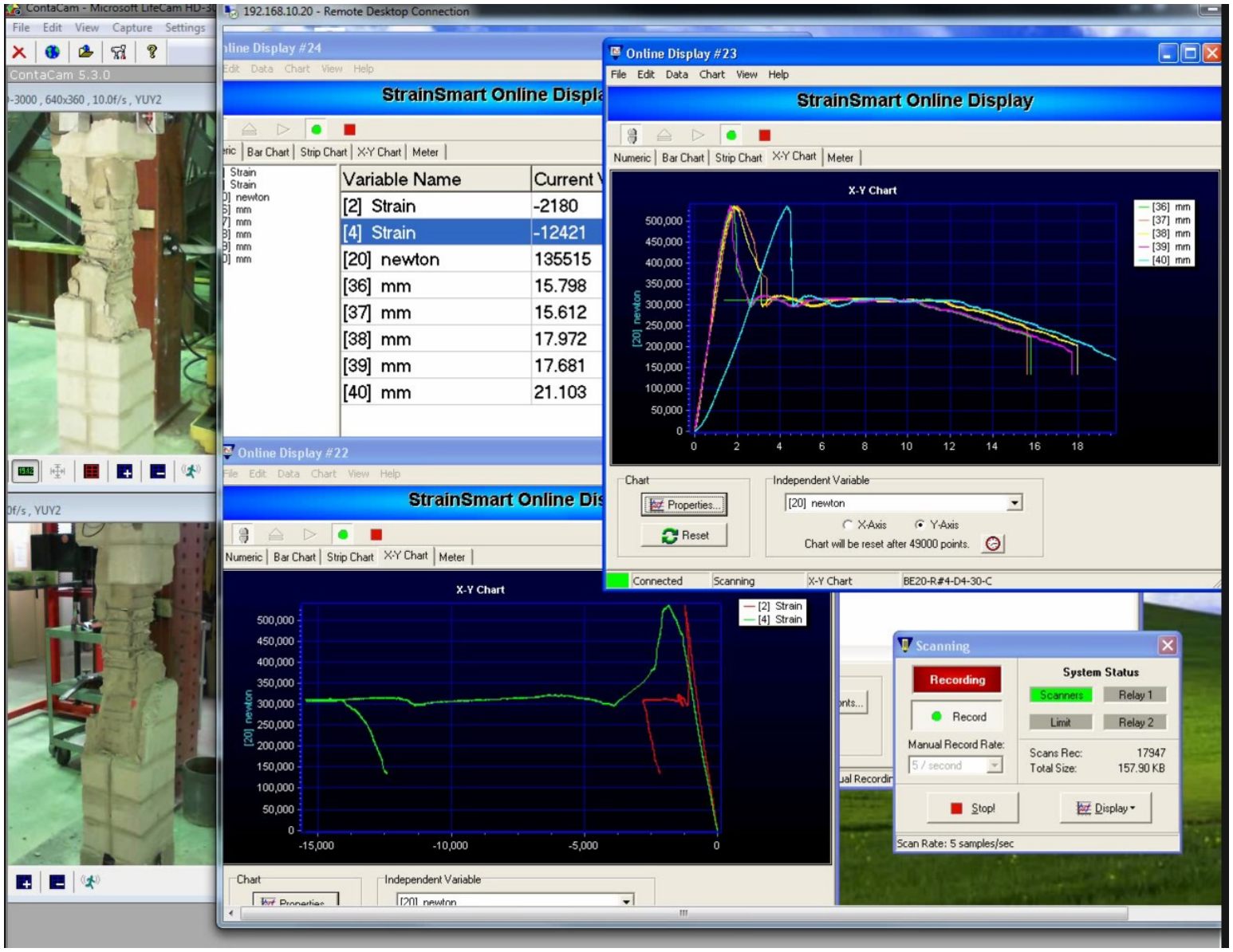

Figure C.29 Observed stress-stress relationship and the damage propagation of the RMBE specimen at the end of the test

C.2 Linear Regression Relationship

From the regression analysis presented in Figure 4.12, the observed trend representing the line of the value of $f_{max\text{-}c}$ compared to the $f_{max\text{-}un}$ based on the experimental average, 95% of the data above it, which is determined by subtracting 1.645 times the standard deviation from the experimental average. The trend line is given by the Eqs. C.1 to C.12 and it is a function of the following:

- Confinement ratio

$f_{\text{max-C}} / f_{\text{max-un}} = 1.02 + 10.33\ Cf$ (Experimental average , RMBE reinforced by #3) Eq. C.1

$f_{\text{max-C}} / f_{\text{max-un}} = 1.24 + 9.04\ Cf$ (Experimental average , RMBE reinforced by #4) Eq. C.2

$f_{\text{max-C}} / f_{\text{max-un}} = 1.05 + 6.66\ Cf$ (95th percentile, RMBE reinforced by #3) Eq. C.3

$f_{\text{max-C}} / f_{\text{max-un}} = 1.11 + 7.97\ Cf$ (95th percentile, RMBE reinforced by #4) Eq. C.4

- Vertical reinforcement ratio

$f_{\text{max-C}} / f_{\text{max-un}} = 1.02 + 0.29\ \rho_v$ (Experimental average , RMBE reinforced by #3) Eq. C.5

$f_{\text{max-C}} / f_{\text{max-un}} = 0.88 + 0.88\ \rho_v$ (Experimental average , RMBE reinforced by #4) Eq. C.6

$f_{\text{max-C}} / f_{\text{max-un}} = 1.06 + 0.18\ \rho_v$ (95th percentile, RMBE reinforced by #3) Eq. C.7

$f_{\text{max-C}} / f_{\text{max-un}} = 0.87 + 0.80\ \rho_v$ (95th percentile, RMBE reinforced by #4) Eq. C.8

- Grout strength

$f_{\text{max-C}} / f_{\text{max-un}} = 1.10 + 0.011\ f_{gr}$ (Experimental average , RMBE reinforced by #3) Eq. C.9

$f_{\text{max-C}} / f_{\text{max-un}} = 1.10 + 0.022\ f_{gr}$ (Experimental average , RMBE reinforced by #4) Eq. C.10

$f_{max\text{-C}} / f_{\text{max-un}} = 1.07 + 0.0092\ f_{gr}$ (95th percentile, RMBE reinforced by #3) Eq. C.11

$f_{\text{max-C}} / f_{\text{max-un}} = 1.005 + 0.021\ f_{gr}$ (95th percentile, RMBE reinforced by #4) Eq. C.12

The strain at peak stress, strain at 75%, and strain at 50% of the peak stress of the RMBE are obtained from equations based on the regression analysis (Figure 4.13 and 4.14) with the confinement ratio, and vertical reinforcement ratio and they are given by the Eqs. (32 to 37) as follows:

- Confinement ratio

$\mathcal{E}_{max} = 0.0014+0.01\ Cf$ (Experimental average, RMBE reinforced by #3) Eq. C.13

$\mathcal{E}_{max} = 0.0019+0.0048\ Cf$ (Experimental average, RMBE reinforced by #4) Eq. C.14

$\mathcal{E}_{max} = 0.0014+0.0067\ Cf$ (95th percentile, RMBE reinforced by #3) Eq. C.15

$\mathcal{E}_{max} = 0.0018+0.0054\ Cf$ (95th percentile, RMBE reinforced by #4) Eq. C.16

$\mathcal{E}_{75\%} = 0.0127+0.01\ Cf$ (Experimental average, RMBE reinforced by #3) Eq. C.17

$\mathcal{E}_{75\%} = 0.0025+0.01\ Cf$ (Experimental average, RMBE reinforced by #4) Eq. C.18

$\mathcal{E}_{75\%} = 0.0018+0.0146\ Cf$ (95th percentile, RMBE reinforced by #3) Eq. C.19

$\mathcal{E}_{75\%} = 0.0024+0.0092\ Cf$ (95th percentile, RMBE reinforced by #4) Eq. C.20

$\mathcal{E}_{50\%} = 0.0044+0.081\ Cf$ (Experimental average, RMBE reinforced by #3) Eq. C.21

$\mathcal{E}_{50\%} = 0.0053+0.13\ Cf$ (Experimental average, RMBE reinforced by #4) Eq. C.22

$\mathcal{E}_{50\%} = 0.004+0.058\ Cf$ (95th percentile, RMBE reinforced by #3) Eq. C.23

$\mathcal{E}_{50\%} = 0.0045+0.11\ Cf$ (95th percentile, RMBE reinforced by #4) Eq. C.24

- Vertical reinforcement ratio

$\mathcal{E}_{max} = 0.0011+0.0006\ \rho_v$ (Experimental average, RMBE constructed with 15 MPa) Eq. C.25

$\mathcal{E}_{max} = 0.0014+0.0005\ \rho_v$ (Experimental average, RMBE constructed with 45 MPa) Eq. C.26

$\mathcal{E}_{max} = 0.001+0.0006\ \rho_v$ (95th percentile, RMBE constructed with 15 MPa strength) Eq. C.27

$\mathcal{E}_{max} = 0.0013+0.0005\ \rho_v$(95th percentile, RMBE constructed with 45 MPa strength) Eq. C.28

$\varepsilon_{75\%} = 0.0018+0.0006\ \rho_v$ (Experimental average, RMBE constructed with 15 MPa) Eq. C.29

$\varepsilon_{75\%} = 0.002+0.0008\ \rho_v$ (Experimental average, RMBE constructed with 45 MPa) Eq. C.30

$\varepsilon_{75\%} = 0.0014+0.0008\ \rho_v$ (95th percentile, RMBE constructed with 15 MPa) Eq. C.31

$\varepsilon_{75\%} = 0.0012+0.0012\ \rho_v$ (95th percentile, RMBE constructed with 45 MPa) Eq. C.32

$\varepsilon_{50\%} = 0.0042+0.0024\ \rho_v$ (Experimental average, RMBE constructed with 15 MPa) Eq. C.33

$\varepsilon_{50\%} = 0.0057+0.0027\ \rho_v$ (Experimental average, RMBE constructed with 45 MPa) Eq. C.34

$\varepsilon_{50\%} = 0.0043+0.0013\ \rho_v$ (95th percentile, RMBE constructed with 15 MPa) Eq. C.35

$\varepsilon_{50\%} = 0.0046+0.0019\ \rho_v$ (95th percentile, RMBE constructed with 45 MPa) Eq. C.36

Appendix D

Pilot Test

D.1 Construction of Pilot Specimens

Four half-scale pilot specimens of boundary elements were constructed and tested up to failure to investigate different aspects prior constructing and testing the half-scale RMBE specimens. The pilot test investigated:

1. The effect of using three different gauge lengths on the axial strain measurements.
2. Measuring the axial strain using different gauge lengths raised the concern of how to fix the potentiometer on the sample. Due to the face shell spalling, fixing the potentiometer on the surface of the sample will not capture the post-peak measurements. Therefore, measuring the vertical strain in the middle zone of the sample by embedding cross bars passing through the core of the boundary element was investigated.
3. The strain gauges measurements compared to that of the potentiometer,
4. The effect of reinforcement detailing at top and bottom ends of the specimen (i.e. comparing reduced spacing hoops to regular spacing hoops),
5. The dimensions of the top and bottom footings, and
6. Using scaled reinforcement cold drawn wires, in the half scale samples, instead of bars, used usually in full-scale samples, as transversal hoops.

Typical dimensions and construction details of these pilot specimens are shown in Figure D.1. Based on the pilot test results the construction details of half-scale RMBE specimens were refined. All pilot specimens were constructed at the structures laboratory at Concordia University. Formwork, C-shape block, and hoops that were used in the construction of these specimens are shown in Figure D.2. Figure D.3 shows the sequence of pilot specimen construction including steel reinforcement cages for big-footing and boundary element, installing of steel reinforcement cages in formwork, building top footing, and building of masonry block units. The pilot specimen under testing and the instrumentations is shown in Figure D.4.

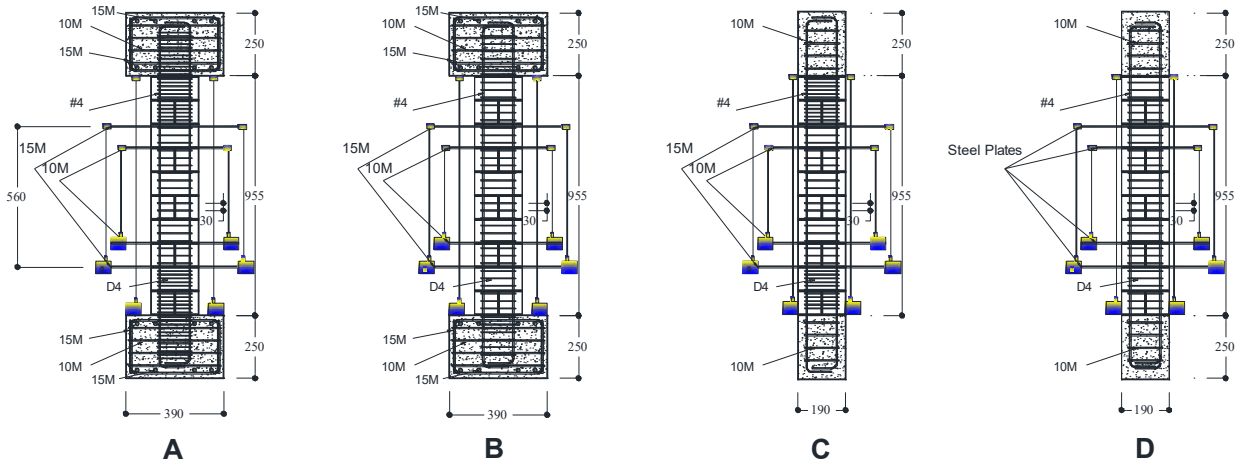

Figure D.1 Construction details of pilot specimens

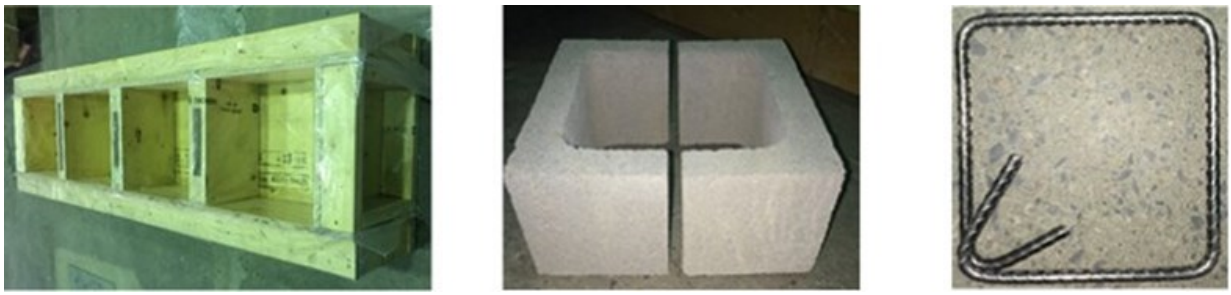

Figure D.2 Formwork, half scale C-shape masonry block, and hoop

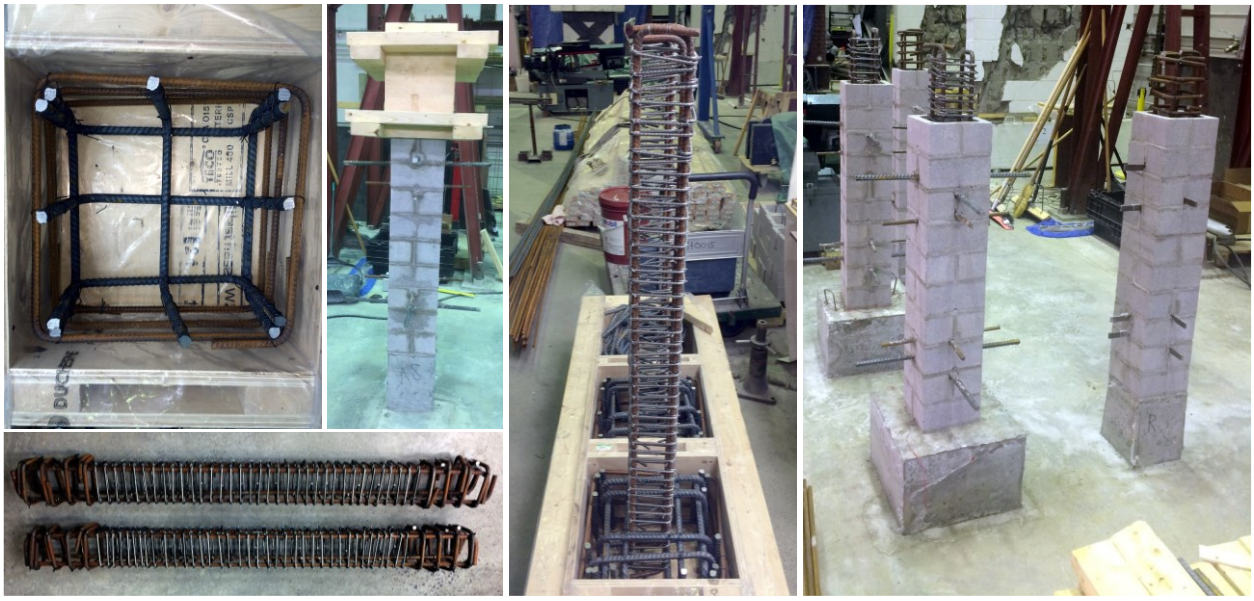

Figure D.3 Sequence of C-RMBE construction

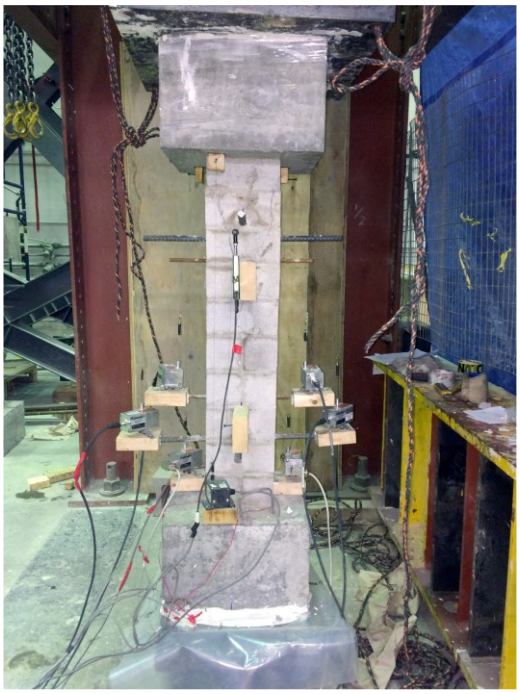

Figure D.4 Pilot specimen under testing

D.2 Pilot Test Results

Based on the test results the following points are concluded:

1. The axial strain measurements based on different gauge lengths were identical up to the peak strength, however, different responses were observed in the post peak. It was observed that as the gauge length increased the calculated strain decreased. However, the results were not consistent for all potentiometers as using embedded cross bars may have affected the reliability of the results.
2. Although measuring the displacement at the core of the sample seems more reliable compared to surface measurements, some of the embedded cross bars were bent and provided an unreliable reading. Only the potentiometers measuring the strain over the sample height were operating up to the end of the test. Consequently, the whole gauge length was used to measure the axial strain in Phase II and III. In addition, measuring the displacement from the core of the sample was reinvestigated in Phase III by taking more precautions on placing the bar through the block and the reinforcement cage.
3. Since the axial strain was measured over the whole sample height, therefore constant hoops spacing will be used. Moreover, based on the pilot test results, no significant

difference between the load-displacement relationships of the samples built detailed with hoops having constant spacing over the height versus those having reduced spacing at the sample ends.

4. It was observed that different strain values were recorded, using strain gauges, in the four reinforcement vertical bars. This was attributed to small eccentricity in the applied load and was avoided in future testing.
5. The specimens with 390 × 390 mm top and bottom footing provided similar results of specimens with 190 × 190 mm top and bottom footing. Therefore, the smaller footings were used in Phases II and III. In addition, a confinement special steel plates were used to confine the top and bottom footing in order to avoid any cracks or damage in the footing during testing.
6. Although the stress-strain behaviour of cold drawn wires (e.g. D4) is comparable to f deformed bars (e.g. 10M), the ductility of cold drawn wires is less than that of the deformed bars. However, cold drawn wire did not rupture during the pilot test except one hoop at 30% of the peak strength (i.e. 70% strength degradation). Consequently, the ductility of the deformed wires did not affect the failure mode of the tested sample and thus was used in half-scale samples as transversal hoops.

Therefore, the pilot test conclusions paved the road for detailing Phases II and III samples based on aforementioned observations as will be shown in the following sections.

D.3 Pilot Mixes of Grout

Table D.1 Mix proportions of grout based on pilot tests

	Mix Proportions			
Constituent Material	**Water**	**Cement**	**Fine Aggregate (Sand)**	**Plasticizer**
20 Mpa-Original	0.75 kg	1 kg	3.9 kg	Not used
40 Mpa-Original	0.5 kg	1 kg	2.6 kg	Not used
20 MPa Trial Mix # 1	0.79 kg	1 kg	3.86 kg	Not used
40 MPa Trial Mix # 1	0.403 kg	1 kg	1.6 kg	Not used
20 MPa Trial Mix # 2	0.81 kg	1 kg	3.92 kg	Not used
40 MPa Trial Mix # 2	0.425 kg	1 kg	1.87 kg	Not used
20 MPa Trial Mix # 3	0.79 kg	1 kg	4 kg	Not used
40 MPa Trial Mix # 3	0.52 kg	1 kg	2.65 kg	Not used

Table D.1 (cont.) Mix proportions of grout based on pilot tests

Trial Mix	Sample #	Slump (mm)	7-Days Compressive Strength (MPa)	28-Days Compressive Strength (MPa)
20 MPa - O	1	280	15.51	-
	2		-	16.68
	3		-	*
	Average		-	-
	C.O.V		-	-
40 MPa - O	1	210	41.23	-
	2		-	54.71
	3		-	54.62
	Average		-	54.67
	C.O.V		-	0.08%
20 MPa - 1	1	280	15.51	-
	2		-	16.68
	3		-	*
	Average		-	-
	C.O.V		-	-
40 MPa - 1	1	210	41.23	-
	2		-	54.71
	3		-	54.62
	Average		-	54.67
	C.O.V		-	0.08%

Table D.1 (cont.) Mix proportions of grout based on pilot tests

Trial Mix	Sample #	Slump (mm)	7-Days Compressive Strength (MPa)	28-Days Compressive Strength (MPa)
20 MPa - 2	1	280	20.04	-
	2		-	30.48
	3		-	30.72
	Average		-	30.60
	C.O.V		-	0.39%
40 MPa - 2	1	220	37.03	-
	2		-	47.08
	3		-	48.57
	Average		-	47.83
	C.O.V		-	1.56%
20 MPa - 3	1	280	14.01	-
	2		-	23.18
	3		-	22.02
	Average		-	22.60
	C.O.V		-	2.57%
40 MPa - 3	1	240	31.97	-
	2		-	45.3
	3		-	42.47
	Average		-	43.89
	C.O.V		-	3.22%